THE ANALYSIS OF THE HUMAN ANTIBODY RESPONSE TO FILOVIRUS INFECTION

By

Andrew I. Flyak

Dissertation

Submitted to the Faculty of the

Graduate School of Vanderbilt University

in partial fulfillment of the requirements

for the degree of

DOCTOR OF PHILOSOPHY

in

Microbiology and Immunology

August, 2016

Nashville, Tennessee

Approved:

James W. Thomas, M.D.

Terence S. Dermody, M.D.

D. Borden Lacy, Ph.D.

Melanie D. Ohi, Ph.D.

James E. Crowe, Jr., M.D.

To survivors of Marburg and Ebola virus infections

who generously donated their blood for this study.

ACKNOWLEDGEMENTS

This work was financially supported by the Defense Threat Reduction Agency (grant HDTRA1-13-1-0034) and U.S. NIH grant U19AI109711. The Vanderbilt Medical Center Flow Cytometry Shared Resource is supported by NIH grants P30 CA68485 and DK058404. I thank all these funding sources; this work would not have been possible without their support.

First and foremost, I would like to thank my mentor, James Crowe for entrusting me with the project that resulted in this thesis. From the very first day in the Crowe Lab, Jim gave me a freedom to explore and supportive environment to learn. There were no limits, no boundaries of what we can do as a team in pursuit of discovery. Jim has taught me to dream big and commit 100% to everything you love.

I would like to express my sincere gratitude to my dissertation committee, Tom Thomas (Chair), Terry Dermody, Borden Lacy, and Melanie Ohi for their scientific guidance over the years. I thank you all for your excellent scientific suggestions and personal advises you shared with me. Your leadership and support enabled me to become a better scientist.

This work would not be possible without numerous people outside the Vanderbilt, who helped me tremendously to advance this project. I use the pronoun “we” throughout this thesis to reflect the collaborative nature of the work I present. First, I would like to thank Alexander Bukreyev’s group at UTMB (including Philipp Ilinykh, Xiaoli Shen, Natalia Kuzmina and a former trainee Tania Garron) for their help with neutralization studies, animal experiments and escape mutants generation. Erica Saphire’s group at Scripps (including Marnie Fusco, former trainees Zachary Bornholdt and Takao Hashiguchi) for providing Ebola and Marburg glycoproteins and advancing this project with X-ray crystallography studies. Andrew Ward’s team at Scripps (including Daniel Murin, Hannah Turner and Joshua David) for mapping antibody-binding sites using electron microscopy techniques.

Benjamin Doranz and Edgar Davidson from Integral Molecular for mapping Ebola-specific antibodies using alanine-scanning mutagenesis.

I would like to thank all past and present members of the Crowe Lab. An early thanks goes to the Hybridoma Master Scott Smith, a brilliant scientist and friend, who taught me the holy grail of human hybridoma generation and helped make me a better scientist. I would like to thank my friend and colleague Natalie Thornburg who would answer every question I had about science and parenting. I would like to thank my scientific colleagues who helped me with my work, including Nurgun Kose who helped me with hybridoma generation and Hannah King who took good care of my hybridomas. I thank present and former lab technicians Rebecca Lampley, Gloria Fritz, Vidisha Singh and Leland Brown who helped me with antibody purification as well as Stephen Graham and Leah Loerinc who provided help with protein expression. I thank Robin Bombardi, Jessica Finn and Andre Branchizio who provided much needed assistance with high-throughput antibody sequencing. I also thank Frances House and Gopal Sapparapu for their excellent technical support.

I would like to thank Pavlo Gilchuk and Sebastian Joyce, my first scientific mentors who helped me to become a scientist and who gave me an opportunity to work here. I also thank the Division of Pediatric Infectious Diseases and Department of Pathology, Microbiology, and Immunology for their dedication to training students. The Vanderbilt Flow Cytometry Core provided much needed assistance with hybridoma sorting. Christopher Gulka, a former graduate student in David Wright's lab, provided help with peptide synthesis.

Finally, I would like to thank my family. All my family in Ukraine, my parents, grandparents and my younger brother, I thank you all for your constant support and encouragement. I thank my wife Solomiia, for supporting me at all times. For bringing light, joy and purpose in my life. To my beautiful daughter Sofia, your smiles and love are worth more than you will ever know.

TABLE OF CONTENTS

LIST OF TABLES

LIST OF FIGURES

LIST OF ABBREVIATIONS

Ab	Antibody
BDBV	Bundibugyo virus
EBOV	Ebola virus
EC_{50}	50% maximum-effective concentration
Fab	Fragment antibody-binding, obtained after papain digest
GP	Glycoprotein
HR	Heptad repeat
IC_{50}	50% maximum-inhibitory concentration
MAb	Monoclonal antibody
MAbs	Monoclonal antibodies
MARV	Marburg virus
MLD	Mucin-like domain
MPER	Membrane proximal external region
NPC1	Niemann-Pick C1 protein
sGP	Secreted/soluble glycoprotein
SUDV	Sudan virus

CHAPTER I

INTRODUCTION

"In biology, nothing is clear, everything is too complicated, everything is a mess, and just when you think you understand something, you peel off a layer and find deeper complications beneath. Nature is anything but simple."

Richard Preston, The Hot Zone: The Terrifying True Story of the Origins of the Ebola Virus

Thesis overview

This document is the culmination of my work on characterizing the human antibody response to Marburg and Ebola virus infections. It is divided into five chapters; chapter I provides necessary background information about filoviruses, the structure and function of filovirus glycoprotein, and filovirus entry into the host cell. This chapter also explores the human humoral response against filovirus infections and provides detailed analysis about what we know about the antibodies that target filovirus glycoprotein.

The beginning of my research starts in chapter II. This part of my research focuses on studying the human antibody response to Marburg virus (MARV). I describe a panel of fifty-one human antibodies against MARV proteins that was isolated using peripheral blood B cells from an individual who survived MARV infection several. I use antibodies from the MARV survivor to define the mechanism of MARV neutralization, and provide the evidence that MARV neutralizing antibodies recognize the receptor-binding site of MARV GP.

Chapter III focuses on the nature of cross-reactive antibody response in human survivors of *Ebolavirus* infections. I describe a panel of ninety human monoclonal antibodies to Ebolavirus glycoprotein isolated from survivors of Bundibugyo virus outbreak. I present structural and functional information about human antibodies that neutralize multiple

Ebolavirus species and a cross-reactive antibody that completely protect guinea pigs from the lethal challenge with Ebola virus. In Chapter IV I describe three naturally-occurring human cross-reactive mAbs that target a new antigenic site in the canonical heptad repeat 2 (HR2) region near the membrane proximal region of EBOV GP. I highlight the structural features formed by conserved residues in the protective site that could be used to develop an epitope-based vaccine against infection caused by diverse *Ebolavirus* species.

In Chapter V I summarize my findings and propose future directions for this work. I believe that understanding the principles underlying molecular recognition of viral protein by potent neutralizing antibodies will have a broad impact on the rational design of therapeutic antibodies and development of vaccines against filoviruses and other emerging viruses.

Epidemiology of Marburg virus infection

Filoviruses are enveloped, negative-sense RNA viruses appearing with a characteristic filamentous shape. The family *Filoviridae* (order Mononegavirales) can be divided into two major genera: *Marburgvirus* and *Ebolavirus* (Kuhn et al., 2013). The genus *Marburgvirus* includes a single species, Marburg marburgvirus and two divergent viruses: Ravn virus and Marburg virus (MARV).

MARV was discovered in August 1967, when laboratory workers in Marburg and Frankfurt (Germany) and Belgrade (former Yugoslavia, now Serbia) were infected with unknown infectious agent. It was determined that African green monkeys that had been imported from Uganda for the purpose of poliovirus vaccine research were the source of infection. The virus was isolated and characterized by multiple groups and named Marburg virus after the city with the most cases (Kissling et al., 1968; Kunz et al., 1968; Siegert et al., 1968). From 31 infected individuals, seven patients died from complications of the disease (23% mortality rate).

In the following years from 1967 though 1998, only sporadic outbreaks of MARV occurred on the African continent affecting small number of individuals (Brauburger et al., 2012) (**Figure 1**). In 1987, an isolated case of Marburg disease was identified in Kenya. The virus was isolated and characterized as a new virus in *Marburgvirus* genus, named Ravn virus (Johnson et al., 1996). The first large outbreak of MARV occurred in 1998-2000 in a gold-mining village of Durba in the northeastern Democratic Republic of Congo (DRC) affecting 154 individuals and killing 83% (Bausch et al., 2006). The outbreak ceased abruptly with the closure of the mine, suggesting that the reservoir of the MARV inhabits mines or caves (Bausch et al., 2006). The largest outbreak of MARV occurred in Angola in 2004-2005 causing 252 cases and 227 deaths (90% mortality) (Towner et al., 2006). In 2007 a small MARV outbreak occurred in western Uganda among miners working in Kitaka Cave. Based on the detection of MARV RNA in bats, virus-specific antibodies in sera, and isolation of MARV virus from bat tissue, the cave-dwelling Egyptian fruit bats (Rousettus aegyptiacus) was identified as a natural host of MARV (Towner et al., 2009). The genome sequences of isolated from miners working in Kitaka Cave and bats from the same cave closely matched (99% identity) (Towner et al., 2009).

While MARV disease remains rare, MARV poses a risk for travelers to Africa. In 2008 two cases of MARV disease were documented in Dutch and American tourists who presumably got infected during a visit to Python Cave in Queen Elizabeth National Park, Uganda. While the Dutch tourist died from MARV disease, the American tourist survived the infection ((CDC), 2009; Timen et al., 2009). In 2012, as I started my thesis studies in the Crowe Lab, I received peripheral blood sample from the American survivor. Using the survivor's peripheral blood mononuclear cells, I isolated a panel of human neutralizing antibodies against MARV that revealed the mechanism of MARV inhibition (further described in Chapter II). In addition to naturally occurring infections, several cases of

Figure 1. Marburg virus outbreaks in Africa. Outbreaks are indicated with corresponding year and color-coded according to virus species. From (Leroy et al., 2011)

laboratory-acquired MARV infection have been reported in Soviet Union (now Russia) of which one had a fatal outcome (Brauburger et al., 2012; Nikiforov et al., 1994).

Including the recent outbreak in Uganda where 4 individuals died from MARV infection (Albarino et al., 2013), to date there have been in total 467 cases and 372 documented deaths due to the MARV infection. The disease burden of MARV infection in Africa is small when compared to other infections diseases such as HIV (1.3 million deaths caused by HIV in 2009 in sub-Saharan Africa alone, (Brauburger et al., 2012)) and malnutrition. However, there are some studies suggesting that the number of MARV infections is underestimated. During the investigation of a 1998-2000 MARV outbreak in a gold-mining village of Durba in the DRC, medical personal reported that the disease was recognized locally as “syndrome hémorragique de Durba”, occurring as far back as 1980s (Bausch et al., 2006).

Epidemiology of Ebola virus infection

In the *Ebolavirus* genus, there are five virus species, four of which are known to cause severe disease in humans: Ebola virus, Bundibugyo virus, Sudan virus and Taï Forest virus. An additional virus, Reston virus (RESTV) was isolated in 1989 from cynomolgus monkeys imported from Philippines and housed in a quarantine facility in Reston, Virginia, USA. While monkeys developed hemorrhagic disease with high lethality, the small number of confirmed human infections did not result in clinical illness despite the presence of RESTV-specific antibodies in some of the workers handling monkeys (Miranda and Miranda, 2011; Miranda et al., 1991).

Ebola virus first appeared in 1976 when similar cases of hemorrhagic fever emerged in two neighboring locations: first in southern Sudan and then in northern Zaire (now Democratic Republic of the Congo, DRC) (WHO, 1978a, b) (**Figure 2**). The virus was isolated from patients in both outbreaks and named Ebola virus after a small river in northwestern DRC. In the follow up study it was determined that these two outbreaks were caused by two different viruses, Sudan virus (SUDV) and Ebola virus (EBOV) (Cox et al., 1983). The SUDV outbreak resulted in 284 cases with a fatality rate of 53% while EBOV outbreak was responsible for 318 cases with a fatality rate of 89%. It is generally recognized now that within the *Ebolavirus* genus EBOV infection has the highest fatality rates (60-90%), followed by SUDV infections (40-60%) (Feldmann and Geisbert, 2011).

A large outbreak of EBOV occurred in 1995 in the Kikwit town, south of DRC affecting 315 individuals and killing 254 patients (81% fatality rate) (Khan et al., 1999). The Kikwit outbreak has provided much of our current knowledge about EBOV and outbreak management. During the outbreak, 80 (25%) of 315 infected individuals were healthcare personal (Khan et al., 1999).

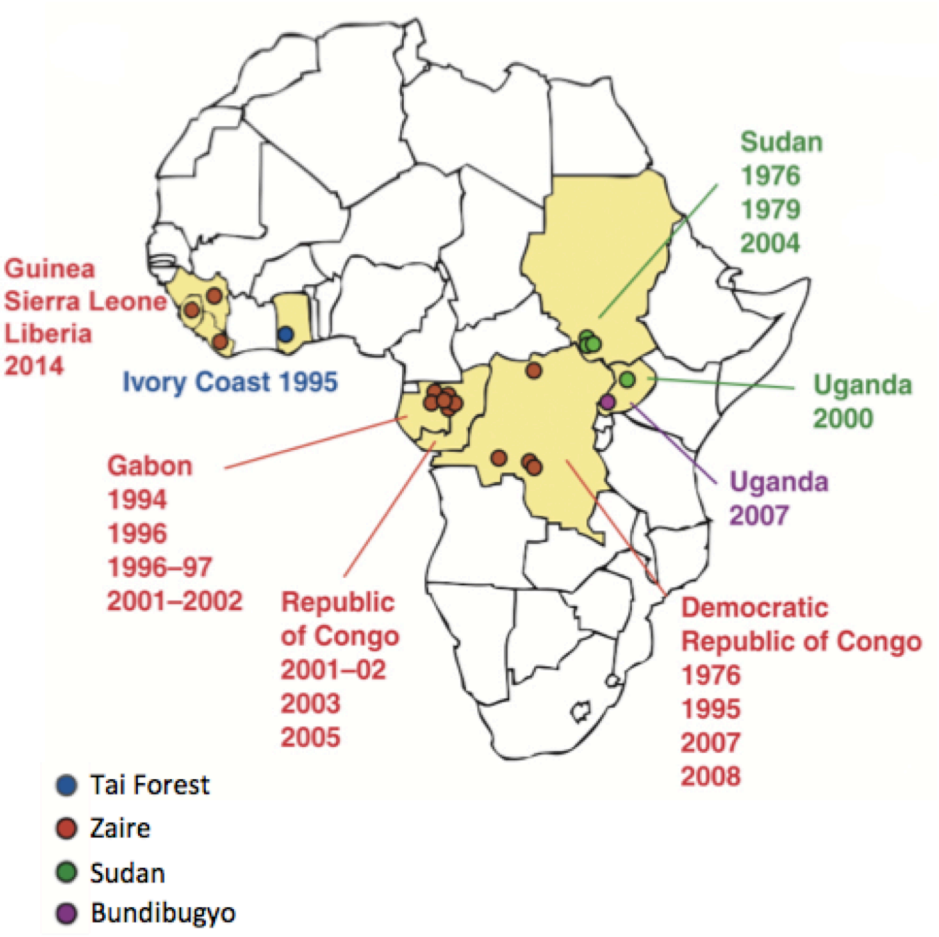

Figure 2. Ebola virus outbreaks in Africa. Outbreaks are indicated with corresponding year and color-coded according to virus species. Modified from (Leroy et al., 2011)

A large outbreak of SUDV occurred in Uganda in 2000, affecting 425 individuals and killing 173 patients (53% fatality rate) (Lamunu et al., 2004). Between 2001 and 2005 there were five EBOV outbreaks in the Republic of Congo and Gabon resulting in a total of 311 cases and 261 fatalities (84% fatality rate) (Formenty et al., 2006; Leroy et al., 2004; Leroy et al., 2002). The last species of the *Ebolavirus* genus, Bundibugyo virus (BDBV), was discovered in 2007 in Uganda causing 149 cases and 37 deaths (Towner et al., 2008). The Crowe lab obtained de-identified peripheral blood mononuclear cells from 30 survivors of the 2007 BDBV outbreak of Uganda from a repository at Makerere University (Kampala,

Uganda), which is part of the Walter Reed Army Institute of Research. Antibodies isolated from BDBV survivors are described in Chapter III of this document.

The only case of Taï Forest virus infection occurred in 1995, when a group of scientists was studying a viral hemorrhagic fever epizootic among western chimpanzees (Pan troglodytes versus) in Taï National Park in Ivory Coast (Formenty et al., 1999; Le Guenno et al., 1995). One of the scientists got infected with the virus when she performed necropsies on chimpanzees found dead in the Taï national park. The individual was transported to Switzerland for treatment and later recovered from infection. This was the first case of Ebola hemorrhagic fever reported in West Africa. Until 2013, the Taï Forest virus infection remained the only case of Ebola hemorrhagic fever reported in West Africa.

2013-2015 Ebola outbreak in West Africa

The 2013-2015 Ebola outbreak in West Africa was caused by EBOV Makona variant (Kuhn et al., 2014). The outbreak began in the forested region of southeastern Guinea in December 2013 and then spread into Liberia in March, Sierra Leone in May, and Nigeria in late July 2014. This is the first EBOV outbreak to reach epidemic proportions and the largest EBOV outbreak on record (Briand et al., 2014). The Ebola epidemic has caused more than 28,000 cases and more than 11,000 deaths (WHO Ebola situation report). According to the initial epidemiologic investigation, the suspected first case of the outbreak occurred in Meliandou in Guéckédou prefecture in Guinea where a 2-year old was infected with virus and died on December 6, 2013 (Baize et al., 2014). After a single introduction into the human population, the outbreak was then sustained exclusively by human-to-human transmission (Baize et al., 2014; Gire et al., 2014).

In 2014 a total of 10 individuals with EBOV disease were treated in U.S. hospitals; of these patients, 8 survived (Epstein et al., 2015) (Lyon et al., 2014). The airlifting of infected

individuals for treatment in selected U.S. hospitals has caused an unprecedented level of media attention to EBOV disease, which likely played a role in increasing public concern (SteelFisher et al., 2015).

High-throughput EBOV genome sequencing has played a major role in understanding EBOV evolution and transmission and also informed public health efforts (Baize et al., 2014; Carroll et al., 2015; Gire et al., 2014; Ladner et al., 2015; Park et al., 2015; Simon-Loriere et al., 2015; Tong et al., 2015). Based on the rate of nonsynonymous to synonymous mutations, it was determined that purifying selection becomes increasingly effective over time, removing deleterious mutants from the viral population (Park et al., 2015). Hotspots for non-synonymous divergence have likely resulted from a lower level of constraint on encoded viral proteins (Ladner et al., 2015), as peaks in non-synonymous divergence largely corresponded to intrinsically disordered regions of proteins (for example the region of the glycoprotein gene encoding mucin-lilke domain) (Olabode et al., 2015). Little evidence was found for EBOV adaptation to the human host suggesting that the frequency of interactions between humans and reservoir hosts may be the dominant factor in controlling the frequency of spillover events (Ladner et al., 2015).

Among survivors of EBOV, chronic health problems, including myalgia, arthralgia, and ocular findings have been considered to be a rheumatologic entity called the post-Ebola syndrome. Recently, the persistence of EBOV in ocular fluid for 9 weeks after the clearance of viremia was reported in EBOV survivor (Varkey et al., 2015). In line with previous reports that EBOV can be cultured from semen samples (Bausch et al., 2007), a recent study has found the first molecular evidence of sexual transmission of EBOV 6 months after patient recovery (Mate et al., 2015), which is more than four times as long as the WHO-defined waiting period for declaring country to be free of EBOV disease.

Filovirus genes and proteins

The family *Filoviridae* belongs to the order of *Mononegavirales*, which contains viruses characterized by a linear, non-segmented, single negative strand of RNA as a genetic material. The EBOV and MARV genomes are about 19 kb in length and they encode seven structural proteins: nucleoprotein (NP), virion protein 35 (VP35), virion protein 40 (VP40), glycoprotein (GP), virion protein 30 (VP30), virion protein 24 (VP24) and RNA-dependent RNA polymerase (L) (**Figure 3**). EBOV but not MARV also encodes one non-structural protein, secreted glycoprotein (sGP). RNA molecule-NP complex is linked to the RNA-depended RNA polymerase and inner matrix proteins VP30 and VP35 to form a ribonucleoprotein complex, which is engaged in replication and transcription (Volchkov et al., 2001). Both VP24 and VP40 link the nucleoprotein complex with the lipid bilayer of the viral envelope and they are also involved in the formation of nucleocapsid, assembly and budding of viral particles (Leroy et al., 2011). Two matrix proteins, VP35 and VP24 play role in the pathogenicity of filovirus infection as they inhibit host antiviral responses (Leroy et al., 2011).

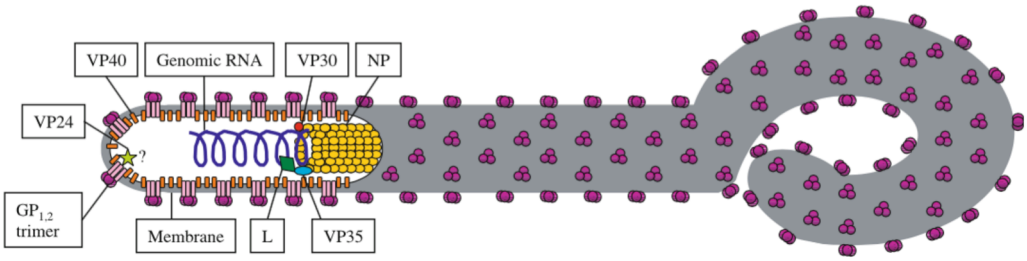

Figure 3. Structure of the filovirus virion particle. The exact position of VP24 in filovirus virions is unclear. From (Kuhn, 2008)

The structure of filovirus glycoprotein

The filovirus glycoprotein (GP) is the only protein on the viral surface. The filovirus GP is a trimer composed of three heavily glycosylated GP1-GP2 heterodimers, which result from furin-like enzyme cleavage of the precursor protein. GP1 and GP2 subunits are linked by a disulphide bond (Volchkov et al., 1998) and mediate all functions necessary for virus to enter the host cell. The GP1 subunit mediates the virus attachment to the cell membrane and receptor recognition. The GP2 subunit anchors the GP spike to the viral membrane and mediates the fusion of viral and host membranes during the viral entry into the host cell.

Crystal structures are available for prefusion GPs of EBOV (Lee et al., 2008a), SUDV (Bale et al., 2012; Dias et al., 2011a), and MARV (Hashiguchi et al., 2015). The crystal structure of EBOV GP in complex with human neutralizing antibody Fab KZ52, illuminated the overall structure of *Ebolavirus* surface protein (Lee et al., 2008a) (**Figure 4**). The EBOV GP trimer adopts a chalice-like shape, in which GP1 subunits form a bowl encircled by helices of GP2 subunits (Lee et al., 2008a). When the virus is internalized inside the endosome, GP2 unwinds from the GP1 subunit and undergoes a series of conformational rearrangements finally collapsing into a six-helix bundle conformation that initiates the fusion of viral and host membranes (Saphire, 2013). Several structures of post-fusion conformations of the GP2 subunit indicate that pre- and post-fusion structures of GP2 differ significantly (Koellhoffer et al., 2012; Malashkevich et al., 1999; Weissenhorn et al., 1998).

The GP1 subunit can be further divided into several subdomains termed base, head, glycan cap, and mucin-like domain (Saphire, 2013) (**Figure 4**). The GP1 base forms a hydrophobic concave surface that clamps GP2 subunits (Lee and Saphire, 2009). The GP1 head contains a receptor-binding site topped by a glycan cap and highly glycosylated mucin-like domain (Lee et al., 2008a). The glycan cap and contains four predicted N-linked glycosylation sites and the mucin-like domain has seven N-linked glycosylation sites and 15-

20 O-linked glycosylation sites. The highly-glycosylated mucin-like domain was excised from GP for crystallization, but a recent study has indicated the relative position of this subdomain using small-angle X-ray scattering (SAXS) in solution (Hashiguchi et al., 2015). The EBOV mucin-like domains extend outwards from the GP core (Hashiguchi et al., 2015) (**Figure 5**). Once inside the endosome, GP is cleaved by host proteases that remove approximately 80% of the mass of the GP1 subunit, including the mucin-like domain and glycan cap and exposing the receptor binding site (Chandran et al., 2005; Dube et al., 2009). Both glycan cap and mucin-like domains are dispensable for pseudovirus attachment or entry in cell culture (Yang et al., 2000). It has been suggested the dense clustering of glycans on the glycan cap and mucin-like domain likely shield much of the surface of EBOV GP from humoral immune surveillance, leaving only a few sites on the EBOV GP protein where neutralizing antibodies could bind without interference by glycans (Cook and Lee, 2013).

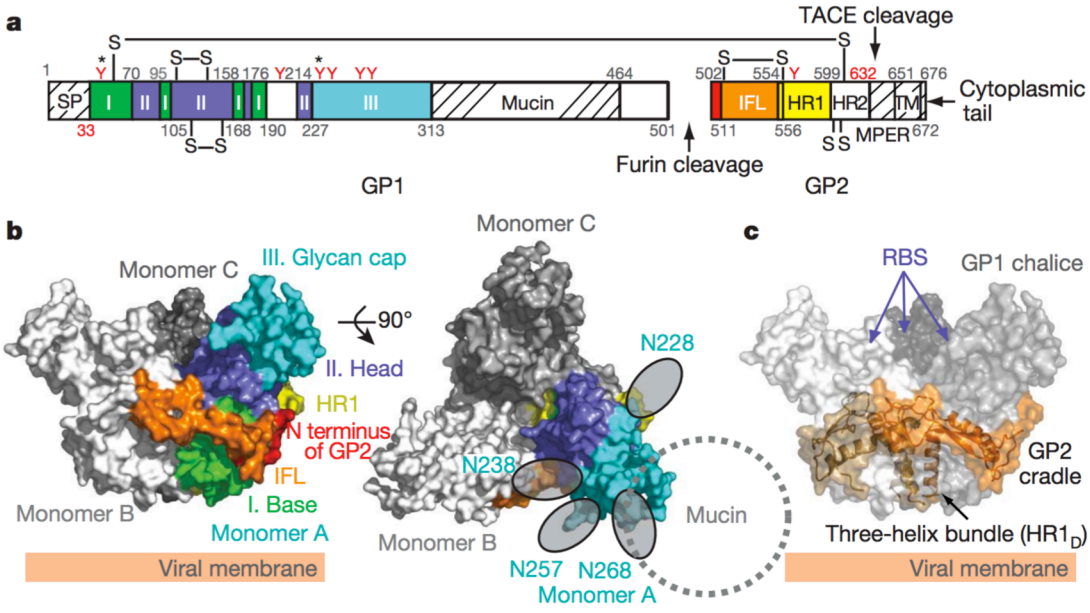

Figure 4. The structure of Ebola virus glycoprotein. (A) Domain schematic of EBOV GP. White regions indicate crystallographically disordered domains and hash-marked regions indicate construct-deleted regions. GP1 base is green (I), GP1 head - blue (II), GP1 glycan cap - cyan (III), N terminus of GP2 – red, GP2 internal fusion loop – orange, GP2 HR1 – yellow. Red Y-shaped symbols indicate predicated N-linked glycosylation sites. Y-symbols marked with an asterisk were mutated. (B) Molecular surface of EBOV GP viewed on its side (left) and top (right). Monomer A is colored according to the scheme in A. (C) Molecular surface of EBOV GP chalice and cradle. From (Lee et al., 2008a)

GP2 mediates the fusion of viral and host cell membranes and contains the internal fusion loop and heptad repeat regions (HR1 and HR2) (Lee et al., 2008a). The crystal structures of post-fusion GP2 subunit have indicated that HR1 and HR2 form antiparallel α-helices (Malashkevich et al., 1999; Weissenhorn et al., 1998).

Recently, a crystal structure of Marburg virus GP in complex with a neutralizing antibody MR78 isolated from a human survivor of Marburg infection has been reported (Hashiguchi et al., 2015). SAXS data collected for full-length EBOV and MARV GPs indicated that while mucin-like domain of EBOV projects more upward, mucin-like domain of MARV is less upward, potentially covering the sides of the GP trimer (**Figure 5**). While the glycan cap and mucin-like domain shield the EBOV receptor-binding sites from humoral immune surveillance (Lee et al., 2008a), new SAXS data suggested that the receptor binding site on MARV GP surface might be accessible for antibody binding (Hashiguchi et al., 2015).

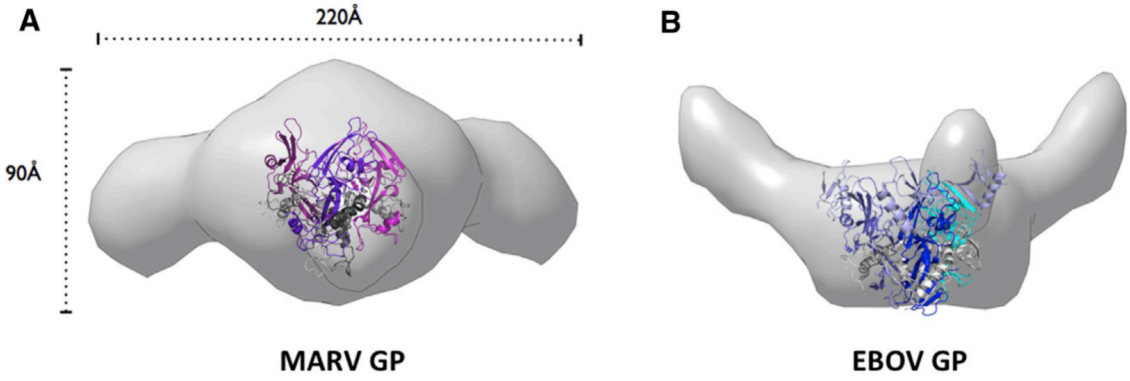

Figure 5. Molecular envelopes of full-length filovirus glycoproteins. Envelopes of mucin-like domain-containing MARV GP (A) and EBOV GP (B) ectodomains determined by Small-Angle X-ray Scattering in solution. Rendered Gaussian distributions of molecular envelopes are shown in gray, crystal structures of cleaved MARV GP (that lacks the glycan cap and mucin-like domain, colored in purple and grey) and EBOV GPΔMuc (that lacks the mucin-like domain, colored in blue and grey) are shown as ribbon models. From (Hashiguchi et al., 2015)

Entry of filoviruses

During viral entry, the mucin-like domain and glycan cap that contain N-linked and O-linked glycans mediate binding to host attachment factors present on the cell membrane, including C-type lectins (DC-SIGN, L-SIGN and mannose-binding lectin) (Alvarez et al., 2002; Lin et al., 2003; Marzi et al., 2004; Marzi et al., 2007). New attachment factors that bind to phosphatidylserine present in the EBOV and MARV viral envelope were identified (Kondratowicz et al., 2011). These phosphatidylserine receptors include members of the T-cell immunoglobulin and mucin domain protein (TIM) family and TAM family of receptor tyrosine kinase (Tyro3/Axl/Mer) (Kondratowicz et al., 2011; Moller-Tank and Maury, 2014; Shimojima et al., 2006). Additional study determined that TIM family receptors can bind to phosphatidylethanolamine, which is also present in the virions of filoviruses (Richard et al., 2015) (**Figure 6**).

Following attachment, filovirus virions are internalized predominantly through macropinocytosis (Nanbo et al., 2010; Saeed et al., 2010). This process is characterized by the actin-mediated membrane ruffling and blebbing followed by the formation of macropinosomes (Mercer and Helenius, 2009). Internalized virions first distribute into early endosomes and then traffic to the late endosomes/lysosomes in a Rab5/Rab7 GTPase-dependent manner (Saeed et al., 2010). Inside the endosome, GP is cleaved by cysteine proteases cathepsin B (CatB) and cathepsin L (CatL) at or around residue 190 (Dube et al., 2009). The cleavage event removes approximately 80% of the mass of the GP1 subunit, including the mucin-like domain and glycan cap (Chandran et al., 2005; Dube et al., 2009).

After cleavage of GP in the endosome, the receptor-binding sites on 19-kDa GP become exposed (Chandran et al., 2005), and the GP1 head then is able to bind to its receptor, Niemann-Pick C1 (NPC1) protein (Carette et al., 2011; Côté et al., 2011) (**Figure 6**). NPC1 is a large thirteen-pass membrane protein that is expressed inside late

endosomes/lysosomes in all cells and functions as a cholesterol transporter (Carstea et al., 1997). Mutations in *NPC1* gene in humans cause a Niemann-Pick type C disease, a rare but fatal neurovisceral disorder, characterized by accumulation of cholesterol inside late endosomes-lysosomes (Carstea et al., 1997). Fibroblasts obtained from patients with Niemann-Pick disease are resistant to EBOV infection (Carette et al., 2011). Chinese hamster ovary-derived cells deficient in NPC1 were completely resistant to viral infection (Carette et al., 2011; Cote et al., 2011). In mouse models of MARV and EBOV infections, heterozygosity for *NPC1* protects animals from lethal filovirus infection (Carette et al., 2011). A single mutation in *NPC1* gene was found in straw-colored fruit bats that are resistant to EBOV infection (Ng et al., 2015). The reported amino acid change decreased the affinity of NPC1 protein to EBOV GP revealing host adaptation to reduce filovirus replication (Ng et al., 2015). Filovirus entry does not require the full-length NPC1 protein, as a single luminal domain C of NPC1 mediates the filovirus entry into the host cell, and NPC1 domain C linked to synthetic membrane protein constituted a receptor for filovirus infection (Miller et al., 2012).

But what is the function of NPC1 in filovirus entry into the host cell? Several models have been proposed to explain the role of NPC1 during the filovirus entry into the host cell (White and Schornberg, 2012). Initial studies proposed that NPC1 triggers the fusion activity of primed GP (Cote et al., 2011; Miller et al., 2012). However, NPC1 binding is not sufficient to trigger the conformational rearrangement, and the additional factors required for fusion remains to be identified (Miller and Chandran, 2012; White and Schornberg, 2012). Recently, endosomal calcium channels called two-pore channels were identified as an additional entry factor for filoviruses and were proposed to trigger the conformational rearrangement in NPC1-negative endosomes (Falzarano and Feldmann, 2015; Sakurai et al., 2015). However, a recent study challenged this idea by showing that glycoprotein fusion events occur in NPC1+ endolysosomes (Mingo et al., 2015).

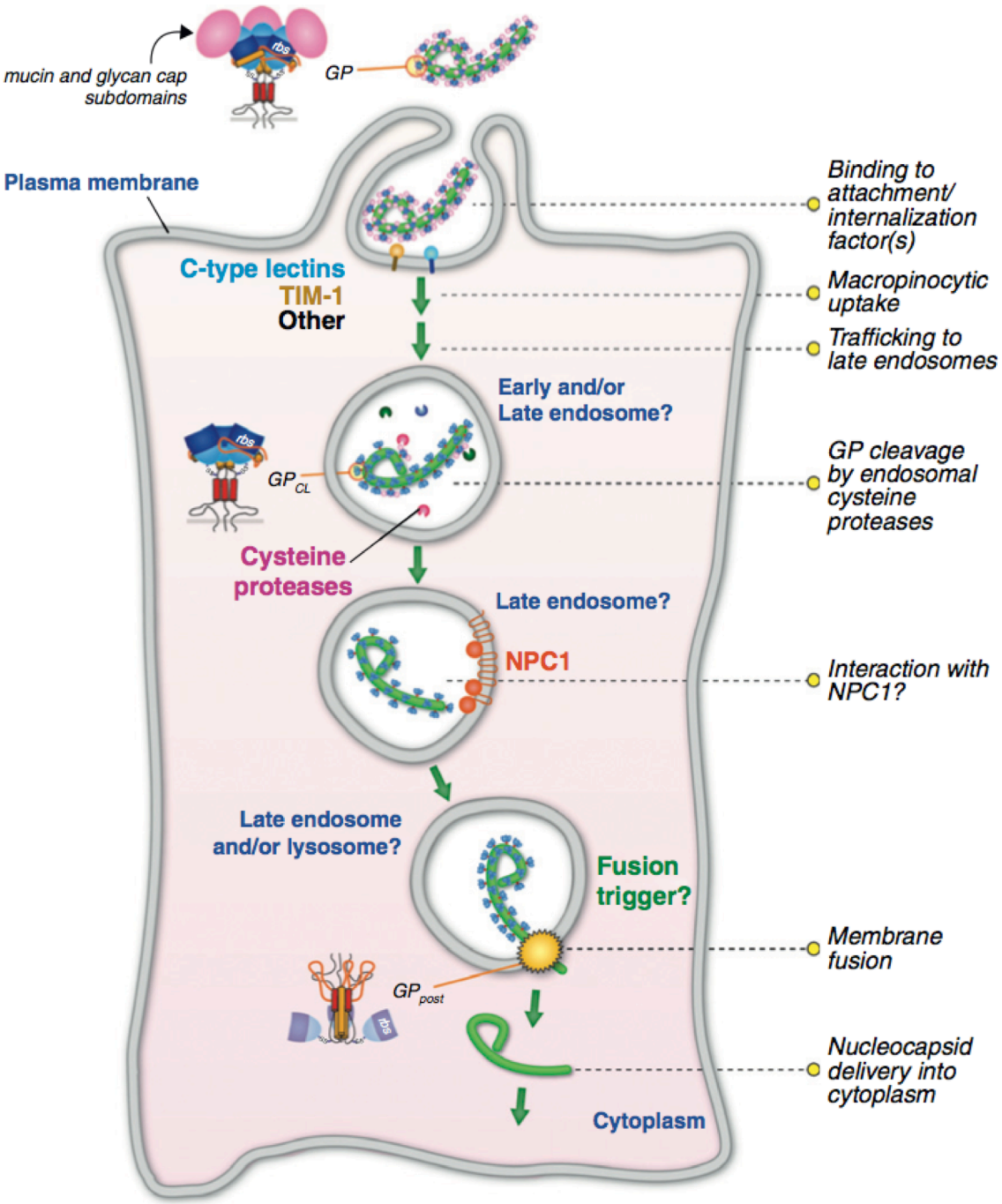

Figure 6. Model of filovirus entry pathway, from (Miller and Chandran, 2012)

Filovirus membrane fusion events are initiated by conformational changes in GP and are though to be similar to the fusion processes described for other viral GPs (White et al., 2008). Triggering expose and reposition the heptad repeat I sequence in GP2 subunit, projecting the hydrophobic GP2 fusion loop into the endosomal membrane (Gregory et al.,

2011). This extended GP2 conformation then unwinds and refolds into six-helix bundle, in which HR1 and HR2 are packed together, and fusion loop and GP transmembrane domain meet (Malashkevich et al., 1999; Weissenhorn et al., 1998). The GP2 conformation rearrangement drives viral and cellular membrane mixing and fusion pore formation, releasing the ribonucleoprotein complex into the cytoplasm (Harrison, 2008) (**Figure 6**).

Human humoral response to filovirus infection

The adaptive immune system contributes to protection against filovirus infections in nonhuman primates and small animal models (reviewed in (Wong et al., 2014)). In accordance with evidence observed in animal models, early upregulation of filovirus-specific antibody responses followed by activation of cytotoxic T cells is associated successful recovery from EBOV infection. In contrast, fatal outcome is associated with impaired antibody responses and early activation of T cells unable to control viral replication (Baize et al., 1999). A follow-study identified asymptomatic infections of EBOV in individuals having direct contact with symptomatic patients. Eleven of 24 asymptomatic individuals developed antibody responses to EBOV antigens, including nucleoprotein and VP40 (Leroy et al., 2000). A large serological survey of rural populations in Gabon found EBOV-specific antibodies in 15% of analyzed individuals (Becquart et al., 2010).

Antigen-specific antibodies persist in humans. Survivors from the 1995 Kikwit outbreak contained EBOV-specific antibodies 2 years after disease onset (Ksiazek et al., 1999a). In another study, antibody responses persisted for 10 years in two survivors of 1976 Yambuku outbreak (Ksiazek et al., 1999b). Survivors from 2000 Gulu outbreak contained SUDV GP-specific antibodies as well as serum-neutralizing activity 12 years after infection (Sobarzo et al., 2013b). Analysis of serum samples collected from SUDV survivors demonstrated the highest number of samples with neutralizing activity 6 months after recovery, with

neutralizing antibodies persisting for prolonged time, even 10 years after infection (Sobarzo et al., 2013a).

A study of immune responses of four survivors of EBOV who received treatment at Emory University Hospital found an extensive T- and B-cell activation in all four patients (McElroy et al., 2015). The frequencies of activated T and B cells were comparable to other acute viral infections, with virus-specific plasmablasts present in the blood even 2 months after disease onset (McElroy et al., 2015).

Ebola virus-specific antibodies

Several dozens of EBOV-specific monoclonal antibodies (mAbs) have been described in the literature, including nearly 20 murine mAbs (Holtsberg et al., 2015; Qiu et al., 2012c; Shedlock et al., 2010; Takada et al., 2003; Wilson et al., 2000), 7 macaque mAbs (Keck et al., 2015; Shedlock et al., 2010), and a single neutralizing human antibody KZ52, which was isolated from a phage-display library constructed from survivors of 1995 EBOV Kikwit outbreak (Maruyama et al., 1999). Additionally, several mAbs have been described for related SUDV, including a single neutralizing antibody that was generated in mice (Dias et al., 2011b) and several synthetic mAbs isolated from a focused phage library (Chen et al., 2014).

Most of our knowledge about humoral response against filovirus infections has come from studies of murine mAbs that recognize EBOV GP (**Figure 7, Table 1**). Several groups isolated EBOV-specific antibodies by infecting mice with replicon systems in which the native surface protein was replaced genetically with EBOV GP (Qiu et al., 2011; Takada et al., 2003; Wilson et al., 2000). After immunization, spleen cells were harvested from mice and fused with myeloma cells followed by hybridoma passaging and antibody purification. Purified mAbs were initially screened in neutralization assays (Qiu et al., 2012c; Shedlock et

al., 2010; Takada et al., 2003; Wilson et al., 2000), and the functional activity for many of them was measured *in vivo* using mouse (Qiu et al., 2012c; Takada et al., 2007; Wilson et al., 2000; Zeitlin et al., 2011), guinea pig (Qiu et al., 2012c; Qiu et al., 2014; Takada et al., 2007) and non-human primate models of EBOV infection (Marzi et al., 2012; Olinger et al., 2012a; Pettitt et al., 2013; Qiu et al., 2012b; Qiu et al., 2014; Qiu et al., 2013) (**Table 1**). In parallel, antigenic sites for several EBOV GP-specific antibodies were determined using X-ray crystallography (Bale et al., 2012; Dias et al., 2011a; Lee et al., 2008a; Olal et al., 2012), negative stain single-particle electron microscopy (Murin et al., 2014), alanine-scanning mutagenesis (Davidson et al., 2015), or linear peptide dot blots (Qiu et al., 2011; Wilson et al., 2000) (**Table 1**). Results from those studies revealed that the highly-glycosylated mucin-like domains shield the EBOV receptor-binding sites from humoral immune surveillance. As a result, mouse antibodies were found to target thee major antigenic regions on the surface of EBOV GP: the mucin-like domain, the glycan cap, and the GP base (Davidson et al., 2015; Murin et al., 2014) (**Figure 7).**

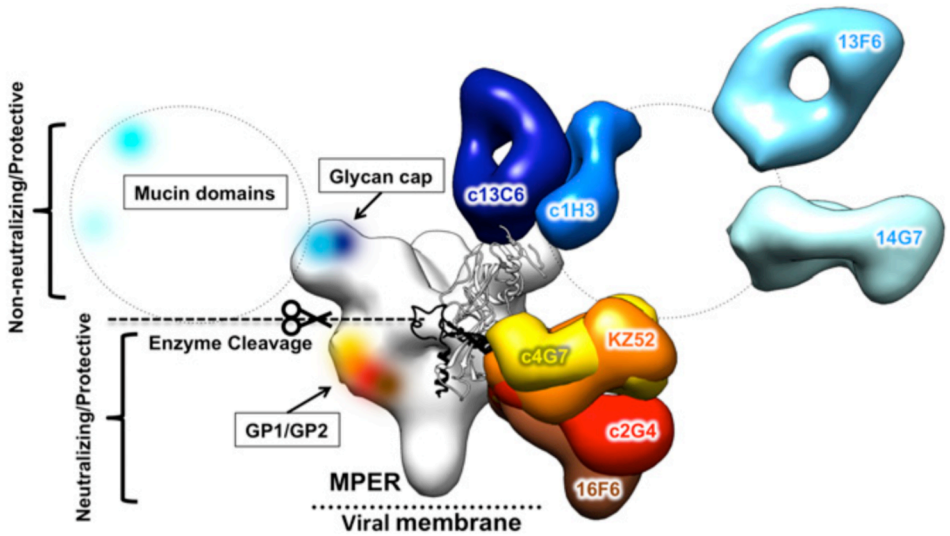

Figure 7. Sites of vulnerability on EBOV GP for protective mAbs. MAbs target the main three sites on GP surface: mucin-like domain, glycan cap and GP base near GP1/GP2 interface. A monomer of GPΔMuc(PDB ID code is 3CSY) is fit into the core GP of the c13C6:c4G7 complex. MPER – membrane proximal external region. From (Murin et al., 2014)

1. Antibodies to the mucin-like domain

Several mouse antibodies were identified that bind to linear polypeptide sequences between glycans in EBOV mucin-like domains (MLD), including mAbs 6D8, 13F6 and 14G7 (Lee et al., 2008c; Olal et al., 2012; Wilson et al., 2000) (**Table 1**). Those mAbs protect mice from lethal EBOV infection but fail to neutralize EBOV *in vitro* (Olal et al., 2012; Shedlock et al., 2010), likely because mucin-like domains, as well as mAbs attached to them, are removed by host cathepsins inside the endosome (Chandran et al., 2005). It has been proposed that the protective effect of the MLD-specific antibodies likely results from the ability of antibodies to recruit immunological effector function rather than preventing binding of virus to the target cell membrane (Olal et al., 2012). Despite the good performance of mAbs specific for the MLD in a mouse model of EBOV infection, both 6D8 and 13F6 failed to protect guinea pigs and non-human primates from lethal EBOV infection when tested individually (Qiu et al., 2014) (**Table 1**).

2. Antibodies to the glycan cap

MAb 13C6 (the key component of MB-003 and ZMapp cocktails) and 1H3 (the key component of ZMab cocktail) were initially isolated in mice (Qiu et al., 2011; Wilson et al., 2000) and later shown by negative-stain single-particle EM and alanine-scanning mutagenesis to target a second antigenic region – the glycan cap (Davidson et al., 2015; Murin et al., 2014). Both 1H3 and 13C6 weakly neutralize EBOV (IC_{50} > 1.0 μg/mL) (Qiu et al., 2012c; Qiu et al., 2014; Wilson et al., 2000) and protected mice against EBOV (Qiu et al., 2012c; Wilson et al., 2000). Despite the high protective efficiency of glycan-cap specific mAbs in mice, 1H3 failed to protect guinea pigs from lethal challenge (all 5 animal died)

Table 1. Protective mAbs against *Ebolavirus* glycoprotein												
MAb	**Isolated from**	**Neutra-lizing?**	**Specificity**			**Protective efficacy**			**References**			
			***Ebolavirus* species**[a]	**GP forms**[b]	**Antigenic regions**	**In mice**[c]	**In guinea pigs**	**In NHPs**	**MAb isolation**	**Epitope information**	**Protective studies**	
KZ52	Human	Yes	Z	GP	Base		4/5	0/4	(Maruyama et al., 1999)	(Davidson et al., 2015; Lee et al., 2008a)	(Oswald et al., 2007; Parren et al., 2002)	
1H3	Mouse	Yes		GP, sGP	Glycan cap	6/15	0/5		(Qiu et al., 2011)	(Davidson et al., 2015; Murin et al., 2014)	(Qiu et al., 2012c)	
13C6	Mouse	Yes	Z, S	GP, sGP	Glycan cap	10/10	1/6	1/3	(Wilson et al., 2000)	(Davidson et al., 2015; Murin et al., 2014)	(Qiu et al., 2014; Wilson et al., 2000)	
2G4	Mouse	Yes	Z	GP	Base	9/15	3/5		(Qiu et al., 2011)	(Davidson et al., 2015; Murin et al., 2014)	(Qiu et al., 2012c)	
4G7	Mouse	Yes	Z	GP	Base	11/15	3/5		(Qiu et al., 2011)	(Davidson et al., 2015; Murin et al., 2014)	(Qiu et al., 2012c)	
13F6	Mouse	No	Z	GP	Mucin-like domain	10/10	1/6	0/3	(Wilson et al., 2000)	(Davidson et al., 2015; Lee et al., 2008c)	(Qiu et al., 2014; Wilson et al., 2000)	
6D8	Mouse	Yes/No	Z	GP	Mucin-like domain	10/10	0/6	0/3	(Wilson et al., 2000)	(Davidson et al., 2015)	(Qiu et al., 2014; Wilson et al., 2000)	
133	Mouse	Yes	Z	GP	Base	7/8	1/3		(Takada et al., 2003)		(Takada et al., 2007)	
226	Mouse	Yes	Z	GP, sGP	GP1	7/8	1/3		(Takada et al., 2003)		(Takada et al., 2007)	
16F6	Mouse	Yes	S	GP	Base	0%[d] / 90%[e]			(Dias et al., 2011a)	(Dias et al., 2011a)	(Chen et al., 2014; Dias et al., 2011a)	

[a] Specificity to various *Ebolavirus* species: Z - Ebola virus, S - Sudan virus,
[b] Specificity to various forms of GP: GP - full length GP, sGP - secreted GP, MLD - mucin-like domain
[c] Number of BALB/c mice surviving challenge of EBOV when 100 μg of mAb is administered on day 1
[d] Percent of SCID mice surviving challenge of SUDV when 100 μg of mAb is administered on days 5, 10, 15 and 20
[e] Percent of Type 1 IFN α/β $R^{-/-}$ mice surviving challenge of SUDV when 500 μg of mAb is administered on days -1, 1 and 4

(Qiu et al., 2012c) and 13C6 provided very marginal protection in guinea pigs (1 of 6 animals survived) or non-human primates (1 of 3 animals survived) (Qiu et al., 2014) (**Table 1**). Similar to the mucin-like domain-specific mAbs, it was suggested that the lower *in vitro* neutralization activity of glycan cap-specific antibodies might be due to the removal of the glycan cap by host proteases (Chandran et al., 2005; Cote et al., 2011; Misasi et al., 2012) inside the endosome before GP engagement with the Niemann-Pick C1 receptor (Carette et al., 2011; Cote et al., 2011).

Murine antibody 226 neutralizes EBOV and protects mice from lethal infection one day before or two days after virus challenge (Takada et al., 2007; Takada et al., 2003). Three neutralization escape mutants with polymorphisms at residues 134, 194 and 199 of GP1 were obtained for mAb 226, suggesting that 226 binds the disordered loop on the surface of GP1, which has been confirmed to be the site of cathepsin cleavage (Lee and Saphire, 2009). MAb 226/8.2 might block cathepsin cleavage, preventing the engagement of GP core with NPC1 receptor.

3. Antibodies to the base region

KZ52 is the only human monoclonal antibody known to bind EBOV GP and represents the group of antibodies that target GP1/GP2 interface at the GP base (**Table 1**). This antibody was isolated from a phage display library that was constructed from bone marrow RNA obtained from a survivor (Maruyama et al., 1999). KZ52 neutralized EBOV *in vitro (Maruyama et al., 1999)*, protected guinea pigs from lethal challenge (Parren et al., 2002), but failed to protect non-human primates from EBOV infection (Oswald et al., 2007). KZ52 mAb is specific for the three discontinuous regions of GP1 and GP2, including the internal fusion loop (Lee et al., 2008c). KZ52 neutralizes EBOV most likely by inhibiting the conformational changes required for fusion of viral and endosomal membranes (Lee et al., 2008a).

Several murine Abs have also been reported to bind to the base region of EBOV GPs (Dias et al., 2011a; Murin et al., 2014). The ZMapp cocktail is composed of three EBOV glycoprotein (GP)-specific mAbs (designated c13C6, c2G4 and c4G7) that were isolated initially from mice (Qiu et al., 2011; Wilson et al., 2000), chimerized with human antibody constant regions, and then produced in *Nicotiana benthamiana* plants (Qiu et al., 2014). Single-particle EM reconstructions of these mAbs in complex with EBOV surface protein have revealed key sites of vulnerability on the EBOV GP (Murin et al., 2014) (**Figure 7**). One such site lies within the GP base at the GP1/GP2 interface; two of three mAbs from the ZMapp cocktail (c2G4 and c4G7) bind to overlapping epitopes located in this region.

Marburg virus-specific antibodies

Most of our knowledge about humoral response against filovirus infections has come from studies of mAbs that recognize EBOV GP. As the result, there is little information available about human or mouse antibodies to other filoviruses, such as MARV. Two murine Abs that bind the mucin-like domain of MARV GP reduce MARV budding from infected cells in culture, but fail to neutralize virus directly (Kajihara et al., 2012). Polyclonal MARV-specific mAbs protect non-human primates when administrated passively after challenge (Dye et al., 2012). The epitopes recognized by such polyclonal neutralizing mAbs, and the mechanism of neutralization by which these Abs act, are unknown.

Recently, a diverse panel of ten mouse mAbs against MARV has been described (Fusco et al., 2015). Four of ten antibodies bind MARV-specific “wing” epitope on GP2 subunit. The wing region is present only on the surface of MARV GP and is a portion of the mucin-like domain attached to GP2 subunit. GP2-specific mAbs provide 60%-100% protection in mice challenged with MARV (Fusco et al., 2015).

Successful treatment with cocktails of antibodies

While there is no FDA-approved treatment for filovirus infections, several experimental therapeutics against EBOV are being investigated, including small interfering RNAs (Geisbert et al., 2010; Thi et al., 2015), antisense oligonucleotides (Warren et al., 2010; Warren et al., 2015), a nucleoside analog (Warren et al., 2014), therapeutic vaccines (Feldmann et al., 2007; Geisbert et al., 2008), and monoclonal antibody (mAb) cocktails (Olinger et al., 2012a; Qiu et al., 2012b; Qiu et al., 2014). Of these, preliminary treatment studies suggest that the effect of the antibody cocktails exceeded the efficacy and treatment window of other experimental therapeutics described so far (Marzi et al., 2012; Pettitt et al., 2013; Qiu et al., 2012a; Qiu et al., 2014; Zeitlin et al., 2011) (**Table 2**).

The ZMapp cocktail is composed of three EBOV glycoprotein (GP)-specific mAbs (designated c13C6, c2G4 and c4G7) that were isolated initially from mice (Qiu et al., 2011; Wilson et al., 2000), chimerized with human antibody constant regions, and then produced in *Nicotiana benthamiana* (Qiu et al., 2014).

Table 2. Efficacy of combined mAb treatment in non-human primates

Cocktail	Components	Dose, mg/kg and time of treatment	No. survivors/total	References
ZMapp	c13C6+c2G4+c4G7	50, 5dpi	6/6	(Qiu et al., 2014)
ZMab	c1H3+c2G4+c4G7	25, 1-3dpi	4/4	(Qiu et al., 2012a)
MB-003	c13C6+h13F6+c6D8	50, 1dpi	1/3	(Qiu et al., 2014)
Two mAb cocktail	133+266	50, -1,1,3 dpi	1/3	(Marzi et al., 2012)

CHAPTER II

MECHANISM OF HUMAN ANTIBODY-MEDIATED NEUTRALIZATION OF MARBURG VIRUS

"…the operators offered a side trip, an option, to a place called the Maramagambo Forest, where the chief attraction was a peculiar site that everyone knew as Python Cave. African rock pythons lived there, languid and content, grown large and fat on a diet of bats."

David Quammen, Spillover: Animal Infections and the Next Human Pandemic

Introduction

Most of our knowledge about humoral response against filovirus infections has come from studies of murine Abs that recognize EBOV GP. From those studies, we learned that mouse nAbs preferentially target peptides exposed in upper, heavily glycosylated domains or lower areas (the GP1 base) where rearrangements occur that drive fusion of viral and host membranes (Saphire, 2013). Abs have not been identified that target protein features of the GP1 head subdomain, where the receptor-binding site to NPC1 protein is located. Ab KZ52, the only reported human EBOV GP-specific mAb, was obtained from a phage display library that was constructed from bone marrow RNA obtained from a survivor (Maruyama et al., 1999). KZ52 binds a site at the base of the GP and neutralizes EBOV, most likely by inhibiting the conformational changes required for fusion of viral and endosomal membranes (Lee et al., 2008).

In contrast, very little is known about the mechanisms by which Abs neutralize MARV. Two murine Abs that bound the mucin-like domain of MARV GP reduced MARV budding from infected cells in culture, but failed to neutralize virus directly (Kajihara et al., 2012).

Polyclonal MARV-specific Abs were shown to protect non-human primates when administrated passively after challenge (Dye et al., 2012). The epitopes recognized by such polyclonal nAbs, and the mechanism of neutralization by which these Abs act, are unknown.

In this chapter, I describe the isolation of a large panel of human nAbs from B cells of an individual who contracted MARV infection in 2008 following exposure to fruit bats in the Python Cave in Queen Elizabeth National Park, Uganda. I used Abs isolated from the human survivor to define the molecular basis of MARV neutralization by Abs. The results show that MARV nAbs recognize the NPC1 receptor-binding site of MARV GP, and in some cases also recognize conserved structural features in the equivalent receptor-binding site on EBOV GP.

I acknowledge Alexander Bukreyev's group for performing neutralization, protection experiments as well as providing help with escape mutants generation, Andrew Ward's group for studying MARV-specific mAbs by negative-stain single-particle EM, and Erica Saphire's group for providing MARV GPs.

Isolation of human monoclonal antibodies against Marburg virus

The success of this project depended on the ability to generate large panels of filovirus-specific neutralizing antibodies. The hybridoma generation technique was used successfully in the Crowe lab in the past to generate hundreds of virus-specific cell lines for dengue and influenza viruses (Krause et al., 2011; Smith et al., 2013). From those studies, it was determined that the frequency of antigen-specific memory B cells in a PBMC sample, the initial transformation efficiency, as well as sensitivity and specificity of the screening assays could impact the total number and functional characteristics of the isolated antibodies.

As the hybridoma generation technique has never been used in the past to obtain filovirus-specific human monoclonal antibodies, I decided to test the overall performance of the method by using PBMCs samples obtained from an individual who survived MARV infection several years earlier. To determine whether the individual was able to mount a successful humoral response, I performed an enzyme-linked immunosorbent assay (ELISA) where antibodies form the subject's serum were tested for binding to MARV proteins. Strong signal was detected for survivor serum but not for control serum, when plates were coated with irradiated cell lysates prepared from MARV-infected cell cultures (**Figure 8A**).

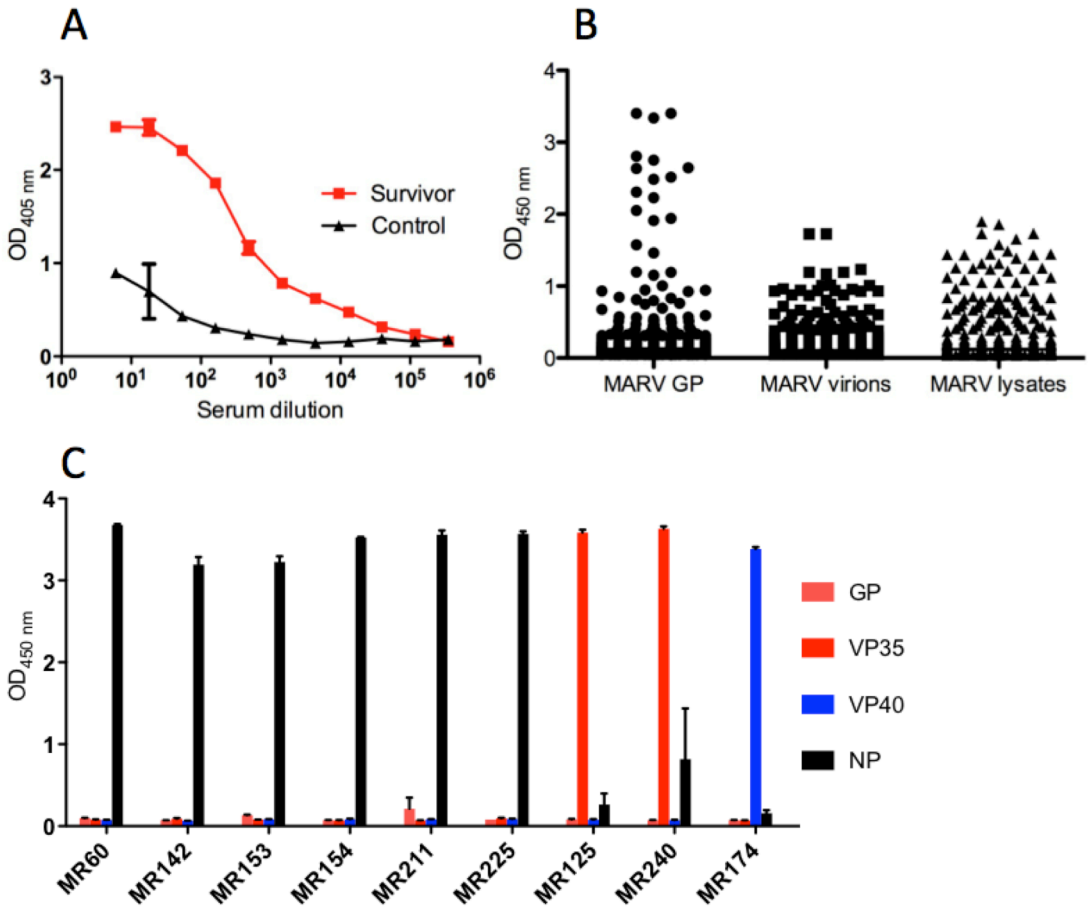

Figure 8. Isolation of human mAbs against Marburg virus. (A) Serum of MARV survivor contains MARV-specific antibodies; plate was coated with irradiated lysates prepared from MARV-infected cells. (B) EBV-transformed B cells secrete MARV-specific antibodies. (C) Mabs that bind to MARV infected-cell lysate but not to GP target MARV internal proteins.

The hybridoma generation protocol developed in the Crowe lab is mostly amenable to isolation of monoclonal antibodies from circulating memory B cells. To show that samples obtained from the MARV survivor contained memory B cells capable of secreting filovirus-specific antibodies, I transformed in total 80 million PBMCs from the subject with Epstein-Barr virus and, after 7 days, I screened supernates from the plates for the presence of MARV antigen-specific B cell lines. I used three different ELISA assays for screening: plates were coated either with recombinant MARV GP expressed in an insect cell line or irradiated MARV virions purified on sucrose gradient or irradiated lysates prepared from MARV-infected cell cultures. Multiple wells with a high signal were observed in all three assays, suggesting that memory B cells capable of secreting antibodies to MARV antigen are present in PBMCs from the MARV survivor and that those cells are transformable by the hybridoma method (**Figure 8B**).

During the next step of the hybridoma generation protocol, cells from wells with supernates reacting in the MARV antigen ELISAs were fused with myeloma cells using an electrofusion technique. This is the most critical step of hybridoma generation, as the success of the fusion can be impacted by multiple factors, such as the initial transformation efficiency, viability of the myeloma and target B cells, and the total number of antigen-specific B cells in the fusion suspension. In total, I fused 247 antigen-specific B cell lines and, after the cloning, I was able to generate 51 monoclonal hybridomas secreting MARV-specific human mAbs (21% success rate).

Thirty-nine of these mAbs were specific to the MARV GP, while 12 bound to infected-cell lysate but not to GP; these latter mAbs were shown in secondary screens to bind to MARV internal proteins (NP, VP35, or VP40) (**Figure 8C**).

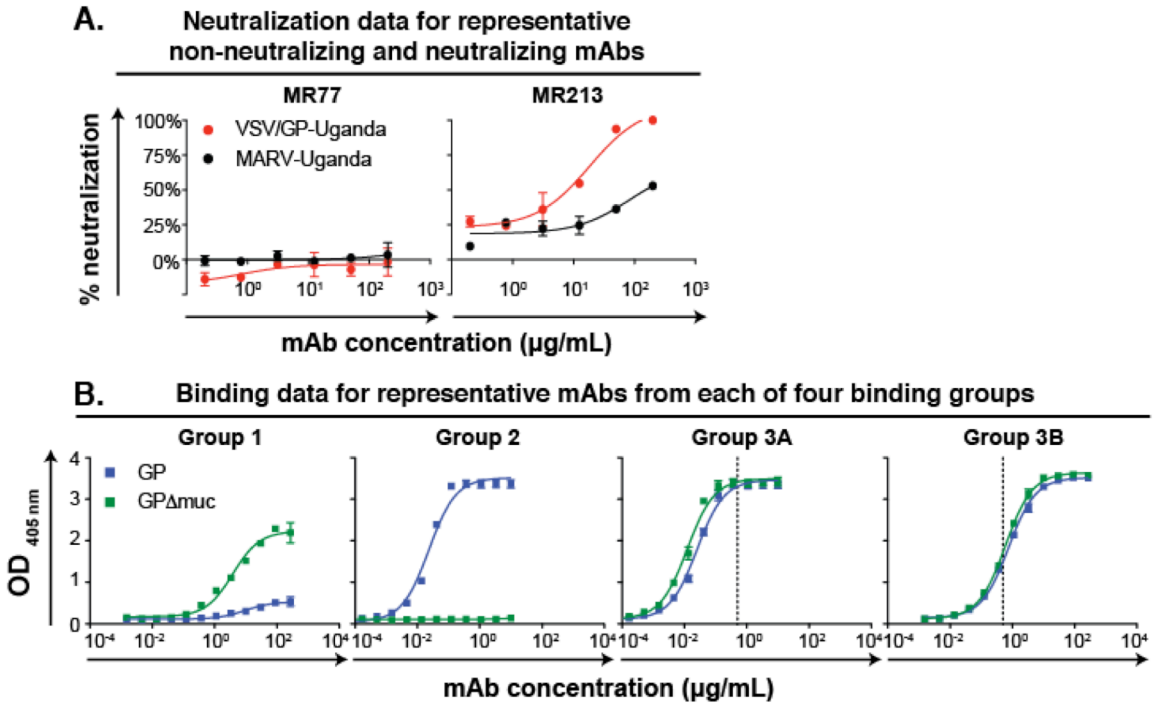

Figure 9. Neutralizing and binding activities of MARV mAbs. (A) Neutralization activity of MR77 (non-neutralizing antibody) or MR213 (neutralizing antibody) against VSV/GP-Uganda (red circles) or MARV-Uganda (black circles). Error bars represent the SE of the experiment performed in triplicate. (B) Binding of representative mAbs from four distinct binding groups to the MARV GP (blue squares) or MARV GPΔmuc (green squares). A dotted line indicates 0.5 µg/ml threshold for categorizing group 3 antibodies as possessing low (3A) or high (3B) EC50 values.

Neutralization activity

To evaluate the inhibitory activity of the mAbs, we collaborated with Dr. Alexander Bukreyev's group at UTMB. The Bukreyev Lab performed *in vitro* neutralization studies using a chimeric vesicular stomatitis virus with MARV GP from Uganda strain on its surface (VSV/GP-Uganda). Eighteen of the 39 MARV GP-specific mAbs exhibited neutralization activity against VSV/GP-Uganda (**Figures 9A, 10**). Of those 18 nAbs, 9 displayed strong (IC_{50} < 10 µg/mL), 8 nAbs displayed moderate (IC_{50}: 10-99 µg/mL), and one displayed weak (IC_{50}: 100-1,000 µg/mL) neutralizing activity against VSV/GP-Uganda. We also tested the neutralization potency of all nAbs that bound to MARV GP in a plaque reduction assay using

Group	mAb	VSV/GP-Uganda	MARV-Uganda
1	MR48	>	>
	MR49	>	>
	MR59	>	>
	MR73	>	>
	MR75	>	>
	MR77	>	>
	MR84	>	>
	MR85	>	>
	MR114	>	>
	MR117	>	>
	MR168	>	>
	MR187	>	>
	MR237	>	>
2	MR228	>	>
	MR235	>	>
3A	MR162	>	>
	MR221	>	>
	MR224	>	>
	MR246	>	>
3B	MR65	224	>
	MR72	13	601
	MR78	5	93
	MR79	>	>
	MR82	7	288
	MR103	28	291
	MR111	8	414
	MR137	>	>
	MR144	37	>
	MR186	2	>
	MR191	6	>
	MR198	12	206
	MR201	8	572
	MR208	55	>
	MR209	12	402
	MR213	10	305
	MR229	7	215
	MR232	4	114
	MR238	10	>
	MR241	12	>

Figure 10. Heatmap showing the neutralization potency of MARV GP-specific mAbs. The IC50 value for each virus-mAb combination is shown, with dark red, orange, yellow, or white shading indicating high, intermediate, low, or no potency, respectively. IC50 values greater than 1,000 µg/ml are indicated by >. Neutralization assays were performed in triplicate.

viable MARV-Uganda virus. Of 18 Abs that neutralized VSV/GP-Uganda, 10 Abs exhibited neutralizing activity against MARV-Uganda (**Figure 9A, 10**). These data suggest that VSV/GP, often used to study neutralizing potency of Abs because of its BSL-2 containment level, is more susceptible to Ab-mediated neutralization than viable MARV. This difference is likely explained by the significantly lower copy number of MARV GP molecules that incorporate into VSV particles compared with the large number of GP molecules on the surface of filovirus filaments (Beniac et al., 2012; Thomas et al., 1985).

Comparison of MARV neutralizing and non-neutralizing antibodies at concentration up to 1.6 mg/mL revealed dose-dependent activity of those mAbs that neutralized. The neutralization activity of nAbs was not enhanced by the presence of complement. As expected, we did not detect neutralizing activity for any of the 12 Abs specific to MARV NP, VP35, or VP40 proteins.

Recognition of varying forms of GP

To characterize the binding of isolated Abs to recombinant MARV GPs, I performed binding assays using either a recombinant MARV GP ectodomain containing the mucin-like domain (MARV GP) or a recombinant GP lacking residues 257-425 of the mucin-like domain (MARV GPΔmuc). Based on OD_{405} values at the highest Ab concentration tested (E_{max}) and 50% effective concentration (EC_{50}), I divided the MARV-GP-specific Abs into four major groups, based on binding phenotype (designated Binding Groups 1, 2, 3A and 3B; **Figure 9B and Figure 12**). Binding Group 1 mAbs had an E_{max} to GP < 2 [*i.e.*, these mAbs never exhibited a maximal binding level to MARV GP]; Binding Group 2 mAbs had an E_{max} to GP >2, with EC_{50} for GP < EC_{50} for GPΔmuc [*i.e.*, these mAbs bound to the mucin-like domain or glycan cap]; Binding Group 3 had an E_{max} to GP > 2, with EC_{50} for GP ≈ EC_{50} for GPΔmuc [*i.e.*, these mAbs bound equally well to full-length and mucin-deleted forms of GP], with the Group 3A mAbs having an EC_{50} for GP < 0.5 μg/mL and the Group 3B mAbs having an EC_{50} for GP > 0.5 μg/mL.

Abs that lacked neutralization activity against VSV/GP-Uganda or MARV-Uganda fell principally into Binding Groups 1, 2, and 3A. Interestingly, all VSV/GP-Uganda nAbs displayed a unique binding pattern and segregated into Binding Group 3B (**Figure 10**). It was interesting that while both mAbs from Groups 3A and 3B bound equally well to the full-length MARV GP and to the GPΔmuc, EC_{50} values for nAbs from Binding Group 3B were higher than those for non-neutralizing Abs from Group 3A.

Competition-binding studies

To determine whether mAbs from distinct binding groups targeted different antigenic regions on the MARV GP surface, I performed a competition-binding assay using a real-time

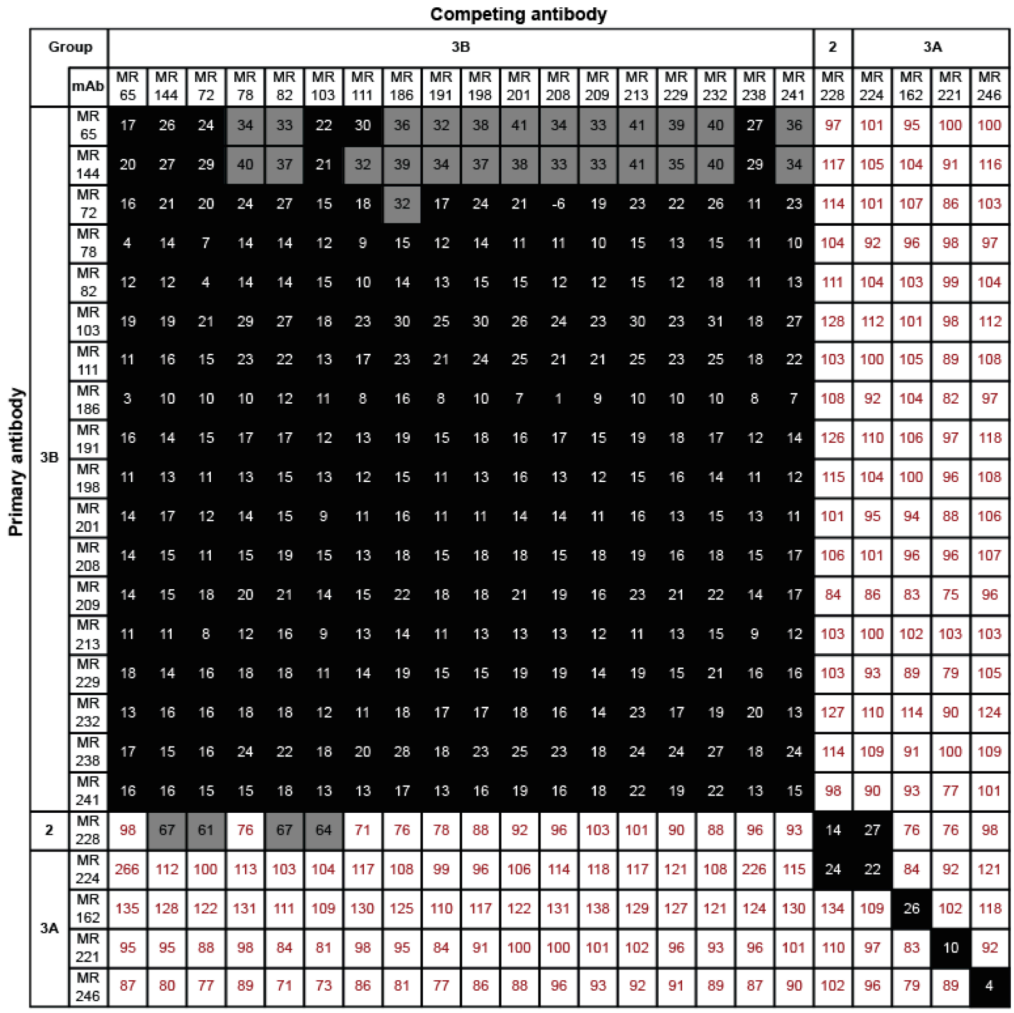

Figure 11. MARV-neutralizing mAbs target a distinct antigenic region on the GP surface. Data from competition binding assays using mAbs from binding groups 2, 3A, or 3B. Numbers indicate the percent binding of the competing mAb in the presence of the first mAb, compared to binding of competing mAb alone. MAbs were judged to compete for the same site if maximum binding of the competing mAb was reduced to <30% of its un-competed binding (black boxes with white numbers). MAbs were considered non-competing if maximum binding of the competing mAb was >70% of its un-competed binding (white boxes with red numbers). Gray boxes with black numbers indicate an intermediate phenotype (between 30 and 70% of un-competed binding).

biosensor. Antibodies are assigned to distinct antigenic regions (or functional regions) if they both can bind the antigen. Antibodies are assigned to the same antigenic region if one antibody blocks the binding of another antibody. I tested 18 MARV nAbs from Binding Group 3B, four Abs from Binding Group 3A, and one Ab from Binding Group 2 in a tandem blocking assay in which biotinylated GPΔmuc was attached to a streptavidin biosensor. Abs from Group 1 and the two non-neutralizing Abs from Binding Group 3B did not bind to biotinylated

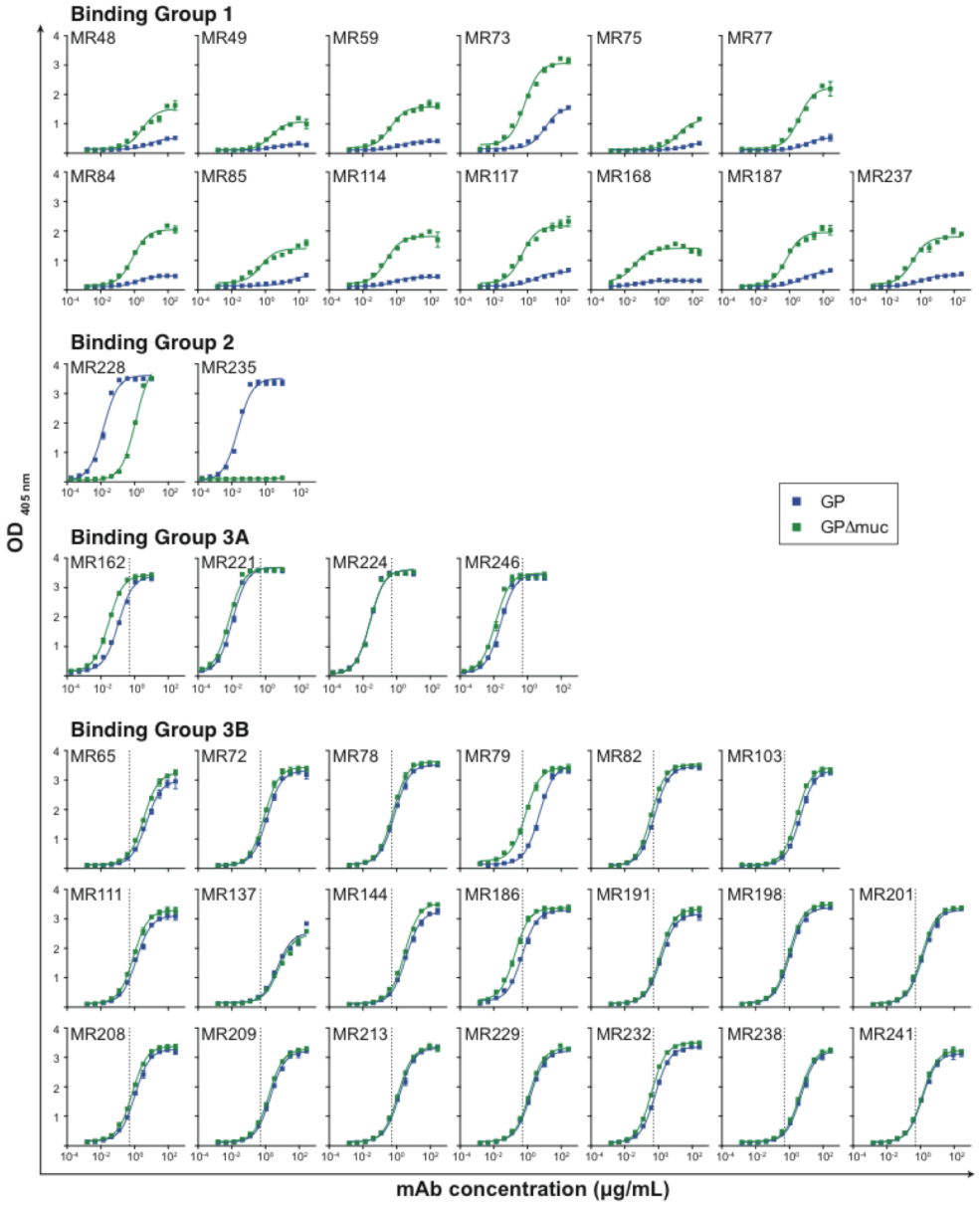

Figure 12. Binding patterns of MARV GP-specific antibodies.
Antibodies were segregated into four Binding Groups based on the binding to MARV GP (blue squares) or MARV GPΔmuc (green squares). Binding was categorized based on the OD405 values at the highest antibody concentration tested (E_{max}) and half maximal effective concentration (EC_{50}).

GPΔmuc in the competition assay and were excluded from the analysis. While non-neutralizing Abs from Binding Groups 2 and 3A did not prevent binding of the Binding Group 3B nAbs to GPΔmuc, all nAbs blocked binding of each of the other nAbs to the antigen and segregated into a single competition-binding group (**Figure 11**). These data suggested that all of the nAbs target a single major antigenic region on the MARV GP surface.

Electron microscopy studies of antigen-antibody complexes

To determine the location of the antigenic region targeted by MARV nAbs, in collaboration with Andrew Ward's group, we performed negative stain single-particle electron microscopy (EM) studies using complexes of GPΔmuc with Fab fragments of seven nAbs from Binding Group 3B. The EM reconstructions clearly showed that Fab fragments for

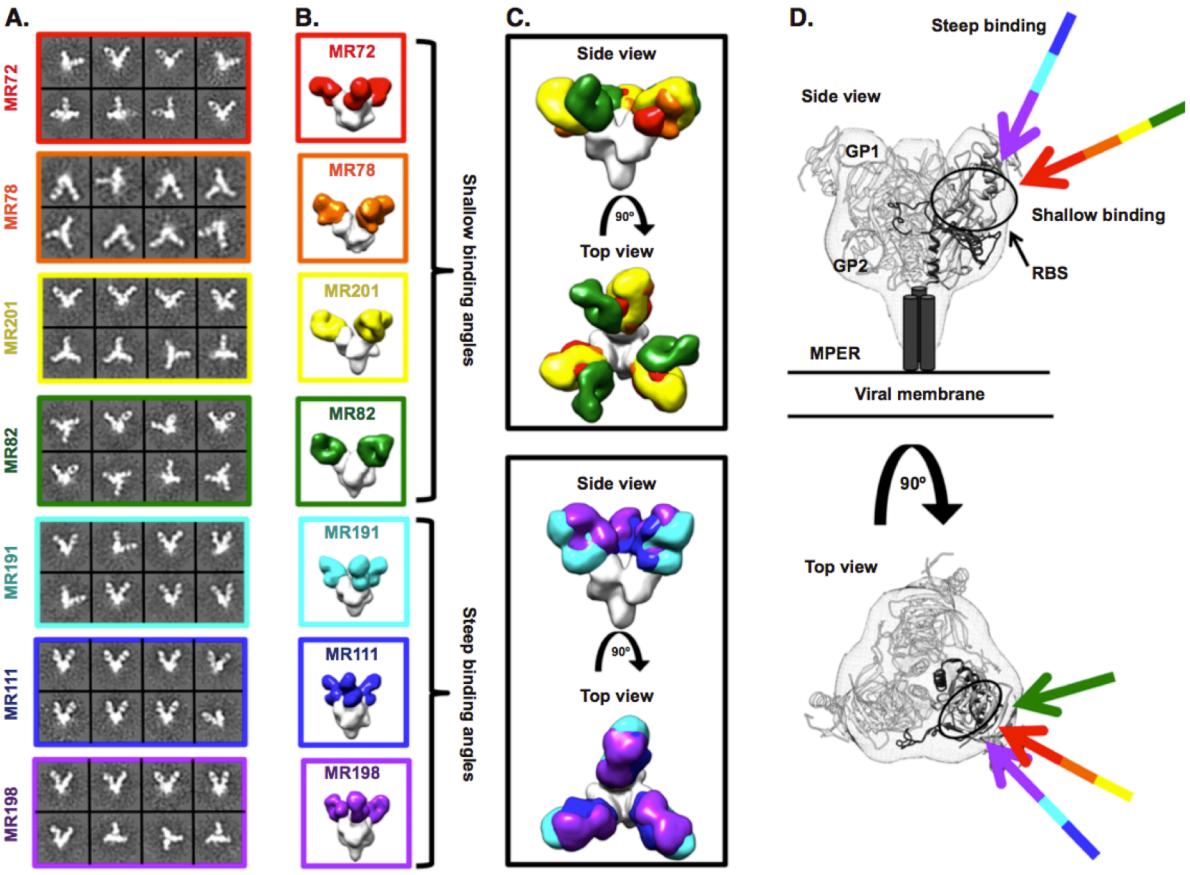

Figure 13. Neutralizing mAbs from a human survivor of MARV bind to the receptor-binding site of GP
(A) Representative reference-free 2D class averages of the MARV GPΔMuc:MR Fab complexes.
(B) EM reconstructions of seven Fab fragments of neutralizing antibodies bound to MARV GPΔmuc (side views). All seven antibodies target a similar epitope on the top of GP.
(C) These antibodies can be subdivided based on their angles of approach: (1) those that bind toward the top and side of GP1 at a shallow angle relative to the central 3-fold axis (MR72 in red, MR78 in orange, MR201 in yellow, or MR82 in green) and (2) those that bind at a steeper angle toward the top of GP1 (MR191 in cyan, MR111 in blue, or MR198 in purple).
(D) The crystal structure of EBOV GPΔmuc (GP1 in white and GP2 in dark gray) is modeled into the MARV GP density (mesh), and the angles of approach of the neutralizing antibodies are indicated with arrows, colored as in (B). The footprint of the antibodies is indicated by a black circle targeting residues in the putative receptor-binding site (RBS) through a variety of approach angles.

all seven nAbs bind at the top of the GP in or near the NPC1 protein receptor-binding site (**Figure 13A,B**). The binding pattern of these Abs could be divided further into two major groups based on their relative angle of approach to the GP head domain. MAbs MR72, MR78, MR201 and MR82 bound toward the top and side of GP1 at a shallow angle relative to the central three-fold axis, while mAbs MR191, MR111 and MR198 bound at a steeper angle toward the top of GP1 (**Figure 13C,D**).

Antibody neutralization escape mutant viruses

As an additional strategy to define residues on MARV GP involved in binding to nAbs, we generated VSV/GP-Uganda variant viruses that escaped neutralization, and then we determined the sequence of the GP of those mAb escape viruses. Vero E6 cells were inoculated with VSV/GP-Uganda in the presence of MR72 or MR78 nAbs. Two escape mutant viruses were isolated: virus variant VSV/GP-72.5 contained three missense mutations in the MARV GP gene (N129S in the putative NPC1 receptor-binding site, S220P in the glycan cap and P455L in the mucin-like domain) and virus variant VSV/GP-78.1 possessed missense mutation C226Y in the glycan cap (**Figure 14A**). Consistent with the EM data, six of seven nAbs tested displayed a higher level of neutralization activity against the wild-type VSV/GP-Uganda than to the VSV/GP-72.5 or VSV/GP-78.1 escape mutant viruses, suggesting these nAbs recognize MARV GP in a similar fashion (**Figure 14B**). MAb MR198 exhibited equal neutralization potency against wild-type VSV/GP-Uganda or the two escape mutant viruses (**Figure 14B**). As all nAbs segregated into one competition group (**Figure 11**), bound the MARV GP at the NPC1 receptor-binding site (**Figure 13**), and displayed a similar profile of neutralization of escape mutant viruses (**Figure 14**), I proposed that blocking of MARV GP binding to NPC1 is the principal mechanism of MARV neutralization by these naturally-occurring human Abs.

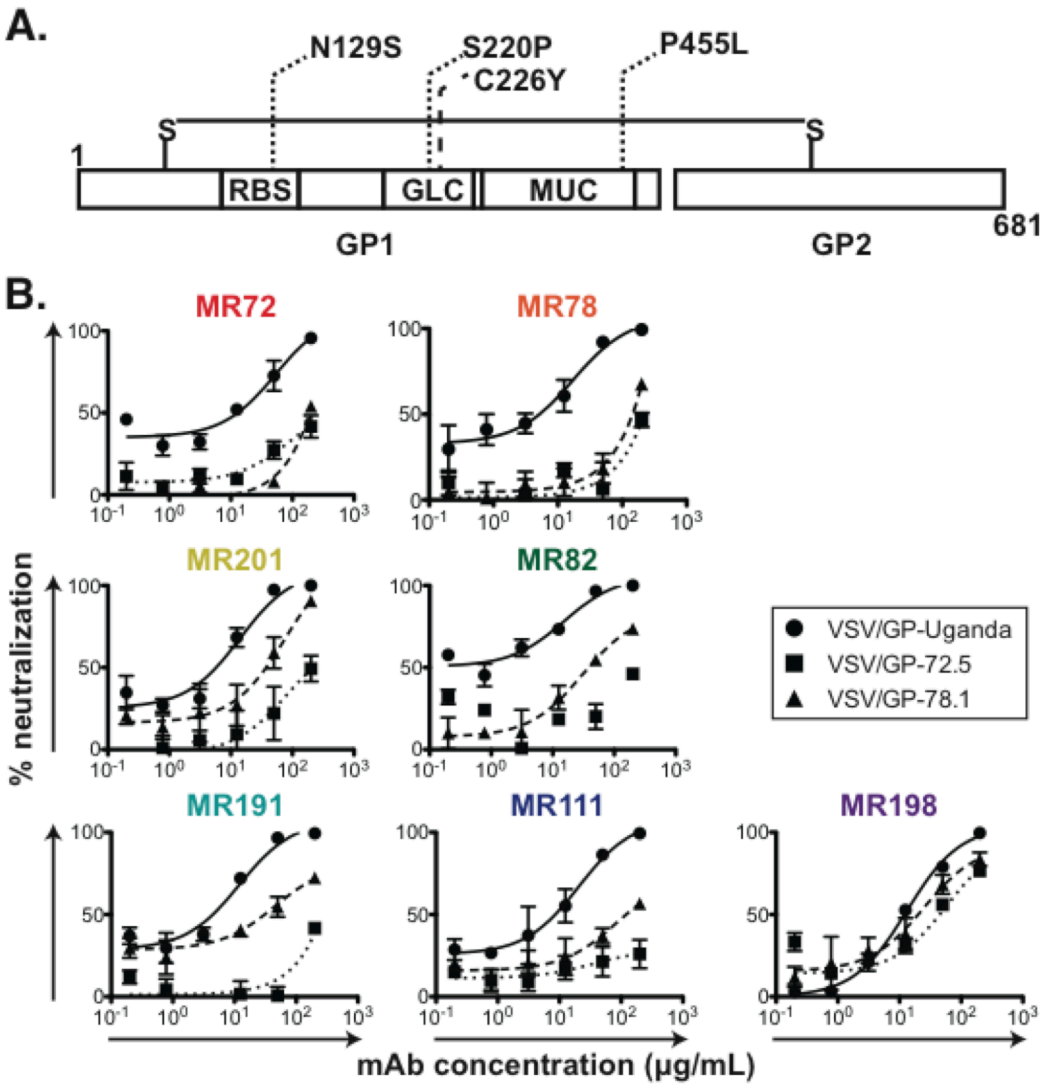

Figure 14. Generation of escape mutants for MARV neutralizing antibodies. (A) VSV-MARV-72.5 (dotted lines) or VSV-MARV-78.1 (dashed line) escape mutations mapped onto the domain schematic of MARV GP. RBS = Receptor-binding site; GLC = glycan cap; MUC = mucin-like domain. (B) Neutralization activity of antibodies from Binding Group 3B against wild-type VSV/GP-Uganda (circles, straight curves), VSV/GP-72.5 (squares, dotted curves) or VSV/GP-78.1 (triangles, dashed curves) escape mutant viruses.

Cross-reactive binding of MARV antibodies with EBOV GP

It is surprising that human MARV nAbs recognize the putative NPC1 protein receptor-binding site on GP, since previous studies suggested that the NPC1 protein receptor-binding

site on EBOV GP may be obscured from Ab binding by the presence of the highly glycosylated glycan cap and mucin-like domain (Lee et al., 2008). To determine whether the MARV nAbs we isolated also could bind in a cross-reactive manner to the EBOV GP receptor-binding site, I performed ELISA binding assays using three recombinant forms of MARV and EBOV GPs: full-length GP ectodomain containing the glycan cap and mucin-like domain (designated MARV or EBOV GP), ectodomains lacking residues 257-425 (MARV) or 314-462 (EBOV) of the mucin-like domain (designated MARV or EBOV GPΔmuc) and cleaved GP ectodomains enzymatically treated to remove the mucin-like domain and glycan cap (designated MARV or EBOV GPcl). Three of the MARV nAbs, designated MR78, MR111 and MR191, recognized the EBOV GPcl that lacked the glycan cap and mucin-like domain (**Figure 15A**). Remarkably, the MARV nAb MR72 bound all three forms of both EBOV and MARV GPs with similar EC_{50} and E_{max} values, indicating that its epitope, and the EBOV receptor-binding site which it likely overlaps, might be partially accessible for Ab binding even in the full-length form (**Figure 15A**). We tested the breadth of neutralization of MARV nAbs for filoviruses using a panel of different MARV and EBOV isolates. While multiple MARV Abs displayed neutralizing activity towards different MARV strains, MARV nAbs did not exhibit detectable neutralization activity against EBOV or VSV/EBOV (**Figure 15B**). Structural analysis of MARV and EBOV GP revealed that the glycan cap and mucin-like domain likely obscure the receptor-binding domain in EBOV but not MARV (Hashiguchi T. *et al*., 2015).

In vivo testing of Marburg virus antibodies

In collaboration with Alexander Bukreyev's group, we tested the *in vivo* protective activity of the mAbs in a murine model using mouse-adapted MARV strain Ci67 (Warfield et al., 2007; Warfield et al., 2009). Inoculation of mice with MARV Ci67 causes clinical disease, and in a proportion of animals causes lethal disease, although typically less than 100%

A. Binding (µg/mL)

mAb	MARV			EBOV		
	GP	GPΔmuc	GPcl	GP	GPΔmuc	GPcl
MR65	8.3	7.5	5.0	>	>	>
MR72	3.0	4.7	0.8	6.1	2.1	<0.1
MR78	1.4	2.3	1.1	>	>	107.4
MR82	1.0	1.5	0.5	>	>	>
MR103	8.8	14.2	4.8	>	>	>
MR111	2.5	4.3	1.5	>	>	21.5
MR144	8.1	8.0	3.3	>	>	>
MR186	1.3	0.9	0.5	>	>	>
MR191	2.5	5.1	1.4	>	>	<0.1
MR198	1.4	1.4	0.8	>	>	>
MR201	1.5	1.9	0.5	>	>	>
MR208	5.6	7.3	2.8	>	>	>
MR209	4.0	5.4	2.0	>	>	>
MR213	2.8	3.6	1.1	>	>	>
MR229	1.8	2.9	1.2	>	>	>
MR232	2.0	1.3	0.5	>	>	>
MR238	6.8	11.7	4.9	>	>	>
MR241	2.2	4.0	1.2	>	>	>

B. Neutralization (µg/mL)

mAb	MARV						EBOV	
	VSV/GP-Musoke	VSV/GP-Uganda	MARV-Musoke	MARV-Uganda	MARV-Angola	MARV-Ravn	VSV/GP-EBOV	EBOV
MR65	31.0	224	>	>	214	>	>	>
MR72	3.6	13.4	>	601	>	368	>	>
MR78	3.8	4.5	>	93	>	286	>	>
MR82	1.8	7.4	234	288	184	185	>	>
MR103	16.5	27.5	>	291	>	>	>	>
MR111	12.2	7.9	370	414	>	444	>	>
MR144	43.1	37.3	900	>	>	354	>	>
MR186	1.5	1.5	24	>	97	64	>	>
MR191	5.5	6.2	441	>	413	>	>	>
MR198	2.7	11.6	290	206	128	30	>	>
MR201	6.6	8.0	343	572	358	832	>	>
MR208	13.8	54.9	896	>	>	106	>	>
MR209	4.2	12.2	577	402	>	93	>	>
MR213	7.6	9.7	>	305	207	121	>	>
MR229	5.1	7.3	103	215	110	59	>	>
MR232	3.9	4.0	>	114	103	127	>	>
MR238	11.9	10.2	264	>	416	>	>	>
MR241	2.7	11.9	376	>	162	>	>	>

Figure 15. Breadth of binding or neutralization of human MARV-specific mAbs for diverse filoviruses. (A) A heat map showing the binding in ELISA of neutralizing mAbs from Binding Group 3B to the MARV and EBOV GPs. EC50 value for each antigen-mAb combination is shown, with dark red shading indicating lower EC50 values and orange or yellow shading indicating intermediate or higher EC50 values. EC50 values greater than 1,000 µg/mL are indicated by >. (B) A heat map showing the neutralization breadth of mAbs from Binding Group 3B. The IC50 value for each virus-mAb combination is shown, with dark red shading indicating increased potency and orange or yellow shading indicating intermediate or low potency. IC50 values greater than 1,000 µg/mL are indicated by >.

lethality in mice (Warren et al., 2014). We selected four mAbs among those with the lowest *in vitro* neutralization IC_{50} values: MR72, MR82, MR213, and MR232. The IC_{50} values in neutralization assays with MARV Uganda or mouse-adapted MARV strain Ci67 were comparable (within two-fold). Seven week-old BALB/c mice were injected with 100 µg of antibody by the intraperitoneal route and challenged with 1,000 PFU of Ci67. Twenty four hours later, antibody treatment was repeated. By day 6, all five control mice developed progressive loss of weight and symptoms of the disease, including dyspnea, recumbency, and unresponsiveness, and on days 8 and 9, two animals were found dead and one animal was found moribund and euthanized. The remaining two animals demonstrated recovery by day 11. In contrast, all animals treated with four antibodies survived and did not display elevation of disease score, with the exception of two animals treated with MR72, which showed a transient marginal loss of weight and increase in disease score on days 6-9, which did not exceed 1 (**Figure 16**). The observed level of protection was remarkable given the relatively modest *in vitro* neutralizing potency of the antibodies.

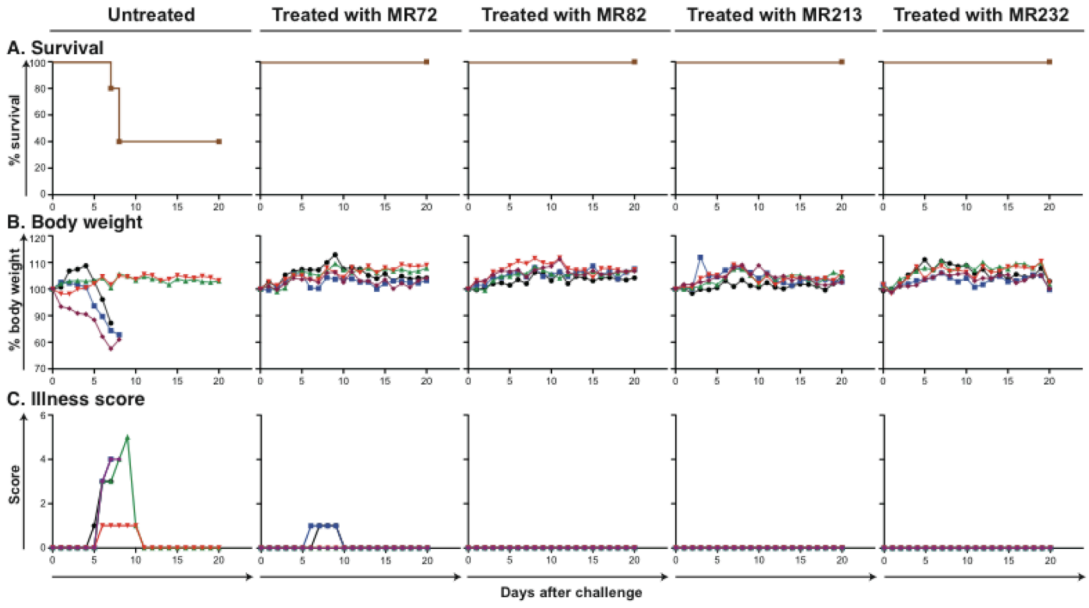

Figure 16. Survival and clinical overview of mice treated with MARV mAbs.
Groups of mice at 5 animals per group were injected with individual mAbs by the intraperitoneal route twice: 1 h prior and 24 h after MARV challenge at 100 µg per treatment. Untreated animals served as controls. (A) Kaplan–Meier survival curves. (B) Body weight (C) Illness score

Discussion

There is an obvious urgent need for prophylactic and therapeutic interventions for filovirus infections given the recurrence of MARV outbreaks including in October 2014 in Uganda and a massive outbreak of EBOV in West Africa in 2013-2015. There is very little information about the structural determinants of neutralization on which to base the rational selection of antibodies, and for MARV there have been no reported human nAbs.

This study reveals that naturally occurring human MARV nAbs isolated from the B cells of a recovered donor principally target the MARV NPC1 protein receptor-binding site, suggesting that a major mechanism of MARV neutralization is inhibition of binding to receptor. Remarkably, some of the isolated antibodies also bound to the EBOV GP. This mechanism of MARV neutralization was unexpected, because previous studies with EBOV showed that the putative receptor-binding domain on GP is obscured on the surface of virions by the presence of the glycan cap and mucin-like domain, only becoming exposed following cleavage by cathepsins in the endosome. These studies suggest that the configuration of the MARV GP differs significantly from that of EBOV GP because the receptor-binding domain must be accessible for immune recognition on MARV GP. Indeed, determination of the structure of the MARV GP and structural analysis of the interaction of mAb MR78 with MARV and EBOV GP molecules shows this to be the case (Hashiguchi *et al.,* 2015).

The information obtained from these studies can be used to inform development of new therapeutics and structure-based vaccine designs against filoviruses. Furthermore, as these nAbs are fully human and exhibit inhibitory activity, they might be useful as a component of a prophylactic or therapeutic approach for filovirus infection and disease. The

challenge studies using mice here show clear evidence of *in vivo* activity and suggest additional preclinical studies in other species such as guinea pigs and macaques are warranted. Their ability to bind a broad range of MARV isolates indicates that they may offer detection of or efficacy against new viral strains yet to emerge. Although some of these mAbs bind to certain forms of EBOV GP, these antibodies are not likely to be effective against natural Ebola infection because the EBOV receptor-binding site is obscured on the viral surface. However, such mAbs might neutralize EBOV if they could be delivered to the endosome where the EBOV receptor-binding site is exposed following GP cleavage.

Material and Methods

Donor

The donor was an otherwise healthy adult woman who contracted Marburg virus (MARV) infection in 2008 following exposure to fruit bats in the Python Cave in Queen Elizabeth National Park, Uganda. The donor's clinical course was documented previously (CDC, 2009). Peripheral blood from the donor was obtained in 2012, four years after the illness, following informed consent. The study was approved by the Vanderbilt University Institutional Review Board.

Viruses

MARV strain 200702854 Uganda (MARV-Uganda) was isolated originally from a subject designated "Patient A" during the outbreak in Uganda in 2007 (CDC, 2009; Towner et al., 2009) and underwent 4 passages in Vero E6 cells. MARV strain Musoke (MARV-Musoke) was isolated during the outbreak in Kenya in 1980 (Smith et al., 1982) and passaged 5 times in Vero E6 cells. MARV strain 200501379 Angola (MARV-Angola) was isolated during the outbreak in Angola in 2005 (Towner et al., 2006) and passaged 3 times

in Vero E6 cells. MARV Ravn virus (Ravn) was isolated from a patient in 1987 in Kenya (Johnson et al., 1996) and passaged 4 times in Vero E6 cells. All strains of MARV were obtained originally from the Special Pathogens Branch, U.S. Centers for Disease Control (CDC) and deposited at the World Reference Center of Emerging Viruses and Arboviruses (WRCEVA) housed at UTMB. The recombinant Ebola Zaire strain Mayinga (EBOV) expressing eGFP was generated in our laboratory by reverse genetics (Lubaki et al., 2013; Towner et al., 2005) from plasmids provided by the Special Pathogens Branch at CDC and passaged 3 times in Vero E6 cells. For analysis of antibody binding by ELISA, viruses were gamma-irradiated with the dose of 5 x 10^6 rad. The recombinant VSV in which the VSV GP protein was replaced with that of MARV strain Musoke (VSV/GP-Musoke) or EBOV strain Mayinga (Garbutt et al., 2004) were provided by Dr. Thomas Geisbert (UTMB) and Dr. Heinz Feldmann (NIH), respectively; a similar virus with GP from MARV (strain 200702854 Uganda) was constructed as described below. All work with EBOV and MARV was performed within the Galveston National Laboratory BSL-4 laboratories.

We used a mouse-adapted strain of MARV for testing the effect of mAbs *in vivo.* The mouse-adapted Ci67 strain of Marburg virus (Warfield et al., 2007) was provided by Dr. Sina Bavari (U.S. Army Medical Research Institute of Infectious Diseases, Fort Detrick, Maryland) and amplified by a single passage in Vero-E6 cells.

Generation of a chimeric strain of VSV in which VSV G protein was replaced with the GP protein of MARV strain Uganda (VSV/GP-Uganda).

The plasmid pVSV-XN2 carrying cDNA of the full-length VSV anti-genome sequence and the support plasmids pBS-N, pBS-L and pBS-P encoding the internal VSV proteins under control of the T7 promoter were kindly provided by Dr. John Rose (Yale University). The plasmid pC-T7, encoding the T7 polymerase, was kindly provided by Dr. Yoshihiro Kawaoka (University of Wisconsin). For generation of the VSV/GP-Uganda construct, Vero

E6 cell monolayers were inoculated with MARV strain 200702854 and total cellular RNA was isolated and reverse-transcribed. MARV GP ORF was PCR-amplified from cDNA using forward primer 5´-CATGTACGACGCGT*CAACATGAGGACTA*-3´ and reverse primer 5´-TCTAGCAGCTCGAG*CTATCCAATATATTTAGTAAAGATACGACAA*-3´ (underlined are MluI and XhoI endonuclease sites, respectively; italicized are the start and the end of MARV GP ORF – direct and complementary sequences, respectively). To replace VSV G with MARV GP, the resulting PCR-product was cloned into pVSV-XN2 using the unique MluI and XhoI endonuclease sites located between the VSV G gene-start and gene-end signals and flanking its ORF, resulting in the plasmid pVSV/GP-Uganda. To recover the recombinant virus, 1 x 10^6 BSR-T7 cells, kindly provided by Dr. Ursula Buchholz (U.S. National Institute of Allergy and Infectious Diseases), were transfected with the following plasmids: pVSV/GP-Uganda, 5 µg; pBS-N, 1.5 µg; pBS-P, 2.5 µg; pBS-L, 1 µg; pC-T7, 5 µg. After 48 hours, transfected BSR-T7 cells were collected with a cell scraper and transferred, along with the supernates, to Vero E6 cell monolayers for amplification of the recovered VSV/GP-Uganda.

Generation of human hybridomas secreting monoclonal antibodies (mAbs)

Peripheral blood mononuclear cells (PBMCs) from the donor were isolated with Ficoll-Histopaque by density gradient centrifugation. The cells were cryopreserved immediately and stored in the vapor phase of liquid nitrogen until use. Previously cryopreserved samples were thawed, and 10 million PBMCs were plated into 384-well plates (Nunc #164688) using: 17 mL of cell culture medium (ClonaCell-HY Medium A, Stemcell Technologies #03801), 8 µg/mL of the TLR agonist CpG (phosphorothioate-modified oligodeoxynucleotide ZOEZOEZZZZZOEEZOEZZZT, Invitrogen), 3 µg/mL Chk2 inhibitor (Sigma #C3742), 1 µg/mL cyclosporine A (Sigma #C1832) and 4.5 mL of clarified supernate from cultures of B95.8 cells (ATCC VR-1492) containing Epstein-Barr virus (EBV). After 7 days, cells from each 384-well culture plate were expanded into four 96-well culture plates (Falcon #353072)

using cell culture medium containing 8 μg/mL CpG, 3 μg/mL Chk2i and 10 million irradiated heterologous human PBMCs (Nashville Red Cross) and incubated for an additional four days. Plates were screened for MARV antigen-specific antibody-secreting cell lines using enzyme-linked immunosorbent assays (ELISAs). Cells from wells with supernates reacting in a MARV antigen ELISA were fused with HMMA2.5 myeloma cells using an established electrofusion technique (Yu et al., 2008). After fusion, hybridomas were resuspended in medium containing 100 μM hypoxanthine, 0.4 μM aminopterin, 16 μM thymidine (HAT Media Supplement, Sigma #HO262) and 7 μg/mL ouabain (Sigma #O3125) and incubated for 18 days before screening hybridomas for antibody production by ELISA.

Human mAb and Fab production and purification

After fusion with HMMA2.5 myeloma cells, hybridomas producing MARV-specific antibodies were cloned biologically by two rounds of limiting dilution and by single-cell fluorescence-activated cell sorting. After cloning, hybridomas were expanded in post-fusion medium (ClonaCell-HY Medium E, STEMCELL Technologies #03805) until 50% confluent in 75-cm^2 flasks (Corning #430641). For antibody production, cells from one 75-cm^2 flask were collected with a cell scraper and expanded to four 225-cm^2 flasks (Corning #431082) in serum-free medium (Hybridoma-SFM, Gibco #12045-076). After 21 days, supernates were clarified by centrifugation and sterile filtered using 0.2-μm pore size filter devices. HiTrap Protein G or HiTrap MabSelectSure columns (GE Healthcare Life Sciences #17040501 and #11003494 respectively) were used to purify antibodies from filtered supernates. Fab fragments were generated by papain digestion (Pierce Fab Preparation Kit, Thermo Scientific #44985) and purified by chromatography using a two-column system where the first column contained protein G resin (GE Healthcare Life Sciences #29048581) and the second column contained either anti-kappa or anti-lambda antibody light chain resins (GE Healthcare Life Sciences #17545811 and #17548211 respectively).

Expression and purification of MARV and EBOV GPs

Angola strain MARV GP ectodomains, containing the mucin-like domain (MARV GP) or lacking residues 257-425 of the mucin-like domain (MARV GPΔmuc), were used to screen supernates of transformed B cells and human hybridomas separately. Recombinant proteins for Ravn strain cleaved GP, EBOV Mayinga strain GP, EBOV Mayinga strain GPΔmuc and EBOV Mayinga strain cleaved GP were designed and expressed similarly. Large-scale production of recombinant GP or GPΔmuc was performed by transfection of *Drosophila* Schneider 2 (S2) cells with modified pMTpuro vectors, followed by stable selection of transfected cells with 6 µg/mL puromycin. Secreted GP ectodomain expression was induced with 0.5 mM $CuSO_4$ for 4 days. Proteins were engineered with a modified double strep tag at the C terminus (enterokinase cleavage site followed by a strep tag/linker/strep tag) to facilitate purification using Strep-Tactin resin (Qiagen #2-1201). Proteins were purified further by Superdex 200 size exclusion chromatography in 10 mM Tris, 150 mM NaCl, pH 7.5 (1X TBS).

Lysates of MARV-infected cells

Lysates were prepared as previously described (Ksiazek et al., 1999). Briefly, Vero E6 cell monolayers in 850 cm^2 roller bottles were inoculated with approximately 10^6 PFU MARV or EBOV and incubated at 37 °C until partial destruction of monolayer occurred (approximately 9-10 days). Cell monolayers were detached using 3 mm glass beads, and cell suspensions were centrifuged at 16,000 x *g* for 10 min at 4 °C. Supernates were discarded, cell pellets were resuspended in 10X excess of borate buffer saline (10 mM $Na_2B_4O_7$, 150 mM NaCl, pH 9.0), and centrifuged at 16,000 x *g* for 10 min at 4 °C. Supernates were discarded, cell pellets were resuspended in cold 1% Triton X-100 (Fisher Scientific) in borate buffer saline, vortexed and gamma-irradiated on dry ice at 5 x 10^6 rad.

The lysates were sonicated with a 600 W Tekmar Sonic Disruptor TM600 (Tekmar) using a cuphorn sonicator at maximum power setting and 50% duty cycle for 10 min, centrifuged at 16,000 x *g* and the supernates aliquoted.

Screening ELISA

ELISA plates were coated with lysates of MARV infected cells (diluted 1:1,000 in Dulbecco phosphate buffered saline, DPBS) or recombinant MARV GP or MARV GPΔmuc proteins (20 µg in 10 mL DPBS per plate) and incubated at 4 °C overnight. Plates were blocked with 100 µL of blocking solution/well for 1 h. Blocking solution consisted of 10 g powdered milk, 10 mL of goat serum, 100 mL of 10X DPBS, and 0.5 mL of Tween-20 mixed to a 1 L final volume with distilled water. The presence of antibodies bound to the GP was determined using goat anti-human IgG horseradish peroxidase conjugated secondary antibodies (Southern Biotech #2040-05, 1:4,000 dilution) and 1-Step Ultra TMB-ELISA substrate (Thermo Scientific #34029), with optical density read at 450 nM after stopping the reaction with 1M HCl.

Half maximal effective concentration (EC_{50}) binding analysis

MARV or EBOV GPs, MARV or EBOV GPΔmuc, or Ravn or EBOV cathepsin-cleaved GPs were coated onto 384-well plates (Thermo Scientific Nunc #265203) in DPBS at 2 µg/mL overnight, then antigen was removed and plates were blocked with blocking solution made as above. Antibodies were applied to the plates at a concentration range of 1.5 µg/mL to 270 ng/mL (Binding Groups #1, #2 and 3A) and 0.1 µg/mL to 10 ng/mL (Binding Group #3B) using three-fold serial dilutions. The presence of antibodies bound to the GP was determined using goat anti-human IgG alkaline phosphatase conjugate (Meridian Life Science #W99008A, 1:4,000 dilution) and p-nitrophenol phosphate substrate tablets (Sigma #S0942), with optical density read at 405 nM after 120 minutes. A non-linear regression

analysis was performed on the resulting curves using Prism version 5 (GraphPad) to calculate EC_{50} values.

MARV and EBOV neutralization experiments

Dilutions of mAbs in triplicate were mixed with 150 PFU of MARV or EBOV expressing eGFP in MEM containing 10% FBS (HyClone), 50 µg/mL gentamicin (Cellgro #30-005-CR) with or without 5% guinea pig complement (MP Biomedicals #642836) in a total volume of 0.1 mL, and incubated for 1 hour at 37 °C for virus neutralization. Following neutralization, virus-antibody mixtures were placed on monolayers of Vero E6 cells in 24-well plates, incubated for 1 hour at 37 °C for virus adsorption, and overlayed with MEM containing 2% FBS and 0.8% methylcellulose (Sigma-Aldrich #M0512-1KG). After incubation for 5 days, medium was removed, cells were fixed with 10% formalin (Fisher Scientific #245-684), plates were sealed in plastic bags and incubated for 24 hours at room temperature. Sealed plates were taken out of the BSL-4 laboratory according to approved SOPs, and monolayers were washed three times with phosphate buffered saline. Viral plaques were immunostained with the serum of rabbits that had been hyperimmunized with MARV, or with a mAb against EBOV, clone 15H10 (BEI Resources #NR-12184). Alternatively, following virus adsorption, monolayers were covered with MEM containing 10% FBS and 1.6% tragacanth (Sigma-Aldrich #G1128). After incubation for 14 days, medium was removed, cells were fixed with 10% formalin, plates were sealed in plastic bags, incubated for 24 hours at room temperature, and taken out of the BSL-4 laboratory as above. Fixed monolayers were stained with 10% formalin containing 0.25% crystal violet (Fisher Scientific #C581-100), and plaques were counted.

VSV-MARV and VSV-EBOV neutralization tests

Neutralization assays were performed in triplicate, as described above for MARV and EBOV. Following neutralization, virus-antibody mixtures were placed on monolayers of Vero E6 cells in duplicate, incubated for 1 hour at 37 °C for virus adsorption, and overlayed with MEM containing 2% FBS containing 0.9% methylcellulose. After incubation for 3 days, medium was removed, monolayers were fixed and stained with 10% formalin containing 0.25% crystal violet, and plaques were counted.

Generation and sequencing of VSV/GP-Uganda escape mutants

Vero E6 cell monolayers with two-fold dilutions of mAbs (12.5 – 200 µg/mL) added to the medium were inoculated with 200 PFU of recombinant VSV/GP-Uganda and incubated at 37 °C for 2-4 days. To determine which samples contained live virus, supernates were collected, virus was titrated in Vero E6 cell monolayers under methylcellulose overlay, monolayers were incubated at 37 °C for 3-4 days, and plaques were counted. Supernates with the highest concentrations of mAbs, which were found to contain live virus by plaque titration, were incubated in presence of serially diluted mAbs followed by titration of virus as above. The procedure was performed a total of three times. Escape mutant viruses harvested after the third passage were cloned biologically by plaque purification. For biological cloning, Vero E6 cell monolayers in 24-well plates were inoculated with dilutions of the escape mutant viruses in the presence of the corresponding mAbs (200 µg/mL of MR72 or 100 µg/mL of MR78) and covered with 0.7% low melting temperature SeaPlaque agarose (Lonza #50100). Monolayers were incubated at 37 °C for 6 days, plaques were visualized with 0.01% neutral red aqueous solution (Electron Microscopy Sciences), picked, resuspended in medium and transferred to Vero E6 cell monolayers in 24-well plates in presence of the corresponding mAbs (200 µg/mL of MR72 or 100 µg/mL of MR78) for virus propagation. In 2-5 days, based on the extent of CPE observed, virus was harvested, and

cells were dissolved in Trizol reagent (Life Technologies 315596018). Total cellular RNA was extracted and reverse-transcribed and amplified by PCR with the primers described above for generation of a chimeric strain of VSV. Two overlapping fragments covering MARV GP ORF were PCR-amplified from cDNA using forward primer 5´-CATGTACGACGCGTCAACATGAGGACTA-3´ and reverse primer 5´-ACTAAGCCCTGCTGCCAGGT-3´ or forward primer 5´-ACAACAATGTACCGAGGCAA-3´ and reverse primer 5´-TCTAGCAGCTCGAGCTATCCAATATATTTAGTAAAGATACGACAA-3´, and the nucleotide sequences of the GP ORFs were determined using standard procedures.

Analysis of growth kinetics of VSV/GP-Uganda escape mutant viruses

Vero E6 cell monolayers in 24-well plates were inoculated in triplicate with VSV/GP-Uganda escape mutants or non-mutated virus at an MOI of 0.00025 PFU/cell in the presence of varying concentrations of the corresponding mAbs. Aliquots of medium were collected every 12 hours and frozen for titration at a later time. Titration of virus in aliquots was performed as above, without adding antibodies to the culture medium.

Biolayer interferometry competition binding assay

Biotinylated GP or GPΔmuc (EZ-link® Micro NHS-PEG_4-Biotinylation Kit, Thermo Scientific #21955) (1 µg/mL) was immobilized onto streptavidin-coated biosensor tips (ForteBio #18-5019) for 2 minutes. After measuring the baseline signal in kinetics buffer (KB: 1X PBS, 0.01% BSA and 0.002% Tween 20) for two minutes, biosensor tips were immersed into the wells containing primary antibody at a concentration of 100 µg/mL for 10 minutes. Biosensors then were immersed into wells containing competing mAbs at a concentration of 100 µg/mL for 5 minutes. The percent binding of the competing mAb in the presence of the first mAb was determined by comparing the maximal signal of competing

mAb applied after the first mAb complex to the maximal signal of competing mAb alone. MAbs were judged to compete for binding to the same site if maximum binding of the competing mAb was reduced to <30% of its un-competed binding. MAbs were considered non-competing if maximum binding of the competing mAb was >70% of its un-competed binding. A level of 30-70% of its un-competed binding was considered intermediate competition.

Sequence analysis of antibody variable region genes

Total cellular RNA was extracted from clonal hybridomas that produced MARV antibodies, and RT-PCR reaction was performed using mixtures of primers designed to amplify all heavy chain or light chain antibody variable regions. The generated PCR products were purified and cloned into the pJet 1.2 plasmid vector (Thermo Scientific, #K1231) for sequence analysis. The nucleotide sequences of plasmid DNAs were determined using an ABI3700 automated DNA sequencer. Heavy chain or light chain antibody variable region sequences were analyzed using the IMGT/V-Quest program (Brochet et al., 2008; Giudicelli et al., 2011). The analysis involved the identification of germline genes that were used for antibody production, location of complementary determining regions (CDRs) and framework regions (FRs) as well as the number and location of somatic mutations that occurred during affinity maturation.

Statistical analysis

EC_{50} values for neutralization were determined by finding the concentration of mAb at which a 50% reduction in plaque counts occurred after incubation of virus with neutralizing antibody. A logistic curve was fit to the data using the count as the outcome and the log-concentration as the predictor variable. The results of the model then were transformed back to the concentration scale. Results are presented as the concentration at the dilution

that achieve a 50% reduction from challenge control with accompanying 95% confidence intervals. Each antibody was treated as a distinct analysis in a Bayesian non-linear regression model.

Sample preparation for EM studies

A Ravn strain MARV GP mucin-deleted construct (GPΔmuc) was produced by stable cell line expression in *Drosophila* S2 cells, as described above. Human Fab proteins for MARV-specific antibodies were generated as described above. Fabs were added in molar excess to GPΔmuc and allowed to incubate overnight at 4 °C. Complexes then were purified by Superdex 200 size exclusion chromatography in TBS.

Electron microscopy and sample preparation

A 4 µL aliquot of each complex that had been diluted to a concentration of ~0.03 µg/mL with TBS buffer was placed for 15 seconds onto carbon-coated 400 Cu mesh grids that had been plasma cleaned for 20 s (Gatan), blotted off on the edge of the grid, then immediately stained for 30 s with 4 µL of 2% uranyl formate. The stain was blotted off on the edge of the grid and the grid was allowed to dry. Data were automatically collected with Leginon (Carragher et al., 2000; Potter et al., 1999; Suloway et al., 2005) using a FEI Tecnai F20 electron microscope operating at 120 keV with an electron dose of 30 $e^-/Å^2$ and a magnification of 52,000X that resulted in a pixel size of 2.65 Å at the specimen plane when collected with Tietz CMOS 4k x 4k CCD camera. Particle orientations appeared to be generally isotropic and images were acquired at a constant defocus value of -1.0 µm at 0° stage tilt.

Image processing of protein complexes

Particles were picked automatically using DoG Picker (*34*) and placed into a particle stack using the Appion software (Lander et al., 2009). Reference-free 2D class averages were generated with the Xmipp clustering 2D alignment software (van Heel et al., 1996) and sorted into an initial 300 classes. Non-GP particles were removed and the stack was further sub-classified into classes with ~100 particles per class in order to generate the final particle stack used for the reconstruction. Various numbers of class averages were chosen to create initial models using EMAN2 common lines software (Tang et al., 2007). A model that best matched its projected classes was then used for refinement against the raw particle stack, imposing C3 symmetry, and the reconstruction was generated with 10 rounds of refinement and increasingly smaller angular sampling rates with EMAN2 (Tang et al., 2007). All model fitting and manipulation was completed using UCSF Chimera (Pettersen et al., 2004).

In vivo testing. The animal protocol for testing of mAbs in mice was approved by the Institutional Animal Care and Use Committee of the University of Texas Medical Branch at Galveston. Seven-week-old BALB/c mice (Harlan) were placed in the ABSL-4 facility of the Galveston National Laboratory. Groups of mice at 5 animals per group were injected with individual mAbs by the intraperitoneal route twice: one h prior and 24 h after MARV challenge, using 100 μg per treatment. Untreated animals served as controls. For the challenge, mice were injected with 1,000 PFU of the mouse-adapted MARV strain Ci67 by the intraperitoneal route. Animals were weighed and monitored daily over the three-week period after challenge. Once animals were symptomatic, they were examined twice per day. The disease was scored using the following parameters: dyspnea (possible scores 0-5), recumbency (0-9), unresponsiveness (0-5), and bleeding/hemorrhage (0-5); the individual scores for each animal were summarized.

CHAPTER III

CROSS-REACTIVE AND POTENT NEUTRALIZING ANTIBODY RESPONSES IN HUMAN SURVIVORS OF EBOLAVIRUS INFECTION

> "The putative index patient was a 26-year-old woman from Kabango village, Kasitu subcounty, in Bundibugyo district. Hunting spears were found at her home, but hunting as a practice was denied."
>
> (Wamala et al., 2010)

Introduction

The ability of mAbs to bind conserved neutralizing epitopes present on the surface of highly variable viral proteins has been documented extensively for HIV (Burton et al., 2012), influenza viruses (Pappas et al., 2014), dengue virus (Rouvinski et al., 2015), paramyxoviruses (Corti et al., 2013), and alphaviruses (Fox et al., 2015). Despite similar requirements for virus entry into the cell (Misasi et al., 2012), GPs from BDBV, EBOV, and SUDV strains differ by over 30% at the amino acid level (Towner et al., 2008). This overall genetic divergence between species of genus *Ebolavirus* has hampered the development of ebolavirus cross-neutralizing Abs. The key components of multiple antibody cocktails developed over the last decade neutralize only viruses of species *Zaire ebolavirus*. A weakly neutralizing mAb c13C6 cross-reacts with SUDV GPs (Wilson et al., 2000), but it is unknown whether this mAb neutralizes SUDV. Cross-reactive antibodies in serum can be elicited during natural infection in humans or vaccination of animals. The serum of individuals who survived BDBV, EBOV, or SUDV infections contained ebolavirus cross-reactive IgG but not IgM (Macneil et al., 2011). Other studies demonstrated that mice immunized with a vaccine bearing the GP of EBOV generated cross-reactive polyclonal mAbs to other ebolaviruses such as BDBV and SUDV (Meyer et al., 2015; Ou et al., 2012). Four broadly reactive non-

neutralizing mAbs were isolated in mice after vaccinating animals with recombinant vesicular stomatitis virus (rVSV) expressing EBOV GP and then boosting initial immune response with the heterologous virus containing SUDV GP (Hernandez et al., 2015). The epitopes recognized by such cross-reactive mAbs are unknown.

In this chapter, I describe the isolation of a large panel of BDBV-specific and *Ebolavirus* cross-reactive mAbs from B cells of survivors of BDBV infection. The results show that a large proportion of mAbs with potent neutralizing activity against BDBV bind to the glycan cap and recognize diverse epitopes within this major antigenic site. We identified several glycan cap-specific mAbs that neutralized multiple *Ebolavirus* species and a cross-reactive mAb that completely protected guinea pigs from the lethal challenge with heterologous EBOV when used as monotherapy. Several of these naturally occurring antibodies exhibit the most potent protective capacity reported, and they possessed unprecedented cross-reactivity for multiple *Ebolavirus* species including SUDV for which neutralizing human mAbs have not been reported.

I acknowledge Alexander Bukreyev's group for performing neutralization, protection experiments as well as escape mutants generation, Andrew Ward's group for studying EBOV-specific mAbs by negative-stain single-particle EM, Erica Saphire's group for providing *Ebolavirus* GPs, and Ben Doranz team for performing epitope mapping of selected mAbs using saturation mutagenesis.

Isolation of Human MAbs

To generate human cell lines secreting human mAbs to BDBV, I transformed peripheral blood B cells from seven survivors of the 2007 Uganda BDBV outbreak with EBV. To determine the breadth of antibody response in survivors of ebolavirus infection, I

screened supernatants from EBV-transformed B cell lines for binding to GPs from diverse representatives of filovirus species: BDBV, EBOV, or MARV (**Figure 17**). I also used the same GP panel to screen supernatants from transformed B cell lines derived from a survivor of the 2014 EBOV outbreak (**Figure 17B**) or from a donor who survived MARV infection (**Figure 17**). I color-coded GP-reactive supernatants based on the cross-reactivity pattern: species-specific cell lines are highlighted in black; cross-reactive lines to 2 or 3 species are shown in yellow or blue, respectively (**Figure 17A-C**). While approximately half of GP-specific B cell lines obtained from BDBV survivors produced antibodies specific to BDBV GP, 24-50% of GP-reactive B cell culture supernatants also cross-reacted with EBOV GP (**Figure 17A, Table 3**). Similarly, 36% of GP-specific B cell lines obtained from the EBOV survivor cross-reacted with the heterologous BDBV GP (**Figure 17B, Table 3**). Despite the apparent presence of B cells encoding cross-reactive antibodies in survivors of BDBV or EBOV infections to GPs from heterologous *Ebolavirus* species, I detected a very limited cross-reactivity with GPs from MARV, which belongs to a different genus in the family *Filoviridae* (**Figure 17A, Table 3**). In line with this finding, 90% of GP-reactive B cell lines obtained from the MARV survivor reacted with autologous GP, and only 2% of antigen-specific B cell lines produced *Ebolavirus* cross-reactive Abs (**Figure 17C, Table 3**). The limited cross-reactivity of mAbs to GPs from *Ebolavirus* and *Marburgvirus* species likely is due in part to low sequence conservation between GPs from two genera (only 27% amino acid identity between BDBV and MARV GP) as well as differences in epitope availability caused by different positions of the mucin-like domains on the GP surface of *Ebolavirus* and *Marburgvirus* (Flyak et al., 2015; Fusco et al., 2015; Hashiguchi et al., 2015).

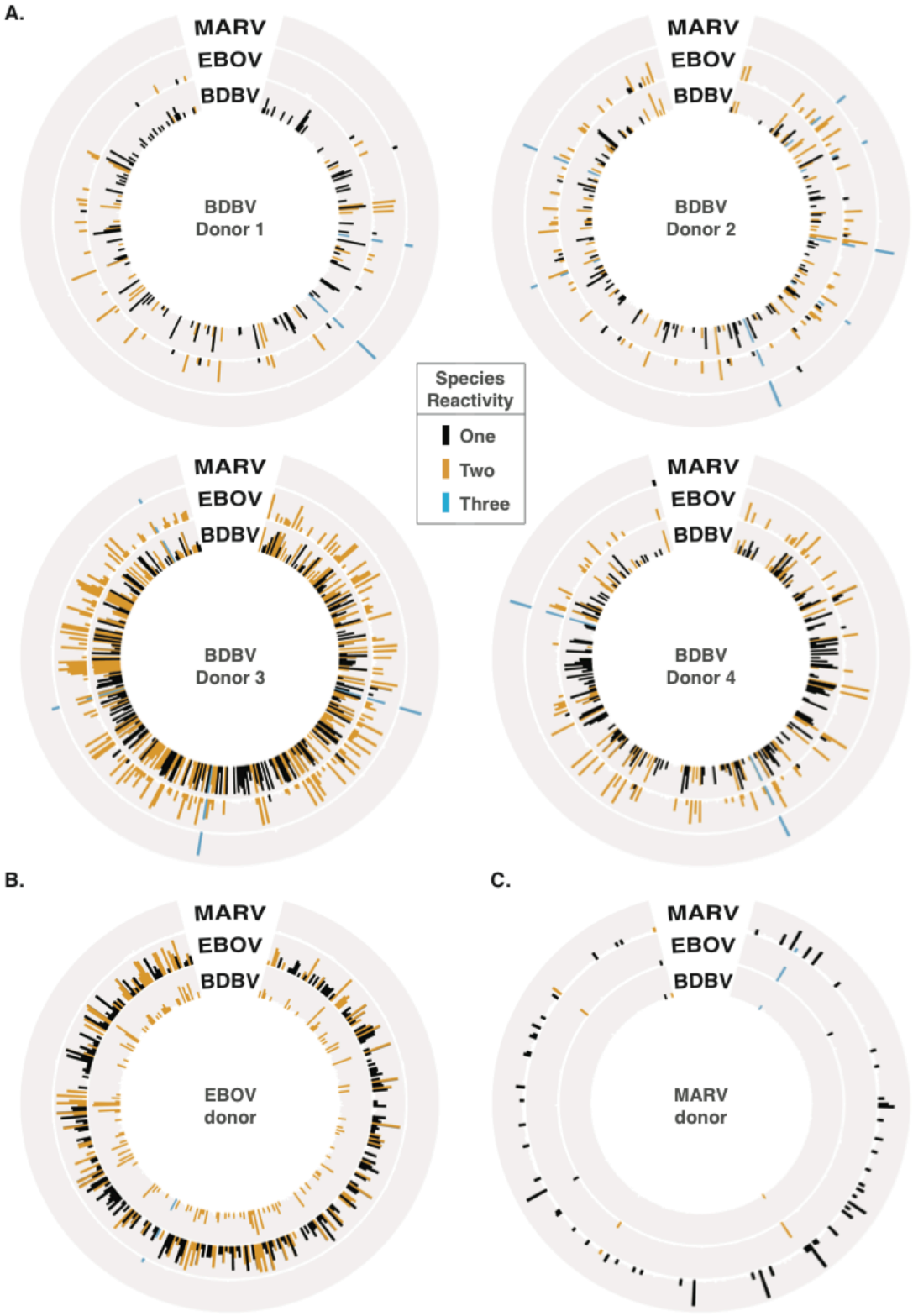

Figure 17. Cross-reactive B cell responses in filovirus immune donors. Supernatants from EBV-transformed PBMC samples isolated from survivors were screened in ELISA binding assays using BDBV, EBOV or MARV GPs (A-C). Results for four BDBV survivors (A), one EBOV survivor (B) or one MARV survivor (C) are shown. Height of the bars indicates OD_{405} nm values in ELISA binding to full-length extracellular domain of GP of the indicated virus species. Reactive supernates are color-coded based on the cross-reactivity pattern: species-specific cell lines are highlighted in black; cross-reactive lines to 2 or 3 species are shown in yellow or blue, respectively.

Binding and Neutralizing Activity of Human MAbs

I fused transformed cells from B cell lines producing BDBV GP-reactive Abs with myeloma cells and generated 90 cloned hybridomas secreting BDBV GP-reactive human mAbs. To determine the breadth of mAb binding, I screened the mAbs in ELISA binding assays using recombinant GPs from multiple filoviruses: BDBV, EBOV, SUDV, or MARV GPs. While 33 Abs recognized only the autologous BDBV GP (designated Groups 1A, 1B), 20 Abs recognized both BDBV and EBOV GPs (Groups 2A, B), and 37 Abs recognized GPs from BDBV, EBOV and SUDV (Groups 3A, B) (**Figure 18A, 19A**). The relative proportions of antibodies that recognize glycoproteins from 1, 2, or 3 *Ebolavirus* species did not correlate fully with the B cell line frequencies in the initial screen, which can be explained by our prioritization on recovery of a high number of cross-reactive mAbs. I was not able to isolate Abs that bind to the heterologous MARV GP (**Figure 18A**).

I further characterized the binding of species-specific or cross-reactive mAbs to recombinant GPs by performing a binding assay with the recombinant form of GP that is secreted from the cell to the extracellular space during natural infection (sGP, secreted GP) (Sanchez et al., 1996; Volchkov et al., 1995). While the *Ebolavirus* GP is a trimer, sGP forms dimers in which each protomer shares only the amino-terminal 295 amino acids with GP. The majority of mAbs recognized epitopes shared between BDBV GP and BDBV sGP

Subject	Total number of GP-specific lines	Reactivity of GP-specific B cell lines with diverse GPs (%)				
		BDBV-specific	BDBV/EBOV cross-reactive	EBOV-specific	BDBV/EBOV/MARV cross-reactive	MARV-specific
BDBV						
Donor 1	127	65.0	24.0	8.0	2.0	1.0
Donor 2	158	46.2	39.2	9.5	4.4	0.6
Donor 3	318	46.9	50.0	1.9	1.3	0
Donor 4	208	63.0	32.2	3.4	1.0	0.5
EBOV	281	0	36.3	63.3	0.4	0
MARV	64	1.6	1.6	4.8	1.6	90.3

Table 3. Percentages of lines secreting antibodies species-specific, or cross-reactive antibodies

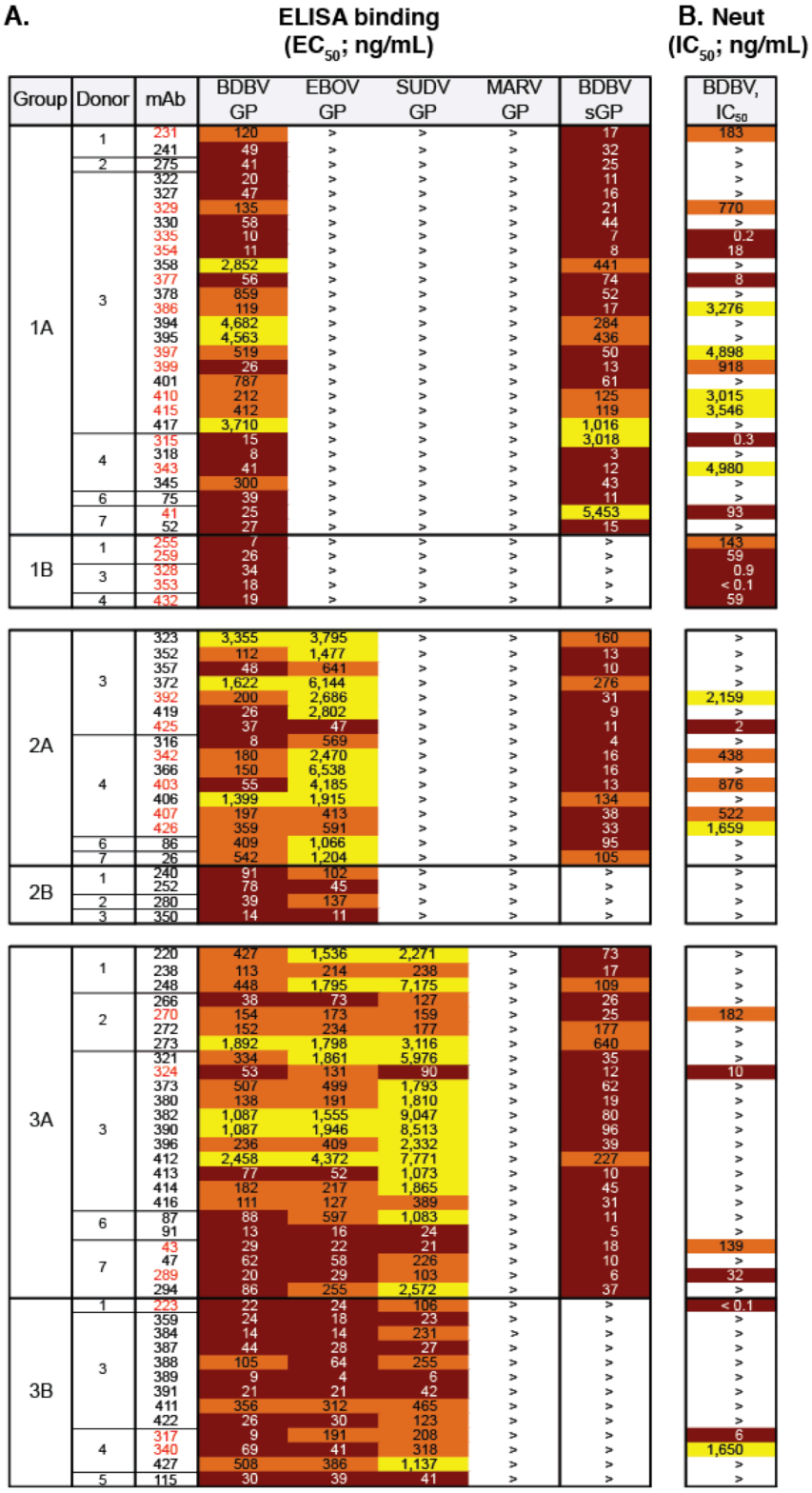

Figure 18. Cross-neutralizing antibodies from survivors of natural BDBV infection. (A) Heat map showing the binding of BDBV mAbs to a panel of filovirus GPs. The EC_{50} value for each GP-mAb combination is shown, with dark red, orange, yellow, or white shading indicating high, intermediate, low, or no detectable binding, respectively. EC_{50} values greater than 10,000 ng/mL are indicated by the > symbol. NAb names are highlighted in red. (B) Heat map showing the neutralization potency of BDBV GP-specific mAbs against BDBV. IC_{50} values greater than 10,000 ng/mL are indicated by the > symbol.

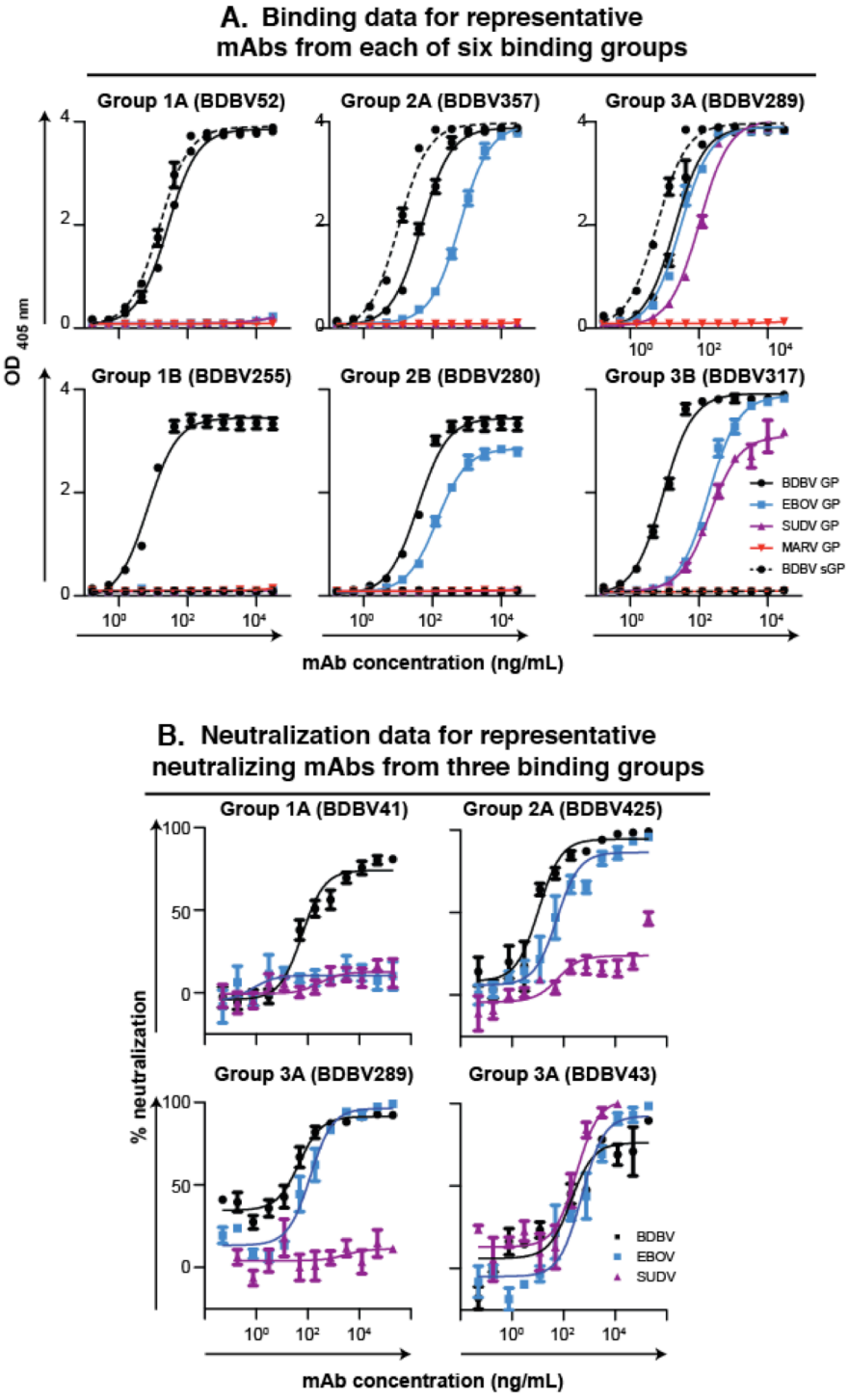

Figure 19. Binding and neutralizing activities of BDBV mAbs. (C) Binding of representative mAbs from six distinct binding groups to the filovirus GP. (D) Neutralization activity of representative neutralizing mAbs from three binding groups against BDBV, EBOV or SUDV. Error bars represent the SE of the experiment, performed in triplicate.

BDBV sGP in ELISA (designated Groups 1B, 2B, or 3B) (**Figure 18A, 19A**). Antibodies from Groups 1B, 2B, or 3B also bound the recombinant GP form that lacks highly glycosylated mucin-like domains (BDBV GPΔmuc), suggesting that mAbs from these three groups target epitopes outside of mucin-like domains (**Figure 20**).

To evaluate the inhibitory activity of isolated mAbs, in collaboration with Dr. Bukreyev's group, we tested mAbs in a BDBV neutralization assay. Thirty-one of the 90 BDBV GP-reactive mAbs had half-maximal inhibitory concentration (IC_{50}) values < 10 μg/mL, and we defined these as neutralizing antibodies (nAbs) (**Figure 18B where nAb names are highlighted in red**). Several nAbs displayed an extremely high neutralizing potency, with IC_{50} values below 1 ng/mL (**Figure 18B**). Eighteen of 31 nAbs bound only to BDBV GP in ELISA, 6 nAbs recognized BDBV and EBOV GPs, and the remaining 7 nAbs bound to GPs from representatives of three *Ebolavirus* species: BDBV, EBOV, and SUDV. These results suggest that cross-reactive mAbs in our panel possess neutralizing activity to multiple ebolaviruses. To test this hypothesis, we screened BDBV425 (a Group 2A nAb) in an EBOV neutralization assay as the nAb with the lowest EC_{50} value to the heterologous EBOV GP, and we determined that BDBV425 neutralized the heterologous EBOV. Encouraged by this result, we tested nAbs from Groups 3A and 3B in EBOV or SUDV neutralization assays to determine whether cross-reactive nAbs can neutralize three *Ebolavirus* species. We found two cross-reactive nAbs from Group 3A (BDBV43 and BDBV324) that neutralized all three *Ebolaviruses*: BDBV, EBOV and SUDV (**Figure 19B, BDBV43**). The remaining 5 nAbs from Group 3A and 3B neutralized BDBV and EBOV but failed to neutralize SUDV (**Figure 19B, BDBV289)**.

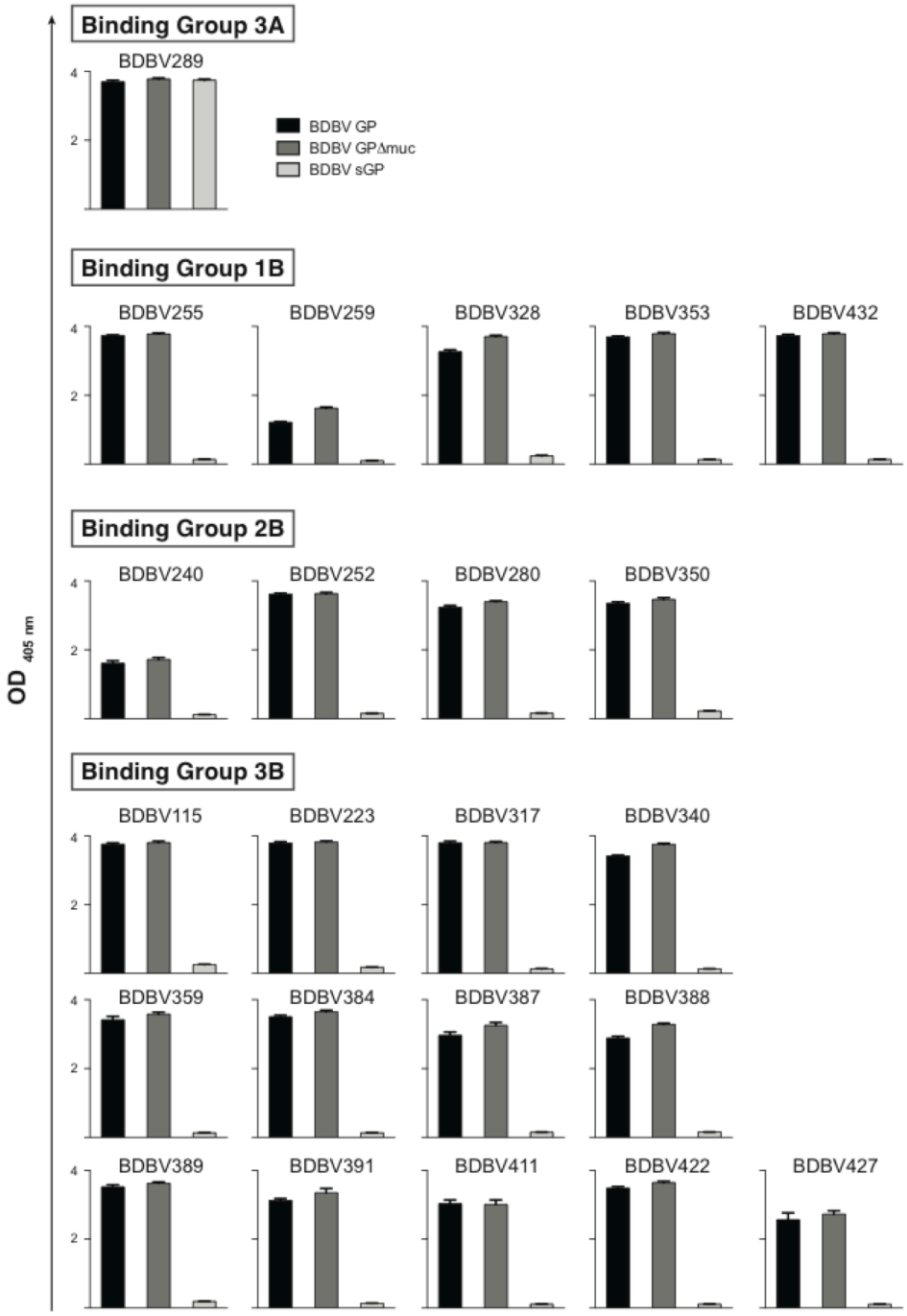

Figure 20. Antibodies from groups 1B, 2B and 3B recognize BDBV GP and BDBV GPΔmuc but not BDBV sGP in ELISA binding assay. The binding of selected antibodies to BDBV GP, BDBV GPΔmuc and BDBV sGP proteins was tested at a single mAb concentration 10 µg/mL.

Major Antigenic Sites Recognized by Human MAbs

To determine whether Abs from distinct binding groups targeted different antigenic regions on the BDBV GP surface, I performed a quantitative competition-binding assay using a real-time biosensor. I tested 4 BDBV nAbs from binding Group 1A, 5 nAbs from binding Group 1B, 4 nAb from Group 3A and 3 nAbs from Group 3B in a tandem blocking assay in which BDBV GP was attached to the biosensor. I also tested 5 non-neutralizing antibodies from Group 1A to determine whether non-neutralizing antibodies target a unique epitope on GP surface.

Non-neutralizing and neutralizing mAbs from Group 1A and nAbs from Group 3A blocked binding of each other to the GP antigen and segregated into a single competition-binding group (**Figure 21**). These results suggest that mAbs from Group 1A and Group 3A target a single antigenic region that contains epitopes shared between GP and sGP (**Figure 18A**). NAbs from Group 3B that did not recognize sGP in ELISA (**Figure 18A**) segregated into a separate competition-binding group. Group 1B antibodies were interesting in that two nAbs in this group competed for binding with Group 3B nAbs, while three nAbs from the group competed for binding with antibodies from Group 3A (**Figure 21**).

These findings suggest based on competition-binding studies that there are at least two major antigenic regions recognized by human BDBV nAbs. The first major antigenic region contains epitopes which both sGP and GP share (recognized by mAbs from Groups 1A, 3A) as well as epitopes that are present only on the GP surface (recognized by three mAbs from Group 1B). The second major antigenic region contains only epitopes that are present on the GP surface but not sGP (recognized by two mAbs from Group 1B and three mAbs from Group 3B).

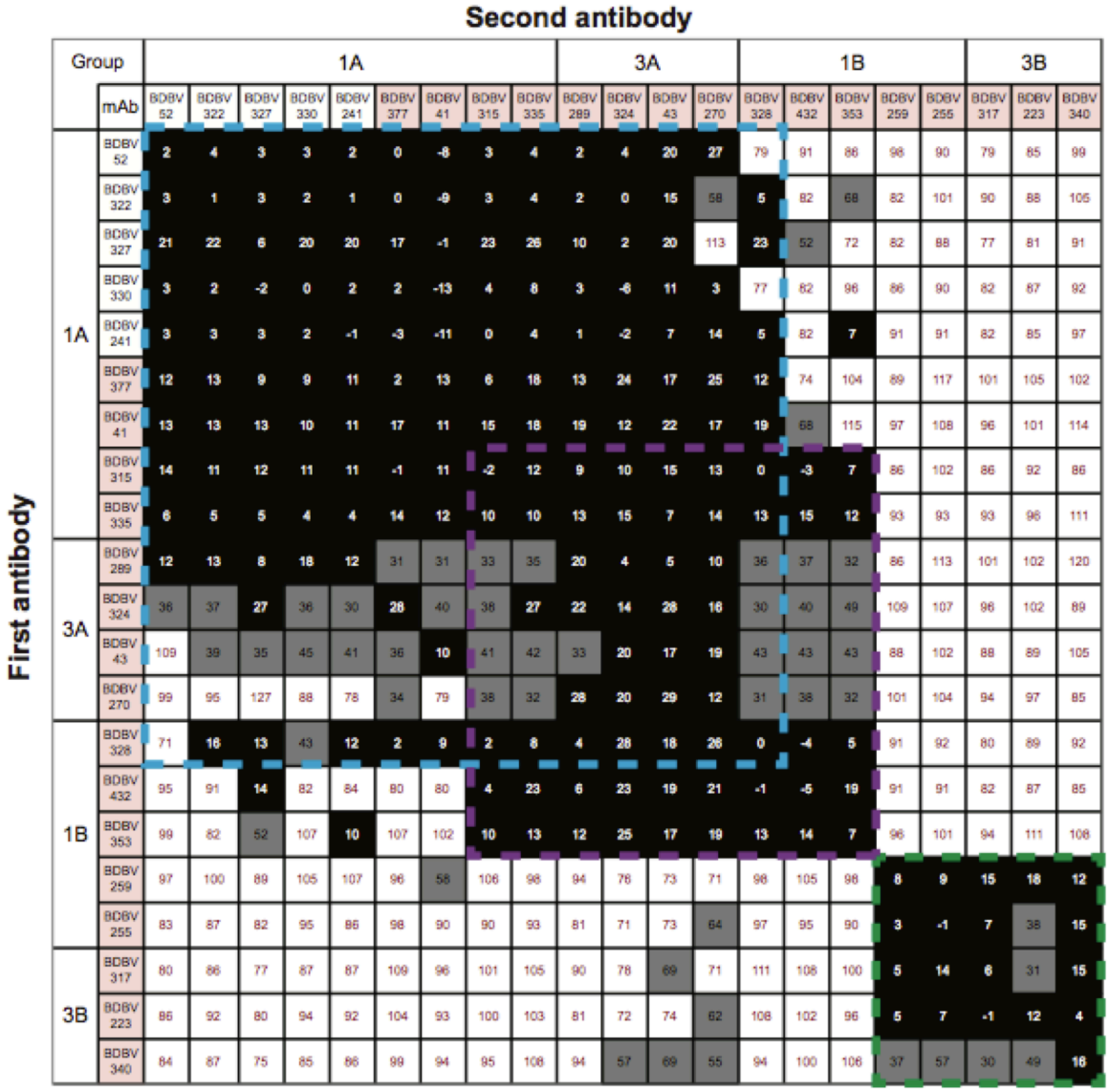

Figure 21. BDBV-neutralizing antibodies target at least two distinct antigenic regions of the GP surface. Data from competition-binding assays using non-neutralizing mAbs from binding Group 1A (white background) and neutralizing mAbs from binding Groups 1A, 1B, 3A or 3B (pink background). Numbers indicate the percent binding of second mAb in the presence of the first mAb, compared to binding of un-competed second mAb. MAbs were judged to compete for the same site if maximum binding of second mAb was reduced to <30% of its un-competed binding (black boxes with white numbers). MAbs were considered non-competing if maximum binding of second mAb was >70% of its un-competed binding (white boxes with red numbers). Grey boxes with black numbers indicate an intermediate phenotype (competition resulted in between 30 and 70% of un-competed binding). Blue, purple, and green dashed lines indicate what appear to be major competition groups; the blue and purple groups overlap substantially but not completely.

Diverse Patterns of Molecular Recognition Defined by Negative Stain Electron Microscopy

To determine the location of the two major antigenic regions targeted by human BDBV nAbs, we performed negative-stain single-particle electron microscopy (EM) studies using antibodies from Groups 1A and 1B, in collaboration with Andrew Ward's group. The EM class averages and reconstructions showed clearly that the two major antigenic regions, defined in competition-binding experiments, corresponded to two distinct sites on GP surface: the glycan cap and the GP base.

Comparison of the structures of glycan cap-directed mAbs from Group 1A with those in Group 1B revealed that the antibodies have partially overlapping epitopes, but approach the glycan cap at distinct angles (**Figure 22A, B**). We fitted a previously determined atomic resolution structure of Sudan virus (SUDV) GPΔmuc (Bale et al., 2012), which reveals more residues of the glycan cap region than the equivalent EBOV structure, into the envelope of GP from the EM reconstructions and determined the regions targeted by each mAb (**Figure 22D, E**). BDBV335, which binds GP and sGP equally well, mainly targets a region between residues 274-282. This region appears well defined in the BDBV335 EM map, indicated by the large lobe on the outside of the glycan cap that closely resembles that region in the GP crystal structure. When viewed along the three-fold axis of GP, BDBV41 binds to the right of BDBV335, further up on the glycan cap, close to a loop that extends from residue 266 to 277. BDBV41 also may make contacts with a loop that extends toward the mucin-like domains, from residue 309 to 312 or further in regions that were unresolved in the GP crystal structure. BDBV432 binds to the left of BDBV335, at the top of a helix-loop at residues 259-266, and likely makes extensive contacts with a loop from residues around 302-312. Despite a lack of binding to sGP, BDBV432, as well as BDBV353, bind in the

glycan cap region, suggesting that these mAbs make contacts with residues that are exclusive to GP.

The other antibodies in Group 1B bind an epitope at the base of GP. These antibodies, including BDBV255 and BDBV259, bind further down on GP than has been observed previously with murine mAbs, possibly contacting residues within GP2 that are part of the membrane proximal external region (MPER) (**Figure 22C, D, and E**). These antibodies were refractory to a reconstruction by EM due to predominant side views of the particles and also apparent flexibility. The class averages, however, clearly show that these antibodies bind an epitope that extends below the base of GP. Three Fabs can be seen in some of the class averages, indicating that despite the apparent small size of this region, three antibodies can be accommodated on one GP trimer. Although the Fabs adopt various positions in each class average, there is not a continuous range of flexibility since the Fabs themselves are well resolved. These antibodies may require the full MPER and transmembrane (TM) regions, as well as a membrane, in order to bind stably. These features are all lacking in the current recombinant protein used here, a soluble form of the extracellular domain of GP. While the GP2 region is well conserved across the filoviruses, these BDBV-specific mAbs likely bind non-conserved regions in GP2 proximal to the TM region.

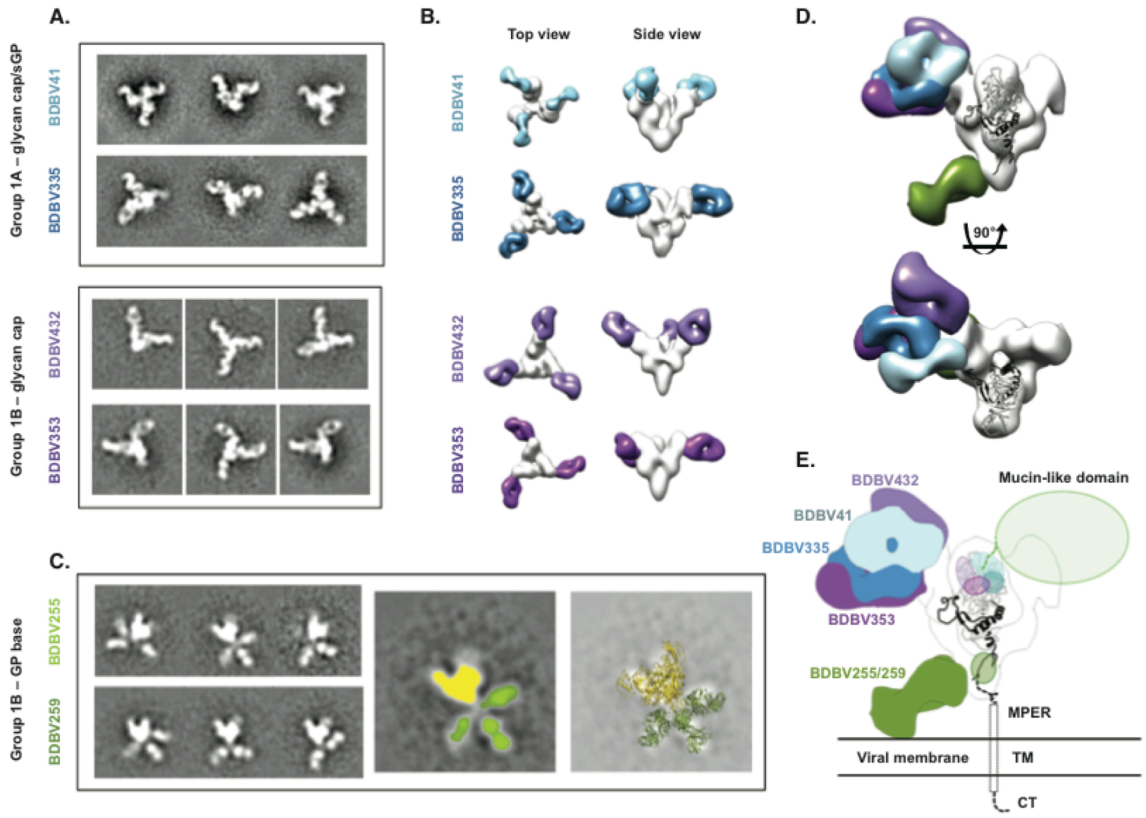

Figure 22. BDBV-neutralizing antibodies bind to the glycan cap or base region of GP. (A) Shown are negative-stain electron microscopy reference-free 2D class averages of Group 1A antibodies that bind both the glycan cap of GP and sGP, and Group 1B antibodies that bind the glycan cap of GP but not sGP. BDBV GP or GPΔmuc was used to generate complexes. (B) 3D reconstructions of glycan cap binders from Groups 1A and 1B reveal that these antibodies bind the glycan cap at overlapping but distinct epitopes. Top (left) and side (right) views of the complexes are shown. (C) Reference free 2D class averages of Group 1B antibodies (left) reveals that these antibodies bind an epitope below the base of GP that is flexible. In the middle image, GP is colored yellow and each Fab colored green. The right-hand panel illustrates a superimposition of crystal structures of SUDV GPΔmuc (PDB 3VE0) and Fabs (PDB 3CSY) to demonstrate how Fabs may bind to GP. (D) The composite model delineates the epitopes of the glycan cap mAbs in Group 1A or 1B. Side (above) and top (below) views are shown. (E) Docking a crystal structure of SUDV GPΔmuc (PDB 3VE0) (Bale et al., 2012), which contains a more complete model of the glycan cap region targeted by Group 1A/B mAbs, reveals how Group 1A/B mAbs target a broad region in the GP1 centered on the glycan cap, near the beginning of the mucin-like domains. Group 1B mAbs that target the base likely bind to a loop near the membrane proximal external region) that is flexible and has not yet been resolved at high resolution. TM = transmembrane region; CT = cytoplasmic tail.

Epitope Mapping of Group 3A MAbs Using Saturation Mutagenesis and Negative Stain Electron Microscopy

As the Group 3A (cross-reactive) nAbs competed for binding with Group 1A (BDBV-specific) nAbs (**Figure 18**), I hypothesized that some structural features of the glycan cap are conserved between GPs from multiple *Ebolavirus* species. In collaboration with Ben Doranz's group at Integral Molecular, we sought to identify amino acids that define epitopes for three Group 3 nAbs (BDBV270, BDBV289, and BDBV324) using a comprehensive EBOV GP alanine-scanning mutation library. Epitope mapping identified critical residues for binding by each nAb, W275 for BDBV270, W275 and Y241 for BDBV289, W275 and L273 for BDBV324. Residues for which mutation reduced binding of three nAbs from Group 3A were visualized on the surface of the high-resolution structure of EBOV GP (PDB ID 3CSY). This finding suggests that each of these antibodies recognize overlapping epitopes in the GP glycan cap (**Figure 23A, B**). The previously described murine nAbs 2G4 and 4G7 and the human nAb KZ52 bind the base region of the GP (Lee et al., 2008a; Murin et al., 2014), and mutations of the W275 or L273 residues did not reduce the binding of these nAbs (**Figure 23C**). Dr. Bukreyev's lab tied to passage VSV/BDBV-GP in the presence of BDBV223 or BDBV289 in an attempt to generate escape mutant viruses, but could not isolate neutralization-resistant viruses. An isolate passaged in the presence of BDBV223 with a R574H polymorphism in heptad repeat 1 (HR1) region was identified, and for BDBV289 an isolate with an I584M polymorphism in the HR1 region alone or in combination with an E149K substitution in the receptor-binding domain. However, none of these mutations was associated with the ability of those viruses to resist neutralization by the corresponding mAb.

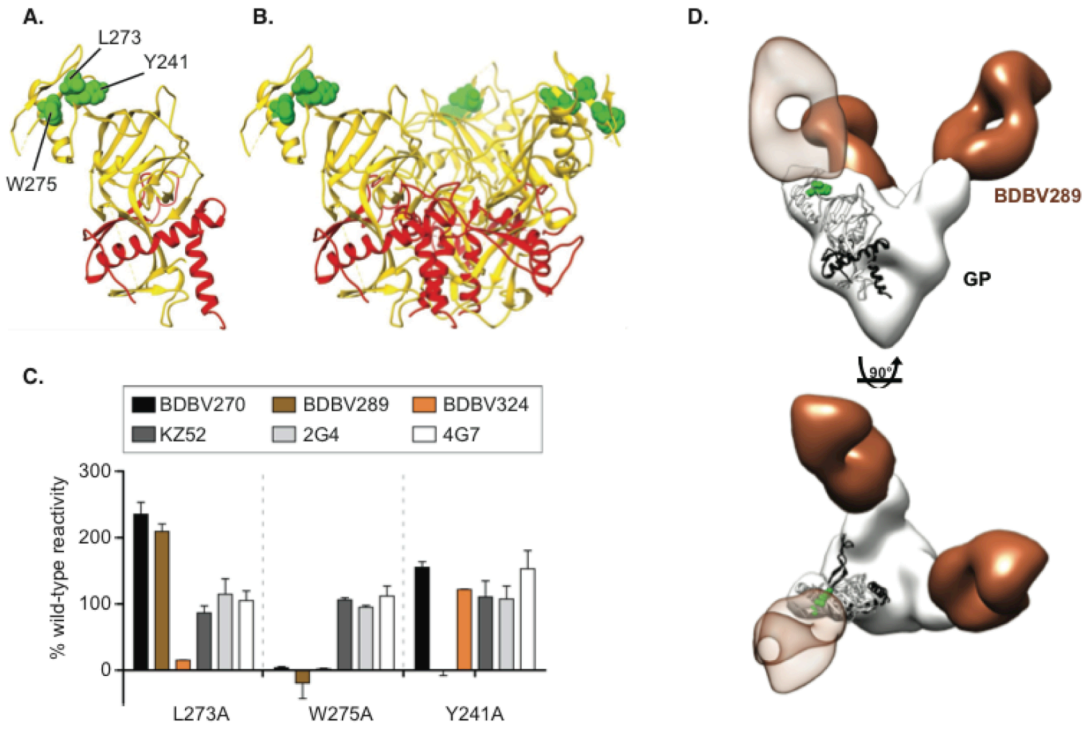

Figure 23. Epitope mapping of Group 3A mAbs using saturation mutagenesis and negative stain electron microscopy. Epitope residues for three nAbs from Group 3A (BDBV270, BDBV289 and BDBV324) were identified as those for which mutation to alanine specifically reduced binding of these antibodies (A-B). GP residue W275 was common to all three nAbs, while L273 was specific for BDBV324, and Y241 was specific for BDBV289. The mutated residues are shown in space filling forms on a ribbon diagram of the EBOV GP structure, based on PDB 3CSY. (C) Binding values for nAbs and previously isolated mAbs KZ52, 2G4 and 4G7 to library clones with mutations at residues L273, W275 and Y241. The Ab reactivities against each mutant EBOV GP clone were calculated relative to reactivity with wild-type EBOV GP. (D) BDBV289 (brown) binds at the top of the viral GP near the glycan cap region. Complexes are of BDBV antibody Fab fragments bound to BDBV GPΔTM with side view (top panel) or top view (bottom panel). A representative Fab crystal structure is fit in the Fab density for each reconstruction (from PDBID 3CSY). A monomer of the GP trimer crystal structure (PDBID 3CSY) is also fit in the GP density, with white corresponding to GP1 and black to GP2. Two critical residues for binding by BDBV289 (W275 and Y241, determined using saturation mutagenesis) are highlighted in green.

In collaboration with Andrew Ward's group, we further characterized the antibody BDBV289 by single particle EM studies of antibody in complex with GP. BDBV289 binds the glycan cap region of GP, centered on the residues W275 and Y241 (**Figure 23D**). The angle of approach resembles that of the mAb 1H3 from the antibody cocktail ZMab, although 1H3 is specific to EBOV and is weakly neutralizing (Murin et al., 2014; Qiu et al., 2011). Further, BDBV289 also binds sGP, which shares the first 295 amino acids of GP1 with GP, including the glycan cap region (Sanchez et al., 1996; Volchkov et al., 1995). Therefore, despite

previous hypotheses that propose that sGP is an immune decoy and that cleavage of the glycan cap prevents neutralizing antibodies from binding this region (Mohan et al., 2012; Murin et al., 2014), we have now identified several antibodies that challenge these ideas. Interestingly, BDBV289 targets an overlapping epitope with antibodies that we identified to be specific to BDBV and that do not bind sGP (**Figure 19**). Therefore, the glycan cap region is a major antigenic site that contains epitopes with subtle features that influence sGP and GP binding, neutralization, and species cross-reactivity of targeting mAbs.

Therapeutic Efficacy of Human MAbs in Small Animal Models of EBOV Infection

Finally, in collaboration with Alexander Bukreyev's group, we set out to test the *in vivo* efficacy of the cross-reactive nAbs using a guinea pig model of EBOV infection. We selected two nAbs from Groups 3A (BDBV289) and 3B (BDBV223) that bound non-overlapping antigenic regions in the competition-binding experiments (**Figure 21**). Five to six week-old guinea pigs, strain Hartley, were injected with 5 mg of antibody by the IP route once (day 1) or twice (days 1 and 3) after inoculation with 1,000 PFU of guinea pig-adapted EBOV, strain Mayinga. BDBV223 provided marginal protection, as only 1 of 5 animals survived the lethal challenge (**Figure 24**). Surprisingly, a glycan cap-specific nAb, BDBV289, fully protected guinea pigs when delivered twice after the virus challenge. The protective efficiency of BDBV289 with a single treatment against a heterologous EBOV (**Figure 24,** 3 of 5 survived) was higher than the protective efficiency of the equivalent glycan-cap-specific mAb c13C6, a component of the ZMapp cocktail (1 of 6 survived) (Qiu et al., 2014). To determine whether a combination of two mAbs that target two neutralizing epitopes on EBOV GP surface confer better protection than treatment with a single mAb alone, we tested the combination of BDBV223 and BDBV289 in guinea pigs. The combination of two antibodies provided

complete protection against a heterologous EBOV with only a single treatment (**Figure 24**). We isolated viral RNA from blood of representative animals that were treated with mAbs BDBV223 or BDBV289 but died and then sequenced the genes encoding the GP. Several polymorphisms were detected, but none appeared to be directly related to the epitope specificity of the mAb used for treatment.

Discussion

This study reveals that natural BDBV infection in humans induces the development of ebolavirus cross-reactive antibodies that target epitopes on the GP surface that are conserved in diverse species of genus *Ebolavirus*. During these studies we isolated 90 human mAbs from humans following BDBV infection and found 57 cross-reactive mAbs that recognized heterologous EBOV GPs. Remarkably, some of the isolated cross-reactive mAbs not only bound but also neutralized multiple *Ebolavirus* species. The majority of cross-reactive mAbs neutralized BDBV and EBOV, but we also isolated two antibodies that displayed potent neutralizing activity against representatives of three *Ebolavirus* species – BDBV, EBOV, and SUDV. We tested two cross-neutralizing mAbs in mice and guinea pigs and showed that they protected animals from lethal challenge with a heterologous species of EBOV. These data suggest that cross-neutralizing mAbs can be used to develop a universal treatment against multiple ebolaviruses and imply that highly immunogenic vaccines with proper presentation of GP from one species could induce some measure of cross-protection against viruses of the other species. The ability of these mAbs to bind and neutralize a broad range of *Ebolavirus* species also suggest that such antibodies might offer protection against emerging filoviruses in the future.

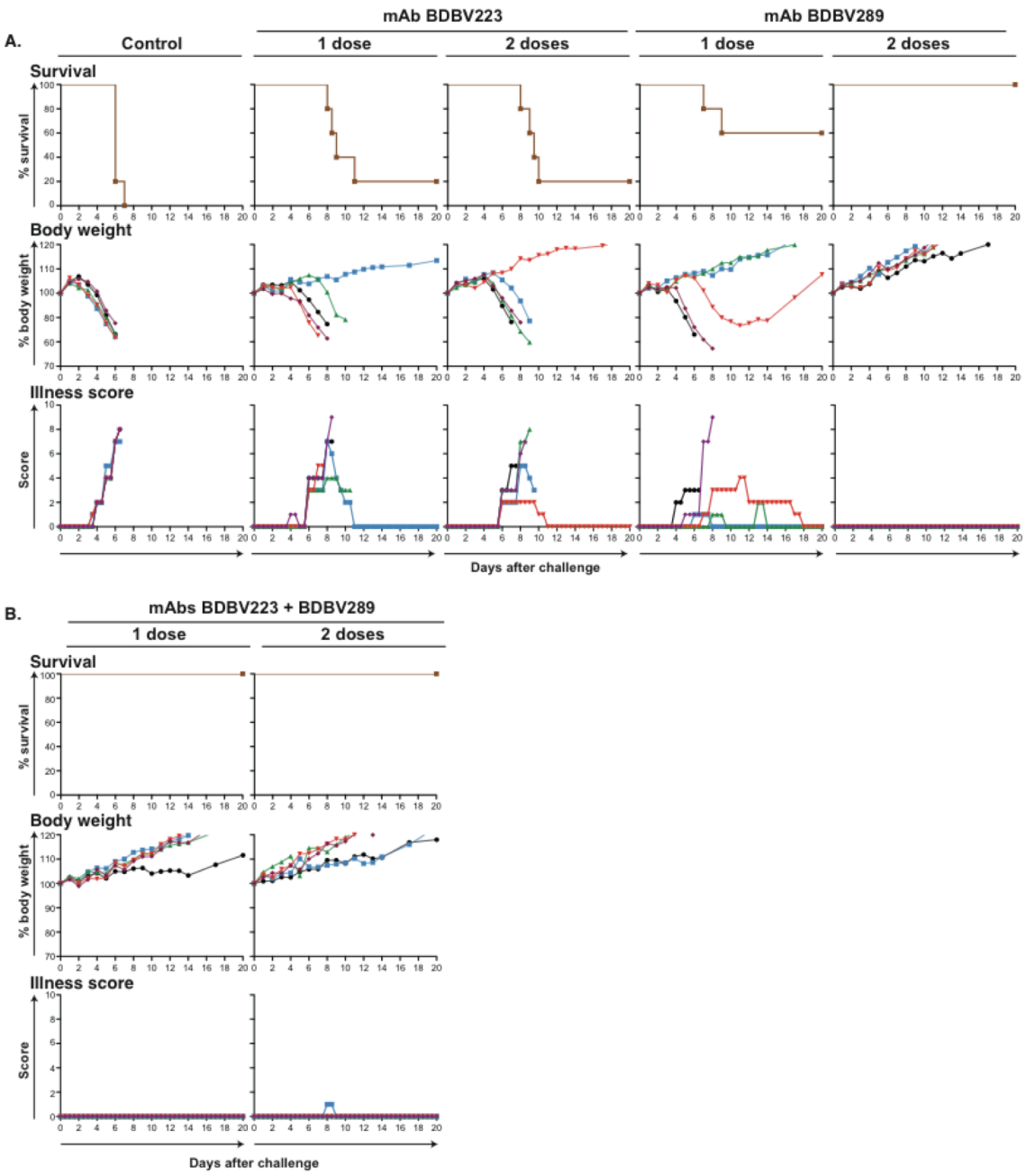

Figure 24. Survival and clinical signs of EBOV inoculated guinea pigs treated with BDBV mAbs. Groups of 5 guinea pigs per group were injected with individual mAbs by the intraperitoneal route 1 day or 1 and 3 days after EBOV challenge, using 5 mg of individual mAb (A) or 5 mg of the combination of two mAbs per treatment (B), as indicated. Animals treated with dengue virus-specific human mAb 2D22 served as controls. The survival curves are based on morning and evening observations. Mortality in the morning is shown in whole day numbers, in the evening in 1/2 day values. The body weight and illness scores are shown with one value per day

Several antibody-based treatments provided complete species-specific protection from EBOV in non-human primate model of infection (Qiu et al., 2014). However, antibody-based therapeutics against other members of the *Ebolavirus* genus, such and BDBV and SUDV, are not available. While one strategy would be to develop separate antibody treatments for each filovirus infection, an alternative strategy would be to have a universal treatment effective against diverse *Ebolavirus* species. The development of universal antibody treatments for ebolaviruses seems inevitable, given recent progress in the identification of broad and potent neutralizing antibodies against viruses that exhibit more antigenic diversity than the filoviruses such as HIV (Burton et al., 2012), influenza viruses (Pappas et al., 2014), dengue virus (Rouvinski et al., 2015), alphaviruses (Fox et al., 2015), and paramyxoviruses (Corti et al. 2013). Our results provide a roadmap to develop a single antibody-based treatment effective against multiple *Ebolavirus* infections. I propose that the principal components of such treatment should include cross-neutralizing mAbs that target conserved elements of the non-overlapping major neutralizing antigenic sites on the GP surface.

Materials and Methods

Donors

De-identified peripheral blood mononuclear cells (PBMCs) from 7 survivors of the 2007 BDBV outbreak in Uganda (Towner et al., 2008) were obtained from a repository at Makerere University (Kampala, Uganda) managed in collaboration with the U.S. Military HIV Research Program MHRP, which is part of the Walter Reed Army Institute of Research. PBMCs were obtained after informed consent from a U.S. survivor of Ebola virus Zaire (EBOV) infection who was infected while delivering health care in Liberia during the 2014

Ebola virus outbreak with Makona virus. Cells from the EBOV survivor were obtained about 11 weeks after infection and about 7 weeks after discharge from hospital, following several negative PCR tests for presence of virus. PBMCs were obtained from a U.S. survivor of Marburg virus (MARV) infection who developed the disease in early 2008 following exposure to fruit bats in the Python Cave in Queen Elizabeth National Park, Uganda. This donor's clinical course was documented previously (Centers for Disease and Prevention, 2009), and we have previously reported isolation of human antibodies from this donor (Flyak et al., 2015). Peripheral blood from the donor was obtained in 2012, four years after the illness, following informed consent. The studies were approved by the Vanderbilt University Institutional Review Board.

Viruses

BDBV strain 200706291 Uganda was isolated originally from the serum of a patient during the first recorded outbreak caused by this virus (Towner et al., 2008) and passaged three times in Vero E6 cells. The virus was provided originally by the Special Pathogens Branch of the U.S. Centers for Disease Control and Prevention (CDC) and deposited at the World Reference Center of Emerging Viruses and Arboviruses (WRCEVA), housed at the University of Texas Medical Branch (UTMB), Galveston, TX. The mouse-adapted EBOV strain Mayinga was originally generated by Dr. Mike Bray (U.S. Army Medical Research Institute of Infectious Diseases, Fort Detrick, Frederick, Maryland) (Bray et al., 1998). The virus was provided originally by the Special Pathogens Branch of CDC, deposited at WRCEVA, and amplified by one passage in Vero-E6 cells. The guinea pig-adapted EBOV strain Mayinga was generated originally by Dr. Brett Cononolly (U.S. Army Medical Research Institute of Infectious Diseases) (Connolly et al., 1999) and was provided by Dr. Alexander Freiberg (UTMB) through Dr. Heinz Feldmann (Special Pathogens Program, National Microbiology Laboratory, Canadian Science Centre for Human and Animal Health,

Winnipeg, Canada) and amplified by one passage in Vero-E6 cells. The recombinant EBOV strain Mayinga expressing eGFP was generated by a reverse genetics technique (Lubaki et al., 2013) as previously described (Towner et al., 2005) from plasmids provided by Drs. Jonathan Towner and Stuart Nichol (CDC) and Drs. Yoshihiro Kawaoka (University of Wisconsin) and Heinz Feldmann (NIH), and passaged three times in Vero E6 cells. The EBOV Makona strain from the 2014-2015 West African outbreak, which was provided by Dr. T. Geisbert (UTMB), was isolated originally from serum of a fatally infected patient in early 2014 in Guekedou, Guinea, and was passaged two times in Vero E6 cells. The chimeric EBOV/BDBV-GP, EBOV/MARV-GP and EBOV/SUDV-GP constructs expressing eGFP were obtained by replacing the gene encoding EBOV GP with that of BDBV, MARV or SUDV, respectively (Ilinykh P., unpublished data) , and passaged two times in Vero E6 cells.

Generation of human hybridomas secreting monoclonal antibodies (mAbs)

Human hybridomas were generated as described previously (Flyak et al., 2015). In brief, previously cryopreserved samples were transformed with Epstein-Barr virus, CpG and additional supplements. After 7 days, cells from each well of the 384-well culture plates were expanded into four 96-well culture plates using cell culture medium containing irradiated heterologous human PBMCs (recovered from blood unit leukofiltration filters, Nashville Red Cross) and incubated for an additional four days. Plates were screened for BDBV GP antigen-specific antibody-secreting cell lines using enzyme-linked immunosorbent assays (ELISAs). Cells from wells with supernates reacting with antigen in an ELISA were fused with HMMA2.5 myeloma cells using an established electrofusion technique (Yu et al., 2008).

Human mAb and Fab production and purification

After fusion, hybridoma cell lines were cloned by single-cell fluorescence-activated cell sorting and expanded in post-fusion medium as previously described (Flyak et al., 2015). HiTrap Protein G or HiTrap MabSelectSure columns were used to purify antibodies from filtered supernates. Fab fragments were generated by papain digestion, as described previously (Flyak et al., 2015).

Expression and purification of filovirus GPs

BDBV GP ectodomain (BDBV GP, residues 1-637) or the secreted glycoprotein dimer (BDBV sGP, residues 1-316) were used to screen supernatants of transformed B cells. Recombinant glycoproteins were engineered with a C-terminal double strep tag and cloned into a modified pMTpuro vector for expression in Drosophila S2 cells. Briefly, plasmids were transfected into S2 cells using Effectene reagent (Qiagen) followed by stable cell selection with 6 μg/mL puromycin. S2 cells first were cultured in Schneider's medium supplemented with 10% (v/v) FCS (Lonza), and later adapted to Insect Xpress medium for large-scale expression in 2L shaker flasks. Stable cells were induced with 0.5 mM $CuSO_4$ and harvested after 4 to 5 days at 27°C. Tangential flow filtration then was used to buffer exchange the supernatants into 100 mM Tris-HCl, 150 mM NaCl, 1 mM EDTA, 15 μg/mL avidin pH 8.0, and target proteins were purified using Streptactin Superflow affinity (Qiagen). GP ectodomains were purified further with S200 size exclusion chromatography (SEC); sGP was purified with S75 SEC. Recombinant ectodomains for EBOV, SUDV or MARV were designed and expressed similarly.

Screening and half maximal effective concentration (EC_{50}) ELISA binding analysis. Soluble forms of the full-length extracellular domain of BDBV, EBOV, SUDV or MARV GPs or the sGP form of BDBV GP were coated overnight onto 384-well plates at 1 μg/mL. For

screening ELISA, 10 µL of supernate from a well of a tissue-culture plate were transferred to each well of a 384-well ELISA plate. For EC_{50} binding analysis by ELISA, purified antibodies were applied to the plates at a concentration range of 30 µg/mL to 170 ng/mL, using three-fold serial dilutions. The presence of antibodies bound to the GP was determined using goat anti-human IgG alkaline phosphatase conjugate and p-nitrophenol phosphate substrate tablets, with optical density read at 405 nm after 120 minutes. A non-linear regression analysis was performed on the resulting curves using Prism version 5 (GraphPad) to calculate EC_{50} values. The Circos software package was used for data visualization (Krzywinski et al., 2009).

EBOV and MARV neutralization experiments

Isolated mAbs were screened initially in a high-throughput neutralization assay using EBOV/BDBV-GP with or without 5% guinea pig complement (MP Biomedicals, Santa Ana, CA) (Ilinykh P., unpublished data). The mAbs that exhibited neutralizing activity also were screened for neutralization of eGFP-expressing EBOV (Towner et al., 2005). BDBV223 was tested for neutralization of EBOV/SUDV-GP and EBOV/MARV-GP by the same approach. In addition, neutralizing activity of BDBV223 was tested against the EBOV Makona strain by a classic plaque reduction assay, which was performed as follows. Triplicate samples of 150 PFU of the virus were mixed with serial dilutions of mAbs, with or without 5% guinea pig complement in a total volume of 100 µL, incubated for 1 hour at 37°C, and placed on Vero E6 cell monolayers. After a 1 hour-long virus adsorption at 37°C, cells were overlaid with 0.8% tragacanth (Spectrum Chemical Mfg. Corp., New Brunswick, NJ) solution in Minimal Essential Medium containing 10% FBS (HyClone, Logan, Utah) and 0.1% gentamicin (Mediatech, Manassas, VA), and incubated for 14 days. Plaques were visualized by staining of monolayers with 0.25% crystal violet (Thermo Fisher Scientific, Waltham, MA) in 10% formalin.

Biolayer interferometry competition binding assay

Competition binding studies using biolayer interferometry and biotinylated BDBV GP (EZ-link® Micro NHS-PEG_4-Biotinylation Kit, Thermo Scientific #21955) (5 µg/mL) were performed on an Octet RED biosensor (ForteBio, Menlo Park, CA), as described previously (Flyak et al., 2015). In brief, the antigen was immobilized onto streptavidin-coated biosensor tips. After a brief washing step, biosensor tips were immersed first into the wells containing first antibody at a concentration of 100 µg/mL and then into the wells containing a second mAb at a concentration of 100 µg/mL. The percent binding of the second mAb in the presence of first mAb was determined by comparing the maximal signal of the second mAb applied after the first mAb complex to the maximal signal of the second mAb alone.

Sequence analysis of antibody variable region genes

Antibody variable gene sequence analysis was performed as previously described (Flyak et al., 2015). Heavy chain antibody variable region sequences were analyzed using the IMGT/V-Quest program (Brochet et al., 2008; Giudicelli et al., 2011).

Electron microscopy and sample preparation

Fabs were added in 10 molar excess to BDBV GPdMuc and subsequently purified and stained as previously described (Murin et al., 2014).

Image processing of protein complexes

Particles were automatically picked using DoG Picker (Voss et al., 2009) and particle stacks were generated using Appion (Lander et al., 2009). Subsequently, reference-free 2D class averages were generated using iterative MRA/MSA (van Heel et al., 1996). Non-GP complexes and those with a clear lack of full saturation by Fab were removed to generate a

final stack for reconstructions. In some cases, orientation bias or flexibility of Fabs prevented convergence of an acceptable model, although examination of class averages allowed a general assignment of the epitope. Final stack class averages were used to generate initial models using EMAN2 common lines (Tang et al., 2007). A model matching its reference projections was further refined using the entire raw particle stack with EMAN2, as described previously (Murin et al., 2014). For the BDBV41 reconstruction, the EMAN2 reconstruction lacked important features that were present in the class averages, indicating that perhaps some particles lacked full Fab saturation. In order to circumvent this problem, we utilized the Relion package, which allows 3D-classification to remove particles that may only contain 2 Fabs, significantly improving the quality of the final EM map (Scheres, 2012). Modeling fitting and EM figures were generated using UCSF Chimera (Pettersen et al., 2004).

Epitope mapping using an EBOV GP alanine-scan mutation library

Comprehensive high-throughput alanine scanning ('shotgun mutagenesis') was carried out on an expression construct for EBOV GP (Yambuku-Mayinga variant GP; Uniprot accession number Q05320). Residues 33-676 of full-length EBOV GP were mutagenized to create a library of clones, each representing an individual point mutant. Residues were changed to alanine (with alanine residues changed to serine). GP residues 1-32, which constitute the GP signal peptide, were not mutagenized. The resulting EBOV GP alanine-scan library covered 99.5% of target residues (641 of 644). Clones were arrayed into 384-well plates, one mutant per well. The EBOV GP mutation library was transfected into HEK-293T cells and allowed to express for 22 hours. Cells were fixed in 4% paraformaldehyde in PBS plus calcium and magnesium, or were left unfixed, and were then incubated with an Ab diluted in 10% normal goat serum (NGS) (Sigma-Aldrich, St. Louis, MO). The cells were incubated with primary antibody for 1 hour at room temperature, followed by a 30 minute incubation with Alexa Fluor 488-conjugated secondary antibody (Jackson ImmunoResearch

Laboratories, Westgrove, PA) in 10% NGS. Cells were washed twice with PBS without calcium or magnesium and resuspended in Cellstripper (Cellgro, Manassas, VA) plus 0.1% BSA (Sigma-Aldrich, St. Louis, MO). Cellular fluorescence was detected using the Intellicyt high throughput flow cytometer (Intellicyt, Albuquerque, NM). Background fluorescence was determined by fluorescence measurement of vector-transfected control cells. Ab reactivities against each mutant EBOV GP clone were calculated relative to wild-type EBOV GP reactivity by subtracting the signal from mock-transfected controls and normalizing to the signal from wild-type GP-transfected controls.

Before screening, the immunoreactivities of MAbs BDBV270, BDBV289, and BDBV324 were optimized by determining reactivity with fixed or unfixed cells over a range of mAb concentrations to identify optimal signal-to-background ratios (>5:1) and to ensure that signals were within the linear range of detection. MAb BDBV289 also screened as a Fab after conversion by papain digestion. Control mAbs 2G4 and 4G7 were kindly provided by Gary Kobinger, Public Health Agency of Canada.

Mutated residues within critical clones were identified as critical to the Ab epitope if they did not support reactivity of the test Ab but did support reactivity of other control EBOV mAbs. This counter-screen strategy facilitates the exclusion of GP mutants that are locally misfolded or that have an expression defect. The detailed algorithms used to interpret shotgun mutagenesis data are described elsewhere (patent application 61/938,894), (Davidson and Doranz, 2014).

Generation and Sequence Analysis of VSV/BDBV GP Escape Mutants

Briefly, 200 PFUs of VSV/BDBV-GP virus were pre-incubated with 2-fold decreasing concentrations of mAbs before each passage, starting from 200 µg/mL, and serially

passaged 3-10 times under selective pressure of the corresponding mAbs. After each passage, virus aliquots were harvested and titrated. A suspension containing 200 PFUs from the virus-positive aliquot with the highest mAb concentration was used for the next passage. Finally, viruses were plaque-purified, and the genes encoding the BDBV GPs were sequenced. Viral samples derived from plaques containing any amino acid substitutions were propagated further in the presence of the corresponding mAb, and tested for neutralization resistance by plaque reduction assay.

In vivo testing

The animal protocols for testing of mAbs in mice and guinea pigs were approved by the Institutional Animal Care and Use Committee of the University of Texas Medical Branch at Galveston. Seven-week-old BALB/c mice (Charles River Laboratories) were placed in the ABSL-4 facility of the Galveston National Laboratory. Groups of mice at 5 animals per group were injected with 1,000 PFU of the mouse-adapted EBOV by the intraperitoneal route. Twenty-four or seventy four hours later, animals were injected with individual mAbs by the intraperitoneal route using 100 μg per treatment. Animals treated with the antibody specific to dengue virus 2D22 served as controls. Animals were weighed and monitored daily over the two-week period after challenge. Once animals were symptomatic, they were examined no less than twice per day. The disease was scored using the following parameters: dyspnea (possible scores 0-5), recumbency (0-9), unresponsiveness (0-5), and bleeding/hemorrhage (0-5). To test the protective efficacy of mAbs in guinea pigs, five to six week-old animals (strain Hartley) were placed in the ABSL-4 facility of the Galveston National Laboratory. Groups of 5 animals per group were injected with 1,000 PFU of guinea pig-adapted EBOV, by the intraperitoneal route. Twenty-four hours later and 72 hours later, animals were injected with individual mAbs (5 mg per treatment), or a cocktail of two mAbs (2.5 mg of each mAb per treatment). Animals were weighted and monitored daily for 14

days. After animals became symptomatic, they were examined no less than twice per day. The disease was scored using the following parameters: appearance (possible scores 0-3), body condition (0-3), natural behavior (0-3), and provoked behavior (0-3).

CHAPTER IV

*C*ROSS-REACTIVE HUMAN ANTIBODIES TO THE HR2/MPER REGION OF EBOLA GLYCOPROTEIN

"…the warriors against Ebola understand that they face a long struggle against a formidable enemy. Many of their weapons will fail, but some will begin to work"

Richard Preston, *Inside the Ebola Wars, The New Yorker*

Introduction

The antibody cocktail ZMapp™ is effective in nonhuman primate models of infection (Qiu et al., 2014) and has been used under compassionate-treatment protocols in humans (Lyon et al., 2014). ZMapp™ is a mixture of three humanized murine mAbs (Olinger et al., 2012b; Qiu et al., 2011; Qiu et al., 2012b; Wilson et al., 2000) that target EBOV-specific epitopes on the surface GP (Davidson et al., 2015; Murin et al., 2014). As a result, ZMapp™ mAbs do not neutralize other viruses from the *Ebolavirus* genus, such as BDBV or SUDV.

In this chapter, I describe three naturally-occurring human cross-reactive mAbs from BDBV survivors that target a new antigenic site in the canonical heptad repeat 2 (HR2) region near the membrane proximal region of EBOV GP. I found that cross-reactive HR2/MPER-specific antibodies do not compete with previously isolated EBOV-specific mAbs that recognize other regions in the GP, such as the glycan cap, base, or mucin-like domain, but rather they bind a site near the viral membrane. The identification of a conserved protective antigenic site in the GP suggests that these mAbs can be used to design antibody therapeutics against multiple filovirus infection. Furthermore, structural

features formed by conserved residues in the protective site could be used to develop an epitope-based vaccine against infection caused by diverse *Ebolavirus* species.

I acknowledge Alexander Bukreyev's group for performing neutralization, protection experiments as well as escape mutants generation, Andrew Ward's group for studying EBOV-specific mAbs by negative-stain single-particle EM, Erica Saphire's group for providing *Ebolavirus* GPs, Ben Doranz's team for performing epitope mapping of selected mAbs using saturation mutagenesis, and David Wright's group for peptide synthesis.

Cross-reactive neutralizing antibodies bind a unique region on GP surface

In Chapter III, I described the isolation of a large panel of neutralizing mAbs using peripheral B cells from survivors of the 2007 BDBV outbreak in Uganda. Among seven cross-reactive mAbs that bound to GPs from multiple ebolaviruses (BDBV, EBOV, and SUDV), I found three neutralizing mAbs (designated BDBV223, BDBV317, and BDBV340) that bound to the recombinant trimeric form of GP ectodomain but did not bind to the dimeric form of GP that is secreted from cells during infection (sGP, secreted GP) (**Figure 18A, 19A**). As BDBV223, BDBV317, and BDBV340 recognized all three GPs from BDBV, EBOV, and SUDV (**Figure 18A, Group 3B**), we next sought to determine whether these cross-reactive mAbs could neutralize viruses from those three *Ebolavirus* species. All three mAbs neutralized autologous BDBV as well as heterologous EBOV. Although these human mAbs recognized SUDV GP in ELISA, BDBV223, BDBV317, and BDBV340 failed to neutralize SUDV (**Figure 25A**). Among three mAbs, BDBV223 displayed an extremely high neutralizing potency, with BDBV IC_{50} values – 0.01 ng/mL and EBOV IC_{50} values – 1.8 μg/mL (**Figure 25A**).

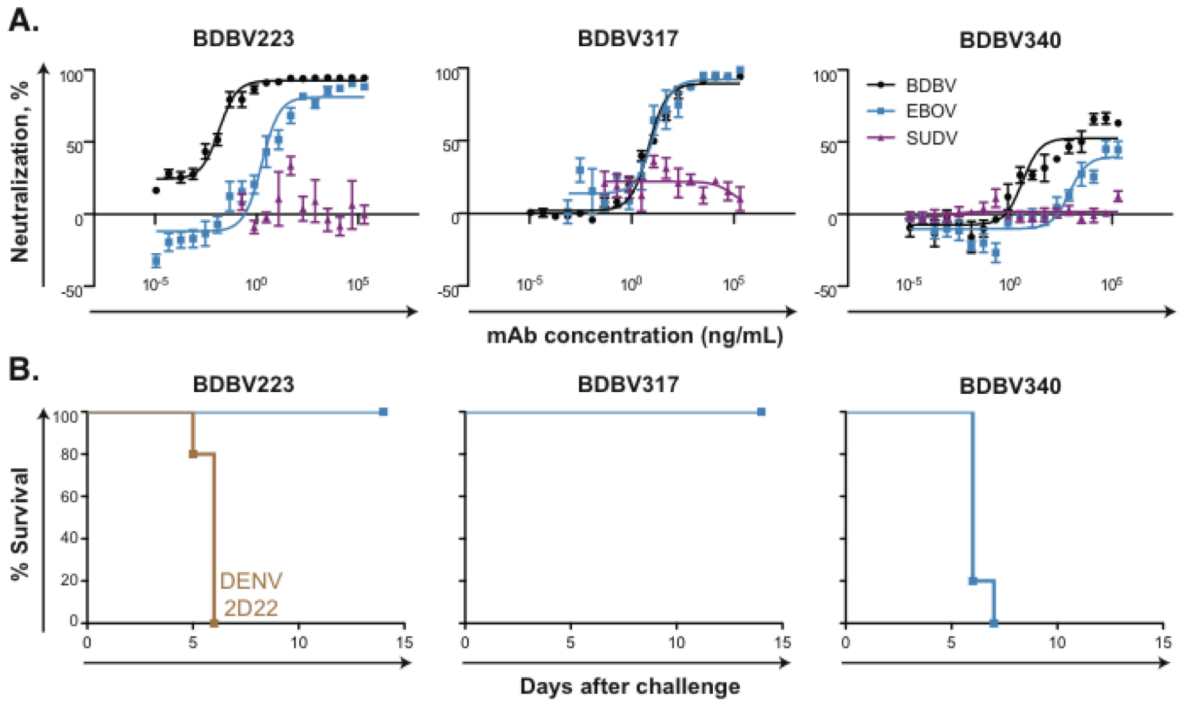

Figure 25. Neutralizing and protective activity of Group 3B cross-reactive mAbs. (A) Neutralization activity of BDBV223, BDBV317 and BDBV340 against BDBV, EBOV, and SUDV. (B) Survival of EBOV inoculated mice treated with Group 3B neutralizing mAbs. Groups of 5 mice per group were injected with individual mAbs by the intraperitoneal route 1 day after EBOV challenge, using 0.1 mg of individual mAb. Animals treated with dengue virus-specific human mAb DENV 2D22 served as controls.

To determine the therapeutic activity of these cross-neutralizing Abs, we tested these three antibodies in mice. Seven week-old BALB/c mice received 100 µg of antibody by the IP route 1 day after inoculation with 1,000 PFU of mouse-adapted EBOV, strain Mayinga (Bray et al., 1998). Both BDBV223 and BDBV317 fully protected mice from lethal challenge with heterologous species of EBOV (**Figure 25B**). We did not observe a protective effect in mice receiving treatment with BDBV340 or dengue-specific antibody 2D22 (**Figure 25B**).

There are several neutralizing mAbs that bind to the base region of the filovirus GP, including two chimerized murin-origin antibodies from the ZMapp^{TM} cocktail (c2G4 and c4G7) (Qiu et al., 2011; Qiu et al., 2012b), the human phage-display library-derived mAb KZ52 (Maruyama et al., 1999), and the murine SUDV-specific mAb 16F6 (Dias et al., 2011a). The epitopes bound by these mAbs were defined crystallographically (KZ52 and 16F6) (Dias et al., 2011a; Lee et al., 2008a), by negative-stain single-particle EM (c2G4 and

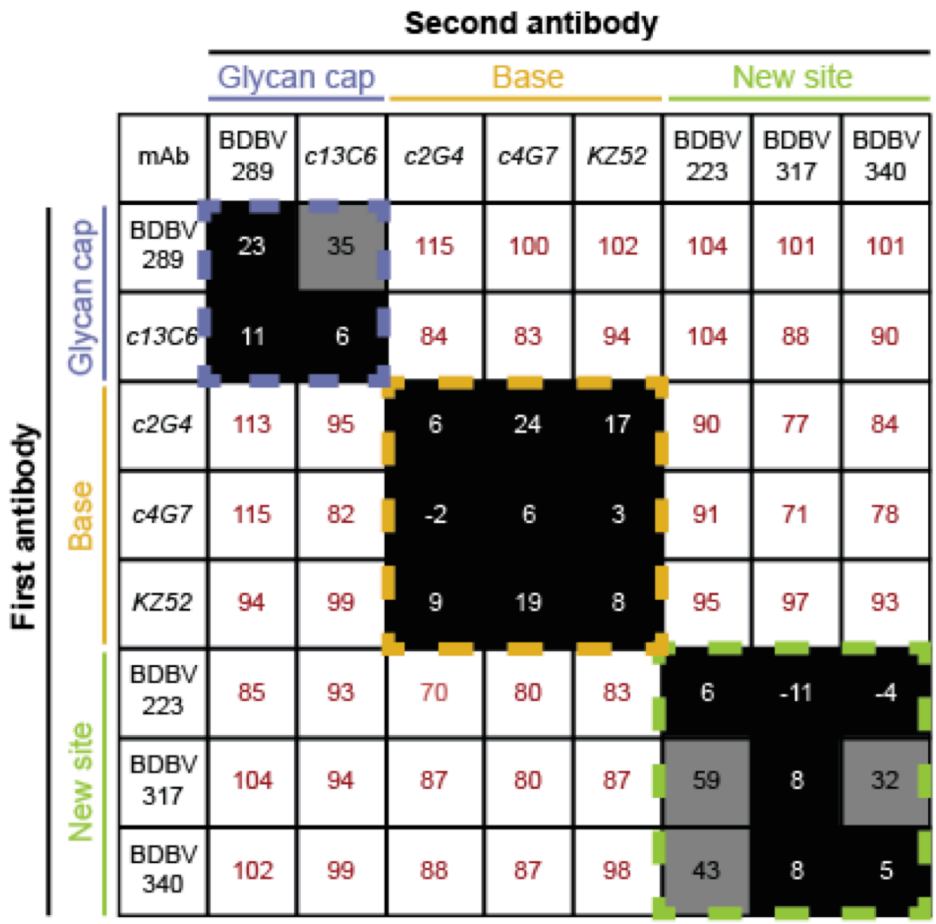

Figure 26. Cross-reactive neutralizing antibodies from Group 3B bind a unique region on GP surface. Data from competition binding assays using BDBV223, BDBV317 and BDBV340; antibodies from ZMapp cocktail (c2G4, c4G7 and 13C6) and previously isolated human antibodies KZ52 and BDBV289. Numbers indicate the percent binding of the second mAb in the presence of the first mAb, compared to binding of second mAb alone. MAbs were judged to compete for the same site if maximum binding of the second mAb was reduced to <30% of its un-competed binding (black boxes with white numbers). MAbs were considered non-competing if maximum binding of the second mAb was >70% of its un-competed binding (white boxes with red numbers). Grey boxes with black numbers indicate an intermediate phenotype (between 30 and 70% of un-competed binding).

c4G7) (Murin et al., 2014), or by alanine-scanning mutagenesis (KZ52, KZ52, c2G4, and c4G7) (Davidson et al., 2015), and mapped to the GP1/GP2 interface, in the vicinity of the heptad repeat 1 (HR1) region.

To determine whether BDBV223, BDBV317, and BDBV340 compete for binding with these *Ebolavirus*-specific mAbs, I performed quantitative competition-binding assay using an Octet biosensor (**Figure 26**). I also included in this analysis a previously isolated potently neutralizing human mAb (BDBV289) that recognizes the glycan cap (**Figure 23**) as well as

the glycan cap-specific mAb c13C6 from the ZMapp^{TM} cocktail (Wilson et al., 2000). As expected, the glycan cap-specific mAbs (c13C6 and BDBV289) and the base region-binding mAbs (KZ52, c2G4, and c4G7) segregated into two independent competition-binding groups (**Figure 26**). BDBV223, BDBV317, and BDBV340 did not compete with either glycan-cap specific mAbs or base region-binding mAbs, suggesting that thesse new mAbs target a unique antigenic region on the GP surface (**Figure 26**).

Electron microscopy studies of cross-reactive mAbs from Group 3B

To determine the location of the cross-reactive antigenic site on the GP base targeted by these human mAbs, we performed negative-stain single-particle EM studies in collaboration with Andrew Ward's group. The EM class averages clearly showed that BDBV223, BDBV317, and BDBV340 each bind to the bottom of GP, in the canonical heptad repeat 2 (HR2) domain near the membrane proximal external region (MPER) (**Figure 27A**). Overlaying a class average of BDBV223 Fab bound to BDBV GP (**Figure 27B**) over a class average of c13C6 Fab:c4G7 Fab bound to EBOV GP (**Figure 27C**) showed that BDBV223, and the two other new mAbs bound more virion proximal on the GP, well below the epitope of the mAb c4G7 site of vulnerability at the GP1/GP2 interface (**Figure 27D**). Measurements of the distance from the bottom of the GP globular head to the mid-point of the Fab in the class averages showed a distance of ~60 Å, which corresponds to the length of the HR2 region previously crystalized as post-fusion GP2 (PDBID 1EBO) (**Figure 27E**). Three BDBV317 Fabs can be seen in the class average images, indicating that three mAbs can bind simultaneously to the HR2/MPER region, which lies in a close proximity to the viral membrane (**Figure 27A**). In Chapter III, I described species-specific neutralizing human

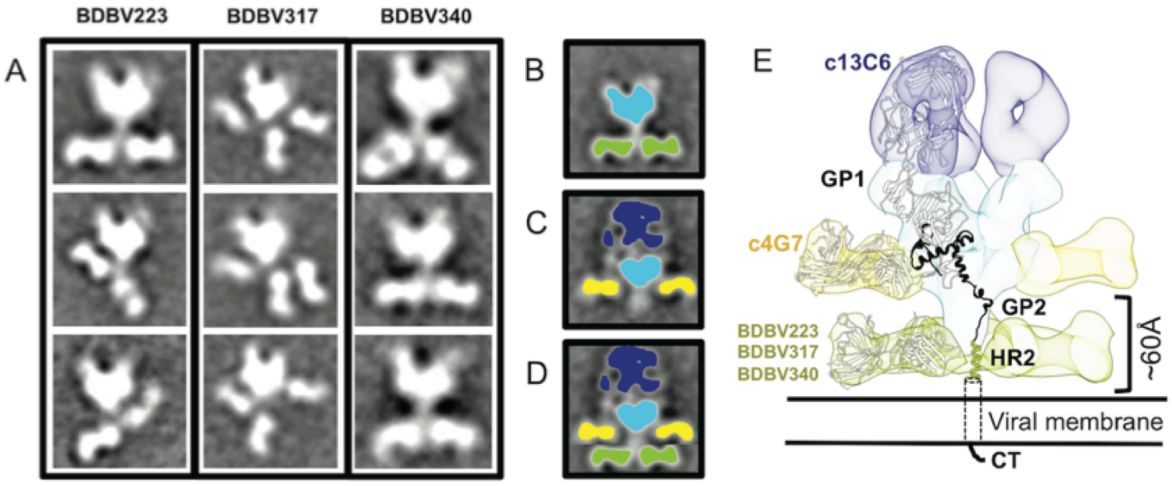

Figure 27 Cross-reactive neutralizing antibodies from Group 3B bind near the membrane proximal region of GP (A) Representative negative stain class averages of antibodies that bind GP2 exclusively in the membrane proximal region. Complexes are of BDBV Fabs bound to BDBV GPdMuc. (B) A class average of BDBV GPdMuc bound to BDBV223 demonstrates the location of each component, with the core GP colored blue and the Fabs in green. Crystal structures of GPdMuc (PDBID 3CSY) and a representative Fab (PDBID 3CSY) are overlaid on their corresponding region in the class average. (C) A class average of c13C6 Fab:c4G7 Fab bound to EBOV GPdTM (Top, with c13C6 in dark blue, c4G7 in yellow and GP core in light blue. (D) Overlaying a class average of c13C6 Fab:c4G7 Fab bound to EBOV GPdTM (Top, with c13C6 in dark blue, c4G7 in yellow and GP core in light blue) over a class average of BDBV223 Fab bound to BDBV GPdTM (with BDBV223 in green and GP core in light blue), demonstrates that BDBV223 binds significantly lower down on GP, well below the epitope of the c4G7 site of vulnerability at the GP1/GP2 interface. (E) A model of the c13C6 Fab:c4G7 Fab bound to EBOV GPdTM is shown with the relative location of BDBV223 Fab. Measurements of the distance from the bottom of the GP core to the mid-point of the Fab in the class averages showed a distance of ~60A, which corresponds to the length of the HR2 region previously crystalized as post-fusion GP2 (PDBID 1EBO).

mAbs that bound the BDBV GP near the MPER region and competed for binding with cross-reactive mAbs BDBV223, BDBV317, and BDBV340, although their epitopes were not determined (**Figure 21, 22**). Also, a previous study described generation of a murine cross-reactive non-neutralizing mAb to the HR2/MPER region (15H10) (Yu et al., 2006). Therefore, HR2 and MPER regions are complex major antigenic sites containing species-specific, cross-reactive as well as neutralizing and non-neutralizing epitopes.

Analysis of GP residues required for mAb cross-reactivity and neutralization

To define the epitope of cross-reactive human mAbs more precisely, we collaborated with Ben Doranz's group at Integral Molecular and tested the binding of BDBV223, BDBV317, and BDBV340 or the ZMapp™ antibody c4G7 to individual GP members of an

alanine-scan mutant library of EBOV GP. Several critical residues were identified previously for c4G7, including D552 in the internal fusion loop and C556, which is part of the HR1 (Davidson et al., 2015). Consistent with the EM data, we identified critical residues in GP2 for BDBV223, BDBV317, and BDBV340 that spanned the C-terminal part of HR2 and N-terminal part of the MPER (**Figure 28A**). A single critical residue in HR2 was identified for BDBV340 (D624), and one residue in MPER was identified for BDBV317 (K633). Two critical residues were identified for BDBV223 (D624 and D632) (**Figure 28A**).

The HR2 α-helix ends at residue D632 (Malashkevich et al., 1999; Weissenhorn et al., 1998), indicating that HR2/MPER peptides might adopt an α-helical conformation that is recognized by the *Ebolavirus* cross-reactive mAbs. To determine whether BDBV223, BDBV317, or BDB340 can recognize a linear conserved epitope in HR2/MPER, we synthesized peptides spanning the GP amino acids 620-635 in the HR2/MPER of three virus species (designated peptides BDBV2, EBOV2, and SUDV2) as well as a control peptide from the N-terminus of HR2 (amino acids 599-613), designated the BDBV1 peptide. I determined that BDBV223, BDBV317, and BDBV340 recognize BDBV2 peptide containing the essential residues determined by alanine-scanning mutagenesis but not the negative control BDBV1 peptide from HR2, as expected (**Figure 28B**). While BDBV223 bound to BDBV2, EBOV2, and SUDV2 peptides, BDBV317 and BDBV340 recognized only BDBV2 and EBOV2 peptides (**Figure 28B**). Interestingly, I noticed similarities between the extent of binding of the three mAbs to the HR2/MPER peptides (**Figure 28B**) and their neutralization potencies *in vitro* (**Figure 25B**). BDBV317 bound equally well to BDBV2 and EBOV2 peptides and neutralized BDBV and EBOV with the same potency. BDBV223 and BDBV340 bound better to BDBV2 peptide, and the same antibodies neutralized BDBV with higher potency than EBOV (**Figure 25B**).

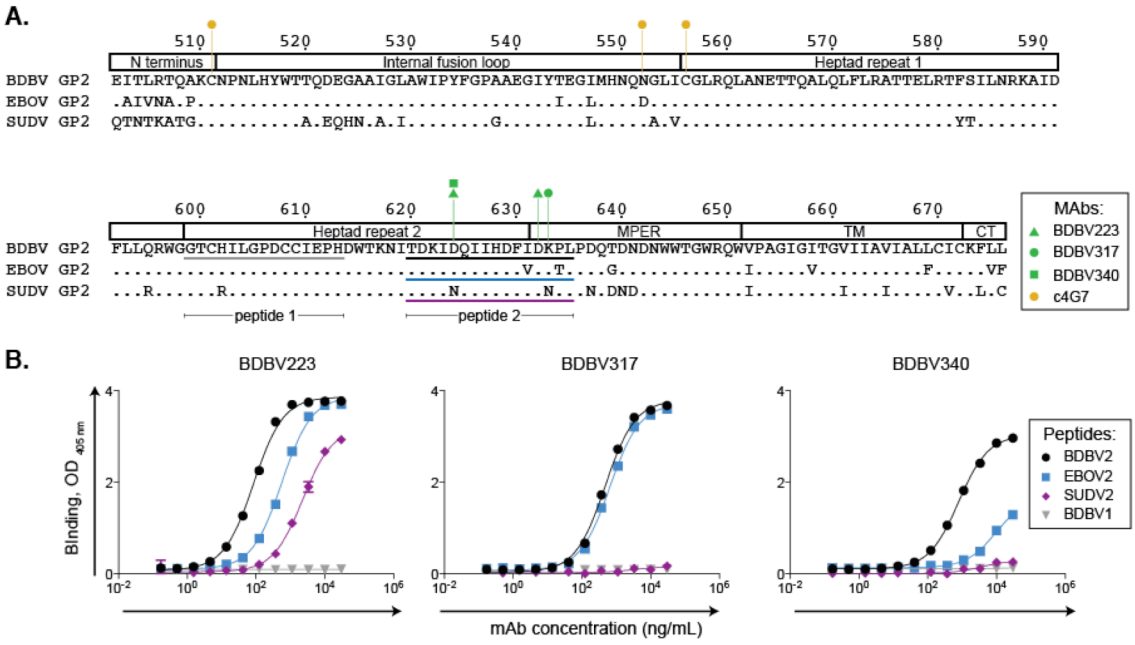

C.

EC50 (ng/mL) for binding of indicated mAb				
Peptide	Sequence	BDBV223	BDBV317	BDBV340
BDBV2	^{620}TDKIDQIIHDFIDKPL^{635}	85	477	791
EBOV2	----------V--T-	558	653	9,668
SUDV2	----N--------N--	2,256	>	>
BDBV2A	----------V----	125	887	4,190
BDBV2B	----------T-	812	15,677	3,628
BDBV2C	----N----------	18,370	>	>
BDBV2D	----------N--	73	>	253

Figure 28. Structural and functional analysis of GP residues important for mAb cross-reactivity and neutralization. (A) Sequence alignment of GP2 from the BDBV, EBOV and SUDV. The numbers above the sequence correspond to the amino acid position in GP. Amino acids identical to BDBV are indicated by dots. Color-coded shapes indicate the position of residues at which alanine substitutions disrupts mAbs binding, as determined by alanine-scanning mutagenesis. BDBV1, BDBV2, EBOV2 and SUDV2 peptide sequences are indicated by grey, black, blue and purple lines, respectively. (B) Binding of BDBV223, BDBV317 and BDBV340 to BDBV1, BDBV2, EBOV2 and SUDV2 peptides. (C) Binding or BDBV223, BDBV317 and BDBV340 to the panel of chimeric BDBV peptides

To determine the basis of mAb cross-reactivity to multiple *Ebolavirus* GPs and peptides, we synthesized a panel of chimeric BDBV peptides containing polymorphic residues from EBOV or SUDV. There are two amino acid differences between BDBV2 and EBOV2 peptides (at residues 631 and 634), located in the C-terminus of the peptide (**Figure**

28C). To identify polymorphisms responsible for the enhanced binding of BDBV223 to BDBV2 peptide, we synthesized two chimeric BDBV peptides with single substitutions at residues 631 or 634 (designated peptides BDBV2A and BDBV2B). While BDBV223 bound equally well to BDBV2 and BDBV2A peptide, it bound relatively weakly to the BDBV2B peptide, suggesting that the P634T substitution in BDBV2B peptide is responsible for reduced binding of BDBV223 to the EBOV2 peptide (**Figure 28C**). We also synthesized chimeric BDBV2C and BDBV2D peptides to introduce two SUDV substitutions at residues 624 and 633. While both BDBV223 and BDBV317 bound equally well to BDBV2D and BDBV2 peptides, they failed to recognize the BDBV2C peptide, suggesting that the N624 residue is required for neutralization of SUDV by MPER/HR-specific mAbs. To investigate the role residue D624 in the context of a live filovirus, we constructed a recombinant BDBV bearing D624N mutation, which was found to be completely resistant to BDBV223 but sensitive to BDBV317 (**Figure 29A**).

We passaged the chimeric filovirus with BDBV GP (Ilinykh et al., 2016) in the presence of HR2/MPER-specific mAbs and generated antibody escape mutant viruses for mAbs BDBV223 and BDBV317. For BDBV223, an isolate with a P634H mutation in the MPER was identified, and for BDBV317 an isolate with a K633R mutation in the MPER was identified (**Figure 29B**). We found that while the BDBV223 escape mutant was resistant to neutralization by both BDBV223 and BDBV317, BDBV223 was able to neutralize the BDBV317 escape mutant (**Figure 29B**). This finding is consistent with the results from the alanine-scanning and peptide ELISA binding experiments, in which the K633 residue was identified as a critical residue only for BDBV317 (**Figure 28A**), Also, BDBV317, but not BDBV223, failed to bind in ELISA to the BDBV3D peptide with a K633N substitution (**Figure 28C)**.

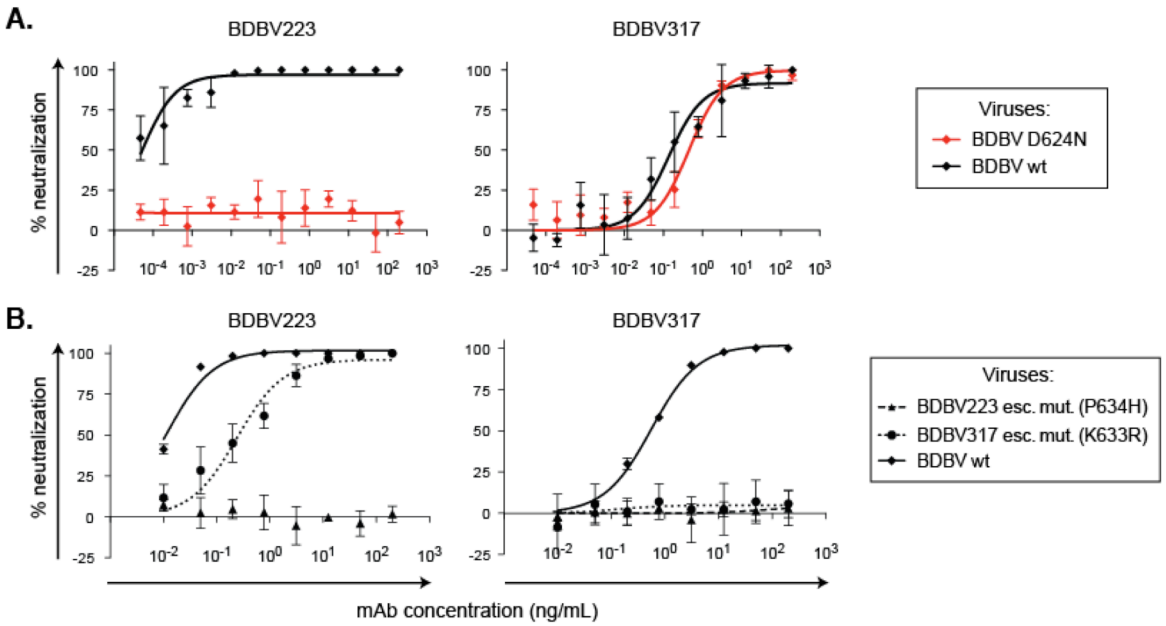

Figure 29. Neutralization activity of Group 3B mAbs against recombinant BDBV isolate and escape mutants. (A) Neutralization activity of BDBV223 or BDBV317 against wild-type BDBV (diamonds, black curves) or a recombinant BDBV D624N isolate (diamonds, red curves). (B) Neutralization activity of BDBV223 or BDBV317 against wild-type BDBV (diamonds, straight curves), BDBV223 escape mutant (triangles, dashed curves), or BDBV317 escape mutant (circles, dotted curves).

Discussion

In this chapter, I describe three human cross-reactive antibodies from Group 3B that target a new antigenic region near the MPER of EBOV GP. These antibodies do not compete with therapeutic antibodies used in the past to treat EBOV infection, suggesting that these MPER-specific mAbs could be used to design a new universal antibody therapeutic cocktail against multiple species of viruses causing *Ebolavirus* infection. Alternatively, the mAbs might be beneficial to include in existing experimental therapeutic antibody cocktails to increase the potency and breadth of those combinations. Although these mAbs are the first reported neutralizing antibodies directed to the MPER of filoviruses, the MPER in the GP of enveloped viruses increasingly is recognized as an important region for recognition by broad and potent human mAbs. Several mAbs that neutralize a broad

range of HIV strains bind conserved epitopes in the HIV gp41 MPER (Muster et al., 1993; Zwick et al., 2001). The identification of potent HIV MPER-specific mAbs has facilitated important progress in the effort to design HIV vaccines rationally using antigens designed to induce such mAbs (Montero et al., 2008). Neutralizing mAbs that recognize the influenza hemagglutinin surface protein stem region (Corti et al., 2011; Ekiert et al., 2009; Sui et al., 2009) also have simulated research into the possibility of a universal influenza vaccine. Here, I report structural and functional information about conserved epitopes in the MPER of EBOV GP that can be used to inform the development of an MPER-based EBOV vaccine effective against multiple filoviruses.

Materials and Methods

Human mAb and Fab expression and purification

Human hybridoma cell lines were expanded in post-fusion medium, as previously described (Flyak et al., 2015). HiTrap Protein G or HiTrap MabSelectSure columns were used to purify antibodies from filtered supernates. Fab fragments were generated by papain digestion, as described previously (Flyak et al., 2015).

Expression and purification of filovirus GPs

Recombinant GP ectodomains containing the mucin-like domain (GPΔTM) or lacking residues 312–463 of the mucin-like domain (GPΔmuc) (Lee et al., 2009; Lee et al., 2008b) were produced by transfection of Drosophila Schneider 2 (S2) cells with modified pMTpuro vectors, followed by stable selection of transfected cells with 6 μg/mL puromycin. Secreted GP ectodomain expression was induced with 0.5 mM $CuSO_4$ for 4 d. Proteins were engineered with a modified double strep tag at the C terminus (enterokinase cleavage site

followed by a strep tag/linker/strep tag) to facilitate purification using Strep-Tactin resin (Qiagen). Proteins were purified further by Superdex 200 (S200) SEC in 10 mM Tris and 150 mM NaCl, pH 7.5 (1× TBS).

Screening and half maximal effective concentration (EC_{50}) ELISA binding analysis

Soluble forms of the full-length extracellular domain of BDBV, EBOV, SUDV or MARV GPs or the sGP forms were coated overnight onto 384-well plates at 1 μg/mL. For screening ELISA, 10 μL of supernate from a well of a tissue-culture plate were transferred to each well of a 384-well ELISA plate. For EC_{50} binding analysis by ELISA, purified antibodies were applied to the plates at a concentration range of 30 μg/mL to 170 ng/mL, using three-fold serial dilutions. The presence of antibodies bound to the GP was determined using goat anti-human IgG alkaline phosphatase conjugate and p-nitrophenol phosphate substrate tablets, with optical density read at 405 nm after 120 minutes. A non-linear regression analysis was performed on the resulting curves using Prism version 5 (GraphPad) to calculate EC_{50} values.

Antibody neutralization experiments

All work with filoviruses, including the chimeric filoviruses, was performed in the BSL-4 facility of the Galveston National Laboratory. Antibody neutralization assays were performed against the recombinant EBOV expressing green fluorescent protein from an added gene (Towner et al., 2005) and its derivatives in which GP was replaced with its counterpart from BDBV (strain 200706291 Uganda) or SUDV (strain 200011676 Gulu) (Ilinykh et al., 2016) to which we refer in Results as EBOV, BDBV and SUDV for simplicity. The assays were performed in a high-throughput format, as previously described (Ilinykh et al., 2016).

Generation of recombinant BDBV with the D624N mutation

To introduce the D624N mutation in BDBV GP of the chimeric filovirus used in the study (Ilinykh et al., 2016) the pEBOwtΔBamHI-SbfI,AscI-PspOMI subclone of the full-length clone encoding the viral genome(Ilinykh et al., 2016) was mutagenized using the QuikChange site-directed mutagenesis kit (Stratagene). Then the ApaI-SacI fragment of the subclone, which includes the mutated GP, was used to replace the corresponding fragment of the chimeric filovirus full-length clone. The mutagenized chimeric virus was recovered as previously as described (Lubaki et al., 2013).

Generation and testing of antibody escape filovirus mutants

To generate escape mutants, 100 PFU of recombinant chimeric EBOV with GP derived from BDBV were combined with 2-fold dilutions of mAbs starting at 200 µg/mL in U-bottom 96-well plates and incubated for 1 hr at 37°C. Mixtures were placed on Vero-E6 cell monolayer clutures in 96-well plates and incubated for 1 hr. Supernatants were removed, fresh mAbs were added at the same concentrations in 200 µL of MEM supplemented with 2% FBS, and plates were incubated for 7 days at 37°C. Viruses that replicated in the presence of the highest concentrations of mAbs, as determined by UV microscopy, were collected. 20 µL aliquots were incubated with 2-fold dilutions of mAbs starting at 200 µg/mL, and viruses were propagated in the presence of mAbs as above. The procedure was repeated once more with mAb dilutions starting at 400 µg/mL. Viruses that replicated at the highest mAb concentrations were amplified in Vero-E6 cell culture monolayers in 24-well plates in the presence of mAbs at 200 µg/mL for 7 days. Cells were used for isolation of RNA using TRIzol reagent, and GP genes were PCR-amplified and sequenced. To determine susceptibility of the isolated escape mutants to mAbs, 100 PFU of the viruses in MEM supplemented with 2% FBS in triplicate were combined in U-bottom 96-well plates with 8 to 12 two-fold dilutions of mAbs, staring at 200 µg/mL, in total volumes of 50 µL, and

incubated for 1 hr at 37°C. The virus/antibody mixtures then were placed in triplicate Vero-E6 cell culture monolayers in 96-well plates, incubated for 1 hr at 37°C, washed with MEM, overlaid with 200 µL of MEM containing 2% FBS and 0.8% methylcellulose, and incubated for 48 hrs at 37°C. Plates were fixed with 10% phosphate-buffered formalin (Fisher) and taken out of the BSL-4 facility according the UTMB BSL-4 standard operating procedures. Plaques were counted using a fluorescence microscope.

Biolayer interferometry competition binding assay

Competition-binding studies using biolayer interferometry and biotinylated EBOV GP (EZ-link® Micro NHS-PEG_4-Biotinylation Kit, Thermo Scientific #21955) (5 µg/mL) were performed on an Octet RED biosensor (ForteBio Menlo Park, CA), as described previously (Flyak et al., 2015). In brief, the antigen was immobilized onto streptavidin-coated biosensor tips. After a brief washing step, biosensor tips were immersed first into the wells containing primary antibody at a concentration of 100 µg/mL and then into the wells containing competing mAbs at a concentration of 100 µg/mL. The percent binding of the competing mAb in the presence of the first mAb was determined by comparing the maximal signal of competing mAb applied after the first mAb complex to the maximal signal of competing mAb alone.

Electron microscopy

To determine the epitope of HR2/MPER-directed mAbs, BDBV223, 317, or 340 Fabs were generated as described above and added in 10M excess to BDBV GPΔmuc and allowed to bind overnight at 4°C (Flyak et al., 2016). Complexes were subsequently purified by size exclusion chromatography on an S200 Increase column (GE) and stained as previously described (Murin et al., 2014). Particles were visualized using an FEI Tecnai

Spirit electron microscope operating at 120kV and images were collected on a TVIPS TemCam-F416 (4k x 4k) CCD camera using Leginon (Suloway et al., 2005) with the following settings: magnification of 52,000X that resulted in a pixel size of 2.05Å at the specimen plane, a constant defocus of -1.00 µm and an electron dosage of ~30e^-/Å^2. Images were processed using the Appion platform (Lander et al., 2009). Particles were picked using DoG Picker (Voss et al., 2009) stacks were created and 2D reference-free class averages were generated using iterative MRA-MSA (van Heel et al., 1996). For all complexes, there was a strong bias toward side-views. Further, the region containing the HR2/MPER epitope in our soluble GP constructs is flexible, as indicated by the variety of positions that bound Fabs adopted in the class averages. Therefore, our data was refractory to a reconstruction, although class averages could be compared to previous class averages of known complexes to determine the spatial location of the epitope on GP.

Epitope mapping using an EBOV GP alanine-scan mutation library

Epitope mapping was carried out as described previously[8]. Comprehensive high-throughput alanine scanning ('shotgun mutagenesis') was carried out on a full-length EBOV GP expression construct (based on the Yambuku-Mayinga variant GP sequence), mutagenizing GP residues 33-676 to create a library of clones, each representing an individual point mutant. Residues were changed to alanine (with alanine residues changed to serine). The resulting library, covering 641 of 644 (99.5%) of target residues was arrayed into 384-well plates, one mutant per well, then transfected into HEK-293T cells and allowed to express for 22 hours. Cells, unfixed or fixed in 4% paraformaldehyde, were incubated with primary antibody then with an Alexa Fluor 488-conjugated secondary antibody (Jackson ImmunoResearch Laboratories, Westgrove, PA). After washing, cellular fluorescence was detected using the Intellicyt high throughput flow cytometer (Intellicyt, Albuquerque, NM). MAb reactivity against each mutant EBOV GP clone was calculated relative to wild-type

EBOV GP reactivity by subtracting the signal from mock-transfected controls and normalizing to the signal from wild-type GP-transfected controls.

Mutated residues within clones were identified as critical to the MAb epitope if they did not support reactivity of the test mAb but did support reactivity of other control EBOV mAbs. This counter-screen strategy facilitated the exclusion of GP mutants that were misfolded locally or that exhibited an expression defect. The detailed algorithms used to interpret shotgun mutagenesis data were described previously (Davidson and Doranz, 2014)

Peptide synthesis and purification

Peptides were synthesized using standard Fmoc solid-phase methods on a Peptide Machines Discovery-4 synthesizer on rink resin (Atherton, 1988; Bodanszky and Bodanszky, 1994; Fields and Noble, 1990; Grant, 1992; Stuber et al., 1989). All coupling reactions were performed with ten-fold excess (vs. load capacity of the resin) of activated amino acid (Aapptec or Advanced Chemtech), using FMOC amino acids/HBTU/HoBt/DIEA (1:1:1:2.5) in DMF for 60 minutes. Deprotection of the FMOC group was accomplished in 20% v/v piperidine diluted in DMF for 30 minutes. Peptides used for ELISA experiments were acetylated at the N-terminus by reaction with 1:1:2 v/v acetic anhydride:DIEA:DMF. Peptides used for biolayer interferometry assays were functionalized with PEG_6-biotin (Quanta BioDesigns) at the N-terminus.

The peptides were cleaved by exposure to a 90:5:3:2 v/v mixture of trifluoroacetic acid, thioanisole, ethanedithiol, and anisole for two hours. Peptides were precipitated by addition of cold diethyl ether, lyophilized and purified by reverse-phase HPLC (Waters Prep LC 4000) equipped with a Waters 2487 detector and C18 column. Final purified fractions were lyophilized until further use. Isolation of the target peptide was confirmed by MALDI mass spectrometry.

CHAPTER V

SUMMARY AND FUTURE DIRECTIONS

"If Ebola can change, we can change, too, and maybe faster than Ebola"

Richard Preston, *Inside the Ebola Wars, The New Yorker*

Thesis summary

Filoviruses cause a highly lethal disease in humans, with untreated mortality rates approaching 90%. Multiple experimental strategies are being investigated for treatment of *Ebolavirus* infection. Among these drug candidates, antibody combinations exceed the efficacy and treatment window of other experimental therapeutics described so far (Qiu et al., 2014). The key components of such therapeutic cocktails contain antibodies that bind to neutralizing epitopes on the GP surface. Most of our knowledge about neutralizing antibody responses against filovirus infections has come from studies of murine mAbs that recognize EBOV GP. As a result, there is little information available about human antibody responses to EBOV infection, and we have very limited knowledge about neutralizing antibodies against other filoviruses, such as BDBV, SUDV and MARV.

I began studies of human antibody responses to filovirus infection by generating a large panel of MARV-specific human mAbs from B cells of an individual who contracted MARV infection in 2008 following exposure to fruit bats in the Python Cave in Queen Elizabeth National Park in Uganda (Chapter II). Among the 39 MARV GP-specific mAbs, we found 18 mAbs that exhibited neutralization activity against chimeric vesicular stomatitis virus with MARV GP from the Uganda strain on its surface (VSV/GP-Uganda). All VSV/GP-Uganda neutralizing Abs displayed unique binding patterns in ELISA and blocked the

binding of each of the other neutralizing Abs to the antigen in an Octet competition experiment. These data suggested that MARV-specific neutralizing Abs bind a single antigenic region on the GP surface.

To determine the location of the antigenic region targeted by MARV neutralizing Abs, we performed negative stain single-particle EM studies using antibody-GP complexes. We observed that all of the neutralizing antibodies bind to MARV GP at or near the predicted region of the NPC1 receptor-binding site. As all neutralizing Abs segregated into a single competition group and bound the MARV GP at the NPC1 receptor-binding site, I proposed that blocking of MARV GP binding to NPC1 is the principal mechanism of MARV neutralization by naturally-occurring human Abs.

To determine whether MARV-specific human Abs could also bind in a cross-reactive manner to the EBOV GP receptor-binding site, I performed ELISAs using EBOV GP. I found that three of the MARV neutralizing Abs recognized the EBOV GPcl that lacked the glycan cap and mucin-like domain. However, structural analysis of MARV and EBOV GPs revealed that the glycan cap and mucin-like domain likely obscure the receptor-binding domain in EBOV. In agreement with the structural data, MARV neutralizing Abs did not exhibit detectable neutralization activity against EBOV or VSV/EBOV.

While I was not able to generate pan-filovirus neutralizing Abs using B cells from a MARV survivor, I decided to test the idea that functionally important regions of GP can be conserved between multiple species from the *Ebolavirus* genus. The serum of individuals who survived BDBV, EBOV, or SUDV infections contained *Ebolavirus* cross-reactive antibodies, suggesting that conserved neutralizing epitopes can be found on the surface of *Ebolavirus* GP. In Chapter III, I describe the isolation and characterization of a large panel of human antibodies using B cells obtained from survivors of a BDBV outbreak.

I found that 57 of 90 mAbs generated from B cells of BDBV survivors recognized heterologous EBOV GPs. Some of the isolated cross-reactive mAbs also neutralized multiple *Ebolavirus* species. The majority of cross-reactive mAbs neutralized BDBV and EBOV, but I also isolated two antibodies that displayed neutralizing activity against representatives of three *Ebolavirus* species – BDBV, EBOV, and SUDV. We tested two cross-neutralizing mAbs in mice and guinea pigs and showed that they protected animals from lethal challenge with a heterologous species of EBOV. We demonstrate that glycan cap-specific mAbs exhibit very potent neutralizing activity, and they recognize diverse epitopes within this major antigenic region.

In Chapter IV, I describe three cross-reactive mAbs isolated from BDBV survivors that bind to a new antigenic site in the HR2 region near the EBOV GP MPER. I found that these cross-reactive HR2/MPER-specific antibodies do not compete with previously isolated EBOV-specific mAbs that recognize other regions in the GP, such as the glycan cap, base, or mucin-like domain. We used a series of protein, virologic, and structural biology studies to define the GP residues important for HR2/MPER mAb cross-reactivity and neutralization.

Collectively, findings presented in this thesis enhance our understanding of human antibody responses to filovirus infection. The new knowledge gained from this study could help develop broad-spectrum protective mAbs and detection capabilities for existing filoviruses, and new viral strains that may emerge in the future. Information gathered from this thesis reveals mechanisms of filovirus neutralization by human mAbs and provides information about conserved epitopes on GP that can be used to inform the development of vaccines effective against multiple filoviruses.

Future directions

Bispecific antibodies as pan-filovirus therapeutic agents

In Chapter II, I described a large panel of MARV neutralizing mAbs isolated from B cells of an individual who contracted MARV infection. Among MARV-specific neutralizing Abs, I found several that recognize the EBOV receptor-binding site (**Figure 15A**), suggesting that the binding site for the essential intracellular receptor NPC1 could be an attractive target for broadly neutralizing Abs. However, the glycan cap and mucin-like domain obscure the receptor-binding site in EBOV GP, complicating the development of pan-filovirus Ab treatment. Protein engineering approaches could be employed to deliver neutralizing Abs that bind to the filovirus receptor-binding site to late endosomes or lysosomes, where the NPC1-binding site is unmasked by host proteases.

Bispecific Abs (bsAbs) combine specificities of two Abs and can simultaneously bind to different antigens or epitopes. The bsAbs have two heavy and two light chains, one each from two different Abs. The two Fab regions are directed against two antigens or epitopes. While the generation of bsAbs in a practical and efficient manner has been a longstanding challenge, platforms have been developed that improve bsAb product homogeneity and yield (Labrijn et al., 2014; Lewis et al., 2014). For example, in a Fab-arm exchange method, two parental Abs containing single matching point mutations in the CH3 domain are mixed under permissive redox conditions to enable recombination of half-molecules (**Figure 30**). This method could be employed to generate pan-filovirus bsAbs. For this approach, a bsAb could be designed to contain variable domains for a human neutralizing Ab that binds to the conserved NPC1 receptor-binding site and an Ebolavirus cross-reactive Ab that binds to the glycan cap.

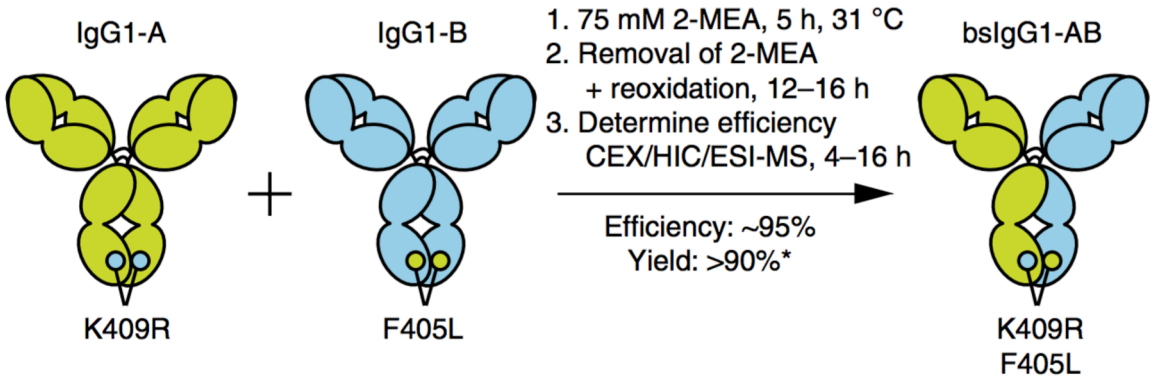

Figure 30. Generation of bsAbs by Fab-arm exchange method. IgG1 molecules containing matching point mutations, K409R and F405L in their CH3 domains are separately expressed and subjected to the controlled Fab-arm exchange protocol. *Yield may be lower when small volumes or low-concentration solutions are used. 2-MEA – 2-mercaptoethylamine, CEX – cation-exchange chromatography, HIC – hydrophobic interaction chromatography, ESI-MS – electrospray ionization mass spectrometry. Adapted from (Labrijn et al., 2014)

During the *Ebolavirus* infection, the cross-reactive glycan cap-specific Fab-fragment would bind to conserved epitopes on EBOV GP surface and deliver neutralizing Fab-fragment that binds to the receptor-binding site to endosomes where EBOV NPC1 receptor-binding site is exposed for Ab binding. Such a bsAb should display neutralizing activity against multiple MARV and EBOV species. Neutralization and protection experiments could be performed to test the inhibitory and protective effect of such bsAb.

Mechanisms of *Ebolavirus* neutralization by glycan cap-specific mAbs

In Chapter III, I highlight the neutralization and protective potencies of human glycan cap-specific antibodies. Glycan cap-binding mAbs might not neutralize well because host cathepsins remove this region during viral entry (Murin et al., 2014). However, several of the BDBV glycan cap-specific mAbs described in Chapter III exhibit very potent neutralizing activity and recognize diverse epitopes within this major antigenic site. Furthermore, a single glycan cap-specific neutralizing Ab, BDBV289, provides complete protection in EBOV-challenged guinea pigs. The mechanism used by glycan cap-binding mAbs to neutralize the

virus *in vitro* is unclear. While the amino acid sequence of the GP1 region is generally less well conserved than that of GP2 in viruses of diverse filovirus species, the five neutralizing glycan cap mAbs described in Chapter III target conserved residues, suggesting that these regions are important to the viral lifecycle. Therefore, these mAbs may inhibit some yet undefined function of the glycan cap.

The glycan cap-specific Abs could neutralize EBOV in several ways: by blocking virion attachment to cells, preventing virus internalization, or inhibiting GP cleavage by host cathepsins, which is required to unmask the NPC1 receptor-binding site. To test whether neutralizing Abs to the glycan cap interfere with virus attachment to host cells, the target Abs can be tested in pre-attachment neutralizing assays where mAbs are pre-incubated with virus or virus-like particles at 4°C before being inoculated onto cell monolayers (1 hour at 4°C). The virus or virus-like particles/antibody mixtures then can be placed onto cell culture monolayers and incubated for 1 hr at 4°C. After non-absorbed virus or virus-like particles are removed, cell monolayers can be overlaid with media contraining methylcellulose and incubated for 48 hrs at 37°C. Plaques can be counted using a fluorescence microscope.

The glycan cap-specific antibodies described here bind to sites distant from the putative cathepsin cleavage site (located at residue 190), so they are unlikely to interfere with GP cleavage. To test whether glycan-cap specific mAbs inhibit the proteolytic cleavage of EBOV surface protein, EBOV GP could be incubated with the mAbs for 1 hour at 37°C and then treated with cathepsins B and L for an additional hour. The cleavage of EBOV GP can be verified in western blot by the presence of a 19 kDa cleaved form of GP.

Mechanisms of *Ebolavirus* neutralization by HR2/MPER-specific mAbs

Multiple neutralizing mAbs bind to the GP base, including two of three murine-origin Abs from the ZMapp™ cocktail (c2G4 and c4G7) and the human neutralizing antibody obtained from a phage-display library (KZ52). The epitopes of these mAbs were mapped to a conformationally-sensitive region at the GP1/GP2 interface in the GP base. These GP1/GP2 interface-specific Abs might neutralize EBOV by blocking fusogenic rearrangement and membrane insertion by GP2, where the HR1 sequence in the pre-fusion GP2 (**GP2pre, Figure 31**) rearrange to form an unbroken α-helix (GP2extended), placing the GP2 internal fusion loop into the target membrane.

In Chapter IV, I describe three neutralizing human Abs (BDBV223, BDBV317 and BDBV340) that bind to a new antigenic region in the HR2/MPER region of GP2. We used a comprehensive alanine-scanning approach and identified critical residues in GP2 for these neutralizing Abs. The critical residues spanned the C-terminal part of HR2 region and the N-terminal part of the MPER which form an α-helix. Therefore, in contrast to GP1/GP2 interface-specific Abs that block the transition from GP2pre to GP2extended conformation, HR2/MPER-specific Abs might block the further rearrangement of GP2 from extended conformation to the six-helix bundle ($GP2_{6HB}$), where HR2 packs against trimeric HR2 coiled coil to form the six-helix bundle (**Figure 32**).

To define the residues in the HR2 α-helix required for binding by HR2/MPER-specific mAbs, crystallographic studies could be performed with cross-reactive mAbs complexed with either recombinant EBOV GP or HR2/MPER peptides. Comparison of crystal structures of neutralizing and protective mAbs (BDBV223 and BDBV317) with the structure of non-protective mAb BDBV340 could further inform the development of an HR2/MPER-based EBOV vaccine effective against multiple filoviruses.

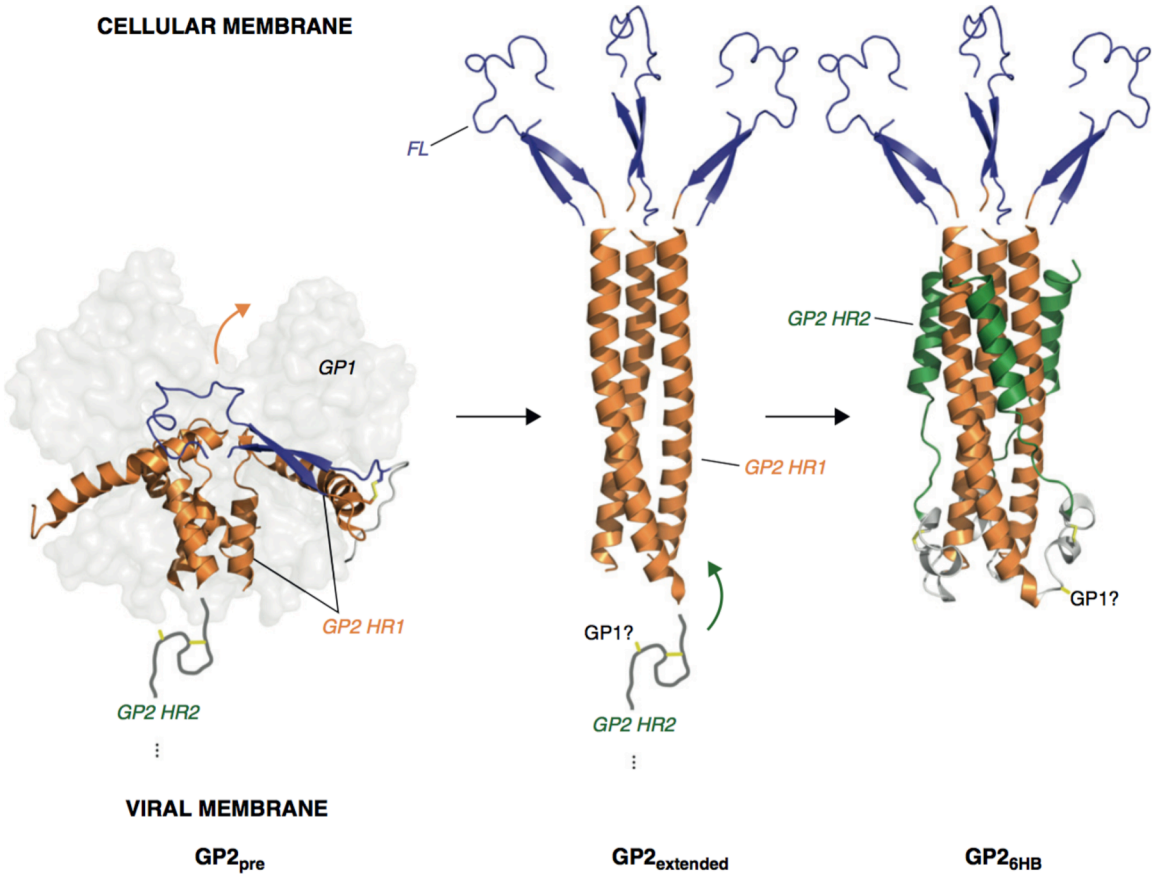

Figure 31. Proposed structural rearrangements in GP2 during entry. Structures from PDB ids: 3CSY (Lee et al., 2008a) and 1EBO (Weissenhorn et al., 1998). Fusion loops in GP2extended and $GP2_{6HB}$ are derived from the GP pre-fusion structure 3CSY, and their positions are indicated for illustration only. GP2extended is hypothetical. From (Miller and Chandran, 2012). GP1/GP2 interface-specific Abs likely neutralize EBOV by blocking the transition of GP2pre to GP2extended conformation. Functional and structural information presented in Chapter IV suggest that HR2/MPER-specific mAbs inhibit the $GP2_{6HB}$ formation.

A real-time assay for EBOV GP triggering and lipid mixing has been described (Spence et al., 2016). This system uses the VSV particles bearing EBOV GP, a fluorescent monomeric NeonGreen protein fused to EBOV phosphoprotein, and lipophilic dye DiD (1,1'-Dioctadecyl-3,3,3',3'-Tetramethylindodicarbocyanine), which is incorporated into the viral membrane. When incorporated into virions, DiD displays fluorescent self-quenching. Lipid mixing between viral and host membranes enables lateral diffusion of DiD dye, which yields a sharp increase in the fluorescent signal. Such real-time systems could be used to determine whether HR2/MPER-specific mAbs inhibit conformational rearrangements of GP2

that ultimately lead to the fusion of viral and host membranes. The HR2/MPER-specific mAbs could be tested in the presence or absence of GP1/GP2 interface-specific mAbs to investigate the type of interaction between mAbs that target two separate antigenic regions on the GP base (additive, synergistic, or antagonistic).

B cell repertoire diversities of filovirus-specific antibodies

High-throughput sequencing technologies can be used to explore Ab gene signatures in humans (Arnaout et al., 2011; Wu et al., 2010). For some neutralizing epitopes, the Ab repertoire is restricted to a limited set of Ab genes (Scheid et al., 2011). Convergent Ab gene rearrangement signatures of the dengue virus-specific B-cell population occur during the acute phase of dengue virus infection (Parameswaran et al., 2013). It is not known whether the limited number of neutralizing epitopes on EBOV or MARV GPs can serve as a constraint mediating the development of convergent Ab sequences that are specific to memory B-cell populations of filovirus survivors.

To analyze the Ab repertoire of filovirus survivors, total RNA could be extracted from PBMC samples of BDBV survivors and, after cDNA synthesis, PCR amplification could be performed with mixtures of primers designed to amplify antibody gene segments (Smith et al., 2009). The purified PCR products could be submitted for high-throughput sequencing using an Illumina platform. The resulting sequence data could be analyzed using the clonal lineage identification methods to identify filovirus-specific signatures in the B-cell repertoire of survivors. The phylogenic analysis could be performed using nucleotide sequences obtained from hybridomas expressing filovirus-specific neutralizing Abs to find sequence families for Ab somatic variants. Ab variants identified by high-throughput sequence analysis could be tested in a binding assays with MARV and EBOV GPs.

LIST OF PUBLICATIONS

1. Flyak AI, Ilinykh PA, Murin CD, Garron T, Shen X, Fusco ML, Hashiguchi T, Bornholdt ZA, Slaughter JC, Sapparapu G, Klages C, Ksiazek TG, Ward AB, Saphire EO, Bukreyev A, Crowe JE Jr. Mechanism of human antibody-mediated neutralization of Marburg virus. *Cell*. 2015 Feb 26;160(5):893-903.

2. Hashiguchi T, Fusco ML, Bornholdt ZA, Lee JE, Flyak AI, Matsuoka R, Kohda D, Yanagi Y, Hammel M, Crowe JE Jr, Saphire EO. Structural basis for Marburg virus neutralization by a cross-reactive human antibody. *Cell*. 2015 Feb 26;160(5):904-12.

3. Ilinykh PA, Shen X, Flyak AI, Kuzmina N, Ksiazek TG, Crowe JE Jr, Bukreyev A. Chimeric Filoviruses for Identification and Characterization of Monoclonal Antibodies. *J Virol.* 2016 Jan 27. pii: JVI.00101-16.

4. Flyak AI, Shen X, Murin CD, Turner HL, David JA, Fusco ML, Lampley R, Kose N, Ilinykh PA, Kuzmina N, Branchizio A, King H, Brown L, Bryan C, Davidson E, Doranz BJ, Slaughter JC, Sapparapu G, Klages C, Ksiazek TG, Saphire EO, Ward AB, Bukreyev A, Crowe JE Jr. Cross-Reactive and Potent Neutralizing Antibody Responses in Human Survivors of Natural Ebolavirus Infection. *Cell*. 2016 Jan 28;164(3):392-405

5. Bornholdt ZA, Ndungo E, Fusco ML, Flyak AI, Crowe JE Jr, Chandran K, and Saphire EO. Host-primed Ebola virus GP exposes a hydrophobic NPC1 receptor-binding pocket, revealing a target for broadly neutralizing antibodies. *mBio.* 2016 Feb 23: 7(1):e02154-15.

BIBLIOGRAPHY

(CDC), C.f.D.C.a.P. (2009). Imported case of Marburg hemorrhagic fever - Colorado, 2008. MMWR Morbidity and mortality weekly report *58*, 1377-1381.

Albarino, C.G., Shoemaker, T., Khristova, M.L., Wamala, J.F., Muyembe, J.J., Balinandi, S., Tumusiime, A., Campbell, S., Cannon, D., Gibbons, A.*, et al.* (2013). Genomic analysis of filoviruses associated with four viral hemorrhagic fever outbreaks in Uganda and the Democratic Republic of the Congo in 2012. Virology *442*, 97-100.

Alvarez, C.P., Lasala, F., Carrillo, J., Muniz, O., Corbi, A.L., and Delgado, R. (2002). C-type lectins DC-SIGN and L-SIGN mediate cellular entry by Ebola virus in cis and in trans. J Virol *76*, 6841-6844.

Arnaout, R., Lee, W., Cahill, P., Honan, T., Sparrow, T., Weiand, M., Nusbaum, C., Rajewsky, K., and Koralov, S.B. (2011). High-resolution description of antibody heavy-chain repertoires in humans. PLoS One *6*, e22365.

Atherton, E.C., L.R.; Sheppard, R.C. (1988). Peptide synthesis : Part 10. Use of pentafluorophenyl esters of fluorenylmethoxycarbonylamino acids in solid phase peptide synthesis. Tetrahedron *44*, 843-857.

Baize, S., Leroy, E.M., Georges-Courbot, M.C., Capron, M., Lansoud-Soukate, J., Debre, P., Fisher-Hoch, S.P., McCormick, J.B., and Georges, A.J. (1999). Defective humoral responses and extensive intravascular apoptosis are associated with fatal outcome in Ebola virus-infected patients. Nat Med *5*, 423-426.

Baize, S., Pannetier, D., Oestereich, L., Rieger, T., Koivogui, L., Magassouba, N.a.F., Soropogui, B., Sow, M.S., Keïta, S., De Clerck, H.*, et al.* (2014). Emergence of Zaire Ebola Virus Disease in Guinea. The New England journal of medicine.

Bale, S., Dias, J.M., Fusco, M.L., Hashiguchi, T., Wong, A.C., Liu, T., Keuhne, A.I., Li, S., Woods, V.L., Jr., Chandran, K.*, et al.* (2012). Structural basis for differential neutralization of ebolaviruses. Viruses *4*, 447-470.

Bausch, D.G., Nichol, S.T., Muyembe-Tamfum, J.J., Borchert, M., Rollin, P.E., Sleurs, H., Campbell, P., Tshioko, F.K., Roth, C., Colebunders, R.*, et al.* (2006). Marburg hemorrhagic fever associated with multiple genetic lineages of virus. N Engl J Med *355*, 909-919.

Bausch, D.G., Towner, J.S., Dowell, S.F., Kaducu, F., Lukwiya, M., Sanchez, A., Nichol, S.T., Ksiazek, T.G., and Rollin, P.E. (2007). Assessment of the risk of Ebola virus transmission from bodily fluids and fomites. J Infect Dis *196 Suppl 2*, S142-147.

Becquart, P., Wauquier, N., Mahlakoiv, T., Nkoghe, D., Padilla, C., Souris, M., Ollomo, B., Gonzalez, J.P., De Lamballerie, X., Kazanji, M.*, et al.* (2010). High prevalence of both

humoral and cellular immunity to Zaire ebolavirus among rural populations in Gabon. PLoS One *5*, e9126.

Beniac, D.R., Melito, P.L., Devarennes, S.L., Hiebert, S.L., Rabb, M.J., Lamboo, L.L., Jones, S.M., and Booth, T.F. (2012). The organisation of Ebola virus reveals a capacity for extensive, modular polyploidy. PLoS One *7*, e29608.

Bodanszky, M., and Bodanszky, A. (1994). The practice of peptide synthesis, 2nd, rev. edn (Berlin ; New York: Springer-Verlag).

Brauburger, K., Hume, A.J., Mühlberger, E., and Olejnik, J. (2012). Forty-five years of Marburg virus research. Viruses *4*, 1878-1927.

Bray, M., Davis, K., Geisbert, T., Schmaljohn, C., and Huggins, J. (1998). A mouse model for evaluation of prophylaxis and therapy of Ebola hemorrhagic fever. J Infect Dis *178*, 651-661.

Briand, S., Bertherat, E., Cox, P., Formenty, P., Kieny, M.P., Myhre, J.K., Roth, C., Shindo, N., and Dye, C. (2014). The international Ebola emergency. N Engl J Med *371*, 1180-1183.

Brochet, X., Lefranc, M.P., and Giudicelli, V. (2008). IMGT/V-QUEST: the highly customized and integrated system for IG and TR standardized V-J and V-D-J sequence analysis. Nucleic Acids Res *36*, W503-508.

Burton, D.R., Poignard, P., Stanfield, R.L., and Wilson, I.A. (2012). Broadly neutralizing antibodies present new prospects to counter highly antigenically diverse viruses. Science *337*, 183-186.

Carette, J.E., Raaben, M., Wong, A.C., Herbert, A.S., Obernosterer, G., Mulherkar, N., Kuehne, A.I., Kranzusch, P.J., Griffin, A.M., Ruthel, G.*, et al.* (2011). Ebola virus entry requires the cholesterol transporter Niemann-Pick C1. Nature *477*, 340-343.

Carroll, M.W., Matthews, D.A., Hiscox, J.A., Elmore, M.J., Pollakis, G., Rambaut, A., Hewson, R., Garcia-Dorival, I., Bore, J.A., Koundouno, R.*, et al.* (2015). Temporal and spatial analysis of the 2014-2015 Ebola virus outbreak in West Africa. Nature *524*, 97-101.

Carstea, E.D., Morris, J.A., Coleman, K.G., Loftus, S.K., Zhang, D., Cummings, C., Gu, J., Rosenfeld, M.A., Pavan, W.J., Krizman, D.B.*, et al.* (1997). Niemann-Pick C1 disease gene: homology to mediators of cholesterol homeostasis. Science *277*, 228-231.

Centers for Disease, C., and Prevention (2009). Imported case of Marburg hemorrhagic fever - Colorado, 2008. MMWR Morb Mortal Wkly Rep *58*, 1377-1381.

Chandran, K., Sullivan, N.J., Felbor, U., Whelan, S.P., and Cunningham, J.M. (2005). Endosomal proteolysis of the Ebola virus glycoprotein is necessary for infection. Science *308*, 1643-1645.

Chen, G., Koellhoffer, J.F., Zak, S.E., Frei, J.C., Liu, N., Long, H., Ye, W., Nagar, K., Pan, G., Chandran, K.*, et al.* (2014). Synthetic antibodies with a human framework that protect mice from lethal Sudan ebolavirus challenge. ACS Chem Biol *9*, 2263-2273.

Connolly, B.M., Steele, K.E., Davis, K.J., Geisbert, T.W., Kell, W.M., Jaax, N.K., and Jahrling, P.B. (1999). Pathogenesis of experimental Ebola virus infection in guinea pigs. J Infect Dis *179 Suppl 1*, S203-217.

Cook, J.D., and Lee, J.E. (2013). The secret life of viral entry glycoproteins: moonlighting in immune evasion. PLoS Pathog *9*, e1003258.

Corti, D., Bianchi, S., Vanzetta, F., Minola, A., Perez, L., Agatic, G., Guarino, B., Silacci, C., Marcandalli, J., Marsland, B.J.*, et al.* (2013). Cross-neutralization of four paramyxoviruses by a human monoclonal antibody. Nature *501*, 439-443.

Corti, D., Voss, J., Gamblin, S.J., Codoni, G., Macagno, A., Jarrossay, D., Vachieri, S.G., Pinna, D., Minola, A., Vanzetta, F.*, et al.* (2011). A neutralizing antibody selected from plasma cells that binds to group 1 and group 2 influenza A hemagglutinins. Science *333*, 850-856.

Cote, M., Misasi, J., Ren, T., Bruchez, A., Lee, K., Filone, C.M., Hensley, L., Li, Q., Ory, D., Chandran, K.*, et al.* (2011). Small molecule inhibitors reveal Niemann-Pick C1 is essential for Ebola virus infection. Nature *477*, 344-348.

Cox, N.J., McCormick, J.B., Johnson, K.M., and Kiley, M.P. (1983). Evidence for two subtypes of Ebola virus based on oligonucleotide mapping of RNA. J Infect Dis *147*, 272-275.

Davidson, E., Bryan, C., Fong, R.H., Barnes, T., Pfaff, J.M., Mabila, M., Rucker, J.B., and Doranz, B.J. (2015). Mechanism of Binding to Ebola Virus Glycoprotein by the ZMapp, ZMAb, and MB-003 Cocktail Antibodies. J Virol *89*, 10982-10992.

Davidson, E., and Doranz, B.J. (2014). A high-throughput shotgun mutagenesis approach to mapping B-cell antibody epitopes. Immunology *143*, 13-20.

Dias, J.M., Kuehne, A.I., Abelson, D.M., Bale, S., Wong, A.C., Halfmann, P., Muhammad, M.A., Fusco, M.L., Zak, S.E., Kang, E.*, et al.* (2011a). A shared structural solution for neutralizing ebolaviruses. Nat Struct Mol Biol *18*, 1424-1427.

Dias, J.M., Kuehne, A.I., Abelson, D.M., Bale, S., Wong, A.C., Halfmann, P., Muhammad, M.A., Fusco, M.L., Zak, S.E., Kang, E.*, et al.* (2011b). A shared structural solution for neutralizing ebolaviruses. Nat Struct Mol Biol *18*, 1424-1427.

Dube, D., Brecher, M.B., Delos, S.E., Rose, S.C., Park, E.W., Schornberg, K.L., Kuhn, J.H., and White, J.M. (2009). The primed ebolavirus glycoprotein (19-kilodalton GP1,2): sequence and residues critical for host cell binding. J Virol *83*, 2883-2891.

Ekiert, D.C., Bhabha, G., Elsliger, M.A., Friesen, R.H., Jongeneelen, M., Throsby, M., Goudsmit, J., and Wilson, I.A. (2009). Antibody recognition of a highly conserved influenza virus epitope. Science *324*, 246-251.

Epstein, L., Wong, K.K., Kallen, A.J., and Uyeki, T.M. (2015). Post-Ebola Signs and Symptoms in U.S. Survivors. N Engl J Med *373*, 2484-2486.

Falzarano, D., and Feldmann, H. (2015). Virology. Delineating Ebola entry. Science *347*, 947-948.

Feldmann, H., and Geisbert, T.W. (2011). Ebola haemorrhagic fever. Lancet *377*, 849-862.

Feldmann, H., Jones, S.M., Daddario-DiCaprio, K.M., Geisbert, J.B., Stroher, U., Grolla, A., Bray, M., Fritz, E.A., Fernando, L., Feldmann, F.*, et al.* (2007). Effective post-exposure treatment of Ebola infection. PLoS Pathog *3*, e2.

Fields, G.B., and Noble, R.L. (1990). Solid phase peptide synthesis utilizing 9-fluorenylmethoxycarbonyl amino acids. Int J Pept Protein Res *35*, 161-214.

Flyak, A.I., Ilinykh, P.A., Murin, C.D., Garron, T., Shen, X., Fusco, M.L., Hashiguchi, T., Bornholdt, Z.A., Slaughter, J.C., Sapparapu, G.*, et al.* (2015). Mechanism of human antibody-mediated neutralization of marburg virus. Cell *160*, 893-903.

Flyak, A.I., Ilinykh, P.A., Murin, C.D., Garron, T., Shen, X., Fusco, M.L., Hashiguchi, T., Bornholdt, Z.A., Slaughter, J.C., Sapparapu, G.*, et al.* (2016). Cross-reactive and potent neutralizing antibody responses in human survivors of natural Ebolavirus infection. Cell.

Formenty, P., Hatz, C., Le Guenno, B., Stoll, A., Rogenmoser, P., and Widmer, A. (1999). Human infection due to Ebola virus, subtype Cote d'Ivoire: clinical and biologic presentation. J Infect Dis *179 Suppl 1*, S48-53.

Formenty, P., Leroy, E.M., Epelboin, A., Libama, F., Lenzi, M., Sudeck, H., Yaba, P., Allarangar, Y., Boumandouki, P., Nkounkou, V.B.*, et al.* (2006). Detection of Ebola virus in oral fluid specimens during outbreaks of Ebola virus hemorrhagic fever in the Republic of Congo. Clin Infect Dis *42*, 1521-1526.

Fox, J.M., Long, F., Edeling, M.A., Lin, H., van Duijl-Richter, M.K., Fong, R.H., Kahle, K.M., Smit, J.M., Jin, J., Simmons, G.*, et al.* (2015). Broadly Neutralizing Alphavirus Antibodies Bind an Epitope on E2 and Inhibit Entry and Egress. Cell.

Fusco, M.L., Hashiguchi, T., Cassan, R., Biggins, J.E., Murin, C.D., Warfield, K.L., Li, S., Holtsberg, F.W., Shulenin, S., Vu, H.*, et al.* (2015). Protective mAbs and Cross-Reactive mAbs Raised by Immunization with Engineered Marburg Virus GPs. PLoS Pathog *11*, e1005016.

Geisbert, T.W., Bausch, D.G., and Feldmann, H. (2010). Prospects for immunisation against Marburg and Ebola viruses. Reviews in medical virology *20*, 344-357.

Geisbert, T.W., Daddario-DiCaprio, K.M., Williams, K.J., Geisbert, J.B., Leung, A., Feldmann, F., Hensley, L.E., Feldmann, H., and Jones, S.M. (2008). Recombinant vesicular stomatitis virus vector mediates postexposure protection against Sudan Ebola hemorrhagic fever in nonhuman primates. J Virol *82*, 5664-5668.

Gire, S.K., Goba, A., Andersen, K.G., Sealfon, R.S.G., Park, D.J., Kanneh, L., Jalloh, S., Momoh, M., Fullah, M., Dudas, G.*, et al.* (2014). Genomic surveillance elucidates Ebola virus origin and transmission during the 2014 outbreak. Science (New York, NY) *345*, 1369-1372.

Giudicelli, V., Brochet, X., and Lefranc, M.P. (2011). IMGT/V-QUEST: IMGT standardized analysis of the immunoglobulin (IG) and T cell receptor (TR) nucleotide sequences. Cold Spring Harb Protoc *2011*, 695-715.

Grant, G.A. (1992). Synthetic peptides : a user's guide (New York: W.H. Freeman).

Gregory, S.M., Harada, E., Liang, B., Delos, S.E., White, J.M., and Tamm, L.K. (2011). Structure and function of the complete internal fusion loop from Ebolavirus glycoprotein 2. Proc Natl Acad Sci U S A *108*, 11211-11216.

Hangartner, L., Zinkernagel, R.M., and Hengartner, H. (2006). Antiviral antibody responses: the two extremes of a wide spectrum. Nature reviews Immunology *6*, 231-243.

Harrison, S.C. (2008). Viral membrane fusion. Nat Struct Mol Biol *15*, 690-698.

Hashiguchi, T., Fusco, M.L., Bornholdt, Z.A., Lee, J.E., Flyak, A.I., Matsuoka, R., Kohda, D., Yanagi, Y., Hammel, M., Crowe, J.E., Jr.*, et al.* (2015). Structural basis for Marburg virus neutralization by a cross-reactive human antibody. Cell *160*, 904-912.

Hernandez, H., Marceau, C., Halliday, H., Callison, J., Borisevich, V., Escaffre, O., Creech, J., Feldmann, H., and Rockx, B. (2015). Development and Characterization of Broadly Cross-reactive Monoclonal Antibodies Against All Known Ebolavirus Species. J Infect Dis.

Holtsberg, F.W., Shulenin, S., Vu, H., Howell, K.A., Patel, S.J., Gunn, B., Karim, M., Lai, J.R., Frei, J.C., Nyakatura, E.K.*, et al.* (2015). Pan-ebolavirus and Pan-filovirus Mouse Monoclonal Antibodies: Protection against Ebola and Sudan Viruses. J Virol *90*, 266-278.

Huang, C.C., Venturi, M., Majeed, S., Moore, M.J., Phogat, S., Zhang, M.Y., Dimitrov, D.S., Hendrickson, W.A., Robinson, J., Sodroski, J.*, et al.* (2004). Structural basis of tyrosine sulfation and VH-gene usage in antibodies that recognize the HIV type 1 coreceptor-binding site on gp120. Proc Natl Acad Sci U S A *101*, 2706-2711.

Ilinykh, P.A., Shen, X., Flyak, A.I., Kuzmina, N., Ksiazek, T.G., Crowe, J.E., Jr., and Bukreyev, A. (2016). Chimeric Filoviruses for Identification and Characterization of Monoclonal Antibodies. J Virol.

Johnson, E.D., Johnson, B.K., Silverstein, D., Tukei, P., Geisbert, T.W., Sanchez, A.N., and Jahrling, P.B. (1996). Characterization of a new Marburg virus isolated from a 1987 fatal case in Kenya. Arch Virol Suppl *11*, 101-114.

Keck, Z.Y., Enterlein, S.G., Howell, K.A., Vu, H., Shulenin, S., Warfield, K.L., Froude, J.W., Araghi, N., Douglas, R., Biggins, J.*, et al.* (2015). Macaque Monoclonal Antibodies Targeting Novel Conserved Epitopes within Filovirus Glycoprotein. J Virol *90*, 279-291.

Khan, A.S., Tshioko, F.K., Heymann, D.L., Le Guenno, B., Nabeth, P., Kerstiens, B., Fleerackers, Y., Kilmarx, P.H., Rodier, G.R., Nkuku, O.*, et al.* (1999). The reemergence of Ebola hemorrhagic fever, Democratic Republic of the Congo, 1995. Commission de Lutte contre les Epidemies a Kikwit. J Infect Dis *179 Suppl 1*, S76-86.

Kissling, R.E., Robinson, R.Q., Murphy, F.A., and Whitfield, S.G. (1968). Agent of disease contracted from green monkeys. Science *160*, 888-890.

Koellhoffer, J.F., Malashkevich, V.N., Harrison, J.S., Toro, R., Bhosle, R.C., Chandran, K., Almo, S.C., and Lai, J.R. (2012). Crystal Structure of the Marburg Virus GP2 Core Domain in Its Postfusion Conformation. Biochemistry *51*, 7665-7675.

Kondratowicz, A.S., Lennemann, N.J., Sinn, P.L., Davey, R.A., Hunt, C.L., Moller-Tank, S., Meyerholz, D.K., Rennert, P., Mullins, R.F., Brindley, M.*, et al.* (2011). T-cell immunoglobulin and mucin domain 1 (TIM-1) is a receptor for Zaire Ebolavirus and Lake Victoria Marburgvirus. Proc Natl Acad Sci U S A *108*, 8426-8431.

Krause, J.C., Tsibane, T., Tumpey, T.M., Huffman, C.J., Briney, B.S., Smith, S.A., Basler, C.F., and Crowe, J.E., Jr. (2011). Epitope-specific human influenza antibody repertoires diversify by B cell intraclonal sequence divergence and interclonal convergence. J Immunol *187*, 3704-3711.

Krzywinski, M., Schein, J., Birol, I., Connors, J., Gascoyne, R., Horsman, D., Jones, S.J., and Marra, M.A. (2009). Circos: an information aesthetic for comparative genomics. Genome Res *19*, 1639-1645.

Ksiazek, T.G., Rollin, P.E., Williams, A.J., Bressler, D.S., Martin, M.L., Swanepoel, R., Burt, F.J., Leman, P.A., Khan, A.S., Rowe, A.K.*, et al.* (1999a). Clinical virology of Ebola hemorrhagic fever (EHF): virus, virus antigen, and IgG and IgM antibody findings among EHF patients in Kikwit, Democratic Republic of the Congo, 1995. J Infect Dis *179 Suppl 1*, S177-187.

Ksiazek, T.G., West, C.P., Rollin, P.E., Jahrling, P.B., and Peters, C.J. (1999b). ELISA for the detection of antibodies to Ebola viruses. J Infect Dis *179 Suppl 1*, S192-198.

Kuhn, J.H. (2008). Filoviruses. A compendium of 40 years of epidemiological, clinical, and laboratory studies. Arch Virol Suppl *20*, 13-360.

Kuhn, J.H., Andersen, K.G., Baize, S., Bao, Y., Bavari, S., Berthet, N., Blinkova, O., Brister, J.R., Clawson, A.N., Fair, J.*, et al.* (2014). Nomenclature- and database-compatible names for the two Ebola virus variants that emerged in Guinea and the Democratic Republic of the Congo in 2014. Viruses *6*, 4760-4799.

Kuhn, J.H., Bao, Y., Bavari, S., Becker, S., Bradfute, S., Brister, J.R., Bukreyev, A.A., Chandran, K., Davey, R.A., Dolnik, O.*, et al.* (2013). Virus nomenclature below the species level: a standardized nomenclature for natural variants of viruses assigned to the family Filoviridae. Arch Virol *158*, 301-311.

Kunz, C., Hofmann, H., and Aspock, H. (1968). [Propagation of "Marburg virus" (Vervet monkey disease agent) in Aedes aegypti]. Zentralblatt fur Bakteriologie, Parasitenkunde, Infektionskrankheiten und Hygiene 1 Abt Medizinisch-hygienische Bakteriologie, Virusforschung und Parasitologie Originale *208*, 347-349.

Labrijn, A.F., Meesters, J.I., Priem, P., de Jong, R.N., van den Bremer, E.T., van Kampen, M.D., Gerritsen, A.F., Schuurman, J., and Parren, P.W. (2014). Controlled Fab-arm exchange for the generation of stable bispecific IgG1. Nat Protoc *9*, 2450-2463.

Ladner, J.T., Wiley, M.R., Mate, S., Dudas, G., Prieto, K., Lovett, S., Nagle, E.R., Beitzel, B., Gilbert, M.L., Fakoli, L.*, et al.* (2015). Evolution and Spread of Ebola Virus in Liberia, 2014-2015. Cell Host Microbe *18*, 659-669.

Lamunu, M., Lutwama, J.J., Kamugisha, J., Opio, A., Nambooze, J., Ndayimirije, N., and Okware, S. (2004). Containing a haemorrhagic fever epidemic: the Ebola experience in Uganda (October 2000-January 2001). Int J Infect Dis *8*, 27-37.

Lander, G.C., Stagg, S.M., Voss, N.R., Cheng, A., Fellmann, D., Pulokas, J., Yoshioka, C., Irving, C., Mulder, A., Lau, P.W.*, et al.* (2009). Appion: an integrated, database-driven pipeline to facilitate EM image processing. J Struct Biol *166*, 95-102.

Le Guenno, B., Formenty, P., Wyers, M., Gounon, P., Walker, F., and Boesch, C. (1995). Isolation and partial characterisation of a new strain of Ebola virus. Lancet *345*, 1271-1274.

Lee, J.E., Fusco, M.L., Abelson, D.M., Hessell, A.J., Burton, D.R., and Saphire, E.O. (2009). Techniques and tactics used in determining the structure of the trimeric ebolavirus glycoprotein. Acta Crystallogr D Biol Crystallogr *65*, 1162-1180.

Lee, J.E., Fusco, M.L., Hessell, A.J., Oswald, W.B., Burton, D.R., and Saphire, E.O. (2008a). Structure of the Ebola virus glycoprotein bound to an antibody from a human survivor. Nature *454*, 177-182.

Lee, J.E., Fusco, M.L., Hessell, A.J., Oswald, W.B., Burton, D.R., and Saphire, E.O. (2008b). Structure of the Ebola virus glycoprotein bound to an antibody from a human survivor. Nature *454*, 177-182.

Lee, J.E., Kuehne, A., Abelson, D.M., Fusco, M.L., Hart, M.K., and Saphire, E.O. (2008c). Complex of a protective antibody with its Ebola virus GP peptide epitope: unusual features of a V lambda x light chain. J Mol Biol *375*, 202-216.

Lee, J.E., and Saphire, E.O. (2009). Neutralizing ebolavirus: structural insights into the envelope glycoprotein and antibodies targeted against it. Curr Opin Struct Biol *19*, 408-417.

Leroy, E.M., Baize, S., Volchkov, V.E., Fisher-Hoch, S.P., Georges-Courbot, M.C., Lansoud-Soukate, J., Capron, M., Debre, P., McCormick, J.B., and Georges, A.J. (2000). Human asymptomatic Ebola infection and strong inflammatory response. Lancet *355*, 2210-2215.

Leroy, E.M., Gonzalez, J.-P., and Baize, S. (2011). Ebola and Marburg haemorrhagic fever viruses: major scientific advances, but a relatively minor public health threat for Africa. Clinical microbiology and infection : the official publication of the European Society of Clinical Microbiology and Infectious Diseases *17*, 964-976.

Leroy, E.M., Rouquet, P., Formenty, P., Souquiere, S., Kilbourne, A., Froment, J.M., Bermejo, M., Smit, S., Karesh, W., Swanepoel, R.*, et al.* (2004). Multiple Ebola virus transmission events and rapid decline of central African wildlife. Science *303*, 387-390.

Leroy, E.M., Souquiere, S., Rouquet, P., and Drevet, D. (2002). Re-emergence of ebola haemorrhagic fever in Gabon. Lancet *359*, 712.

Lewis, S.M., Wu, X., Pustilnik, A., Sereno, A., Huang, F., Rick, H.L., Guntas, G., Leaver-Fay, A., Smith, E.M., Ho, C.*, et al.* (2014). Generation of bispecific IgG antibodies by structure-based design of an orthogonal Fab interface. Nat Biotechnol *32*, 191-198.

Lin, G., Simmons, G., Pohlmann, S., Baribaud, F., Ni, H., Leslie, G.J., Haggarty, B.S., Bates, P., Weissman, D., Hoxie, J.A.*, et al.* (2003). Differential N-linked glycosylation of human immunodeficiency virus and Ebola virus envelope glycoproteins modulates interactions with DC-SIGN and DC-SIGNR. J Virol *77*, 1337-1346.

Lubaki, N.M., Ilinykh, P., Pietzsch, C., Tigabu, B., Freiberg, A.N., Koup, R.A., and Bukreyev, A. (2013). The lack of maturation of Ebola virus-infected dendritic cells results from the cooperative effect of at least two viral domains. J Virol *87*, 7471-7485.

Lyon, G.M., Mehta, A.K., Varkey, J.B., Brantly, K., Plyler, L., McElroy, A.K., Kraft, C.S., Towner, J.S., Spiropoulou, C., Stroher, U.*, et al.* (2014). Clinical care of two patients with Ebola virus disease in the United States. N Engl J Med *371*, 2402-2409.

Macneil, A., Reed, Z., and Rollin, P.E. (2011). Serologic cross-reactivity of human IgM and IgG antibodies to five species of Ebola virus. PLoS Negl Trop Dis *5*, e1175.

Malashkevich, V.N., Schneider, B.J., McNally, M.L., Milhollen, M.A., Pang, J.X., and Kim, P.S. (1999). Core structure of the envelope glycoprotein GP2 from Ebola virus at 1.9-A resolution. Proc Natl Acad Sci U S A *96*, 2662-2667.

Maruyama, T., Rodriguez, L.L., Jahrling, P.B., Sanchez, A., Khan, A.S., Nichol, S.T., Peters, C.J., Parren, P.W., and Burton, D.R. (1999). Ebola virus can be effectively neutralized by antibody produced in natural human infection. J Virol *73*, 6024-6030.

Marzi, A., Gramberg, T., Simmons, G., Moller, P., Rennekamp, A.J., Krumbiegel, M., Geier, M., Eisemann, J., Turza, N., Saunier, B.*, et al.* (2004). DC-SIGN and DC-SIGNR interact with the glycoprotein of Marburg virus and the S protein of severe acute respiratory syndrome coronavirus. J Virol *78*, 12090-12095.

Marzi, A., Moller, P., Hanna, S.L., Harrer, T., Eisemann, J., Steinkasserer, A., Becker, S., Baribaud, F., and Pohlmann, S. (2007). Analysis of the interaction of Ebola virus glycoprotein with DC-SIGN (dendritic cell-specific intercellular adhesion molecule 3-grabbing nonintegrin) and its homologue DC-SIGNR. J Infect Dis *196 Suppl 2*, S237-246.

Marzi, A., Yoshida, R., Miyamoto, H., Ishijima, M., Suzuki, Y., Higuchi, M., Matsuyama, Y., Igarashi, M., Nakayama, E., Kuroda, M.*, et al.* (2012). Protective efficacy of neutralizing monoclonal antibodies in a nonhuman primate model of Ebola hemorrhagic fever. PLoS One *7*, e36192.

Mate, S.E., Kugelman, J.R., Nyenswah, T.G., Ladner, J.T., Wiley, M.R., Cordier-Lassalle, T., Christie, A., Schroth, G.P., Gross, S.M., Davies-Wayne, G.J.*, et al.* (2015). Molecular Evidence of Sexual Transmission of Ebola Virus. N Engl J Med *373*, 2448-2454.

McElroy, A.K., Akondy, R.S., Davis, C.W., Ellebedy, A.H., Mehta, A.K., Kraft, C.S., Lyon, G.M., Ribner, B.S., Varkey, J., Sidney, J.*, et al.* (2015). Human Ebola virus infection results in substantial immune activation. Proc Natl Acad Sci U S A *112*, 4719-4724.

Mercer, J., and Helenius, A. (2009). Virus entry by macropinocytosis. Nat Cell Biol *11*, 510-520.

Meyer, M., Garron, T., Lubaki, N.M., Mire, C.E., Fenton, K.A., Klages, C., Olinger, G.G., Geisbert, T.W., Collins, P.L., and Bukreyev, A. (2015). Aerosolized Ebola vaccine protects primates and elicits lung-resident T cell responses. J Clin Invest *125*, 3241-3255.

Miller, E.H., and Chandran, K. (2012). Filovirus entry into cells - new insights. Curr Opin Virol *2*, 206-214.

Miller, E.H., Obernosterer, G., Raaben, M., Herbert, A.S., Deffieu, M.S., Krishnan, A., Ndungo, E., Sandesara, R.G., Carette, J.E., Kuehne, A.I.*, et al.* (2012). Ebola virus entry

requires the host-programmed recognition of an intracellular receptor. EMBO J *31*, 1947-1960.

Mingo, R.M., Simmons, J.A., Shoemaker, C.J., Nelson, E.A., Schornberg, K.L., D'Souza, R.S., Casanova, J.E., and White, J.M. (2015). Ebola virus and severe acute respiratory syndrome coronavirus display late cell entry kinetics: evidence that transport to NPC1+ endolysosomes is a rate-defining step. J Virol *89*, 2931-2943.

Miranda, M.E., and Miranda, N.L. (2011). Reston ebolavirus in humans and animals in the Philippines: a review. J Infect Dis *204 Suppl 3*, S757-760.

Miranda, M.E., White, M.E., Dayrit, M.M., Hayes, C.G., Ksiazek, T.G., and Burans, J.P. (1991). Seroepidemiological study of filovirus related to Ebola in the Philippines. Lancet *337*, 425-426.

Misasi, J., Chandran, K., Yang, J.Y., Considine, B., Filone, C.M., Cote, M., Sullivan, N., Fabozzi, G., Hensley, L., and Cunningham, J. (2012). Filoviruses require endosomal cysteine proteases for entry but exhibit distinct protease preferences. J Virol *86*, 3284-3292.

Mohan, G.S., Li, W., Ye, L., Compans, R.W., and Yang, C. (2012). Antigenic subversion: a novel mechanism of host immune evasion by Ebola virus. PLoS Pathog *8*, e1003065.

Moller-Tank, S., and Maury, W. (2014). Phosphatidylserine receptors: enhancers of enveloped virus entry and infection. Virology *468-470*, 565-580.

Montero, M., van Houten, N.E., Wang, X., and Scott, J.K. (2008). The membrane-proximal external region of the human immunodeficiency virus type 1 envelope: dominant site of antibody neutralization and target for vaccine design. Microbiol Mol Biol Rev *72*, 54-84, table of contents.

Murin, C.D., Fusco, M.L., Bornholdt, Z.A., Qiu, X., Olinger, G.G., Zeitlin, L., Kobinger, G.P., Ward, A.B., and Saphire, E.O. (2014). Structures of protective antibodies reveal sites of vulnerability on Ebola virus. Proc Natl Acad Sci U S A *111*, 17182-17187.

Muster, T., Steindl, F., Purtscher, M., Trkola, A., Klima, A., Himmler, G., Ruker, F., and Katinger, H. (1993). A conserved neutralizing epitope on gp41 of human immunodeficiency virus type 1. J Virol *67*, 6642-6647.

Nanbo, A., Imai, M., Watanabe, S., Noda, T., Takahashi, K., Neumann, G., Halfmann, P., and Kawaoka, Y. (2010). Ebolavirus is internalized into host cells via macropinocytosis in a viral glycoprotein-dependent manner. PLoS Pathog *6*, e1001121.

Ng, M., Ndungo, E., Kaczmarek, M.E., Herbert, A.S., Binger, T., Kuehne, A.I., Jangra, R.K., Hawkins, J.A., Gifford, R.J., Biswas, R.*, et al.* (2015). Filovirus receptor NPC1 contributes to species-specific patterns of ebolavirus susceptibility in bats. Elife *4*.

Nikiforov, V.V., Turovskii Iu, I., Kalinin, P.P., Akinfeeva, L.A., Katkova, L.R., Barmin, V.S., Riabchikova, E.I., Popkova, N.I., Shestopalov, A.M., Nazarov, V.P*., et al.* (1994). [A case of a laboratory infection with Marburg fever]. Zh Mikrobiol Epidemiol Immunobiol, 104-106.

Olabode, A.S., Jiang, X., Robertson, D.L., and Lovell, S.C. (2015). Ebolavirus is evolving but not changing: No evidence for functional change in EBOV from 1976 to the 2014 outbreak. Virology *482*, 202-207.

Olal, D., Kuehne, A.I., Bale, S., Halfmann, P., Hashiguchi, T., Fusco, M.L., Lee, J.E., King, L.B., Kawaoka, Y., Dye, J.M*., et al.* (2012). Structure of an antibody in complex with its mucin domain linear epitope that is protective against Ebola virus. J Virol *86*, 2809-2816.

Olinger, G.G., Jr., Pettitt, J., Kim, D., Working, C., Bohorov, O., Bratcher, B., Hiatt, E., Hume, S.D., Johnson, A.K., Morton, J*., et al.* (2012a). Delayed treatment of Ebola virus infection with plant-derived monoclonal antibodies provides protection in rhesus macaques. Proc Natl Acad Sci U S A *109*, 18030-18035.

Olinger, G.G., Pettitt, J., Kim, D., Working, C., Bohorov, O., Bratcher, B., Hiatt, E., Hume, S.D., Johnson, A.K., Morton, J*., et al.* (2012b). Delayed treatment of Ebola virus infection with plant-derived monoclonal antibodies provides protection in rhesus macaques. Proc Natl Acad Sci U S A *109*, 18030-18035.

Oswald, W.B., Geisbert, T.W., Davis, K.J., Geisbert, J.B., Sullivan, N.J., Jahrling, P.B., Parren, P.W.H.I., and Burton, D.R. (2007). Neutralizing antibody fails to impact the course of Ebola virus infection in monkeys. PLoS Pathog *3*, e9.

Ou, W., Delisle, J., Jacques, J., Shih, J., Price, G., Kuhn, J.H., Wang, V., Verthelyi, D., Kaplan, G., and Wilson, C.A. (2012). Induction of ebolavirus cross-species immunity using retrovirus-like particles bearing the Ebola virus glycoprotein lacking the mucin-like domain. Virol J *9*, 32.

Pappas, L., Foglierini, M., Piccoli, L., Kallewaard, N.L., Turrini, F., Silacci, C., Fernandez-Rodriguez, B., Agatic, G., Giacchetto-Sasselli, I., Pellicciotta, G*., et al.* (2014). Rapid development of broadly influenza neutralizing antibodies through redundant mutations. Nature *516*, 418-422.

Parameswaran, P., Liu, Y., Roskin, K.M., Jackson, K.K.L., Dixit, V.P., Lee, J.-Y., Artiles, K.L., Zompi, S., Vargas, M.J., Simen, B.B*., et al.* (2013). Convergent antibody signatures in human dengue. Cell host & microbe *13*, 691-700.

Park, D.J., Dudas, G., Wohl, S., Goba, A., Whitmer, S.L., Andersen, K.G., Sealfon, R.S., Ladner, J.T., Kugelman, J.R., Matranga, C.B*., et al.* (2015). Ebola Virus Epidemiology, Transmission, and Evolution during Seven Months in Sierra Leone. Cell *161*, 1516-1526.

Parren, P.W.H.I., Geisbert, T.W., Maruyama, T., Jahrling, P.B., and Burton, D.R. (2002). Pre- and postexposure prophylaxis of Ebola virus infection in an animal model by passive transfer of a neutralizing human antibody. J Virol *76*, 6408-6412.

Pettersen, E.F., Goddard, T.D., Huang, C.C., Couch, G.S., Greenblatt, D.M., Meng, E.C., and Ferrin, T.E. (2004). UCSF Chimera--a visualization system for exploratory research and analysis. J Comput Chem *25*, 1605-1612.

Pettitt, J., Zeitlin, L., Kim, D.H., Working, C., Johnson, J.C., Bohorov, O., Bratcher, B., Hiatt, E., Hume, S.D., Johnson, A.K.*, et al.* (2013). Therapeutic intervention of Ebola virus infection in rhesus macaques with the MB-003 monoclonal antibody cocktail. Sci Transl Med *5*, 199ra113.

Qiu, X., Alimonti, J.B., Melito, P.L., Fernando, L., Stroher, U., and Jones, S.M. (2011). Characterization of Zaire ebolavirus glycoprotein-specific monoclonal antibodies. Clin Immunol *141*, 218-227.

Qiu, X., Audet, J., Wong, G., Pillet, S., Bello, A., Cabral, T., Strong, J.E., Plummer, F., Corbett, C.R., Alimonti, J.B.*, et al.* (2012a). Successful Treatment of Ebola Virus-Infected Cynomolgus Macaques with Monoclonal Antibodies. Sci Transl Med *4*, 138ra181-138ra181.

Qiu, X., Audet, J., Wong, G., Pillet, S., Bello, A., Cabral, T., Strong, J.E., Plummer, F., Corbett, C.R., Alimonti, J.B.*, et al.* (2012b). Successful treatment of ebola virus-infected cynomolgus macaques with monoclonal antibodies. Sci Transl Med *4*, 138ra181.

Qiu, X., Fernando, L., Melito, P.L., Audet, J., Feldmann, H., Kobinger, G., Alimonti, J.B., and Jones, S.M. (2012c). Ebola GP-specific monoclonal antibodies protect mice and guinea pigs from lethal Ebola virus infection. PLoS Negl Trop Dis *6*, e1575.

Qiu, X., Wong, G., Audet, J., Bello, A., Fernando, L., Alimonti, J.B., Fausther-Bovendo, H., Wei, H., Aviles, J., Hiatt, E.*, et al.* (2014). Reversion of advanced Ebola virus disease in nonhuman primates with ZMapp. Nature *514*, 47-53.

Qiu, X., Wong, G., Fernando, L., Audet, J., Bello, A., Strong, J., Alimonti, J.B., and Kobinger, G.P. (2013). mAbs and Ad-Vectored IFN-α Therapy Rescue Ebola-Infected Nonhuman Primates When Administered After the Detection of Viremia and Symptoms. Sci Transl Med *5*, 207ra143.

Richard, A.S., Zhang, A., Park, S.J., Farzan, M., Zong, M., and Choe, H. (2015). Virion-associated phosphatidylethanolamine promotes TIM1-mediated infection by Ebola, dengue, and West Nile viruses. Proc Natl Acad Sci U S A *112*, 14682-14687.

Rouvinski, A., Guardado-Calvo, P., Barba-Spaeth, G., Duquerroy, S., Vaney, M.C., Kikuti, C.M., Navarro Sanchez, M.E., Dejnirattisai, W., Wongwiwat, W., Haouz, A.*, et al.* (2015). Recognition determinants of broadly neutralizing human antibodies against dengue viruses. Nature *520*, 109-113.

Saeed, M.F., Kolokoltsov, A.A., Albrecht, T., and Davey, R.A. (2010). Cellular entry of ebola virus involves uptake by a macropinocytosis-like mechanism and subsequent trafficking through early and late endosomes. PLoS Pathog *6*, e1001110.

Sakurai, Y., Kolokoltsov, A.A., Chen, C.C., Tidwell, M.W., Bauta, W.E., Klugbauer, N., Grimm, C., Wahl-Schott, C., Biel, M., and Davey, R.A. (2015). Ebola virus. Two-pore channels control Ebola virus host cell entry and are drug targets for disease treatment. Science *347*, 995-998.

Sanchez, A., Trappier, S.G., Mahy, B.W., Peters, C.J., and Nichol, S.T. (1996). The virion glycoproteins of Ebola viruses are encoded in two reading frames and are expressed through transcriptional editing. Proc Natl Acad Sci U S A *93*, 3602-3607.

Saphire, E.O. (2013). An update on the use of antibodies against the filoviruses. Immunotherapy *5*, 1221-1233.

Scheid, J.F., Mouquet, H., Ueberheide, B., Diskin, R., Klein, F., Oliveira, T.Y.K., Pietzsch, J., Fenyo, D., Abadir, A., Velinzon, K*., et al.* (2011). Sequence and structural convergence of broad and potent HIV antibodies that mimic CD4 binding. Science (New York, NY) *333*, 1633-1637.

Scheres, S.H. (2012). RELION: implementation of a Bayesian approach to cryo-EM structure determination. J Struct Biol *180*, 519-530.

Shedlock, D.J., Bailey, M.A., Popernack, P.M., Cunningham, J.M., Burton, D.R., and Sullivan, N.J. (2010). Antibody-mediated neutralization of Ebola virus can occur by two distinct mechanisms. Virology *401*, 228-235.

Shimojima, M., Takada, A., Ebihara, H., Neumann, G., Fujioka, K., Irimura, T., Jones, S., Feldmann, H., and Kawaoka, Y. (2006). Tyro3 family-mediated cell entry of Ebola and Marburg viruses. J Virol *80*, 10109-10116.

Siegert, R., Shu, H.L., Slenczka, H.L., Peters, D., and Muller, G. (1968). The aetiology of an unknown human infection transmitted by monkeys (preliminary communication). Ger Med Mon *13*, 1-2.

Simon-Loriere, E., Faye, O., Faye, O., Koivogui, L., Magassouba, N., Keita, S., Thiberge, J.M., Diancourt, L., Bouchier, C., Vandenbogaert, M*., et al.* (2015). Distinct lineages of Ebola virus in Guinea during the 2014 West African epidemic. Nature *524*, 102-104.

Smith, K., Garman, L., Wrammert, J., Zheng, N.Y., Capra, J.D., Ahmed, R., and Wilson, P.C. (2009). Rapid generation of fully human monoclonal antibodies specific to a vaccinating antigen. Nat Protoc *4*, 372-384.

Smith, S.A., de Alwis, R., Kose, N., Durbin, A.P., Whitehead, S.S., de Silva, A.M., and Crowe, J.E., Jr. (2013). Human monoclonal antibodies derived from memory B cells following

live attenuated dengue virus vaccination or natural infection exhibit similar characteristics. J Infect Dis *207*, 1898-1908.

Sobarzo, A., Groseth, A., Dolnik, O., Becker, S., Lutwama, J.J., Perelman, E., Yavelsky, V., Muhammad, M., Kuehne, A.I., Marks, R.S.*, et al.* (2013a). Profile and persistence of the virus-specific neutralizing humoral immune response in human survivors of Sudan ebolavirus (Gulu). The Journal of infectious diseases *208*, 299-309.

Sobarzo, A., Ochayon, D.E., Lutwama, J.J., Balinandi, S., Guttman, O., Marks, R.S., Kuehne, A.I., Dye, J.M., Yavelsky, V., Lewis, E.C.*, et al.* (2013b). Persistent immune responses after Ebola virus infection. The New England journal of medicine *369*, 492-493.

Spence, J.S., Krause, T.B., Mittler, E., Jangra, R.K., and Chandran, K. (2016). Direct Visualization of Ebola Virus Fusion Triggering in the Endocytic Pathway. MBio *7*.

SteelFisher, G.K., Blendon, R.J., and Lasala-Blanco, N. (2015). Ebola in the United States--Public Reactions and Implications. N Engl J Med *373*, 789-791.

Stuber, W., Knolle, J., and Breipohl, G. (1989). Synthesis of peptide amides by Fmoc-solid-phase peptide synthesis and acid labile anchor groups. Int J Pept Protein Res *34*, 215-221.

Sui, J., Hwang, W.C., Perez, S., Wei, G., Aird, D., Chen, L.-m., Santelli, E., Stec, B., Cadwell, G., Ali, M.*, et al.* (2009). Structural and functional bases for broad-spectrum neutralization of avian and human influenza A viruses. Nat Struct Mol Biol *16*, 265-273.

Suloway, C., Pulokas, J., Fellmann, D., Cheng, A., Guerra, F., Quispe, J., Stagg, S., Potter, C.S., and Carragher, B. (2005). Automated molecular microscopy: the new Leginon system. J Struct Biol *151*, 41-60.

Takada, A., Ebihara, H., Jones, S., Feldmann, H., and Kawaoka, Y. (2007). Protective efficacy of neutralizing antibodies against Ebola virus infection. Vaccine *25*, 993-999.

Takada, A., Feldmann, H., Stroeher, U., Bray, M., Watanabe, S., Ito, H., McGregor, M., and Kawaoka, Y. (2003). Identification of protective epitopes on ebola virus glycoprotein at the single amino acid level by using recombinant vesicular stomatitis viruses. J Virol *77*, 1069-1074.

Tang, G., Peng, L., Baldwin, P.R., Mann, D.S., Jiang, W., Rees, I., and Ludtke, S.J. (2007). EMAN2: an extensible image processing suite for electron microscopy. J Struct Biol *157*, 38-46.

Thi, E.P., Mire, C.E., Lee, A.C., Geisbert, J.B., Zhou, J.Z., Agans, K.N., Snead, N.M., Deer, D.J., Barnard, T.R., Fenton, K.A.*, et al.* (2015). Lipid nanoparticle siRNA treatment of Ebola-virus-Makona-infected nonhuman primates. Nature *521*, 362-365.

Thomas, D., Newcomb, W.W., Brown, J.C., Wall, J.S., Hainfeld, J.F., Trus, B.L., and Steven, A.C. (1985). Mass and molecular composition of vesicular stomatitis virus: a scanning transmission electron microscopy analysis. J Virol *54*, 598-607.

Timen, A., Koopmans, M.P.G., Vossen, A.C.T.M., van Doornum, G.J.J., Günther, S., van den Berkmortel, F., Verduin, K.M., Dittrich, S., Emmerich, P., Osterhaus, A.D.M.E.*, et al.* (2009). Response to imported case of Marburg hemorrhagic fever, the Netherland. Emerg Infect Dis *15*, 1171-1175.

Tong, Y.G., Shi, W.F., Liu, D., Qian, J., Liang, L., Bo, X.C., Liu, J., Ren, H.G., Fan, H., Ni, M.*, et al.* (2015). Genetic diversity and evolutionary dynamics of Ebola virus in Sierra Leone. Nature *524*, 93-96.

Towner, J.S., Amman, B.R., Sealy, T.K., Carroll, S.A.R., Comer, J.A., Kemp, A., Swanepoel, R., Paddock, C.D., Balinandi, S., Khristova, M.L.*, et al.* (2009). Isolation of genetically diverse Marburg viruses from Egyptian fruit bats. PLoS Pathog *5*, e1000536.

Towner, J.S., Khristova, M.L., Sealy, T.K., Vincent, M.J., Erickson, B.R., Bawiec, D.A., Hartman, A.L., Comer, J.A., Zaki, S.R., Stroher, U.*, et al.* (2006). Marburgvirus genomics and association with a large hemorrhagic fever outbreak in Angola. J Virol *80*, 6497-6516.

Towner, J.S., Paragas, J., Dover, J.E., Gupta, M., Goldsmith, C.S., Huggins, J.W., and Nichol, S.T. (2005). Generation of eGFP expressing recombinant Zaire ebolavirus for analysis of early pathogenesis events and high-throughput antiviral drug screening. Virology *332*, 20-27.

Towner, J.S., Sealy, T.K., Khristova, M.L., Albarino, C.G., Conlan, S., Reeder, S.A., Quan, P.L., Lipkin, W.I., Downing, R., Tappero, J.W.*, et al.* (2008). Newly discovered ebola virus associated with hemorrhagic fever outbreak in Uganda. PLoS Pathog *4*, e1000212.

van Heel, M., Harauz, G., Orlova, E.V., Schmidt, R., and Schatz, M. (1996). A new generation of the IMAGIC image processing system. J Struct Biol *116*, 17-24.

Varkey, J.B., Shantha, J.G., Crozier, I., Kraft, C.S., Lyon, G.M., Mehta, A.K., Kumar, G., Smith, J.R., Kainulainen, M.H., Whitmer, S.*, et al.* (2015). Persistence of Ebola Virus in Ocular Fluid during Convalescence. N Engl J Med *372*, 2423-2427.

Volchkov, V.E., Becker, S., Volchkova, V.A., Ternovoj, V.A., Kotov, A.N., Netesov, S.V., and Klenk, H.D. (1995). GP mRNA of Ebola virus is edited by the Ebola virus polymerase and by T7 and vaccinia virus polymerases. Virology *214*, 421-430.

Volchkov, V.E., Feldmann, H., Volchkova, V.A., and Klenk, H.D. (1998). Processing of the Ebola virus glycoprotein by the proprotein convertase furin. Proc Natl Acad Sci U S A *95*, 5762-5767.

Volchkov, V.E., Volchkova, V.A., Muhlberger, E., Kolesnikova, L.V., Weik, M., Dolnik, O., and Klenk, H.D. (2001). Recovery of infectious Ebola virus from complementary DNA: RNA editing of the GP gene and viral cytotoxicity. Science *291*, 1965-1969.

Voss, N.R., Yoshioka, C.K., Radermacher, M., Potter, C.S., and Carragher, B. (2009). DoG Picker and TiltPicker: software tools to facilitate particle selection in single particle electron microscopy. J Struct Biol *166*, 205-213.

Wamala, J.F., Lukwago, L., Malimbo, M., Nguku, P., Yoti, Z., Musenero, M., Amone, J., Mbabazi, W., Nanyunja, M., Zaramba, S.*, et al.* (2010). Ebola hemorrhagic fever associated with novel virus strain, Uganda, 2007-2008. Emerg Infect Dis *16*, 1087-1092.

Warren, T.K., Warfield, K.L., Wells, J., Swenson, D.L., Donner, K.S., Van Tongeren, S.A., Garza, N.L., Dong, L., Mourich, D.V., Crumley, S.*, et al.* (2010). Advanced antisense therapies for postexposure protection against lethal filovirus infections. Nat Med *16*, 991-994.

Warren, T.K., Wells, J., Panchal, R.G., Stuthman, K.S., Garza, N.L., Van Tongeren, S.A., Dong, L., Retterer, C.J., Eaton, B.P., Pegoraro, G.*, et al.* (2014). Protection against filovirus diseases by a novel broad-spectrum nucleoside analogue BCX4430. Nature *508*, 402-405.

Warren, T.K., Whitehouse, C.A., Wells, J., Welch, L., Heald, A.E., Charleston, J.S., Sazani, P., Reid, S.P., Iversen, P.L., and Bavari, S. (2015). A single phosphorodiamidate morpholino oligomer targeting VP24 protects rhesus monkeys against lethal Ebola virus infection. MBio *6*.

Weissenhorn, W., Carfi, A., Lee, K.H., Skehel, J.J., and Wiley, D.C. (1998). Crystal structure of the Ebola virus membrane fusion subunit, GP2, from the envelope glycoprotein ectodomain. Mol Cell *2*, 605-616.

White, J.M., Delos, S.E., Brecher, M., and Schornberg, K. (2008). Structures and mechanisms of viral membrane fusion proteins: multiple variations on a common theme. Crit Rev Biochem Mol Biol *43*, 189-219.

White, J.M., and Schornberg, K.L. (2012). A new player in the puzzle of filovirus entry. Nature reviews Microbiology *10*, 317-322.

WHO (1978a). Ebola haemorrhagic fever in Sudan, 1976. Report of a WHO/International Study Team. Bull World Health Organ *56*, 247-270.

WHO (1978b). Ebola haemorrhagic fever in Zaire, 1976. Bull World Health Organ *56*, 271-293.

Wilson, J.A., Hevey, M., Bakken, R., Guest, S., Bray, M., Schmaljohn, A.L., and Hart, M.K. (2000). Epitopes involved in antibody-mediated protection from Ebola virus. Science *287*, 1664-1666.

Wong, G., Kobinger, G.P., and Qiu, X. (2014). Characterization of host immune responses in Ebola virus infections. Expert Rev Clin Immunol *10*, 781-790.

Wu, Y.-C., Kipling, D., Leong, H.S., Martin, V., Ademokun, A.A., and Dunn-Walters, D.K. (2010). High-throughput immunoglobulin repertoire analysis distinguishes between human IgM memory and switched memory B-cell populations. Blood *116*, 1070-1078.

Yang, Z.Y., Duckers, H.J., Sullivan, N.J., Sanchez, A., Nabel, E.G., and Nabel, G.J. (2000). Identification of the Ebola virus glycoprotein as the main viral determinant of vascular cell cytotoxicity and injury. Nat Med *6*, 886-889.

Yu, J.S., Liao, H.X., Gerdon, A.E., Huffman, B., Scearce, R.M., McAdams, M., Alam, S.M., Popernack, P.M., Sullivan, N.J., Wright, D.*, et al.* (2006). Detection of Ebola virus envelope using monoclonal and polyclonal antibodies in ELISA, surface plasmon resonance and a quartz crystal microbalance immunosensor. J Virol Methods *137*, 219-228.

Yu, X., McGraw, P.A., House, F.S., and Crowe, J.E., Jr. (2008). An optimized electrofusion-based protocol for generating virus-specific human monoclonal antibodies. J Immunol Methods *336*, 142-151.

Zeitlin, L., Pettitt, J., Scully, C., Bohorova, N., Kim, D., Pauly, M., Hiatt, A., Ngo, L., Steinkellner, H., Whaley, K.J.*, et al.* (2011). Enhanced potency of a fucose-free monoclonal antibody being developed as an Ebola virus immunoprotectant. Proc Natl Acad Sci U S A *108*, 20690-20694.

Zwick, M.B., Labrijn, A.F., Wang, M., Spenlehauer, C., Saphire, E.O., Binley, J.M., Moore, J.P., Stiegler, G., Katinger, H., Burton, D.R.*, et al.* (2001). Broadly neutralizing antibodies targeted to the membrane-proximal external region of human immunodeficiency virus type 1 glycoprotein gp41. J Virol *75*, 10892-10905.

Article

Cell

Mechanism of Human Antibody-Mediated Neutralization of Marburg Virus

Graphical Abstract

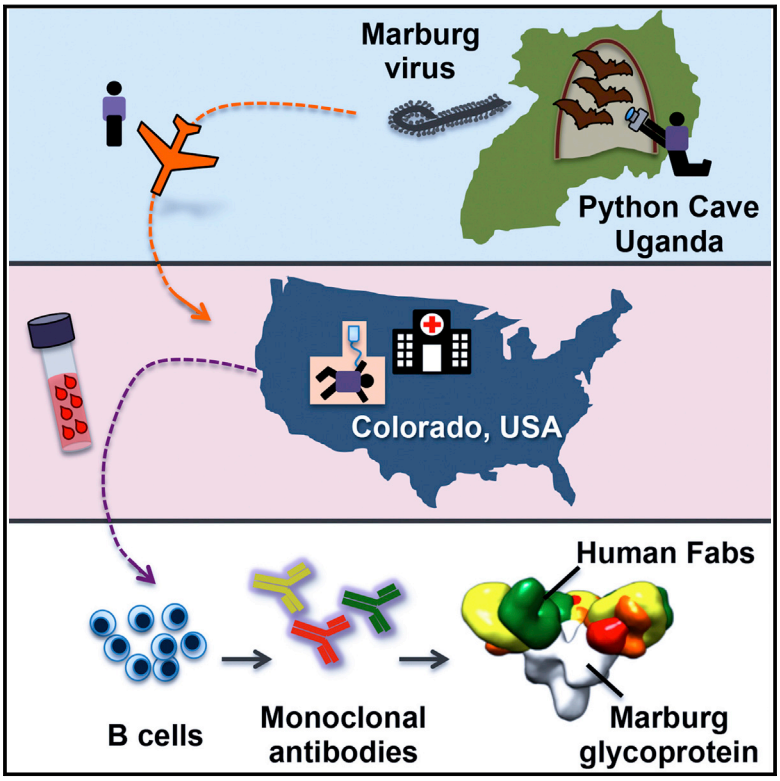

Authors

Andrew I. Flyak, Philipp A. Ilinykh, ..., Alexander Bukreyev, James E. Crowe, Jr.

Correspondence

james.crowe@vanderbilt.edu

In Brief

The characterization of Marburg-specific antibodies in several patients who survived the infection reveals a common binding site in the viral glycoprotein and a mechanism for filovirus inhibition.

Highlights

- Marburg virus survivor-neutralizing antibodies bind to a single antigenic site
- Several of the survivors' antibodies also bind to Ebola virus glycoprotein
- All antibodies identified bind at the predicted region of the receptor-binding site
- Binding to receptor-binding site is a new mechanism of filovirus inhibition

Flyak et al., 2015, Cell *160*, 893–903
February 26, 2015
http://dx.doi.org/10.1016/j.cell.2015.01.031

CellPress

Article

Cell

Mechanism of Human Antibody-Mediated Neutralization of Marburg Virus

Andrew I. Flyak,[1] Philipp A. Ilinykh,[5,6] Charles D. Murin,[7,8] Tania Garron,[5,6] Xiaoli Shen,[5,6] Marnie L. Fusco,[8] Takao Hashiguchi,[8,11] Zachary A. Bornholdt,[8] James C. Slaughter,[3,4] Gopal Sapparapu,[3] Curtis Klages,[5,6] Thomas G. Ksiazek,[5,6] Andrew B. Ward,[7] Erica Ollmann Saphire,[8,9] Alexander Bukreyev,[5,6,10] and James E. Crowe, Jr.[1,2,3,10,*]

[1]Department of Pathology, Microbiology, and Immunology, Vanderbilt University, Nashville, TN 37232, USA
[2]Department of Pediatrics, Vanderbilt University, Nashville, TN 37232, USA
[3]Vanderbilt Vaccine Center, Vanderbilt University, Nashville, TN 37232, USA
[4]Department of Biostatistics, Vanderbilt University, Nashville, TN 37232, USA
[5]Department of Pathology, University of Texas Medical Branch, Galveston, TX 77555, USA
[6]Galveston National Laboratory, Galveston, TX 77550, USA
[7]Department of Integrative Structural and Computational Biology, The Scripps Research Institute, La Jolla, CA 92037, USA
[8]Department of Immunology and Microbial Science, The Scripps Research Institute, La Jolla, CA 92037, USA
[9]The Skaggs Institute for Chemical Biology, The Scripps Research Institute, La Jolla, CA 92037, USA
[10]Co-senior author
[11]Present address: Faculty of Medicine, Department of Virology, Kyushu University, Fukuoka 812-8582, Japan
*Correspondence: james.crowe@vanderbilt.edu
http://dx.doi.org/10.1016/j.cell.2015.01.031

SUMMARY

The mechanisms by which neutralizing antibodies inhibit Marburg virus (MARV) are not known. We isolated a panel of neutralizing antibodies from a human MARV survivor that bind to MARV glycoprotein (GP) and compete for binding to a single major antigenic site. Remarkably, several of the antibodies also bind to Ebola virus (EBOV) GP. Single-particle EM structures of antibody-GP complexes reveal that all of the neutralizing antibodies bind to MARV GP at or near the predicted region of the receptor-binding site. The presence of the glycan cap or mucin-like domain blocks binding of neutralizing antibodies to EBOV GP, but not to MARV GP. The data suggest that MARV-neutralizing antibodies inhibit virus by binding to infectious virions at the exposed MARV receptor-binding site, revealing a mechanism of filovirus inhibition.

INTRODUCTION

Marburg virus (MARV) and Ebola virus (EBOV), which are members of the family *Filoviridae*, infect humans and non-human primates, causing a hemorrhagic fever with mortality rates up to 90% (Brauburger et al., 2012). There have been a dozen outbreaks of Marburg virus infection in humans reported to date, including the most recent report from Uganda of a 30-year-old male health worker who died in September 2014 (WHO, 2014a). As of January 7, 2015, there have been in excess of 20,000 confirmed, probable, and suspected cases of Ebola virus disease (EVD) in the current EBOV outbreak in nine affected countries (Guinea, Liberia, Mali, Nigeria, Senegal, Sierra Leone, Spain, the United Kingdom, and the United States of America), with more than 8,000 deaths (WHO, 2014b).

There is no licensed treatment or vaccine for filovirus infection. Recently, several studies showed that filovirus glycoprotein (GP)-specific neutralizing antibodies (nAbs) can reduce mortality following experimental inoculation of animals with a lethal dose of EBOV (Dye et al., 2012; Marzi et al., 2012; Olinger et al., 2012; Qiu et al., 2012, 2014; Pettitt et al., 2013) or MARV (Dye et al., 2012). The primary target of these nAbs, the filovirus surface GP, is a trimer composed of three heavily glycosylated GP1-GP2 heterodimers (Figure S1). The GP1 subunit can be divided further into base, head, glycan cap, and mucin-like domains (Lee et al., 2008). During viral entry, the mucin-like domain and glycan cap mediate binding to multiple host attachment factors present on the cell membrane. After the virus enters the host cell by macropinocytosis (Nanbo et al., 2010; Saeed et al., 2010), the GP is cleaved by host proteases that remove approximately 80% of the mass of the GP1 subunit, including the mucin-like domain and glycan cap (Chandran et al., 2005; Dube et al., 2009). After cleavage of GP in the endosome, the receptor-binding sites on GP become exposed, and the GP1 head then is able to bind to its receptor, Niemann-Pick C1 (NPC1) protein (Carette et al., 2011; Chandran et al., 2005; Côté et al., 2011). Subsequent conformational changes in GP facilitate fusion between viral and endosomal membranes.

The dense clustering of glycans on the glycan cap and mucin-like domain likely shield much of the surface of EBOV GP from humoral immune surveillance, leaving only a few sites on the EBOV GP protein at which nAbs could bind without interference by glycans (Cook and Lee, 2013). Most of our knowledge about humoral response against filovirus infections has come from studies of murine Abs that recognize EBOV GP. From those studies, we learned that mouse nAbs preferentially target peptides exposed in upper, heavily glycosylated domains or lower areas (the GP1 base), where rearrangements occur that drive

fusion of viral and host membranes (Saphire, 2013). Abs have not been identified that target protein features of the GP1 head subdomain, where the receptor-binding site to NPC1 protein is located. Ab KZ52, the only reported human EBOV GP-specific mAb, was obtained from a phage display library that was constructed from bone marrow RNA obtained from a survivor (Maruyama et al., 1999). KZ52 binds a site at the base of the GP and neutralizes EBOV, most likely by inhibiting the conformational changes required for fusion of viral and endosomal membranes (Lee et al., 2008). Some murine Abs also have been reported to bind to the base region of Ebola virus GPs (Dias et al., 2011, Murin et al., 2014). In contrast, very little is known about the mechanisms by which Abs neutralize MARV. Two murine Abs that bound the mucin-like domain of MARV GP reduced MARV budding from infected cells in culture but failed to neutralize virus directly (Kajihara et al., 2012). Polyclonal MARV-specific Abs were shown to protect non-human primates when administrated passively after challenge (Dye et al., 2012). The epitopes recognized by such polyclonal nAbs, and the mechanism of neutralization by which these Abs act, are unknown. In this study, we isolated a large panel of human nAbs from B cells of a human survivor of severe MARV infection and used these Abs to define the molecular basis of MARV neutralization by human Abs. The results show that MARV nAbs recognize the NPC1 receptor-binding domain of MARV GP and, in some cases, also recognize conserved structural features in the equivalent receptor-binding domain on EBOV GP.

RESULTS

Isolation of Monoclonal Antibodies

We tested plasma of a MARV survivor previously infected in Uganda for the 50% neutralization activity against the Uganda strain of MARV and found a serum-neutralizing titer of 1:1,010. To generate human hybridoma cell lines secreting mAbs to MARV, we screened supernatants from EBV-transformed B cell lines derived from the survivor for binding to several recombinant forms of MARV GP or to irradiated cell lysates prepared from MARV-infected cell cultures. We fused transformed cells from B cell lines producing MARV-reactive Abs to the MARV antigens with myeloma cells and generated 51 cloned hybridomas secreting MARV-specific human mAbs. Thirty-nine of these mAbs were specific to the MARV GP, while 12 bound to infected-cell lysate, but not to GP; these latter mAbs were shown in secondary screens to bind to MARV internal proteins (NP, VP35, or VP40; data not shown). Analysis of the Ab heavy- and light-chain variable domain sequences revealed that all MARV-specific mAbs were encoded by unique Ab genes.

Neutralization Activity

To evaluate the inhibitory activity of the mAbs, we first performed in vitro neutralization studies using a chimeric vesicular stomatitis virus with MARV GP from Uganda strain on its surface (vesicular stomatitis virus/Marburg glycoprotein recombinant VSV/GP-Uganda). Eighteen of the 39 MARV GP-specific mAbs exhibited neutralization activity against VSV/GP-Uganda (Figures 1A and 1C; Figures S2 and S4). Of those 18 nAbs, 9 displayed strong (IC_{50} < 10 μg/ml), 8 nAbs displayed moderate (IC_{50}: 10–99 μg/ml), and one displayed weak (IC_{50}: 100–1,000 μg/ml) neutralizing activity against VSV/GP-Uganda. We also tested the neutralization potency of all nAbs that bound to MARV GP in a plaque reduction assay using live MARV-Uganda virus. Of 18 Abs that neutralized VSV/GP-Uganda, 11 Abs exhibited neutralizing activity against MARV-Uganda (Figures 1A and 1C; Figures S3 and S4). These data suggest that VSV/GP, often used to study neutralizing potency of Abs because of its BSL-2 containment level, is more susceptible to Ab-mediated neutralization than live MARV. This difference is likely explained by the significantly lower copy number of MARV GP molecules that incorporate into VSV particles compared with the large number of GP molecules on the surface of filovirus filaments (Beniac et al., 2012; Thomas et al., 1985). Comparison of MARV-neutralizing and non-neutralizing antibodies at concentration up to 1.6 mg/ml revealed dose-dependent activity of those mAbs that neutralized. The neutralization activity of nAbs was not enhanced by the presence of complement (data not shown). As expected, we did not detect neutralizing activity for any of the 12 Abs specific to MARV NP, VP35, or VP40 proteins.

Recognition of Varying Forms of GP

To characterize the binding of isolated Abs to recombinant MARV GPs, we performed binding assays using either a recombinant MARV GP ectodomain containing the mucin-like domain (MARV GP) or a recombinant GP lacking residues 257–425 of the mucin-like domain (MARV GPΔmuc). Based on OD_{405} values at the highest Ab concentration tested (E_{max}) and 50% effective concentration (EC_{50}), we divided the MARV-GP-specific Abs into four major groups, based on binding phenotype (designated binding groups 1, 2, 3A, and 3B; Figures 1B and S5). Binding group 1 mAbs had an E_{max} to GP <2 (i.e., these mAbs never exhibited a maximal binding level to MARV GP); binding group 2 mAbs had an E_{max} to GP >2, with EC_{50} for GP <EC_{50} for GPΔmuc (i.e., these mAbs bound to the mucin-like domain or glycan cap); and binding group 3 had an E_{max} to GP >2, with EC_{50} for GP ≈ EC_{50} for GPΔmuc (i.e., these mAbs bound equally well to full-length and mucin-deleted forms of GP), with the group 3A mAbs having an EC_{50} for GP <0.5 μg/ml and the group 3B mAbs having an EC_{50} for GP >0.5 μg/ml (suggesting that, as a class, the group 3B mAbs possess a lower steady-state K_D of binding to GP than did group 3A mAbs).

Abs that lacked neutralization activity against VSV/GP-Uganda or MARV-Uganda fell principally into binding groups 1, 2, and 3A. Interestingly, all VSV/GP-Uganda nAbs displayed a unique binding pattern and segregated into binding group 3B (Figure 1C). It was interesting that while both mAbs from groups 3A and 3B bound equally well to the full-length MARV GP and to the GPΔmuc, EC_{50} values for nAbs from binding group 3B were higher than those for non-neutralizing Abs from group 3A.

Competition-Binding Studies

To determine whether mAbs from distinct binding groups targeted different antigenic regions on the MARV GP surface, we performed a competition-binding assay using a real-time biosensor. We tested 18 MARV nAbs from binding group 3B, 4 Abs from binding group 3A, and 1 Ab from binding group 2 in a tandem blocking assay in which biotinylated GPΔmuc was

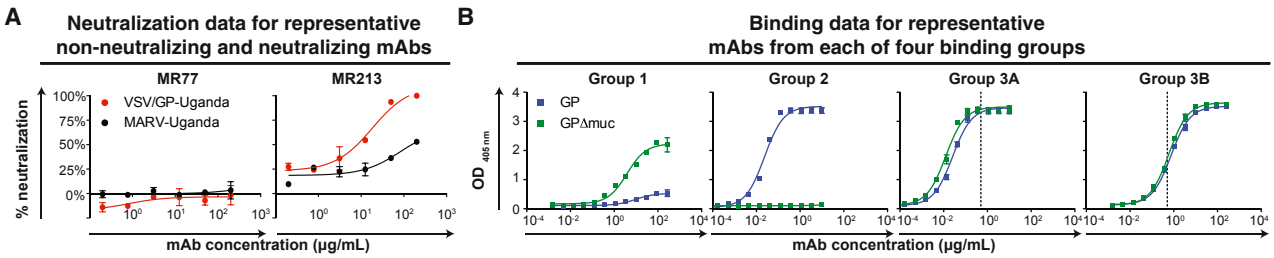

C Neutralization (μg/mL)

Group	mAb	VSV/GP-Uganda	MARV-Uganda
1	MR48	>	>
	MR49	>	>
	MR59	>	>
	MR73	>	>
	MR75	>	>
	MR77	>	>
	MR84	>	>
	MR85	>	>
	MR114	>	>
	MR117	>	>
	MR168	>	>
	MR187	>	>
	MR237	>	>
2	MR228	>	>
	MR235	>	>
3A	MR162	>	>
	MR221	>	>
	MR224	>	>
	MR246	>	>
3B	MR65	224	>
	MR72	13	601
	MR78	5	93
	MR79	>	>
	MR82	7	288
	MR103	28	291
	MR111	8	414
	MR137	>	>
	MR144	37	>
	MR186	2	>
	MR191	6	>
	MR198	12	206
	MR201	8	572
	MR208	55	>
	MR209	12	402
	MR213	10	305
	MR229	7	215
	MR232	4	114
	MR238	10	>
	MR241	12	>

D Competitive binding

Primary antibody: Group	Primary antibody: mAb	Competing antibody: 3B MR65	MR144	MR72	MR78	MR82	MR103	MR111	MR186	MR191	MR198	MR201	MR208	MR209	MR213	MR229	MR232	MR238	MR241	2 MR228	3A MR224	MR162	MR221	MR246
3B	MR65	17	26	24	34	33	22	30	36	32	38	41	34	33	41	39	40	27	36	97	101	95	100	100
	MR144	20	27	29	40	37	21	32	39	34	37	38	33	33	41	35	40	29	34	117	105	104	91	116
	MR72	16	21	20	24	27	15	18	32	17	24	21	-6	19	23	22	26	11	23	114	101	107	86	103
	MR78	4	14	7	14	14	12	9	15	12	14	11	11	10	15	13	15	11	10	104	92	96	98	97
	MR82	12	12	4	14	14	15	10	14	13	15	15	12	12	15	12	18	11	13	111	104	103	99	104
	MR103	19	19	21	29	27	18	23	30	25	30	26	24	23	30	23	31	18	27	128	112	101	98	112
	MR111	11	16	15	23	22	13	17	23	21	24	25	21	21	25	23	25	18	22	103	100	105	89	108
	MR186	3	10	10	10	12	11	8	16	8	10	7	1	9	10	10	10	8	7	108	92	104	82	97
	MR191	16	14	15	17	17	12	13	19	15	18	16	17	15	19	18	17	12	14	126	110	106	97	118
	MR198	11	13	11	13	15	13	12	15	11	13	16	13	12	15	16	14	11	12	115	104	100	96	108
	MR201	14	17	12	14	15	9	11	16	11	11	14	14	11	16	13	15	13	11	101	95	94	88	106
	MR208	14	15	11	15	19	15	13	18	15	18	18	15	18	19	16	18	15	17	106	101	96	96	107
	MR209	14	15	18	20	21	14	15	22	18	18	21	19	16	23	21	22	14	17	84	86	83	75	96
	MR213	11	11	8	12	16	9	13	14	11	13	13	13	12	11	13	15	9	12	103	100	102	103	103
	MR229	18	14	16	18	18	11	14	19	15	15	19	19	14	19	15	21	16	16	103	93	89	79	105
	MR232	13	16	16	18	18	12	11	18	17	17	18	16	14	23	17	19	20	13	127	110	114	90	124
	MR238	17	15	16	24	22	18	20	28	18	23	25	23	18	24	24	27	18	24	114	109	91	100	109
	MR241	16	16	15	15	18	13	13	17	13	16	19	16	18	22	19	22	13	15	98	90	93	77	101
2	MR228	98	67	61	76	67	64	71	76	78	88	92	96	103	101	90	88	96	93	14	27	76	76	98
3A	MR224	266	112	100	113	103	104	117	108	99	96	106	114	118	117	121	108	226	115	24	22	84	92	121
	MR162	135	128	122	131	111	109	130	125	110	117	122	131	138	129	127	121	124	130	134	109	26	102	118
	MR221	95	95	88	98	84	81	98	95	84	91	100	100	101	102	96	93	96	101	110	97	83	10	92
	MR246	87	80	77	89	71	73	86	81	77	86	88	96	93	92	91	89	87	90	102	96	79	89	4

Figure 1. MARV-Neutralizing mAbs Display a Unique Binding Pattern and Target a Distinct Antigenic Region on the GP Surface

(A) Neutralization activity of MR77 (non-neutralizing antibody) or MR213 (neutralizing antibody) against VSV/GP-Uganda (red circles) or MARV-Uganda (black circles). Error bars represent the SE of the experiment performed in triplicate.

(B) Binding of representative mAbs from four distinct binding groups to the MARV GP (blue squares) or MARV GPΔmuc (green squares). A dotted line indicates 0.5 μg/ml threshold for categorizing group 3 antibodies as possessing low (3A) or high (3B) EC_{50} values.

(C) Heatmap showing the neutralization potency of MARV GP-specific mAbs against VSV/GP-Uganda or MARV-Uganda. The IC_{50} value for each virus-mAb combination is shown, with dark red, orange, yellow, or white shading indicating high, intermediate, low, or no potency, respectively. IC_{50} values greater than 1,000 μg/ml are indicated by >. Neutralization assays were performed in triplicate.

(D) Data from competition binding assays using mAbs from binding groups 2, 3A, or 3B. Numbers indicate the percent binding of the competing mAb in the presence of the first mAb, compared to binding of competing mAb alone. MAbs were judged to compete for the same site if maximum binding of the competing mAb was reduced to <30% of its un-competed binding (black boxes with white numbers). MAbs were considered non-competing if maximum binding of the competing mAb was >70% of its un-competed binding (white boxes with red numbers). Gray boxes with black numbers indicate an intermediate phenotype (between 30 and 70% of un-competed binding).

See also Figures S2, S3, S4, and S5.

attached to a streptavidin biosensor. Abs from group 1 and the two non-neutralizing Abs from binding group 3B did not bind to biotinylated GPΔmuc in the competition assay and were excluded from the analysis. While non-neutralizing Abs from binding groups 2 and 3A did not prevent binding of the binding group 3B nAbs to GPΔmuc, all nAbs blocked binding of each of the other nAbs to the antigen and segregated into a single competition-binding group (Figure 1D). These data suggested

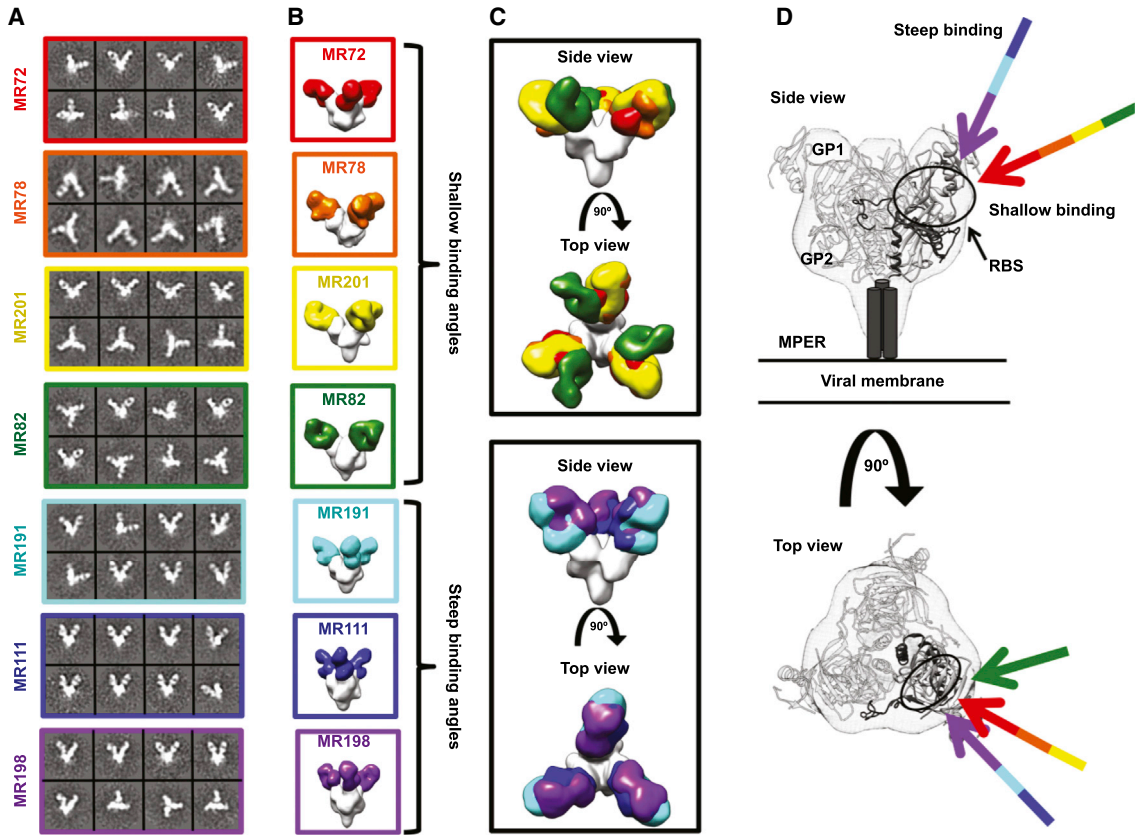

Figure 2. Neutralizing Antibodies from a Human Survivor of MARV Bind to the Receptor-Binding Site of GP at Two Distinct Angles of Approach

(A) Representative reference-free 2D class averages of the MARV GPΔMuc:MR Fab complexes.

(B) EM reconstructions of seven Fab fragments of neutralizing antibodies bound to MARV GPΔmuc (side views). All seven antibodies target a similar epitope on the top of GP.

(C) These antibodies can be subdivided based on their angles of approach: (1) those that bind toward the top and side of GP1 at a shallow angle relative to the central 3-fold axis (MR72 in red, MR78 in orange, MR201 in yellow, or MR82 in green) and (2) those that bind at a steeper angle toward the top of GP1 (MR191 in cyan, MR111 in blue, or MR198 in purple).

(D) The crystal structure of EBOV GPΔmuc (GP1 in white and GP2 in dark gray) is modeled into the MARV GP density (mesh), and the angles of approach of the neutralizing antibodies are indicated with arrows, colored as in (B). The footprint of the antibodies is indicated by a black circle targeting residues in the putative receptor-binding site (RBS) through a variety of approach angles.

See also Figure S1.

that all of the nAbs target a single major antigenic region on the MARV GP surface.

Electron Microscopy Studies of Antigen-Antibody Complexes

To determine the location of the antigenic region targeted by MARV nAbs, we performed negative stain single-particle electron microscopy (EM) studies using complexes of GPΔmuc with Fab fragments of seven nAbs from Binding Group 3B. The EM reconstructions clearly showed that Fab fragments for all seven nAbs bind at the top of the GP in or near the NPC1 protein receptor-binding site (Figures 2A and 2B). The binding pattern of these Abs could be divided further into two major groups based on their relative angle of approach to the GP head domain. MAbs MR72, MR78, MR201, and MR82 bound toward the top and side of GP1 at a shallow angle relative to the central 3-fold axis, while mAbs MR191, MR111, and MR198 bound at a steeper angle toward the top of GP1 (Figures 2C and 2D). When we compared IC_{50} values for nAbs that bound in the two binding poses, we did not detect a significant difference in neutralization potency based on the angle of approach (Figure 1C).

Antibody Neutralization Escape Mutant Viruses

As an additional strategy to determine residues on MARV GP involved in binding to nAbs, we generated VSV/GP-Uganda variant viruses that escaped neutralization, and then we determined the sequence of the GP of those mAb escape viruses. Vero E6 cells were inoculated with VSV/GP-Uganda in the presence of MR72 or MR78 nAbs. Two escape mutant viruses were isolated: virus variant VSV/GP-72.5 contained three missense mutations in the MARV GP gene (N129S in the putative NPC1 receptor-binding site, S220P in the glycan cap and P455L in the

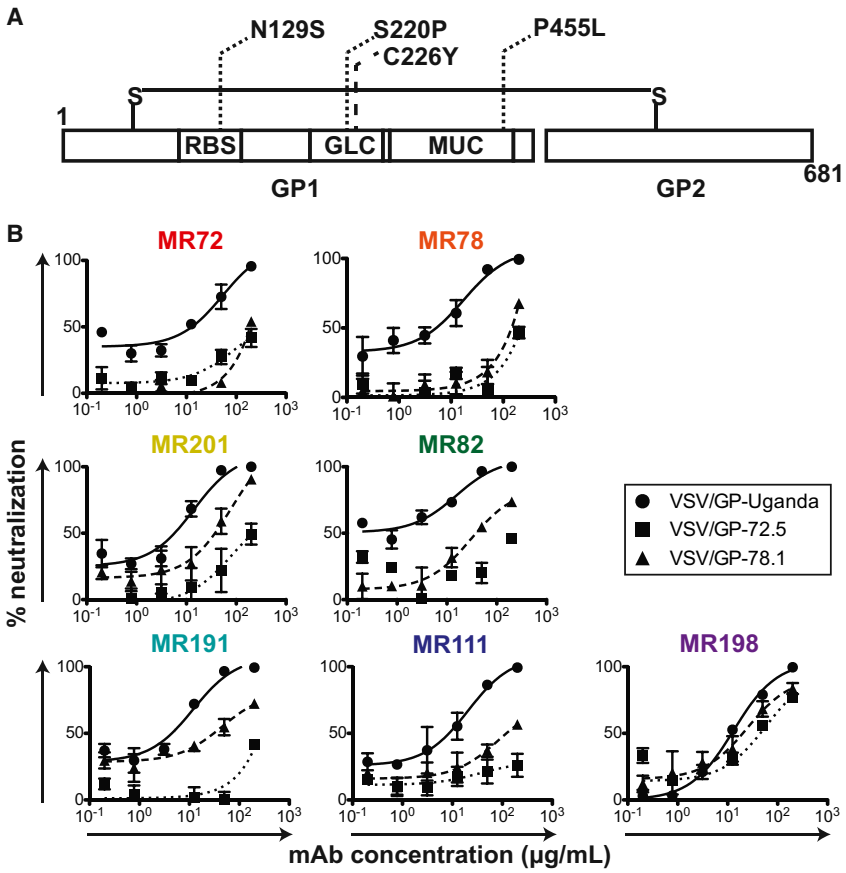

Figure 3. Generation of Escape Mutants for MARV-Neutralizing Antibodies

(A) VSV-MARV-72.5 (dotted lines) or VSV-MARV-78.1 (dashed line) escape mutations mapped onto the domain schematic of MARV GP. RBS, receptor binding site; GLC, glycan cap; MUC, mucin-like domain.

(B) Neutralization activity of antibodies from binding group 3B against wild-type VSV/GP-Uganda (circles, straight curves), VSV/GP-72.5 (squares, dotted curves), or VSV/GP-78.1 (triangles, dashed curves) escape mutant viruses.

mucin-like domain), and virus variant VSV/GP-78.1 possessed missense mutation C226Y in the glycan cap (Figure 3A). Consistent with the EM data, six out of seven nAbs tested displayed a higher level of neutralization activity against the wild-type VSV/GP-Uganda than to the VSV/GP-72.5 or VSV/GP-78.1 escape mutant viruses, suggesting these nAbs recognize MARV GP in a similar fashion (Figure 3B). MAb MR198 exhibited equal neutralization potency against wild-type VSV/GP-Uganda or the two escape mutant viruses (Figure 3B). As all nAbs segregated into one competition group (Figure 1D), bound the MARV GP at the NPC1 receptor-binding site (Figures 2A–2D), and displayed a similar profile of neutralization of escape mutant viruses (Figure 3B), we propose that blocking of MARV GP binding to NPC1 is the principal mechanism of MARV neutralization by these naturally occurring human Abs. This model is supported by the data in the accompanying paper by Hashiguchi et al. (2015; this issue of *Cell*) showing that MR78 inhibits binding of NPC1 domain C to MARV GP.

Cross-Reactive Binding of MARV Antibodies with EBOV GP

It is surprising that human MARV nAbs recognize the putative NPC1 protein receptor-binding site on GP, since previous studies suggested that the NPC1 protein receptor-binding site on EBOV GP may be obscured from Ab binding by the presence of the highly glycosylated glycan cap and mucin-like domain (Lee et al., 2008). To determine whether the MARV nAbs we isolated also could bind in a cross-reactive manner to the EBOV GP receptor-binding site, we performed ELISA using three recombinant forms of MARV and EBOV GPs: full-length GP ectodomain containing the glycan cap and mucin-like domain (designated MARV or EBOV GP), ectodomains lacking residues 257–425 (MARV) or 314–462 (EBOV) of the mucin-like domain (designated MARV or EBOV GPΔmuc), and cleaved GP ectodomains enzymatically treated to remove the mucin-like domain and glycan cap (designated MARV or EBOV GPcl). Three of the MARV nAbs, designated MR78, MR111, and MR191, recognized the EBOV GPcl that lacked the glycan cap and mucin-like domain (Figure 4A). Remarkably, the MARV nAb MR72 bound all three forms of both EBOV and MARV GPs with similar EC_{50} and E_{max} values, indicating that its epitope, and the EBOV receptor-binding site, which it likely overlaps, might be partially accessible for Ab binding even in the full-length form (Figure 4A). We tested the breadth of neutralization of MARV nAbs for filoviruses using a panel of different MARV and EBOV isolates. While multiple MARV Abs displayed neutralizing activity toward different MARV strains, MARV nAbs did not exhibit detectable neutralization activity against EBOV or VSV/EBOV (Figure 4B). Structural analysis of MARV and EBOV GP in the accompanying paper by Hashiguchi et al. (2015) reveals that the glycan cap and mucin-like domain likely obscure the receptor-binding domain in EBOV, but not in MARV.

In Vivo Testing

We tested the in vivo protective activity of the mAbs in a murine model using mouse-adapted MARV strain Ci67 (Warfield et al., 2007, 2009). Inoculation of mice with MARV Ci67 causes clinical disease and, in a proportion of animals, causes lethal disease, although typically less than 100% lethality in mice (Warren et al., 2014). We selected four of the mAbs among those with the lowest in vitro neutralization IC_{50} values: MR72, MR82, MR213, and MR232. The IC_{50} values in neutralization assays with MARV Uganda or mouse-adapted MARV strain Ci67 were comparable (within 2-fold). Seven-week-old BALB/c mice were

A Binding (μg/mL)

mAb	MARV			EBOV		
	GP	GPΔmuc	GPcl	GP	GPΔmuc	GPcl
MR65	8.3	7.5	5.0	>	>	>
MR72	3.0	4.7	0.8	6.1	2.1	<0.1
MR78	1.4	2.3	1.1	>	>	107.4
MR82	1.0	1.5	0.5	>	>	>
MR103	8.8	14.2	4.8	>	>	>
MR111	2.5	4.3	1.5	>	>	21.5
MR144	8.1	8.0	3.3	>	>	>
MR186	1.3	0.9	0.5	>	>	>
MR191	2.5	5.1	1.4	>	>	<0.1
MR198	1.4	1.4	0.8	>	>	>
MR201	1.5	1.9	0.5	>	>	>
MR208	5.6	7.3	2.8	>	>	>
MR209	4.0	5.4	2.0	>	>	>
MR213	2.8	3.6	1.1	>	>	>
MR229	1.8	2.9	1.2	>	>	>
MR232	2.0	1.3	0.5	>	>	>
MR238	6.8	11.7	4.9	>	>	>
MR241	2.2	4.0	1.2	>	>	>

B Neutralization (μg/mL)

mAb	MARV						EBOV	
	VSV/GP-Musoke	VSV/GP-Uganda	MARV-Musoke	MARV-Uganda	MARV-Angola	MARV-Ravn	VSV/GP-EBOV	EBOV
MR65	31.0	224	>	>	214	>	>	>
MR72	3.6	13.4	>	601	>	368	>	>
MR78	3.8	4.5	>	93	>	286	>	>
MR82	1.8	7.4	234	288	184	185	>	>
MR103	16.5	27.5	>	291	>	>	>	>
MR111	12.2	7.9	370	414	>	444	>	>
MR144	43.1	37.3	900	>	>	354	>	>
MR186	1.5	1.5	24	>	97	64	>	>
MR191	5.5	6.2	441	>	413	>	>	>
MR198	2.7	11.6	290	206	128	30	>	>
MR201	6.6	8.0	343	572	358	832	>	>
MR208	13.8	54.9	896	>	>	106	>	>
MR209	4.2	12.2	577	402	>	93	>	>
MR213	7.6	9.7	>	305	207	121	>	>
MR229	5.1	7.3	103	215	110	59	>	>
MR232	3.9	4.0	>	114	103	127	>	>
MR238	11.9	10.2	264	>	416	>	>	>
MR241	2.7	11.9	376	>	162	>	>	>

Figure 4. Breadth of Binding or Neutralization of Human MARV-Specific mAbs for Diverse Filoviruses

(A) A heatmap showing the binding in ELISA of neutralizing mAbs from binding group 3B to the MARV and EBOV GPs. EC_{50} value for each antigen-mAb combination is shown, with dark red shading indicating lower EC_{50} values and orange or yellow shading indicating intermediate or higher EC_{50} values. EC_{50} values greater than 1,000 μg/ml are indicated by >.

(B) A heatmap showing the neutralization breadth of mAbs from binding group 3B. The IC_{50} value for each virus-mAb combination is shown, with dark red shading indicating increased potency and orange or yellow shading indicating intermediate or low potency. IC_{50} values greater than 1,000 μg/ml are indicated by >. Neutralization assays were performed in triplicate.

injected with 100 μg of antibody by the IP route and challenged with 1,000 plaque-forming unit (PFU) of Ci67. Twenty-four hours later, antibody treatment was repeated. By day 6, all five control (untreated) mice developed progressive loss of weight and symptoms of the disease, including dyspnea, recumbency, and unresponsiveness, and on days 8 and 9, two animals were found dead and one animal was found moribund and euthanized. The remaining two animals demonstrated recovery by day 11. In contrast, all animals treated with any antibody survived and did not display the elevation of the disease score, with the exception of two animals treated with MR72, which showed a transient marginal loss of weight and increase of the disease score on days 6–9, which did not exceed 1 (Figure 5). The observed level of protection was remarkable given the relatively modest in-vitro-neutralizing potency of the antibodies.

DISCUSSION

There is an obvious urgent need for prophylactic and therapeutic interventions for filovirus infections given the recurrence of MARV outbreaks, including that in Uganda in October 2014 and a massive outbreak of EBOV infections in West Africa in 2014. There is very little information about the structural determinants of neutralization on which to base the rational selection of antibodies, and for MARV there have been no reported human nAbs.

This study reveals that naturally occurring human MARV nAbs isolated from the B cells of a recovered donor principally target the MARV NPC1 protein receptor-binding site, suggesting that a major mechanism of MARV neutralization could be inhibition of binding to receptor. Remarkably, some of the isolated antibodies also bound to the EBOV GP. This mechanism of MARV neutralization was unexpected, because previous studies with EBOV showed that the putative receptor-binding domain on GP is obscured on the surface of virions by the presence of the glycan cap and mucin-like domain, only becoming exposed following cleavage by cathepsin in the endosome. These studies suggest that the configuration of the MARV GP differs significantly from that of EBOV GP because the receptor-binding domain must be accessible for immune recognition on MARV GP. Indeed, determination of the structure of the MARV GP and structural analysis of the interaction of mAb MR78 with MARV and EBOV GP molecules shows this to be the case (see Hashiguchi et al., 2015).

The information obtained from these studies can be used to inform development of new therapeutics and structure-based vaccine designs against filoviruses. Furthermore, as these nAbs are fully human and exhibit inhibitory activity, they might be useful as a component of a prophylactic or therapeutic approach for filovirus infection and disease. The challenge studies using a murine model here show clear evidence of in vivo activity and suggest additional preclinical studies in other species, such as guinea pigs and macaques, are warranted. Their ability to bind a broad range of MARV isolates indicates they may offer detection of or efficacy against new viral strains yet to emerge. Although some of these mAbs bind to certain forms of EBOV GP, these antibodies are not likely to be effective against natural Ebola infection because the EBOV receptor-binding site is obscured on the viral surface. However, such mAbs might neutralize EBOV if they could be delivered to the endosome, where the EBOV receptor-binding site is exposed following GP cleavage.

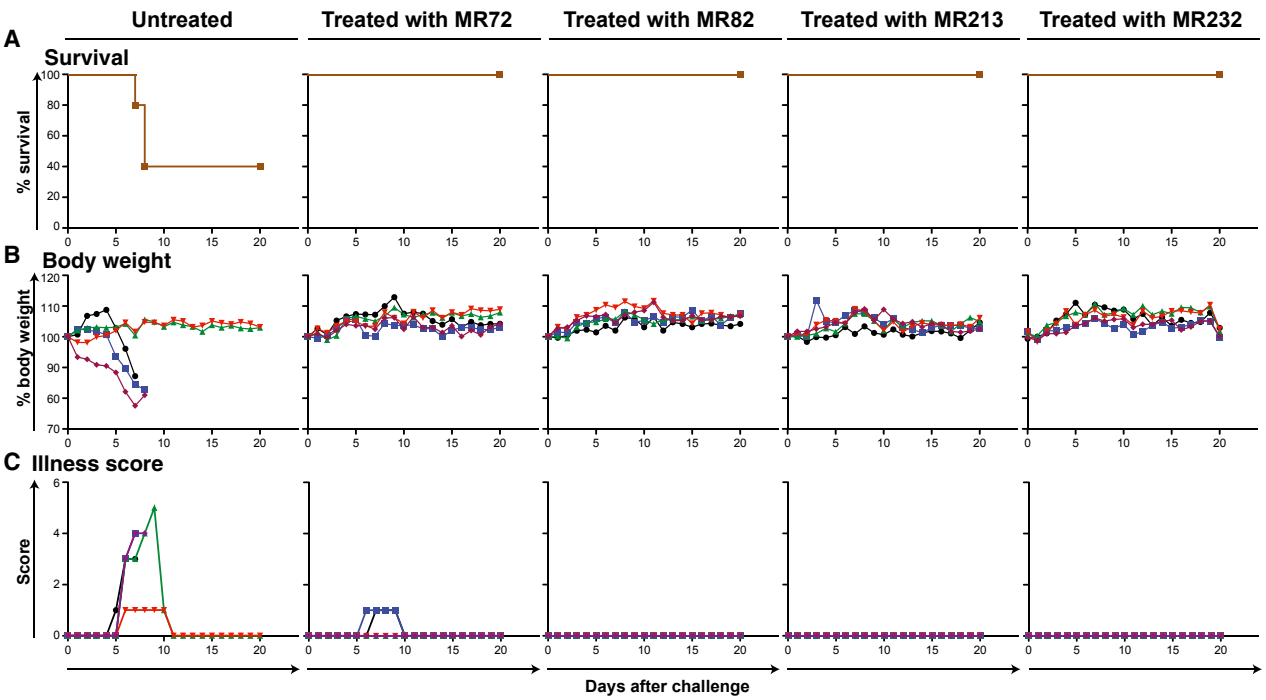

Figure 5. Survival and Clinical Overview of Mice Treated with MARV mAbs

(A–C) Groups of mice at five animals per group were injected with individual mAbs by the intraperitoneal route twice: 1 hr prior and 24 hr after MARV challenge at 100 μg per treatment. Untreated animals served as controls. (A) Kaplan-Meier survival curves. (B) Body weight. (C) Illness score.

EXPERIMENTAL PROCEDURES

Donor

The donor was an otherwise healthy adult woman who contracted Marburg virus (MARV) infection in 2008 following exposure to fruit bats in the Python Cave in Queen Elizabeth National Park, Uganda. The donor's clinical course was documented previously (CDC, 2009). Peripheral blood from the donor was obtained in 2012, four years after the illness, following informed consent. The study was approved by the Vanderbilt University Institutional Review Board.

Viruses

MARV strain 200702854 Uganda (MARV-Uganda) was isolated originally from a subject designated "patient A" during the outbreak in Uganda in 2007 (CDC, 2009; Towner et al., 2009) and underwent four passages in Vero E6 cells. MARV strain Musoke (MARV-Musoke) was isolated during the outbreak in Kenya in 1980 (Smith et al., 1982) and passaged five times in Vero E6 cells. MARV strain 200501379 Angola (MARV-Angola) was isolated during the outbreak in Angola in 2005 (Towner et al., 2006) and passaged three times in Vero E6 cells. MARV Ravn virus (Ravn) was isolated from a patient in 1987 in Kenya (Johnson et al., 1996) and passaged four times in Vero E6 cells. All strains of MARV were obtained originally from the Special Pathogens Branch, U.S. Centers for Disease Control (CDC), and deposited at the World Reference Center of Emerging Viruses and Arboviruses (WRCEVA) housed at UTMB. The recombinant Ebola Zaire strain Mayinga (EBOV) expressing eGFP was generated in our laboratory by reverse genetics (Lubaki et al., 2013; Towner et al., 2005) from plasmids provided by the Special Pathogens Branch at CDC and passaged three times in Vero E6 cells. For analysis of antibody binding by ELISA, viruses were gamma-irradiated with the dose of 5×10^6 rad. The recombinant VSV in which the VSV/GP protein was replaced with that of MARV strain Musoke (VSV/GP-Musoke) or EBOV strain Mayinga (Garbutt et al., 2004) were provided by Dr. Thomas Geisbert (UTMB) and Dr. Heinz Feldmann (NIH), respectively; a similar virus with GP from MARV (strain 200702854 Uganda) was constructed as described below. All work with EBOV and MARV was performed within the Galveston National Laboratory BSL-4 laboratories.

We used a mouse-adapted strain of MARV for testing the effect of mAbs in vivo. The mouse-adapted Ci67 strain of Marburg virus (Warfield et al., 2007) was provided by Dr. Sina Bavari (U.S. Army Medical Research Institute of Infectious Diseases) and amplified by a single passage in Vero-E6 cells.

Generation of a Chimeric Strain of VSV in which VSV G Protein Was Replaced with the GP Protein of MARV Strain Uganda

The plasmid pVSV-XN2 carrying cDNA of the full-length VSV anti-genome sequence and the support plasmids pBS-N, pBS-L, and pBS-P encoding the internal VSV proteins under control of the T7 promoter were kindly provided by Dr. John Rose (Yale University). The plasmid pC-T7, encoding the T7 polymerase, was kindly provided by Dr. Yoshihiro Kawaoka (University of Wisconsin). For generation of the VSV/GP-Uganda construct, Vero E6 cell monolayers were inoculated with MARV strain 200702854, and total cellular RNA was isolated and reverse transcribed. MARV GP open reading frame (ORF) was PCR amplified from cDNA using forward primer 5′-CATGTACG ACGCGTC*AACATGAGGACTA*-3′ and reverse primer 5′-TCTAGCAGCTC GAG*CTATCCAATATATTTAGTAAAGATACGACAA*-3′ (MluI and XhoI endonuclease sites are underlined, respectively; the start and end of MARV GP ORF direct and complementary sequences are italicized, respectively). To replace VSV G with MARV GP, the resulting PCR product was cloned into pVSV-XN2 using the unique MluI and XhoI endonuclease sites located between the VSV G gene-start and gene-end signals and flanking its ORF, resulting in the plasmid pVSV/GP-Uganda. To recover the recombinant virus, 1×10^6 BSR-T7 cells, kindly provided by Dr. Ursula Buchholz (U.S. National Institute of Allergy and Infectious Diseases), were transfected with the following plasmids: pVSV/GP-Uganda, 5 μg, pBS-N, 1.5 μg, pBS-P, 2.5 μg, pBS-L, 1 μg, and pC-T7, 5 μg. After 48 hr, transfected BSR-T7 cells were collected with a cell scraper and transferred, along with the supernates, to Vero E6 cell monolayers for amplification of the recovered VSV/GP-Uganda.

Generation of Human Hybridomas Secreting Monoclonal Antibodies

Peripheral blood mononuclear cells (PBMCs) from the donor were isolated with Ficoll-Histopaque by density gradient centrifugation. The cells were cryopreserved immediately and stored in the vapor phase of liquid nitrogen until use. Previously cryopreserved samples were thawed, and ten million PBMCs were plated into 384-well plates (Nunc #164688) using 17 ml of cell culture medium (ClonaCell-HY Medium A, StemCell Technologies, #03801), 8 μg/ml of the TLR agonist CpG (phosphorothioate-modified oligodeoxynucleotide ZOEZOEZZZZZOEEZOEZZZT, Invitrogen), 3 μg/ml of the Chk2 inhibitor (Sigma #C3742), 1 μg/ml of cyclosporine A (Sigma #C1832), and 4.5 ml of clarified supernate from cultures of B95.8 cells (ATCC VR-1492) containing Epstein-Barr virus (EBV). After 7 days, cells from each 384-well culture plate were expanded into four 96-well culture plates (Falcon #353072) using cell culture medium containing 8 μg/ml CpG, 3 μg/ml Chk2i, and ten million irradiated heterologous human PBMCs (Nashville Red Cross) and incubated for an additional 4 days. Plates were screened for MARV antigen-specific antibody-secreting cell lines using ELISAs. Cells from wells with supernates reacting in a MARV antigen ELISA were fused with HMMA2.5 myeloma cells using an established electrofusion technique (Yu et al., 2008). After fusion, hybridomas were resuspended in medium containing 100 μM hypoxanthine, 0.4 μM aminopterin, 16 μM thymidine (HAT Media Supplement, Sigma #HO262), and 7 μg/ml ouabain (Sigma #O3125) and incubated for 18 days before screening hybridomas for antibody production by ELISA.

Human mAb and Fab Production and Purification

After fusion with HMMA2.5 myeloma cells, hybridomas producing MARV-specific antibodies were cloned biologically by two rounds of limiting dilution and by single-cell fluorescence-activated cell sorting. After cloning, hybridomas were expanded in post-fusion medium (ClonaCell-HY Medium E, STEMCELL Technologies #03805) until 50% confluent in 75-cm^2 flasks (Corning #430641). For antibody production, cells from one 75-cm^2 flask were collected with a cell scraper and expanded to four 225-cm^2 flasks (Corning #431082) in serum-free medium (Hybridoma-SFM, GIBCO #12045-076). After 21 days, supernates were clarified by centrifugation and sterile filtered using 0.2-μm pore size filter devices. HiTrap Protein G or HiTrap MabSelectSure columns (GE Healthcare Life Sciences #17040501 and #11003494, respectively) were used to purify antibodies from filtered supernates. Fab fragments were generated by papain digestion (Pierce Fab Preparation Kit, Thermo Scientific #44985) and purified by chromatography using a two-column system in which the first column contained protein G resin (GE Healthcare Life Sciences #29048581) and the second column contained either anti-kappa or anti-lambda antibody light chain resins (GE Healthcare Life Sciences #17545811 and #17548211, respectively).

Expression and Purification of MARV and EBOV GPs

Angola strain MARV GP ectodomains, containing the mucin-like domain (MARV GP) or lacking residues 257–425 of the mucin-like domain (MARV GPΔmuc), were used to screen supernates of transformed B cells and human hybridomas separately. Recombinant proteins for Ravn strain cleaved GP, EBOV Mayinga strain GP, EBOV Mayinga strain GPΔmuc, and EBOV Mayinga strain cleaved GP were designed and expressed similarly. Large-scale production of recombinant GP or GPΔmuc was performed by transfection of *Drosophila* Schneider 2 (S2) cells with modified pMTpuro vectors, followed by stable selection of transfected cells with 6 μg/ml puromycin. Secreted GP ectodomain expression was induced with 0.5 mM $CuSO_4$ for 4 days. Proteins were engineered with a modified double strep tag at the C terminus (enterokinase cleavage site followed by a strep tag/linker/strep tag) to facilitate purification using Strep-Tactin resin (QIAGEN #2-1201). Proteins were purified further by Superdex 200 size-exclusion chromatography in 10 mM Tris and 150 mM NaCl (pH 7.5) (1× TBS).

Lysates of MARV-Infected Cells

Lysates were prepared as previously described (Ksiazek et al., 1999). Briefly, Vero E6 cell monolayers in 850 cm^2 roller bottles were inoculated with approximately 10^6 PFU MARV or EBOV and incubated at 37°C until partial destruction of monolayer occurred (approximately 9–10 days). Cell monolayers were detached using 3-mm glass beads, and cell suspensions were centrifuged at 16,000 × *g* for 10 min at 4°C. Supernates were discarded; cell pellets were resuspended in 10× excess of borate buffer saline (10 mM $Na_2B_4O_7$ and 150 mM NaCl [pH 9.0]) and centrifuged at 16,000 × *g* for 10 min at 4°C. Supernates were discarded; cell pellets were resuspended in cold 1% Triton X-100 (Fisher Scientific) in borate buffer saline, vortexed, and gamma-irradiated on dry ice at 5 × 10^6 rad. The lysates were sonicated with a 600 W Tekmar Sonic Disruptor TM600 (Tekmar) using a cuphorn sonicator at maximum power setting and 50% duty cycle for 10 min and centrifuged at 16,000 × *g*, and the supernates were aliquoted.

Screening ELISA

ELISA plates were coated with lysates of MARV-infected cells (diluted 1:1,000 in Dulbecco's PBS [DPBS]) or recombinant MARV GP or MARV GPΔmuc proteins (20 μg in 10 ml DPBS per plate) and incubated at 4°C overnight. Plates were blocked with 100 μl of blocking solution/well for 1 hr. Blocking solution consisted of 10 g powdered milk, 10 ml of goat serum, 100 ml of 10× DPBS, and 0.5 ml of Tween-20 mixed to a 1 l final volume with distilled water. The presence of antibodies bound to the GP was determined using goat anti-human immunoglobulin G (IgG) horseradish peroxidase-conjugated secondary antibodies (Southern Biotech #2040-05, 1:4,000 dilution) and 1-Step Ultra TMB-ELISA substrate (Thermo Scientific #34029), with optical density read at 450 nM after stopping the reaction with 1M HCl.

Half-Maximal Effective Concentration Binding Analysis

MARV or EBOV GPs, MARV or EBOV GPΔmuc, or Ravn or EBOV cathepsin-cleaved GPs were coated onto 384-well plates (Thermo Scientific Nunc #265203) in DPBS at 2 μg/ml overnight, then antigen was removed, and plates were blocked with blocking solution made as above. Antibodies were applied to the plates at a concentration range of 1.5 μg/ml to 270 ng/ml (binding groups #1, #2, and 3A) and 0.1 μg/ml to 10 ng/ml (binding group #3B) using 3-fold serial dilutions. The presence of antibodies bound to the GP was determined using goat anti-human IgG alkaline phosphatase conjugate (Meridian Life Science #W99008A, 1:4,000 dilution) and p-nitrophenol phosphate substrate tablets (Sigma #S0942), with optical density read at 405 nM after 120 min. A non-linear regression analysis was performed on the resulting curves using Prism (v. 5) (GraphPad) to calculate EC_{50} values.

MARV and EBOV Neutralization Experiments

Dilutions of mAbs in triplicate were mixed with 150 PFU of MARV or EBOV expressing eGFP in MEM containing 10% fetal bovine serum (FBS) (HyClone) and 50 μg/ml gentamicin (Cellgro #30-005-CR) with or without 5% guinea pig complement (MP Biomedicals #642836) in a total volume of 0.1 ml and incubated for 1 hr at 37°C for virus neutralization. Following neutralization, virus-antibody mixtures were placed on monolayers of Vero E6 cells in 24-well plates, incubated for 1 hr at 37°C for virus adsorption, and overlayed with MEM containing 2% FBS and 0.8% methylcellulose (Sigma-Aldrich #M0512). After incubation for 5 days, medium was removed, cells were fixed with 10% formalin (Fisher Scientific #245-684), and plates were sealed in plastic bags and incubated for 24 hr at room temperature. Sealed plates were taken out of the BSL-4 laboratory according to approved SOPs, and monolayers were washed three times with PBS. Viral plaques were immunostained with the serum of rabbits that had been hyperimmunized with MARV, or with a mAb against EBOV, clone 15H10 (BEI Resources #NR-12184). Alternatively, following virus adsorption, monolayers were covered with MEM containing 10% FBS and 1.6% tragacanth (Sigma-Aldrich #G1128). After incubation for 14 days, medium was removed, cells were fixed with 10% formalin, and plates were sealed in plastic bags, incubated for 24 hr at room temperature, and taken out of the BSL-4 laboratory as above. Fixed monolayers were stained with 10% formalin containing 0.25% crystal violet (Fisher Scientific #C581-100), and plaques were counted.

VSV-MARV and VSV-EBOV Neutralization Tests

Neutralization assays were performed in triplicate, as described above for MARV and EBOV. Following neutralization, virus-antibody mixtures were placed on monolayers of Vero E6 cells in duplicate, incubated for 1 hr at 37°C for virus adsorption, and overlayed with MEM containing 2% FBS containing 0.9% methylcellulose. After incubation for 3 days, medium was

removed, monolayers were fixed and stained with 10% formalin containing 0.25% crystal violet, and plaques were counted.

Generation and Sequencing of VSV/GP-Uganda Escape Mutants

Vero E6 cell monolayers with 2-fold dilutions of mAbs (12.5–200 μg/ml) added to the medium were inoculated with 200 PFU of recombinant VSV/GP-Uganda and incubated at 37°C for 2–4 days. To determine which samples contained live virus, supernates were collected, virus was titrated in Vero E6 cell monolayers under methylcellulose overlay, monolayers were incubated at 37°C for 3–4 days, and plaques were counted. Supernates with the highest concentrations of mAbs, which were found to contain live virus by plaque titration, were incubated in presence of serially diluted mAbs, followed by titration of virus as above. The procedure was performed a total of three times. Escape mutant viruses harvested after the third passage were cloned biologically by plaque purification. For biological cloning, Vero E6 cell monolayers in 24-well plates were inoculated with dilutions of the escape mutant viruses in the presence of the corresponding mAbs (200 μg/ml of MR72 or 100 μg/ml of MR78) and covered with 0.7% low melting temperature SeaPlaque agarose (Lonza #50100). Monolayers were incubated at 37°C for 6 days; plaques were visualized with 0.01% neutral red aqueous solution (Electron Microscopy Sciences), picked, resuspended in medium, and transferred to Vero E6 cell monolayers in 24-well plates in the presence of the corresponding mAbs (200 μg/ml of MR72 or 100 μg/ml of MR78) for virus propagation. In 2–5 days, based on the extent of CPE observed, virus was harvested, and cells were dissolved in Trizol reagent (Life Technologies 315596018). Total cellular RNA was extracted, reverse transcribed, and amplified by PCR with the primers described above for generation of a chimeric strain of VSV. Two overlapping fragments covering MARV GP ORF were PCR amplified from cDNA using forward primer 5′-CATGTACGACGCGTCAACATGAGGACTA-3′ and reverse primer 5′-ACTAAGCCCTGCTGCCAGGT-3′ or forward primer 5′-ACAACAATGTACCGAGGCAA-3′ and reverse primer 5′-TCTAGCAGCTCGAGCTATCCAATATATTTAGTAAAGATACGACAA-3′, and the nucleotide sequences of the GP ORFs were determined using standard procedures.

Analysis of Growth Kinetics of VSV/GP-Uganda Escape Mutant Viruses

Vero E6 cell monolayers in 24-well plates were inoculated in triplicate with VSV/GP-Uganda escape mutants or non-mutated virus at an MOI of 0.00025 PFU/cell in the presence of varying concentrations of the corresponding mAbs. Aliquots of medium were collected every 12 hr and frozen for titration at a later time. Titration of virus in aliquots was performed as above, without adding antibodies to the culture medium.

Biolayer Interferometry Competition Binding Assay

Biotinylated GP or GPΔmuc (EZ-link Micro NHS-PEG_4-Biotinylation Kit, Thermo Scientific #21955) (1 μg/ml) was immobilized onto streptavidin-coated biosensor tips (ForteBio #18-5019) for 2 min. After measuring the baseline signal in kinetics buffer (KB; 1× PBS, 0.01% BSA, and 0.002% Tween 20) for 2 min, biosensor tips were immersed into the wells containing primary antibody at a concentration of 100 μg/ml for 10 min. Biosensors then were immersed into wells containing competing mAbs at a concentration of 100 μg/ml for 5 min. The percent binding of the competing mAb in the presence of the first mAb was determined by comparing the maximal signal of competing mAb applied after the first mAb complex to the maximal signal of competing mAb alone. MAbs were judged to compete for binding to the same site if maximum binding of the competing mAb was reduced to <30% of its un-competed binding. MAbs were considered non-competing if maximum binding of the competing mAb was >70% of its un-competed binding. A level of 30%–70% of its un-competed binding was considered intermediate competition.

Sequence Analysis of Antibody Variable Region Genes

Total cellular RNA was extracted from clonal hybridomas that produced MARV antibodies, and RT-PCR reaction was performed using mixtures of primers designed to amplify all heavy-chain or light-chain antibody variable regions. The generated PCR products were purified and cloned into the pJet 1.2 plasmid vector (Thermo Scientific, #K1231) for sequence analysis. The nucleotide sequences of plasmid DNAs were determined using an ABI3700 automated DNA sequencer. Heavy-chain or light-chain antibody variable region sequences were analyzed using the IMGT/V-Quest program (Brochet et al., 2008; Giudicelli et al., 2011). The analysis involved the identification of germline genes that were used for antibody production, location of complementary determining regions (CDRs), and framework regions (FRs), as well as the number and location of somatic mutations that occurred during affinity maturation.

Statistical Analysis

EC_{50} values for neutralization were determined by finding the concentration of mAb at which a 50% reduction in plaque counts occurred after incubation of virus with neutralizing antibody. A logistic curve was fit to the data using the count as the outcome and the log-concentration as the predictor variable. The results of the model then were transformed back to the concentration scale. Results are presented as the concentration at the dilution that achieves a 50% reduction from challenge control with accompanying 95% confidence intervals. Each antibody was treated as a distinct analysis in a Bayesian nonlinear regression model.

Sample Preparation for EM Studies

A Ravn strain MARV GP mucin-deleted construct (GPΔmuc) was produced by stable cell line expression in *Drosophila* S2 cells, as described above. Human Fab proteins for MARV-specific antibodies were generated as described above. Fabs were added in molar excess to GPΔmuc and allowed to incubate overnight at 4°C. Complexes then were purified by Superdex 200 size-exclusion chromatography in TBS.

Electron Microscopy and Sample Preparation

A 4 μl aliquot of each complex that had been diluted to a concentration of ~0.03 μg/ml with TBS buffer was placed for 15 s onto carbon-coated 400 Cu mesh grids that had been plasma cleaned for 20 s (Gatan), blotted off on the edge of the grid, and then immediately stained for 30 s with 4 μl of 2% uranyl formate. The stain was blotted off on the edge of the grid, and the grid was allowed to dry. Data were automatically collected with Leginon (Carragher et al., 2000; Potter et al., 1999; Suloway et al., 2005) using a FEI Tecnai F20 electron microscope operating at 120 keV with an electron dose of 30 $e^-/Å^2$ and a magnification of 52,000× that resulted in a pixel size of 2.65 Å at the specimen plane when collected with Tietz CMOS 4k × 4k CCD camera. Particle orientations appeared to be generally isotropic, and images were acquired at a constant defocus value of −1.0 μm at 0° stage tilt.

Image Processing of Protein Complexes

Particles were picked automatically using DoG Picker (34) and placed into a particle stack using the Appion software (Lander et al., 2009). Reference-free 2D class averages were generated with the Xmipp clustering 2D alignment software (van Heel et al., 1996) and sorted into an initial 300 classes. Non-GP particles were removed, and the stack was further subclassified into classes with ~100 particles per class in order to generate the final particle stack used for the reconstruction. Various numbers of class averages were chosen to create initial models using EMAN2 common lines software (Tang et al., 2007). A model that best matched its projected classes was then used for refinement against the raw particle stack, imposing C3 symmetry, and the reconstruction was generated with ten rounds of refinement and increasingly smaller angular sampling rates with EMAN2 (Tang et al., 2007). All model fitting and manipulation was completed using UCSF Chimera (Pettersen et al., 2004).

In Vivo Testing

The animal protocol for testing of mAbs in mice was approved by the Institutional Animal Care and Use Committee of the University of Texas Medical Branch at Galveston. Seven-week-old BALB/c mice (Harlan) were placed in the ABSL-4 facility of the Galveston National Laboratory. Groups of mice at five animals per group were injected with individual mAbs by the intraperitoneal route twice: 1 hr prior and 24 hr after MARV challenge, using 100 μg per treatment. Untreated animals served as controls. For the challenge, mice were injected with 1,000 PFU of the mouse-adapted MARV strain Ci67 by the intraperitoneal route. Animals were weighed and monitored daily over the 3-week period after challenge. Once animals were symptomatic, they

were examined twice per day. The disease was scored using the following parameters: dyspnea (possible scores 0–5), recumbency (0–9), unresponsiveness (0–5), and bleeding/hemorrhage (0–5); the individual scores for each animal were summarized.

ACCESSION NUMBERS

EM reconstructions have been deposited in the Electron Microscopy Data Bank under the accession codes EMD-6232 through 6238.

SUPPLEMENTAL INFORMATION

Supplemental Information includes five figures and can be found with this article online at http://dx.doi.org/10.1016/j.cell.2015.01.031.

AUTHOR CONTRIBUTIONS

A.I.F., P.A.I., and C.D.M. planned, performed, and analyzed experiments and wrote the paper. T.G., X.S., C.K., M.L.F., T.H., Z.A.B., and G.S. performed and analyzed experiments. J.C.S. performed statistical analysis. T.G.K. and A.B.W. planned and analyzed experiments. E.O.S., A.B., and J.E.C. planned and analyzed experiments and wrote the paper.

ACKNOWLEDGMENTS

This project received support from the Defense Threat Reduction Agency (HDTRA1-13-1-0034) (to J.E.C.) and the U.S. NIH (1U19AI109711 to J.E.C. and A.B.; U19AI109762 to E.O.S. and A.B.W.; R01AI089498 and U01AI082156 to E.O.S.). E.O.S. is an Investigator in the Pathogenesis of Infectious Disease of the Burroughs Wellcome Fund. The project was supported by the NCRR (UL1 RR024975-01) and is now at the National Center for Advancing Translational Sciences (UL1 TR000445-06). T.H. received support from MEXT and JSPS Postdoctoral Fellowships for Research Abroad and a Research Fellowship of The Uehara Memorial Foundation. The content of this paper is solely the responsibility of the authors and does not necessarily represent the official views of the NIH. We thank Dr. Eugene Agapov (Washington University in St. Louis) for useful suggestions concerning the generation of VSV/GP-Uganda escape mutants. We thank the donor, Dr. Norman Fujit (Wheat Ridge, Colorado), and the Vanderbilt Clinical Trials Center for help in sample acquisition. We thank Frances Smith-House, Gloria Fritz, Vidisha Singh, and Leland Brown for excellent technical support and Dr. Scott A. Smith for thoughtful comments and discussions. Flow cytometry experiments were performed in the VMC Flow Cytometry Shared Resource and supported by NIH grants (P30 CA68485 and DK058404). The EM work was conducted at the National Resource for Automated Molecular Microscopy at The Scripps Research Institute, which is supported by the Biomedical Technology Research Center program (GM103310) of the National Institute of General Medical Sciences.

Received: October 18, 2014
Revised: January 9, 2015
Accepted: January 14, 2015
Published: February 26, 2015

REFERENCES

Beniac, D.R., Melito, P.L., Devarennes, S.L., Hiebert, S.L., Rabb, M.J., Lamboo, L.L., Jones, S.M., and Booth, T.F. (2012). The organisation of Ebola virus reveals a capacity for extensive, modular polyploidy. PLoS ONE *7*, e29608.

Brauburger, K., Hume, A.J., Mühlberger, E., and Olejnik, J. (2012). Forty-five years of Marburg virus research. Viruses *4*, 1878–1927.

Brochet, X., Lefranc, M.P., and Giudicelli, V. (2008). IMGT/V-QUEST: the highly customized and integrated system for IG and TR standardized V-J and V-D-J sequence analysis. Nucleic Acids Res. *36*, W503–W508.

Carette, J.E., Raaben, M., Wong, A.C., Herbert, A.S., Obernosterer, G., Mulherkar, N., Kuehne, A.I., Kranzusch, P.J., Griffin, A.M., Ruthel, G., et al. (2011). Ebola virus entry requires the cholesterol transporter Niemann-Pick C1. Nature *477*, 340–343.

Carragher, B., Kisseberth, N., Kriegman, D., Milligan, R.A., Potter, C.S., Pulokas, J., and Reilein, A. (2000). Leginon: an automated system for acquisition of images from vitreous ice specimens. J. Struct. Biol. *132*, 33–45.

Centers for Disease Control and Prevention (CDC) (2009). Imported case of Marburg hemorrhagic fever - Colorado, 2008. MMWR Morb. Mortal. Wkly. Rep. *58*, 1377–1381.

Chandran, K., Sullivan, N.J., Felbor, U., Whelan, S.P., and Cunningham, J.M. (2005). Endosomal proteolysis of the Ebola virus glycoprotein is necessary for infection. Science *308*, 1643–1645.

Cook, J.D., and Lee, J.E. (2013). The secret life of viral entry glycoproteins: moonlighting in immune evasion. PLoS Pathog. *9*, e1003258.

Côté, M., Misasi, J., Ren, T., Bruchez, A., Lee, K., Filone, C.M., Hensley, L., Li, Q., Ory, D., Chandran, K., and Cunningham, J. (2011). Small molecule inhibitors reveal Niemann-Pick C1 is essential for Ebola virus infection. Nature *477*, 344–348.

Dias, J.M., Kuehne, A.I., Abelson, D.M., Bale, S., Wong, A.C., Halfmann, P., Muhammad, M.A., Fusco, M.L., Zak, S.E., Kang, E., et al. (2011). A shared structural solution for neutralizing ebolaviruses. Nat. Struct. Mol. Biol. *18*, 1424–1427.

Dube, D., Brecher, M.B., Delos, S.E., Rose, S.C., Park, E.W., Schornberg, K.L., Kuhn, J.H., and White, J.M. (2009). The primed ebolavirus glycoprotein (19-kilodalton GP1,2): sequence and residues critical for host cell binding. J. Virol. *83*, 2883–2891.

Dye, J.M., Herbert, A.S., Kuehne, A.I., Barth, J.F., Muhammad, M.A., Zak, S.E., Ortiz, R.A., Prugar, L.I., and Pratt, W.D. (2012). Postexposure antibody prophylaxis protects nonhuman primates from filovirus disease. Proc. Natl. Acad. Sci. USA *109*, 5034–5039.

Garbutt, M., Liebscher, R., Wahl-Jensen, V., Jones, S., Möller, P., Wagner, R., Volchkov, V., Klenk, H.D., Feldmann, H., and Ströher, U. (2004). Properties of replication-competent vesicular stomatitis virus vectors expressing glycoproteins of filoviruses and arenaviruses. J. Virol. *78*, 5458–5465.

Giudicelli, V., Brochet, X., and Lefranc, M.P. (2011). IMGT/V-QUEST: IMGT standardized analysis of the immunoglobulin (IG) and T cell receptor (TR) nucleotide sequences. Cold Spring Harb Protoc *2011*, 695–715.

Hashiguchi, T., Fusco, M.L., Bornholdt, Z.A., Lee, J.E., Flyak, A.I., Matsuoka, R., Kohda, D., Yanagi, Y., Hammel, M., Crowe, J.E., Jr., and Saphire, E.O. (2015). Structural basis for Marburg virus neutralization by a cross-reactive human antibody. Cell *160*, this issue, 904–912.

Johnson, E.D., Johnson, B.K., Silverstein, D., Tukei, P., Geisbert, T.W., Sanchez, A.N., and Jahrling, P.B. (1996). Characterization of a new Marburg virus isolated from a 1987 fatal case in Kenya. Arch. Virol. Suppl. *11*, 101–114.

Kajihara, M., Marzi, A., Nakayama, E., Noda, T., Kuroda, M., Manzoor, R., Matsuno, K., Feldmann, H., Yoshida, R., Kawaoka, Y., and Takada, A. (2012). Inhibition of Marburg virus budding by nonneutralizing antibodies to the envelope glycoprotein. J. Virol. *86*, 13467–13474.

Ksiazek, T.G., West, C.P., Rollin, P.E., Jahrling, P.B., and Peters, C.J. (1999). ELISA for the detection of antibodies to Ebola viruses. J. Infect. Dis. *179* (*Suppl 1*), S192–S198.

Lander, G.C., Stagg, S.M., Voss, N.R., Cheng, A., Fellmann, D., Pulokas, J., Yoshioka, C., Irving, C., Mulder, A., Lau, P.W., et al. (2009). Appion: an integrated, database-driven pipeline to facilitate EM image processing. J. Struct. Biol. *166*, 95–102.

Lee, J.E., Fusco, M.L., Hessell, A.J., Oswald, W.B., Burton, D.R., and Saphire, E.O. (2008). Structure of the Ebola virus glycoprotein bound to an antibody from a human survivor. Nature *454*, 177–182.

Lubaki, N.M., Ilinykh, P., Pietzsch, C., Tigabu, B., Freiberg, A.N., Koup, R.A., and Bukreyev, A. (2013). The lack of maturation of Ebola virus-infected dendritic cells results from the cooperative effect of at least two viral domains. J. Virol. *87*, 7471–7485.

Maruyama, T., Rodriguez, L.L., Jahrling, P.B., Sanchez, A., Khan, A.S., Nichol, S.T., Peters, C.J., Parren, P.W., and Burton, D.R. (1999). Ebola virus can be

effectively neutralized by antibody produced in natural human infection. J. Virol. *73*, 6024–6030.

Marzi, A., Yoshida, R., Miyamoto, H., Ishijima, M., Suzuki, Y., Higuchi, M., Matsuyama, Y., Igarashi, M., Nakayama, E., Kuroda, M., et al. (2012). Protective efficacy of neutralizing monoclonal antibodies in a nonhuman primate model of Ebola hemorrhagic fever. PLoS ONE *7*, e36192.

Murin, C.D., Fusco, M.L., Bornholdt, Z.A., Qiu, X., Olinger, G.G., Zeitlin, L., Kobinger, G.P., Ward, A.B., and Saphire, E.O. (2014). Structures of protective antibodies reveal sites of vulnerability on Ebola virus. Proc. Natl. Acad. Sci. USA *111*, 17182–17187.

Nanbo, A., Imai, M., Watanabe, S., Noda, T., Takahashi, K., Neumann, G., Halfmann, P., and Kawaoka, Y. (2010). Ebolavirus is internalized into host cells via macropinocytosis in a viral glycoprotein-dependent manner. PLoS Pathog. *6*, e1001121.

Olinger, G.G., Jr., Pettitt, J., Kim, D., Working, C., Bohorov, O., Bratcher, B., Hiatt, E., Hume, S.D., Johnson, A.K., Morton, J., et al. (2012). Delayed treatment of Ebola virus infection with plant-derived monoclonal antibodies provides protection in rhesus macaques. Proc. Natl. Acad. Sci. USA *109*, 18030–18035.

Pettersen, E.F., Goddard, T.D., Huang, C.C., Couch, G.S., Greenblatt, D.M., Meng, E.C., and Ferrin, T.E. (2004). UCSF Chimera—a visualization system for exploratory research and analysis. J. Comput. Chem. *25*, 1605–1612.

Pettitt, J., Zeitlin, L., Kim, D.H., Working, C., Johnson, J.C., Bohorov, O., Bratcher, B., Hiatt, E., Hume, S.D., Johnson, A.K., et al. (2013). Therapeutic intervention of Ebola virus infection in rhesus macaques with the MB-003 monoclonal antibody cocktail. Sci. Transl. Med *5*, 199ra113.

Potter, C.S., Chu, H., Frey, B., Green, C., Kisseberth, N., Madden, T.J., Miller, K.L., Nahrstedt, K., Pulokas, J., Reilein, A., et al. (1999). Leginon: a system for fully automated acquisition of 1000 electron micrographs a day. Ultramicroscopy *77*, 153–161.

Qiu, X., Audet, J., Wong, G., Pillet, S., Bello, A., Cabral, T., Strong, J.E., Plummer, F., Corbett, C.R., Alimonti, J.B., et al. (2012). Successful treatment of Ebola virus-infected cynomolgus macaques with monoclonal antibodies. Sci. Trans. Med *4*, 138ra181–138ra181.

Qiu, X., Wong, G., Audet, J., Bello, A., Fernando, L., Alimonti, J.B., Fausther-Bovendo, H., Wei, H., Aviles, J., Hiatt, E., et al. (2014). Reversion of advanced Ebola virus disease in nonhuman primates with ZMapp. Nature *514*, 47–53.

Saeed, M.F., Kolokoltsov, A.A., Albrecht, T., and Davey, R.A. (2010). Cellular entry of ebola virus involves uptake by a macropinocytosis-like mechanism and subsequent trafficking through early and late endosomes. PLoS Pathog. *6*, e1001110.

Saphire, E.O. (2013). An update on the use of antibodies against the filoviruses. Immunotherapy *5*, 1221–1233.

Smith, D.H., Johnson, B.K., Isaacson, M., Swanapoel, R., Johnson, K.M., Killey, M., Bagshawe, A., Siongok, T., and Keruga, W.K. (1982). Marburg-virus disease in Kenya. Lancet *1*, 816–820.

Suloway, C., Pulokas, J., Fellmann, D., Cheng, A., Guerra, F., Quispe, J., Stagg, S., Potter, C.S., and Carragher, B. (2005). Automated molecular microscopy: the new Leginon system. J. Struct. Biol. *151*, 41–60.

Tang, G., Peng, L., Baldwin, P.R., Mann, D.S., Jiang, W., Rees, I., and Ludtke, S.J. (2007). EMAN2: an extensible image processing suite for electron microscopy. J. Struct. Biol. *157*, 38–46.

Thomas, D., Newcomb, W.W., Brown, J.C., Wall, J.S., Hainfeld, J.F., Trus, B.L., and Steven, A.C. (1985). Mass and molecular composition of vesicular stomatitis virus: a scanning transmission electron microscopy analysis. J. Virol. *54*, 598–607.

Towner, J.S., Paragas, J., Dover, J.E., Gupta, M., Goldsmith, C.S., Huggins, J.W., and Nichol, S.T. (2005). Generation of eGFP expressing recombinant Zaire ebolavirus for analysis of early pathogenesis events and high-throughput antiviral drug screening. Virology *332*, 20–27.

Towner, J.S., Khristova, M.L., Sealy, T.K., Vincent, M.J., Erickson, B.R., Bawiec, D.A., Hartman, A.L., Comer, J.A., Zaki, S.R., Ströher, U., et al. (2006). Marburgvirus genomics and association with a large hemorrhagic fever outbreak in Angola. J. Virol. *80*, 6497–6516.

Towner, J.S., Amman, B.R., Sealy, T.K., Carroll, S.A.R., Comer, J.A., Kemp, A., Swanepoel, R., Paddock, C.D., Balinandi, S., Khristova, M.L., et al. (2009). Isolation of genetically diverse Marburg viruses from Egyptian fruit bats. PLoS Pathog. *5*, e1000536.

van Heel, M., Harauz, G., Orlova, E.V., Schmidt, R., and Schatz, M. (1996). A new generation of the IMAGIC image processing system. J. Struct. Biol. *116*, 17–24.

Warfield, K.L., Alves, D.A., Bradfute, S.B., Reed, D.K., VanTongeren, S., Kalina, W.V., Olinger, G.G., and Bavari, S. (2007). Development of a model for marburgvirus based on severe-combined immunodeficiency mice. Virol. J. *4*, 108.

Warfield, K.L., Bradfute, S.B., Wells, J., Lofts, L., Cooper, M.T., Alves, D.A., Reed, D.K., VanTongeren, S.A., Mech, C.A., and Bavari, S. (2009). Development and characterization of a mouse model for Marburg hemorrhagic fever. J. Virol. *83*, 6404–6415.

Warren, T.K., Wells, J., Panchal, R.G., Stuthman, K.S., Garza, N.L., Van Tongeren, S.A., Dong, L., Retterer, C.J., Eaton, B.P., Pegoraro, G., et al. (2014). Protection against filovirus diseases by a novel broad-spectrum nucleoside analogue BCX4430. Nature *508*, 402–405.

World Health Organization (2014a). Ebola situation report. W.H.O. Global Alert and Response. January 2015. http://www.who.int/csr/disease/ebola/situation-reports/en/?m=20150121.

World Health Organization (2014b). Marburg virus disease - Uganda. W.H.O. Global Alert and Response. October 2014. http://www.who.int/csr/don/10-october-2014-marburg/en/.

Yu, X., McGraw, P.A., House, F.S., and Crowe, J.E., Jr. (2008). An optimized electrofusion-based protocol for generating virus-specific human monoclonal antibodies. J. Immunol. Methods *336*, 142–151.

Article

Cell

Structural Basis for Marburg Virus Neutralization by a Cross-Reactive Human Antibody

Graphical Abstract

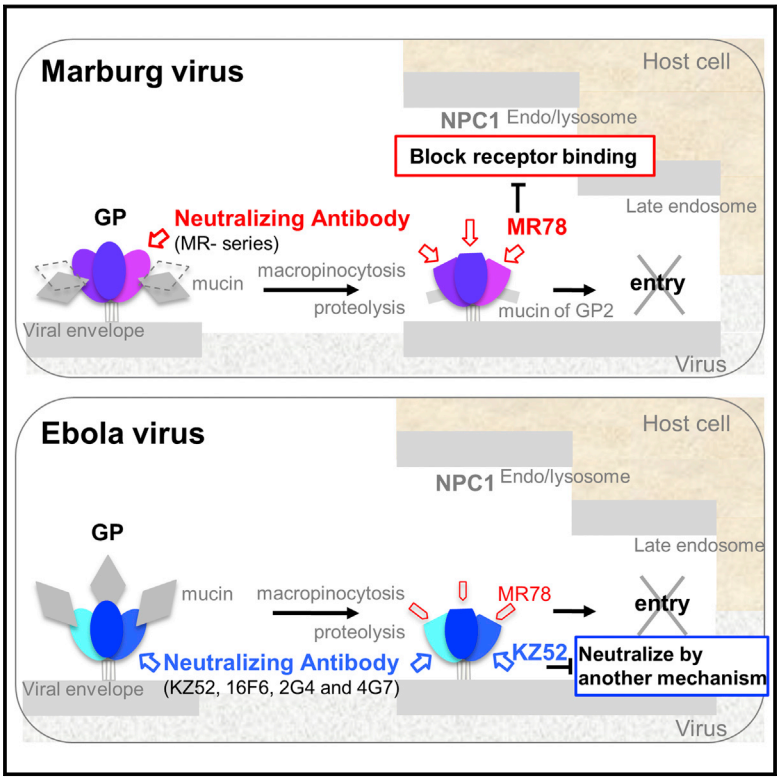

Highlights

- Structure of the Marburg virus GP bound by MR78, a cross-reactive human antibody
- The epitope is conserved among filoviruses and is the likely receptor-binding site
- The antibody-GP interaction mimics that made by the Ebola virus glycan cap
- Mucin domain structure may cause mAbs to react to Ebola and Marburg differently

Authors

Takao Hashiguchi, Marnie L. Fusco, ..., James E. Crowe, Jr., Erica Ollmann Saphire

Correspondence

erica@scripps.edu

In Brief

The structures of Marburg virus glycoprotein in complex with a cross-reactive human antibody, as well as of the Ebola virus glycoprotein bound to the same antibody, reveal that there is a conserved epitope among filoviruses that overlaps with the putative receptor-binding site. These studies provide a map by which therapy with cross-reactive antibodies and inhibitors of entry could be developed.

Accession Numbers

3X2D

Hashiguchi et al., 2015, Cell *160*, 904–912
February 26, 2015
http://dx.doi.org/10.1016/j.cell.2015.01.041

CellPress

Cell

Article

Structural Basis for Marburg Virus Neutralization by a Cross-Reactive Human Antibody

Takao Hashiguchi,[1,2] Marnie L. Fusco,[1] Zachary A. Bornholdt,[1] Jeffrey E. Lee,[1,3] Andrew I. Flyak,[4] Rei Matsuoka,[5] Daisuke Kohda,[5] Yusuke Yanagi,[2] Michal Hammel,[6] James E. Crowe, Jr.,[4,7] and Erica Ollmann Saphire[1,8,*]

[1]Department of Immunology and Microbial Science, The Scripps Research Institute, La Jolla, CA 92037, USA
[2]Department of Virology, Faculty of Medicine, Kyushu University, Fukuoka, 812-8582, Japan
[3]Current address: Department of Laboratory Medicine and Pathobiology, University of Toronto, Toronto, ON M5S 1A1, Canada
[4]Department of Pathology, Microbiology, and Immunology, Vanderbilt University, Nashville, TN 37232, USA
[5]Division of Structural Biology, Medical Institute of Bioregulation, Kyushu University, Fukuoka, 812-8582, Japan
[6]Life Sciences Division, Lawrence Berkeley National Laboratory, Berkeley, CA 94720 USA
[7]Vanderbilt Vaccine Center, Vanderbilt University, Nashville, TN 37232, USA
[8]The Skaggs Institute for Chemical Biology, The Scripps Research Institute, La Jolla, CA 92037, USA
*Correspondence: erica@scripps.edu
http://dx.doi.org/10.1016/j.cell.2015.01.041

SUMMARY

The filoviruses, including Marburg and Ebola, express a single glycoprotein on their surface, termed GP, which is responsible for attachment and entry of target cells. Filovirus GPs differ by up to 70% in protein sequence, and no antibodies are yet described that cross-react among them. Here, we present the 3.6 Å crystal structure of Marburg virus GP in complex with a cross-reactive antibody from a human survivor, and a lower resolution structure of the antibody bound to Ebola virus GP. The antibody, MR78, recognizes a GP1 epitope conserved across the filovirus family, which likely represents the binding site of their NPC1 receptor. Indeed, MR78 blocks binding of the essential NPC1 domain C. These structures and additional small-angle X-ray scattering of mucin-containing MARV and EBOV GPs suggest why such antibodies were not previously elicited in studies of Ebola virus, and provide critical templates for development of immunotherapeutics and inhibitors of entry.

INTRODUCTION

The filovirus family includes Marburg virus and five ebolaviruses (Ebola, Sudan, Reston, Bundibugyo, and Taï Forest viruses), most of which cause highly lethal hemorrhagic fever and multiple outbreaks among humans. Among the filoviruses, Marburg virus was the first to be identified when it sickened laboratory workers in Europe in 1967 (Malherbe and Strickland-Cholmley, 1968; Siegert et al., 1968). Marburg virus has since re-emerged multiple times, with modern strains conferring greater lethality (~90%) (Geisbert et al., 2007; Towner et al., 2006). Sudan virus has caused at least six outbreaks between 1976 and 2013 (Albariño et al., 2013; Bowen et al., 1977; Sanchez and Rollin, 2005; Shoemaker et al., 2012), Bundibugyo virus emerged in 2007 (Towner et al., 2008; Wamala et al., 2010) and again in 2012 (Albariño et al., 2013), and Reston virus was found to infect ranches of swine being raised for human consumption in Asia in 2009 and 2011 (Barrette et al., 2009; Pan et al., 2014; Sayama et al., 2012). Ebola virus is typically found in Central Africa, but re-emerged in Western Africa in 2014 to cause an outbreak unprecedented in magnitude and geographic spread (WHO Ebola Response Team, 2014). During this outbreak, an experimental Ebola virus-specific monoclonal antibody (mAb) cocktail (Qiu et al., 2014) was used compassionately in several patients. No such treatment yet exists that could be used against Marburg virus or the other four ebolaviruses.

Filoviruses express a single protein on their envelope surface, a glycoprotein termed GP, which is responsible for attachment to, and entry of, host cells (Sanchez et al., 1996). GP forms a trimer on the viral surface. In the trimer, each monomer is comprised of GP1 and GP2 subunits that are anchored together by a GP1-GP2 disulfide bond (Volchkov et al., 1998). GP1 contains a receptor-binding core topped by a glycan cap and a heavily glycosylated mucin-like domain (Lee et al., 2008), while GP2 contains two heptad repeats and a transmembrane domain. Filoviruses initially enter cells via macropinocytosis (Aleksandrowicz et al., 2011; Nanbo et al., 2010; Saeed et al., 2010; Mulherkar et al., 2011). Once in the endosome, the viral surface GP is cleaved by host cathepsins. Cleavage removes the mucin-like domains and glycan cap (Chandran et al., 2005; Schornberg et al., 2006; Hood et al., 2010; Marzi et al., 2012a; Brecher et al., 2012) and renders GP competent to bind the Niemann Pick C1 (NPC1) receptor (Carette et al., 2011; Côté et al., 2011). Interestingly, Ebola virus entry requires cleavage by cathepsin B (Chandran et al., 2005; Martinez et al., 2010; Schornberg et al., 2006), while Marburg virus entry is independent of cathepsin B (Gnirss et al., 2012; Misasi et al., 2012). The reasons underlying these differences are unknown. After enzymatic cleavage and receptor binding, the GP2 subunit unwinds from its GP1 clamp and rearranges irreversibly into a six-helix bundle (Malashkevich et al., 1999; Weissenhorn et al., 1998a; Weissenhorn et al., 1998b) to drive fusion of virus and host membranes.

Antibody therapies recently have demonstrated effective post-exposure protection against filoviruses in animal models (Dye et al., 2012; Marzi et al., 2012b; Olinger et al., 2012; Pettitt et al., 2013; Qiu et al., 2012; Qiu et al., 2014). MAbs can be produced on large scale and offer more reproducible effects than polyclonal sera from survivors. However, most mAbs available only recognize Ebola virus. Very few are yet described against Marburg virus, and no antibodies are yet described that cross-react among the filoviruses. Indeed, Marburg and Ebola GP are 72% different in protein sequence, and the filoviruses are thought to be antigenically distinct. Further, there is no structure available for the unique Marburg virus GP, by which we may interpret differences in requirements for viral entry, or develop immunotherapeutics or inhibitors of entry.

Here, we report the crystal structure of the trimeric, receptor-competent form of Marburg virus GP in complex with a neutralizing antibody, termed MR78, that was identified in a recent human survivor of Marburg virus infection (Flyak et al., 2015). Atypically, MR78 cross-reacts to cleaved Ebola virus GP. An additional structure of MR78 in complex with Ebola virus GP illustrates the basis of the cross-reactivity: the antibody binds a hydrophobic ''trough'' at the top of GP1, the sequence and structure of which are conserved across the filoviruses. We propose that this trough is the binding site of the critical domain C of the NPC1 receptor. Indeed, MR78 blocks binding of domain C to Marburg GP. Further, the extended third complementarity-determining region of the heavy chain (CDR H3) of MR78 mimics the glycan cap that shields this site on Ebola virus prior to entry and may mimic the receptor itself. These crystal structures plus additional biophysical analysis of complete, mucin-containing Ebola and Marburg GP ectodomains reveal that the receptor-binding site is masked on the surface of Ebola virus but more exposed on the surface of Marburg virus. These findings may explain why a cross-reactive antibody such as MR78 has not been identified in studies of Ebola virus.

RESULTS

Structure Determination

Trimeric GP ectodomains for Marburg virus (MARV; strain Ravn) or Ebola virus (EBOV, also known as Ebola Zaire; strain Mayinga) were expressed in *Drosophila* S2 cells, with or without their mucin-like domains (GP and GPΔmuc, respectively). MARV and EBOV GPΔmuc were further proteolyzed by trypsin or thermolysin, respectively, to produce cleaved GP (GPcl) resembling the version of GP competent for receptor binding in the endosome (Figure S1A). Three hundred versions of MARV GP were engineered and complexed with 22 different mAbs in order to find a crystallizable combination. Hundreds of crystals of the final MARV GPcl-MR78 combination were grown and screened for X-ray diffraction: just one crystal yielded suitable diffraction.

Diffraction to 3.6 Å resolution was obtained from a single crystal of the MARV GPcl-Fab MR78 complex. The structure was determined by molecular replacement using EBOV GP and Fab KZ52 (Lee et al., 2008) as search models and was refined to R_{work} of 24.7 % and R_{free} of 27.9 % (Table S1). Four GP-Fab complexes are contained in the asymmetric unit: one complete trimer and one other monomer, which forms its biologically relevant trimer around a crystallographic 3-fold axis.

Differences in GP Structure between EBOV and MARV

Although the overall organization is similar between Marburg and Ebola GPs (1.8 Å rmsd among 212 Cα atoms) (Figures 1A and 1B), several structural differences exist that may explain their differing requirements for cellular entry. The first difference is that the intra-GP1 disulfide bond formed by C121 and C147 in ebolavirus GP structures (Ebola [Lee et al., 2008] and Sudan [Bale et al., 2012; Dias et al., 2011]) does not exist in MARV. In MARV, the two cysteines are replaced instead with L105 and H131 (Figure 1C and Figure S1B). As a result, the equivalent polypeptides, which form the crest of the receptor-binding subunit, differ in structure and flexibility. In the ebolaviruses, the polypeptide bearing C147 (residues 145 to 150) turns inward, toward the trimer center to disulfide bond to C121. In MARV, the equivalent polypeptide (residues 129 to 134) turns outward into solvent, away from the trimer center.

A second difference between MARV and the ebolaviruses lies at the base of the cathepsin cleavage loop. In MARV, these residues (172-180) form a clear alpha helix (α2), which packs against the outside of the GP2 fusion loop, interacting with both the N- and C-terminal strands of the fusion loop (Figure 1D). In ebolaviruses, the equivalent residues predict to form a loop rather than a helix and are disordered (Bale et al., 2012; Dias et al., 2011; Lee et al., 2008). In MARV GP, the peptide connecting this α2 helix to β14 in the glycan cap would necessarily and immediately cover the both N- and C-terminal arms of the GP2 fusion loop, and if uncleaved, would hinder the conformational changes of fusion. Structural differences in α2 of MARV may prevent effective processing by cathepsin B.

The third difference in the MARV GP structure lies at the N terminus, in the base of the β sheet that forms the GP1 spool, about which the metastable GP2 subunit is wound. In EBOV, the base of the spool connects to the anchoring GP1-GP2 disulfide bond by a short stretch of polypeptide that intimately interacts with GP2. This short connecting polypeptide contains an N-linked glycan at Asn40, and also contains residue Asp47, which renders EBOV dependent on cathepsin B for entry (Misasi et al., 2012). In EBOV entry, cathepsin B removes an additional and critical 1 kDa of mass from GP beyond that removed by cathepsin L, but the site and consequences of that extra cleavage event are not yet known. We propose that if cathepsin B cleaves this connecting loop, EBOV GP2 would be freed from the constraints of the disulfide bond and better able to undergo the conformational rearrangements of fusion. Our crystal structure reveals that MARV, which is cathepsin B-independent, is structured differently from EBOV at the same site. In MARV, the base of the GP1 spool is more mobile and is shifted toward the center of the trimer, inside of the fusion loop. Further, unlike in ebolaviruses (Dias et al., 2011; Bale et al., 2012), the polypeptide connection to the MARV GP1-GP2 disulfide could not be visualized and the N-linked glycan is absent. The nearest glycan is instead attached to residue 171 on the MARV GP1 β sheet itself (Figure 1E). These differences in sequence, glycosylation, mobility, and conformation likely allow MARV to be cleaved by other enzymes and render MARV cathepsin B-independent.

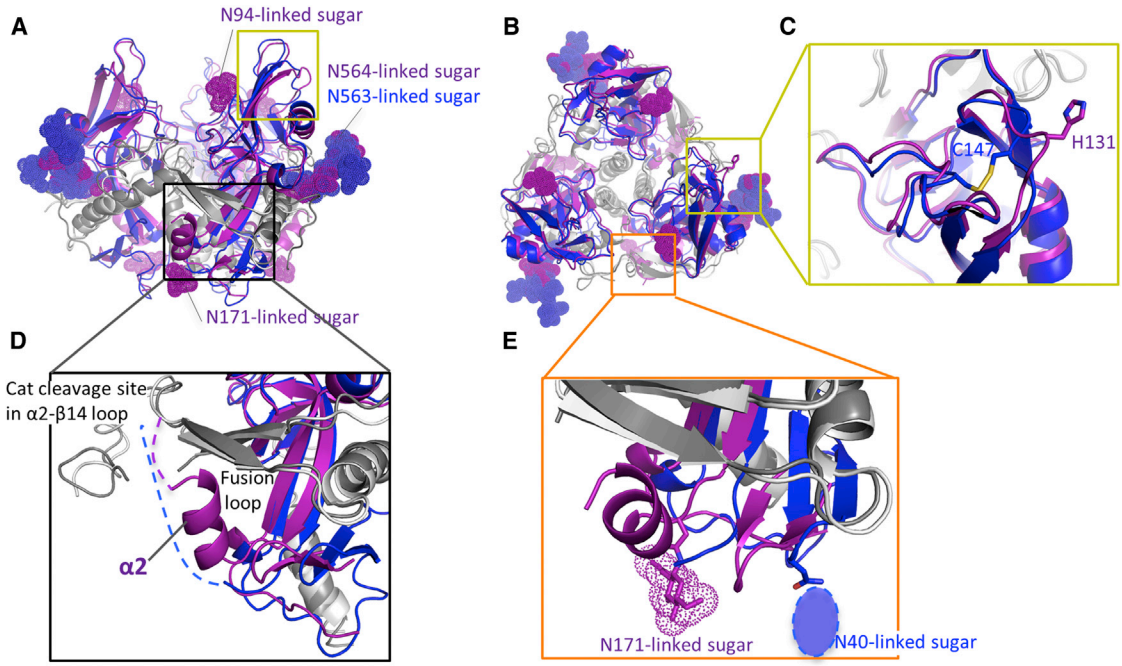

Figure 1. Structure of Marburg Virus GP

(**A**) Crystal structure of MARV GPcl (GP1, purple and GP2, dark gray) superimposed with the equivalent structure of EBOV (PDB ID, 3CSY; GP1, blue; and GP2, light gray). The glycan cap of EBOV GP is deleted for clarity. The yellow box outlines the MR78 epitope and putative receptor-binding site. The black box outlines the interaction site of the MARV-specific helix α2 of GP1 (purple) with the fusion loop of GP2 (dark gray). The visible N-linked sugars on MARV and EBOV GPcl crystal structures are shown as dot models. MARV GPcl bears glycans at positions N94 and N171, which are not glycosylated in EBOV. See also Figure S1.

(B) Top view of GP.

(C) MARV GP lacks the intra-GP1 disulfide bond of EBOV. C147 of EBOV (blue) is replaced by H131 in MARV (purple), and the corresponding polypeptide traces outward from the trimer center. The orange box outlines the glycan attachment sites at the base of each GP.

(D) Residues 172–180 of MARV form an α helix (α2) that packs against both N- and C-terminal arms of the fusion loop. In ebolaviruses, the equivalent residues are predict to form a loop rather than a helix and are disordered in crystal structures.

(E) At the base of GP, MARV bears a glycan attached to N171 while EBOV bears a glycan attached to N40 (drawn as an oval as it was not included in the EBOV crystal structure).

Overall Organization of the MARV or EBOV GPcl Bound to Fab MR78

The crystal structure of MARV GPcl in complex with the Fab fragment of MR78 indicates that MR78 binds the membrane-distal head of GP1 (Figure 2A). We determined an additional, low-resolution structure of EBOV GPcl bound to both MR78 and KZ52. The ternary EBOV complex, determined by molecular replacement, demonstrates that the MR78 antibody recognizes a similar site on both MARV and EBOV (Figures 2B, S2, and Table S1). MR78 binds into a highly conserved hydrophobic trough revealed at the top of the EBOV GP1 core, after removal of the glycan cap by proteolytic cleavage in the endosome. Although MARV and EBOV diverge significantly in sequence overall, residues contained in this site, the MR78 epitope, are 85% similar between the viruses (Figures 3A and S1B).

Likely Receptor-Binding Site

The location and structural conservation of this site suggest that it could be the binding site of the NPC1 receptor, used by all known filoviruses (Carette et al., 2011; Côté et al., 2011; Miller et al., 2012; Ng et al., 2014). Indeed, in ELISA, MR78 inhibits binding of NPC1 domain C to MARV GP (Figure S3A). This site, at the apex of cleaved GP1, resembles an ocean wave morphology, with a lower trough beneath a rising crest. The trough is hydrophobic and is formed by α1, β4 and the loop that connects them (residues 63-74 in MARV). It is 22 Å wide and 8 Å deep at F72. The crest is hydrophilic, includes charged residues previously identified as essential for virus entry (Dube et al., 2009; Manicassamy et al., 2005; Manicassamy et al., 2007), and is formed by strands β7, β9 and their connecting loops (residues 92–106 and 120–134 in MARV). The 120–134 loop contains H131, which replaces the cysteine and the intra-GP1 disulfide bond of EBOV (Figure 3B).

Here, we show by ELISA that a Q128S and N129S double mutant in MARV GP abrogates binding to NPC1 domain C (Figure S4A). Q128 and N129 are at the tip of the crest and could make direct hydrophilic interaction with NPC1. The trough itself is formed by hydrophobic side chains, such as F72 (equivalent to F88 in EBOV). Also forming the trough are the main chains of hydrophilic residues; these polar side chains reach away from the trough into the trimer to make key stabilizing contacts to GP2. Two examples are R73 and K79, previously shown to be essential for MARV infectivity (Manicassamy et al., 2007). In the crystal structure, R73 makes multiple hydrogen bonds to the fusion loop

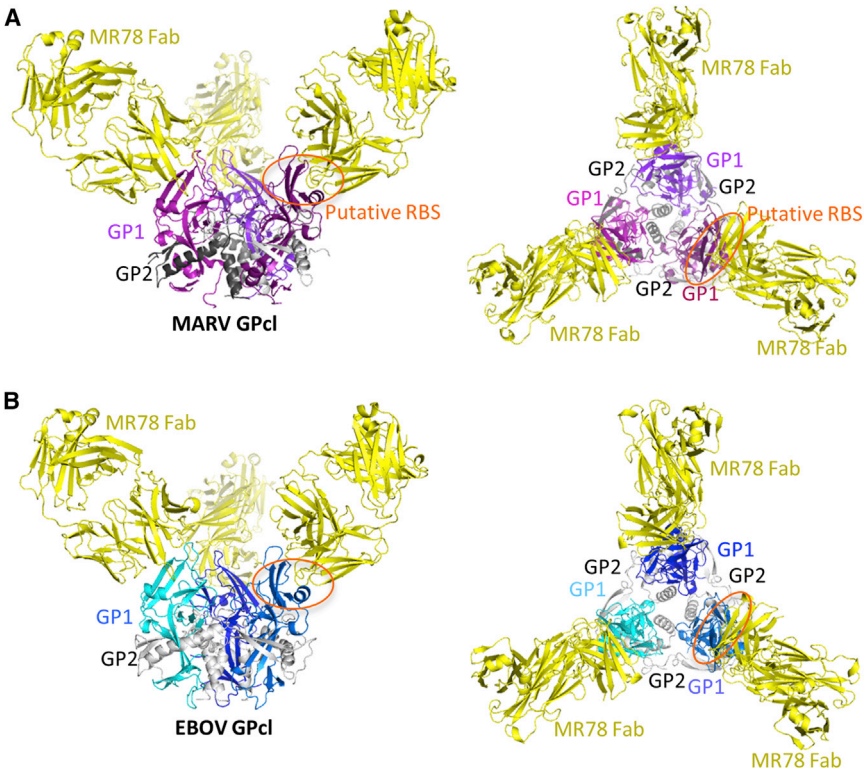

Figure 2. MR78 Binds Both MARV and EBOV GPcl at the Apex of GP1

(A) 3.6 Å crystal structure of MARV GPcl in complex with Fab MR78. Each GP1 is colored a different shade of purple, GP2 is gray, and the MR78 Fab is in yellow.

(B) 8 Å structure of EBOV GPcl in complex with Fab MR78, determined by molecular replacement and rigid body refinement. Each EBOV GP1 is colored a different shade of blue and GP2 is gray. See also Figure S2. Fab MR78 (yellow) binds the apex of GP1 of both viruses.

of the neighboring protomer in the trimer (Figure S4B) and likely plays a key role in maintaining the prefusion structure or transmitting a conformational change to the fusion loop after receptor binding. K79 interacts with the main chain of residues 574–577 of GP2 (Figure S4C), residues that connect the separated helical segments of the first heptad repeat. We propose that binding of NPC1 domain C involves contact with the hydrophilic crest and hydrophobic trough, and that binding in the trough may transmit conformational changes to GP2 via R73 and K79 (equivalent to R89 and K95 in EBOV). Although MR78 binds both MARV and EBOV GPcl, it only outcompetes NPC1 domain C for binding of MARV GPcl (Figure S3B). MR78 may have lower affinity for EBOV GPcl than MARV GPcl or domain C may bind the GPs slightly differently.

GP-MR78 Interactions

The interaction surface between the MR78 antibody and MARV GP buries 976 Å^2 of molecular surface and is primarily hydrophobic. Contact is mediated by both the heavy and light chains, but the primary region of interaction is the 17-residue CDR H3 (Figures 3C and S3CD), which penetrates the hydrophobic trough in MARV GP1. In this interaction, F111.2 and Y112.2 of the CDR H3 interact with P63, S67, W70, F72, I95 and I125 of MARV GP (IMGT numbering, Figure 4A).

Notably, these interactions are similar to those made by the Ebola virus glycan cap, which occupies this site prior to enzymatic cleavage in the endosome. In Ebola virus, the equivalent interactions are made by F225 and Y232 of the EBOV glycan cap interacting with P80, T83, W86, F88, L111 and V141 on EBOV GP (Figure 4B). Similarity may even extend to the key domain C of the NPC1 receptor itself, as domain C contains similar Phenylalanine and Tyrosine residues that are essential for binding GP (Ndundo and Chandran, personal communication). Further, F72 in MARV, which is equivalent to F88 in EBOV, interacts with CDR H3 in the bottom of the trough. Both F72 of MARV and F88 of EBOV are critical for attachment and entry (Martinez et al., 2013; Mpanju et al., 2006) and may interact directly with essential hydrophobic residues of domain C. The binding mode of MR78 is reminiscent of anti-influenza virus human mAbs in which long CDR H3s similarly reach into the conserved receptor-binding site (Barbey-Martin et al., 2002; Bizebard et al., 1995; Hong et al., 2013; Lee et al., 2014; Schmidt et al., 2013; Whittle et al., 2011; Xu et al., 2013). In many cases those influenza mAbs also use Phe or Tyr aromatic residues to interact with an aromatic residue in the viral receptor binding domain, suggesting that the favorable energetics and intermolecular interactions of common aromatic molecules may constitute a canonical mode of binding of antiviral antibodies to recessed receptor-binding sites.

Although the MR78 epitope is largely conserved in sequence and structure between MARV and EBOV, it differs in its exposure at different stages of virus entry. MR78 binds MARV GP equally well whether MARV GP is in its uncleaved, viral-surface form or its cleaved, endosomal form. In contrast, MR78 does not bind uncleaved EBOV GP. It only binds the endosomal, cleaved form from which the glycan cap has been removed. Together, these results suggest that in EBOV, the glycan cap effectively blocks the MR78 epitope and putative receptor-binding site on the (uncleaved) viral surface, but that in MARV, the epitope and at least part of the receptor-binding site is fully exposed on the viral surface. Better exposure of this site may explain why antibodies against the putative receptor-binding site were elicited by MARV infection (see companion paper by Flyak et al., 2015), but seem to be more rarely elicited and have not yet been described against EBOV.

Differences in Mucin-Like Domains between MARV and EBOV, and Possible Effect on Antibody Reactivity

In addition to a glycan cap, the GP spike on the viral surface includes three heavily glycosylated mucin-like domains that are ~75 kDa each in mass and are predicted to have little secondary

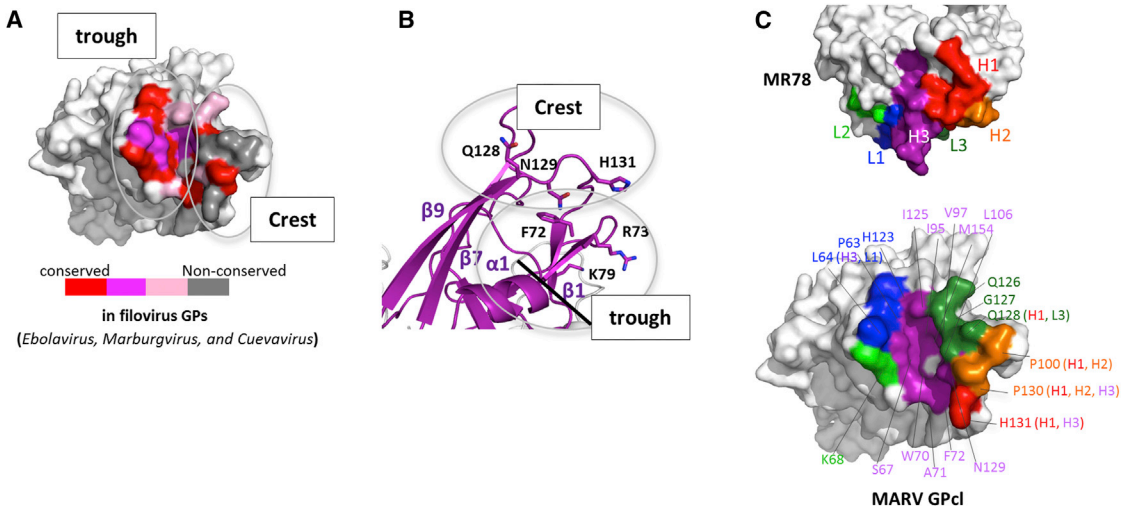

Figure 3. MR78 Recognizes a Conserved Epitope at the Apex of Cleaved GP1

(**A**) Conservation of the MR78 epitope among filovirus GPs, mapped onto one monomer of MARV GPcl. Sequence alignment was performed in *ebolavirus* (*Ebola, Sudan, Reston, Tai Forest, Bundibugyo*), *marburgvirus* (Musoke, Angola, Popp, Ci67, DRC1999, Ravn), and *cuevavirus* (Lloviu) genuses. Residues identical across the filoviruses are colored red; residues that possess strong similarity, magenta; weak similarity, pink; no similarity, gray.

(B) The apex of cleaved MARV GP1, where Fab MR78 binds, forms a wave crest-and-trough morphology (magenta). The hydrophilic crest and the hydrophobic trough each contain residues previously shown to be critical for virus entry (Dube et al., 2009; Manicassamy et al., 2005; Manicassamy et al., 2007; Mpanju et al., 2006). The diagonal black line indicates the base of the trough. See also Figure S4.

(C) Surface representation of the interface between one monomer of MARV GPcl (bottom) and Fab MR78 (top). CDR H1 is colored red; CDR H2, orange; CDR H3, purple; CDR L1, blue; CDR L2, green; CDR L3, forest green. The footprint on MARV GPcl is colored according to the CDR that mediates the contact. GP residues contacted by MR78 are indicated and colored according to the CDR that mediates the contact (CDR names in parentheses).

structure. All mucin-containing GPs thus far have been refractory to crystallization. In order to visualize the native glycoprotein ectodomain and position of the mucin-like domain relative to the receptor-binding core, we turned to Small-Angle X-ray Scattering (SAXS) in solution. SAXS data collected for mucin-containing EBOV or MARV GP trimers indicate that the mucin-like domains of both viruses are large and extend outward from the GP core. The radius of gyration, R_G, for mucin-deleted and mucin-containing MARV GPs are 50 and 72 Å, respectively, and maximum dimension, D_{max}, for mucin-deleted and mucin-containing GPs are 160 and 250Å, respectively, indicating that the mucin-like domain of MARV widens the molecule up to 90 Å (Figures 5A and S5). The mucin-like domains of MARV are a bit larger than those of EBOV (67 Å R_G and 225 Å D_{max} for mucin-containing EBOV GP), consistent with their greater volume determined by SAXS (Figure S5C) and mass noted by SDS-PAGE (Figure S5D). The mucin-like domains of EBOV appear to project more upward (consistent with EM tomography [Tran et al., 2014]), while those of MARV appear to project less upward, more equatorially, and to cover the sides of the GP trimer (Figures 5A and 5B). Although the mucin-like domains are likely flexible (see Porod-Debey coefficient P in Figure S5C), an equatorial, rather than upward projection is consistent with attachment points of the mucin-like domain to both GP1 and GP2 in MARV. In EBOV, a different position of the furin cleavage site results in all of mucin-like domain being attached to GP1. The MARV GP2 portion of the mucin-like domain, residues 436–509, is attached to residue 510 on the side of the MARV GP trimer, but is flexible and disordered.

A differing position of the mucin-like domains between MARV and EBOV would leave different surfaces exposed for immune recognition. The equatorial projection of the MARV mucin-like domain, for example, would leave the expected receptor-binding site at the top more accessible on MARV than EBOV, and further supports the notion that antibodies against the expected receptor-binding site would be more likely to be elicited using marburgvirus antigens than ebolavirus antigens. The accompanying paper (Flyak et al., 2015) and other immunization studies (Qiu et al., 2011; Wilson et al., 2000) support this notion.

In contrast, on EBOV, the upward projection of the mucin-like domains and the absence of mucin attached to EBOV GP2 would leave the EBOV base more exposed for antibody surveillance, compared to that of MARV. Indeed, in the accompanying paper by Flyak et al., none of the 18 neutralizing antibodies raised against MARV appear to bind the base of the MARV GP, while multiple neutralizing antibodies elicited by ebolaviruses are known to bind, or thought to bind, to the base of ebolavirus GP (Dias et al., 2011; Lee et al., 2008; Qiu et al., 2012; Murin et al., 2014) (Figure 5C).

DISCUSSION

In summary, the crystal structures and accompanying experiments indicate that MR78 binds a conserved site on the apex of GP1 that is available on the surface of MARV GP, but masked on EBOV GP prior to enzymatic cleavage. The epitope of MR78 likely overlaps with the receptor-binding site, and hydrophobic contacts made by CDR H3 to the hydrophobic trough may mimic

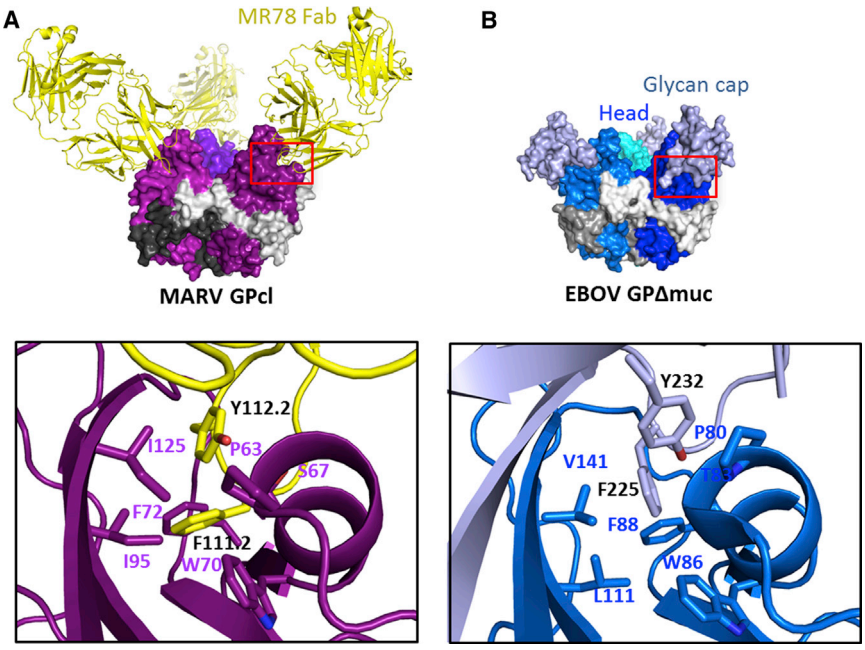

Figure 4. Similarity in Recognition of the Putative Receptor-Binding Site by MR78 and the Ebola Virus Glycan Cap

(**A**) The CDR H3 of MR78 (yellow) reaches into the hydrophobic trough of GP1 (purple). F111.2 and Y112.2 of CDR H3 interact with P63, S67, W70, F72, I95, and I125 of MARV GP.

(B) Similar residues of the EBOV glycan cap (light blue) bind into this trough on the surface of EBOV GP (blue), prior to enzymatic cleavage. Here, F225 and Y232 of the glycan cap interact with P80, T83, W86, F88, L111, and V141 in the trough (PDB ID; 3CSY).

those of the as-yet-unvisualized NPC1 domain C. MR78 does not neutralize authentic EBOV, likely because its epitope is masked on the EBOV surface by the mucin-like domain and glycan cap on the virus surface. MR78 does, however, neutralize authentic MARV (Flyak et al., 2015) and could be a valuable monoclonal antibody therapeutic against this extremely lethal virus. Importantly, no mAb therapeutic yet exists against MARV, and few mAbs are yet known against MARV from which such a therapeutic could be developed. The crystal structure of MARV GP presented here, and the highly conserved MR78 epitope, provide strategies for immunotherapy and templates for development of potentially broad-spectrum inhibitors of filovirus entry.

EXPERIMENTAL PROCEDURES

Construction, Expression, and Purification of MARV/EBOV GP

DNA encoding the MARV GPΔmuc ectodomain (residues 1–636 with a mucin deletion of residues 257–425), point mutants of MARV GPΔmuc and the EBOV GPΔmuc ectodomain (residues 1–637 with a mucin deletion of residues 314–462) were amplified by PCR using codon-optimized and whole-gene synthesized MARV or EBOV GPs as templates. Four point mutations in MARV GPΔmuc, F438L, W439A, F445G, and F447N, on GP2, located around the furin cleavage site were found to improve the efficiency of furin cleavage. GP constructs were cloned into a derivative of the expression vector pMT. This derivative vector contains the puromycin resistant gene and a C-terminal double-strep tag sequence. Expression plasmids were transfected using Effectin (QIAGEN) into 80% confluent *Drosophila* Schneider S2 cells. The cells were first cultured in complete Schneider's medium supplemented with 10% (v/v) FCS (LONZA), and were adapted to Insect Xpress medium by progressively modifying the Schneider/Insect Xpress medium ratio with 6.0 μg/ml puromycin. Large-scale expression of the MARV/EBOV GPΔmuc was performed using stable S2 cell lines in 2 l Erlenmeyer flask at 27.0°C, induced with 0.5 mM $CuSO_4$. Supernatants containing the expressed proteins were harvested 4 days after induction, and mixed with the Strept-Tactin affinity column binding buffer (100 mM Tris-HCl, 150 mM NaCl, 1 mM EDTA, 15 μg/ml Avidin [pH8.0]). The proteins were purified via Strept-Tactin affinity, followed by Superdex 200GL 10/300 (GE Healthcare Life Sciences) size-exclusion chromatography (S200 SEC).

Preparation and Crystallization of GP-Antibody Complexes

To mimic endosomal protease cleavage and produce MARV GPcl, MARV GPΔmuc was incubated with 0.01 mg trypsin at 37°C for 1 hr in 20 mM TBS [pH 8.0], 100 mM NaCl. The reaction was stopped using 0.5 mM 4-(2-Aminoethyl) benzenesulfonyl fluoride hydrochloride (AEBSF), and the protein was purified by S200 SEC. EBOV GPcl was produced by incubating EBOV GPΔmuc with 0.02 mg thermolysin overnight at room temperature in 20 mM TBS [pH 7.5], 100 mM NaCl, 1 mM $CaCl_2$, and purified by S200 SEC. Hybridoma cells expressing the human MR78 antibody were generated from peripheral blood mononuclear cells (PBMCs) from a donor, who contracted MARV infection in the Python Cave in Queen Elizabeth National Park, Uganda in 2008 (see Flyak et al., 2015). MR78 was expressed in serum-free medium (Hybridoma-SFM, GIBCO), and culture supernatants were centrifuged, sterile-filtered, and purified over HiTrap Protein G columns (GE Healthcare Life Sciences). Fab fragments were generated by standard papain digestion, with released Fc and undigested IgG removed by Protein A chromatography, and remaining Fab fragments further purified by MonoQ ion-exchange chromatography. For crystallization, purified MARV GPcl was mixed with excess Fab MR78 for 2 days at 4°C. Complexes were separated from unbound Fab via S200 SEC. Crystals were grown by hanging-drop vapor diffusion at 20°C using 0.8 μl protein (13.0 mg ml^{-1}, in 20 mM Tris-HCl [pH 8.0], 100 mM NaCl) and 0.8 μl of mother liquor (100 mM NaCl, 50 mM MES [pH 6.5], 13 % PEG 4000, 0.5 % ethyl acetate). These crystals were cryoprotected with 25% glycerol plus mother liquor before flash cooling in liquid nitrogen. One crystal diffracted to a resolution of 3.6 Å. EBOV GPcl was complexed with Fabs KZ52 and MR78 and crystallized using hanging-drop vapor diffusion at 20°C with 1.0 μl of protein (6 mg/ml, 150 mM NaCl, 10 mM Tris [pH 7.5]) and 1.0 μl of mother liquor (100 mM NaAcetate [pH 4.6], 200 mM NH4SO4, 10% PEG 3350, 2% PEG 400). The crystals were then cryoprotected by washing in 100 mM NaAcetate [pH 4.6], 200 mM NH4SO4, 12% PEG 3350, 10% PEG 400, 10% ethylene glycol. Only diffraction to 8 Å was obtained, but this data permitted molecular replacement using Phaser (McCoy et al., 2007) and EBOV GP and KZ52 (Lee et al., 2008) as search models.

ACCESSION NUMBERS

Coordinates and structure factors have been deposited into the Protein Data Bank under the accession code 3X2D.

SUPPLEMENTAL INFORMATION

Supplemental Information includes Extended Experimental Procedures, five figures, and one table and can be found with this article online at http://dx.doi.org/10.1016/j.cell.2015.01.041.

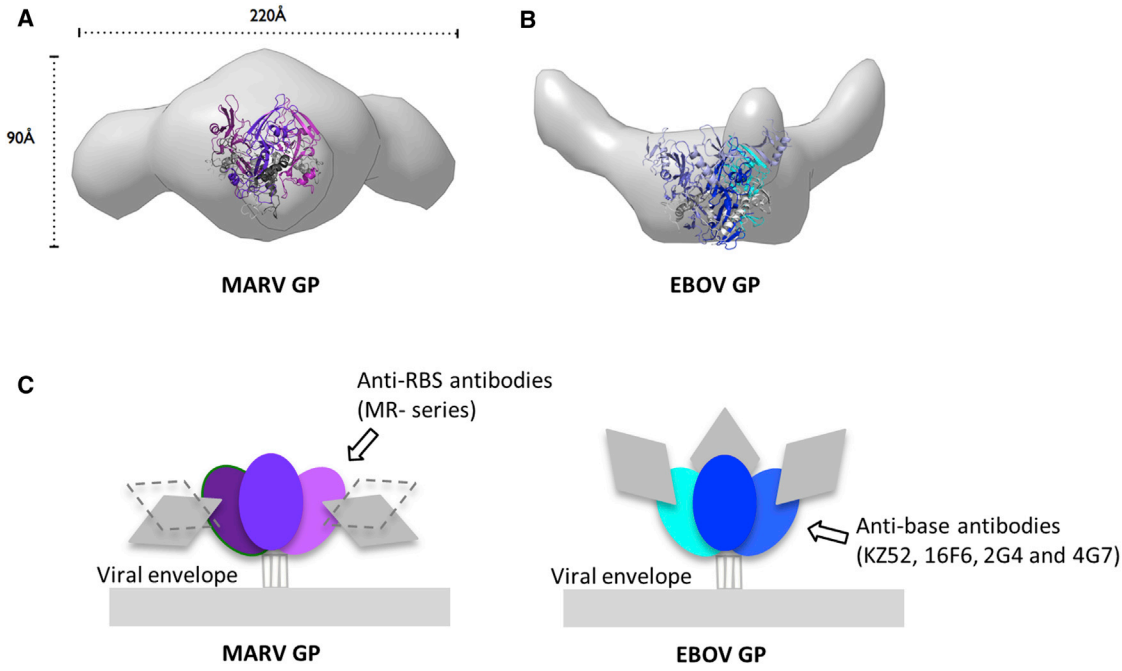

Figure 5. MARV and EBOV Present Different Surfaces for Antibody Recognition

(A and B) Molecular envelopes of mucin-containing MARV and EBOV GP ectodomains determined by SAXS. Rendered Gaussian distributions of molecular envelopes are illustrated in light gray, with ribbon models of the crystallized MARV GPcl and EBOV GPΔmuc trimers to scale and overlaid for comparison. The trimers are illustrated as ribbons. Note that the glycan cap was removed from MARV GP used in crystallization in order to improve diffraction but was contained in the complete MARV GP used for SAXS. The glycan cap did not inhibit diffraction of EBOV GP and is included in the EBOV GP crystal structure. MARV GPcl is colored in purple (GP1) and gray (GP2). EBOV GPΔmuc is colored blue (GP1), white blue (GP1 glycan cap), and gray (GP2). MARV GP is drawn in two possible orientations because definitive placement of polypeptide is challenging at this resolution. In either orientation however, the mucin-like domains of MARV project sideways, equatorially or downward from the core of GP. In MARV, the mucin-like domain is attached to both GP1 and GP2. By contrast, in EBOV, the mucin-like domain is attached solely to GP1, there is no anchor at the base. Both these SAXS experiments and previous electron tomography (Tran et al., 2014) agree on the upward projection of the mucin-like domains in EBOV. See also Figure S5.

(C) Differing positions of the mucin-like domains between MARV and EBOV may lead to elicitation of different types of antibodies. The lower position and GP2 anchor of the mucin-like domain of MARV may better mask the base of GP but expose its upper surfaces, allowing antibodies like mAb MR78 to be elicited. The upward projection of the EBOV mucin-like domain and absence of any GP2 anchor, appear to better mask upper surfaces, but expose the base, allowing antibodies such as KZ52 (Lee et al., 2008), 2G4, 4G7 (Murin et al., 2014), and 16F6 (directed against Sudan ebolavirus [Dias et al., 2011; Bale et al., 2012]) to be elicited.

AUTHOR CONTRIBUTIONS

Experiments were conceived by E.O.S. with T.H., M.L.F., J.E.L., and Z.A.B. All structural and biochemical work was performed by T.H., M.L.F., Z.A.B., J.E.L., A.I.F. and analyzed by T.H., M.L.F., Z.A.B., J.E.L., A.I.F., R.M., D.K., Y.Y., M.H., J.E.C., and E.O.S. The manuscript was written by E.O.S. and T.H. All authors contributed to editing the manuscript and support the conclusions.

ACKNOWLEDGMENTS

We would like to thank Dr. Adrianna P.P. Zhang (TSRI) for help with data collection, Dr. Sebastien Igonet (TSRI and Calixar) for assistance with S2 cell expression, Dr. Kartik Chandran (Albert Einstein College of Medicine), C. Daniel Murin, and Dr. Andrew Ward (TSRI) for valuable discussions, and the beamline staff of Photon Factory (Tsukuba, Japan) for technical help during data collection. We thank NIAID CETR U19 AI109762 (E.O.S.), R01 AI089498, and R21AI069347 (E.O.S.); Defense Threat Reduction Agency grant HDTRA1-13-1-0034; NIAID grant U19 AI109711 (J.E.C.); MEXT KAKENHI grant numbers 26713018 (T.H.) and 24115005 (Y.Y.); MEXT Platform for Drug Discovery Informatics and Structural Life Science (T.H.), JSPS Postdoctoral Fellowships (DC2 [R.M.], Research Abroad [T.H.]); a Research Fellowship of The Uehara Memorial Foundation (T.H.); an Investigators in the Pathogenesis of Infectious Disease award from the Burroughs Wellcome Fund (E.O.S.); and an NIH grant MINOS GM105404 (M.H.) for support. SIBYLS beamline efforts to combine SAXS and crystallography at the Advanced Light Source of Lawrence Berkeley National Laboratory are supported in part by US DOE program Integrated Diffraction Analysis Technologies (IDAT). This is manuscript # 28060 from The Scripps Research Institute.

Received: October 18, 2014
Revised: January 8, 2015
Accepted: January 27, 2015
Published: February 26, 2015

REFERENCES

Albariño, C.G., Shoemaker, T., Khristova, M.L., Wamala, J.F., Muyembe, J.J., Balinandi, S., Tumusiime, A., Campbell, S., Cannon, D., Gibbons, A., et al. (2013). Genomic analysis of filoviruses associated with four viral hemorrhagic fever outbreaks in Uganda and the Democratic Republic of the Congo in 2012. Virology *442*, 97–100.

Aleksandrowicz, P., Marzi, A., Biedenkopf, N., Beimforde, N., Becker, S., Hoenen, T., Feldmann, H., and Schnittler, H.J. (2011). Ebola virus enters host cells

by macropinocytosis and clathrin-mediated endocytosis. J. Infect. Dis. *204* (3), S957–S967.

Bale, S., Dias, J.M., Fusco, M.L., Hashiguchi, T., Wong, A.C., Liu, T., Keuhne, A.I., Li, S., Woods, V.L., Jr., Chandran, K., et al. (2012). Structural basis for differential neutralization of ebolaviruses. Viruses *4*, 447–470.

Barbey-Martin, C., Gigant, B., Bizebard, T., Calder, L.J., Wharton, S.A., Skehel, J.J., and Knossow, M. (2002). An antibody that prevents the hemagglutinin low pH fusogenic transition. Virology *294*, 70–74.

Barrette, R.W., Metwally, S.A., Rowland, J.M., Xu, L., Zaki, S.R., Nichol, S.T., Rollin, P.E., Towner, J.S., Shieh, W.J., Batten, B., et al. (2009). Discovery of swine as a host for the Reston ebolavirus. Science *325*, 204–206.

Bizebard, T., Gigant, B., Rigolet, P., Rasmussen, B., Diat, O., Bösecke, P., Wharton, S.A., Skehel, J.J., and Knossow, M. (1995). Structure of influenza virus haemagglutinin complexed with a neutralizing antibody. Nature *376*, 92–94.

Bowen, E.T., Lloyd, G., Harris, W.J., Platt, G.S., Baskerville, A., and Vella, E.E. (1977). Viral haemorrhagic fever in southern Sudan and northern Zaire. Preliminary studies on the aetiological agent. Lancet *1*, 571–573.

Brecher, M., Schornberg, K.L., Delos, S.E., Fusco, M.L., Saphire, E.O., and White, J.M. (2012). Cathepsin cleavage potentiates the Ebola virus glycoprotein to undergo a subsequent fusion-relevant conformational change. J. Virol. *86*, 364–372.

Carette, J.E., Raaben, M., Wong, A.C., Herbert, A.S., Obernosterer, G., Mulherkar, N., Kuehne, A.I., Kranzusch, P.J., Griffin, A.M., Ruthel, G., et al. (2011). Ebola virus entry requires the cholesterol transporter Niemann-Pick C1. Nature *477*, 340–343.

Chandran, K., Sullivan, N.J., Felbor, U., Whelan, S.P., and Cunningham, J.M. (2005). Endosomal proteolysis of the Ebola virus glycoprotein is necessary for infection. Science *308*, 1643–1645.

Côté, M., Misasi, J., Ren, T., Bruchez, A., Lee, K., Filone, C.M., Hensley, L., Li, Q., Ory, D., Chandran, K., and Cunningham, J. (2011). Small molecule inhibitors reveal Niemann-Pick C1 is essential for Ebola virus infection. Nature *477*, 344–348.

Dias, J.M., Kuehne, A.I., Abelson, D.M., Bale, S., Wong, A.C., Halfmann, P., Muhammad, M.A., Fusco, M.L., Zak, S.E., Kang, E., et al. (2011). A shared structural solution for neutralizing ebolaviruses. Nat. Struct. Mol. Biol. *18*, 1424–1427.

Dube, D., Brecher, M.B., Delos, S.E., Rose, S.C., Park, E.W., Schornberg, K.L., Kuhn, J.H., and White, J.M. (2009). The primed ebolavirus glycoprotein (19-kilodalton GP1,2): sequence and residues critical for host cell binding. J. Virol. *83*, 2883–2891.

Dye, J.M., Herbert, A.S., Kuehne, A.I., Barth, J.F., Muhammad, M.A., Zak, S.E., Ortiz, R.A., Prugar, L.I., and Pratt, W.D. (2012). Postexposure antibody prophylaxis protects nonhuman primates from filovirus disease. Proc. Natl. Acad. Sci. USA *109*, 5034–5039.

Flyak, A.I., Ilinykh, P.A., Murin, C.D., Garron, T., Shen, X., Fusco, M.L., Hashiguchi, T., Bornholdt, Z.A., Slaughter, J.C., Sapparapu, G., et al. (2015). Mechanism of Human Antibody-Mediated Neutralization of Marburg virus. Cell *160*, this issue, 893–903.

Geisbert, T.W., Daddario-DiCaprio, K.M., Geisbert, J.B., Young, H.A., Formenty, P., Fritz, E.A., Larsen, T., and Hensley, L.E. (2007). Marburg virus Angola infection of rhesus macaques: pathogenesis and treatment with recombinant nematode anticoagulant protein c2. J. Infect. Dis. *196* (2), S372–S381.

Gnirss, K., Kühl, A., Karsten, C., Glowacka, I., Bertram, S., Kaup, F., Hofmann, H., and Pöhlmann, S. (2012). Cathepsins B and L activate Ebola but not Marburg virus glycoproteins for efficient entry into cell lines and macrophages independent of TMPRSS2 expression. Virology *424*, 3–10.

Hong, M., Lee, P.S., Hoffman, R.M., Zhu, X., Krause, J.C., Laursen, N.S., Yoon, S.I., Song, L., Tussey, L., Crowe, J.E., Jr., et al. (2013). Antibody recognition of the pandemic H1N1 Influenza virus hemagglutinin receptor binding site. J. Virol. *87*, 12471–12480.

Hood, C.L., Abraham, J., Boyington, J.C., Leung, K., Kwong, P.D., and Nabel, G.J. (2010). Biochemical and structural characterization of cathepsin L-processed Ebola virus glycoprotein: implications for viral entry and immunogenicity. J. Virol. *84*, 2972–2982.

Lee, J.E., Fusco, M.L., Hessell, A.J., Oswald, W.B., Burton, D.R., and Saphire, E.O. (2008). Structure of the Ebola virus glycoprotein bound to an antibody from a human survivor. Nature *454*, 177–182.

Lee, P.S., Ohshima, N., Stanfield, R.L., Yu, W., Iba, Y., Okuno, Y., Kurosawa, Y., and Wilson, I.A. (2014). Receptor mimicry by antibody F045-092 facilitates universal binding to the H3 subtype of influenza virus. Nat. Commun. *5*, 3614.

Malashkevich, V.N., Schneider, B.J., McNally, M.L., Milhollen, M.A., Pang, J.X., and Kim, P.S. (1999). Core structure of the envelope glycoprotein GP2 from Ebola virus at 1.9-A resolution. Proc. Natl. Acad. Sci. USA *96*, 2662–2667.

Malherbe, H., and Strickland-Cholmley, M. (1968). Human disease from monkeys (Marburg virus). Lancet *1*, 1434.

Manicassamy, B., Wang, J., Jiang, H., and Rong, L. (2005). Comprehensive analysis of ebola virus GP1 in viral entry. J. Virol. *79*, 4793–4805.

Manicassamy, B., Wang, J., Rumschlag, E., Tymen, S., Volchkova, V., Volchkov, V., and Rong, L. (2007). Characterization of Marburg virus glycoprotein in viral entry. Virology *358*, 79–88.

Martinez, O., Johnson, J., Manicassamy, B., Rong, L., Olinger, G.G., Hensley, L.E., and Basler, C.F. (2010). Zaire Ebola virus entry into human dendritic cells is insensitive to cathepsin L inhibition. Cell. Microbiol. *12*, 148–157.

Martinez, O., Ndungo, E., Tantral, L., Miller, E.H., Leung, L.W., Chandran, K., and Basler, C.F. (2013). A mutation in the Ebola virus envelope glycoprotein restricts viral entry in a host species- and cell-type-specific manner. J. Virol. *87*, 3324–3334.

Marzi, A., Reinheckel, T., and Feldmann, H. (2012a). Cathepsin B & L are not required for ebola virus replication. PLoS Negl. Trop. Dis. *6*, e1923.

Marzi, A., Yoshida, R., Miyamoto, H., Ishijima, M., Suzuki, Y., Higuchi, M., Matsuyama, Y., Igarashi, M., Nakayama, E., Kuroda, M., et al. (2012b). Protective efficacy of neutralizing monoclonal antibodies in a nonhuman primate model of Ebola hemorrhagic fever. PLoS ONE *7*, e36192.

McCoy, A.J., Grosse-Kunstleve, R.W., Adams, P.D., Winn, M.D., Storoni, L.C., and Read, R.J. (2007). Phaser crystallographic software. J. Appl. Cryst. *40*, 658–674.

Miller, E.H., Obernosterer, G., Raaben, M., Herbert, A.S., Deffieu, M.S., Krishnan, A., Ndungo, E., Sandesara, R.G., Carette, J.E., Kuehne, A.I., et al. (2012). Ebola virus entry requires the host-programmed recognition of an intracellular receptor. EMBO J. *31*, 1947–1960.

Misasi, J., Chandran, K., Yang, J.Y., Considine, B., Filone, C.M., Côté, M., Sullivan, N., Fabozzi, G., Hensley, L., and Cunningham, J. (2012). Filoviruses require endosomal cysteine proteases for entry but exhibit distinct protease preferences. J. Virol. *86*, 3284–3292.

Mpanju, O.M., Towner, J.S., Dover, J.E., Nichol, S.T., and Wilson, C.A. (2006). Identification of two amino acid residues on Ebola virus glycoprotein 1 critical for cell entry. Virus Res. *121*, 205–214.

Mulherkar, N., Raaben, M., de la Torre, J., Whelan, S., and Chandran, K. (2011). The Ebola virus glycoprotein mediates entry via a non-classical dynamin-dependent macropinocytic pathway. Virology *418*, 72–83.

Murin, C.D., Fusco, M.L., Bornholdt, Z.A., Qiu, X., Olinger, G.G., Zeitlin, L., Kobinger, G.P., Ward, A.B., and Saphire, E.O. (2014). Structures of protective antibodies reveal sites of vulnerability on Ebola virus. Proc. Natl. Acad. Sci. USA *111*, 17182–17187.

Nanbo, A., Imai, M., Watanabe, S., Noda, T., Takahashi, K., Neumann, G., Halfmann, P., and Kawaoka, Y. (2010). Ebolavirus is internalized into host cells via macropinocytosis in a viral glycoprotein-dependent manner. PLoS Pathog. *6*, e1001121.

Ng, M., Ndungo, E., Jangra, R.K., Cai, Y., Postnikova, E., Radoshitzky, S.R., Dye, J.M., Ramírez de Arellano, E., Negredo, A., Palacios, G., et al. (2014). Cell entry by a novel European filovirus requires host endosomal cysteine proteases and Niemann-Pick C1. Virology *468-470*, 637–646.

Olinger, G.G., Jr., Pettitt, J., Kim, D., Working, C., Bohorov, O., Bratcher, B., Hiatt, E., Hume, S.D., Johnson, A.K., Morton, J., et al. (2012). Delayed treatment of Ebola virus infection with plant-derived monoclonal antibodies provides protection in rhesus macaques. Proc. Natl. Acad. Sci. USA *109*, 18030–18035.

Pan, Y., Zhang, W., Cui, L., Hua, X., Wang, M., and Zeng, Q. (2014). Reston virus in domestic pigs in China. Arch. Virol. *159*, 1129–1132.

Pettitt, J., Zeitlin, L., Kim do, H., Working, C., Johnson, J.C., Bohorov, O., Bratcher, B., Hiatt, E., Hume, S.D., Johnson, A.K., et al. (2013). Therapeutic intervention of Ebola virus infection in rhesus macaques with the MB-003 monoclonal antibody cocktail. Sci. Transl. Med. *5*, 199ra113.

Pflugrath, J.W. (1999). The finer things in X-ray diffraction data collection. Acta Crystallogr. D Biol. Crystallogr. *55*, 1718–1725.

Qiu, X., Alimonti, J.B., Melito, P.L., Fernando, L., Ströher, U., and Jones, S.M. (2011). Characterization of Zaire ebolavirus glycoprotein-specific monoclonal antibodies. Clin. Immunol. *141*, 218–227.

Qiu, X., Audet, J., Wong, G., Pillet, S., Bello, A., Cabral, T., Strong, J.E., Plummer, F., Corbett, C.R., Alimonti, J.B., et al. (2012). Successful treatment of ebola virus-infected cynomolgus macaques with monoclonal antibodies. Sci. Transl. Med. *4*, 138ra181.

Qiu, X., Wong, G., Audet, J., Bello, A., Fernando, L., Alimonti, J.B., Fausther-Bovendo, H., Wei, H., Aviles, J., Hiatt, E., et al. (2014). Reversion of advanced Ebola virus disease in nonhuman primates with ZMapp. Nature *514*, 47–53.

Saeed, M.F., Kolokoltsov, A.A., Albrecht, T., and Davey, R.A. (2010). Cellular entry of ebola virus involves uptake by a macropinocytosis-like mechanism and subsequent trafficking through early and late endosomes. PLoS Pathog. *6*, e1001110.

Sanchez, A., and Rollin, P.E. (2005). Complete genome sequence of an Ebola virus (Sudan species) responsible for a 2000 outbreak of human disease in Uganda. Virus Res. *113*, 16–25.

Sanchez, A., Trappier, S.G., Mahy, B.W., Peters, C.J., and Nichol, S.T. (1996). The virion glycoproteins of Ebola viruses are encoded in two reading frames and are expressed through transcriptional editing. Proc. Natl. Acad. Sci. USA *93*, 3602–3607.

Sayama, Y., Demetria, C., Saito, M., Azul, R.R., Taniguchi, S., Fukushi, S., Yoshikawa, T., Iizuka, I., Mizutani, T., Kurane, I., et al. (2012). A seroepidemiologic study of Reston ebolavirus in swine in the Philippines. BMC Vet. Res. *8*, 82.

Schmidt, A.G., Xu, H., Khan, A.R., O'Donnell, T., Khurana, S., King, L.R., Manischewitz, J., Golding, H., Suphaphiphat, P., Carfi, A., et al. (2013). Preconfiguration of the antigen-binding site during affinity maturation of a broadly neutralizing influenza virus antibody. Proc. Natl. Acad. Sci. USA *110*, 264–269.

Schornberg, K., Matsuyama, S., Kabsch, K., Delos, S., Bouton, A., and White, J. (2006). Role of endosomal cathepsins in entry mediated by the Ebola virus glycoprotein. J. Virol. *80*, 4174–4178.

Shoemaker, T., MacNeil, A., Balinandi, S., Campbell, S., Wamala, J.F., McMullan, L.K., Downing, R., Lutwama, J., Mbidde, E., Ströher, U., et al. (2012). Re-emerging Sudan Ebola virus disease in Uganda, 2011. Emerg. Infect. Dis. *18*, 1480–1483.

Siegert, R., Shu, H.L., and Slenczka, W. (1968). [Isolation and identification of the "Marburg virus"]. Dtsch. Med. Wochenschr. *93*, 604–612.

Towner, J.S., Khristova, M.L., Sealy, T.K., Vincent, M.J., Erickson, B.R., Bawiec, D.A., Hartman, A.L., Comer, J.A., Zaki, S.R., Ströher, U., et al. (2006). Marburgvirus genomics and association with a large hemorrhagic fever outbreak in Angola. J. Virol. *80*, 6497–6516.

Towner, J.S., Sealy, T.K., Khristova, M.L., Albariño, C.G., Conlan, S., Reeder, S.A., Quan, P.L., Lipkin, W.I., Downing, R., Tappero, J.W., et al. (2008). Newly discovered ebola virus associated with hemorrhagic fever outbreak in Uganda. PLoS Pathog. *4*, e1000212.

Tran, E.E., Simmons, J.A., Bartesaghi, A., Shoemaker, C.J., Nelson, E., White, J.M., and Subramaniam, S. (2014). Spatial localization of the Ebola virus glycoprotein mucin-like domain determined by cryo-electron tomography. J. Virol. *88*, 10958–10962.

Volchkov, V.E., Feldmann, H., Volchkova, V.A., and Klenk, H.D. (1998). Processing of the Ebola virus glycoprotein by the proprotein convertase furin. Proc. Natl. Acad. Sci. USA *95*, 5762–5767.

Wamala, J.F., Lukwago, L., Malimbo, M., Nguku, P., Yoti, Z., Musenero, M., Amone, J., Mbabazi, W., Nanyunja, M., Zaramba, S., et al. (2010). Ebola hemorrhagic fever associated with novel virus strain, Uganda, 2007-2008. Emerg. Infect. Dis. *16*, 1087–1092.

Weissenhorn, W., Calder, L.J., Wharton, S.A., Skehel, J.J., and Wiley, D.C. (1998a). The central structural feature of the membrane fusion protein subunit from the Ebola virus glycoprotein is a long triple-stranded coiled coil. Proc. Natl. Acad. Sci. USA *95*, 6032–6036.

Weissenhorn, W., Carfí, A., Lee, K.H., Skehel, J.J., and Wiley, D.C. (1998b). Crystal structure of the Ebola virus membrane fusion subunit, GP2, from the envelope glycoprotein ectodomain. Mol. Cell *2*, 605–616.

Whittle, J.R., Zhang, R., Khurana, S., King, L.R., Manischewitz, J., Golding, H., Dormitzer, P.R., Haynes, B.F., Walter, E.B., Moody, M.A., et al. (2011). Broadly neutralizing human antibody that recognizes the receptor-binding pocket of influenza virus hemagglutinin. Proc. Natl. Acad. Sci. USA *108*, 14216–14221.

WHO Ebola Response Team (2014). Ebola Virus Disease in West Africa - The First 9 Months of the Epidemic and Forward Projections. N. Engl. J. Med. *371*, 1481–1495.

Wilson, J.A., Hevey, M., Bakken, R., Guest, S., Bray, M., Schmaljohn, A.L., and Hart, M.K. (2000). Epitopes involved in antibody-mediated protection from Ebola virus. Science *287*, 1664–1666.

Xu, R., Krause, J.C., McBride, R., Paulson, J.C., Crowe, J.E., Jr., and Wilson, I.A. (2013). A recurring motif for antibody recognition of the receptor-binding site of influenza hemagglutinin. Nat. Struct. Mol. Biol. *20*, 363–370.

JVI Accepted Manuscript Posted Online 27 January 2016
J. Virol. doi:10.1128/JVI.00101-16

Chimeric Filoviruses for Identification and Characterization of Monoclonal Antibodies

Running title: Chimeric Filoviruses

Philipp A. Ilinykh,[1, 2] Xiaoli Shen,[1, 2] Andrew I. Flyak,[3] Natalia Kuzmina,[1, 2] Thomas G. Ksiazek,[1, 2] James E. Crowe, Jr., [3,4,5 *] Alexander Bukreyev[1, 2* **]

Affiliations:

[1]Department of Pathology, University of Texas Medical Branch, Galveston, TX, 77555, USA.

[2]Galveston National Laboratory, Galveston, TX, 77550, USA.

[3]Department of Pathology, Microbiology, and Immunology, Vanderbilt University, Nashville, TN, 37232, USA.

[4]Vanderbilt Vaccine Center, Vanderbilt University, Nashville, TN, 37232, USA.

[5]Department of Pediatrics, Vanderbilt University, Nashville, TN, 37232, USA.

* Co-senior authors

** Address correspondence to: Alexander Bukreyev, Departments of Pathology and Microbiology & Immunology, Galveston National Laboratory, Keiller Building, Room 3.145, University of Texas Medical Branch, 301 University Boulevard, Galveston, Texas 77555-0609. Phone: 409-772-2829; E-mail: alexander.bukreyev@utmb.edu.

Abstract words: 248 / 150

Text words: 5,444

ABSTRACT

Recent experiments suggest that some glycoprotein (GP) specific monoclonal antibodies (mAbs) can protect experimental animals against the filovirus Ebola virus (EBOV). There is a need for isolation of mAbs capable of neutralizing multiple filoviruses. Antibody neutralization assays for filoviruses frequently use surrogate systems such as the rhabdovirus vesicular stomatitis Indiana virus (VSV), lentiviruses or gammaretroviruses with their envelope proteins replaced with EBOV glycoprotein (GP) or pseudotyped with EBOV GP. It is optimal for both screening and in-depth characterization of newly identified neutralizing mAbs to generate recombinant filoviruses that express a reporter fluorescent protein in order to more easily monitor and quantify the infection. Our study showed that unlike neutralization-sensitive chimeric VSV, authentic filoviruses are highly resistant to neutralization by mAbs. We used reverse genetics techniques to replace EBOV GP with its counterpart from the heterologous filoviruses Bundibugyo virus (BDBV), Sudan virus (SUDV), and even Marburg virus (MARV) and Lloviu virus (LLOV), which belong to the heterologous genera in the filovirus family. This work resulted in generation of multiple chimeric filoviruses, demonstrating the ability of filoviruses to tolerate swapping of the envelope protein. The sensitivity of chimeric filoviruses to neutralizing mAbs was similar to that of authentic biologically derived filoviruses with the same GP. Moreover, disabling the expression of the secreted GP (sGP) resulted in an increased susceptibility of an engineered virus to the BDBV52 mAb isolated from a BDBV survivor, suggesting a role for sGP in evasion of antibody neutralization in the context of a human filovirus infection.

IMPORTANCE

The study demonstrated that chimeric rhabdoviruses in which G protein is replaced with filovirus GP, widely used as surrogate targets for characterization of filovirus neutralizing antibodies, do not accurately predict the ability of antibodies to neutralize authentic filoviruses, which appeared to be resistant to neutralization. However, a recombinant EBOV expressing a fluorescent protein tolerated swapping of GP with counterparts from heterologous filoviruses, allowing high-throughput screening of B cell lines to isolate mAbs of any filovirus specificity. Human mAb BDBV52, that was isolated from a survivor of BDBV infection, was capable of partially neutralizing a chimeric EBOV carrying BDBV GP in which expression of sGP was disabled. In contrast, the parental virus expressing sGP was resistant to the mAb. Thus, the ability of filoviruses to tolerate swapping of GP can be used for identification of neutralizing mAbs specific to any filovirus and for characterization of mAb specificity and mechanism of action.

63 **INTRODUCTION**

64

65 The family *Filoviridae* is composed of the genus *Ebolavirus*, which includes Ebola (EBOV), Sudan (SUDV), Taï
66 Forest (TAFV), Reston (RESTV), and Bundibugyo (BDBV) viruses, the genus *Marburgvirus*, which includes
67 Marburg (MARV) and Ravn (RAVV) viruses, and the putative genus *Cuevavirus*, which includes Lloviu virus
68 (LLOV) (1). All of these viruses, with the exception of TAFV, RESTV and LLOV, are known to cause disease
69 outbreaks in humans with high case fatality (2, 3). The recent outbreak of EBOV disease in Western Africa (4)
70 demonstrated that filoviruses can cause large epidemics. In addition, identification of the "new" filoviruses
71 BDBV and LLOV was reported as recently as in 2007 or 2011, respectively (5, 6), suggesting the possibility of
72 emergence or identification of previously unknown filoviruses.

73

74 For decades, no treatment demonstrated protective efficacy against filoviruses in the non-human primate
75 model, which is considered the best model of filovirus disease predictive for a similar effect in humans.
76 However, recently developed treatments based on polyclonal (7) or monoclonal antibodies (mAbs) (8-10) have
77 shown impressive levels of efficacy in non-human primates. Development of mAb-based treatments and
78 understanding of mechanisms of antibody neutralization of RNA viruses can be greatly facilitated by
79 development of reverse genetics systems, which allow recovery of recombinant viruses from DNA copies of
80 their genomes or antigenomes. The advantages of such systems for work with polyclonal or monoclonal Abs
81 include the possibility of introduction of mutations in genes encoding major protective antigens, such as the
82 glycoprotein (GP), which is the sole envelope protein of filoviruses. GP is expressed as a precursor protein that
83 is cleaved post-translationally to GP1 and GP2 subunits, and the mature integral membrane protein is present
84 on the surface of viral particles as two disulfide-linked subunits (11, 12). The GP gene of ebolaviruses encodes
85 two proteins: the full-length GP, which is a part of the viral particles and a type I transmembrane protein, and
86 the secreted GP (sGP). It also encodes a much less abundant small soluble GP (ssGP). The GP gene does
87 not have a continuous open reading frame, and thus the expression of full-length GP and ssGP result from
88 transcriptional editing. In contrast, sGP does not require transcriptional editing, and has an identical N-terminal
89 part of GP, but a unique C-terminal part (13-15). Unlike ebolaviruses, marburgvirus GP genes have a

90 continuous open reading frame that encodes full-length GP but not sGP (16, 17). Another advantage of
91 reverse genetics techniques is the possibility to engineer viruses expressing green fluorescent protein (GFP) or
92 another reporter protein to visualize infection. However, development of reverse genetics systems is very labor
93 and time consuming and is not always successful. To date, such systems have been developed only for three
94 filoviruses: EBOV, MARV and RESTV (reviewed in reference 18) , and are not available for the other
95 filoviruses causing a severe disease, including SUDV, BDBV or RAVV. In the absence of reverse genetics
96 systems and/or biosafety level 4 (BSL-4) facilities required for work with filoviruses, researchers use various
97 surrogate systems for characterization of filovirus-specific mAbs or investigation of various steps of filovirus life
98 cycle involving GP. These systems include chimeric vesicular stomatitis Indiana viruses (VSV) with the G
99 protein replaced with filovirus GP (19-21), and pseudotyped gammaretroviruses (22, 23) and lentiviruses (24-
100 26), which have their respective envelope proteins replaced with a filovirus GP provided in trans. It is generally
101 assumed that these surrogate systems can be used to accurately characterize neutralizing properties of
102 filovirus polyclonal or monoclonal Abs.
103
104 In the present study, we used the EBOV reverse genetics system to show that the virus can tolerate
105 replacement of GP with its counterpart not only from heterologous ebolaviruses, but remarkably also from a
106 more distantly related marburgvirus and cuevavirus. The generated chimeric viruses were used, in parallel,
107 with chimeric VSVs, for characterization of filovirus-reactive mAbs isolated from human survivors of previous
108 BDBV or MARV infection. We show here that filoviruses, including the chimeric filoviruses, are more resistant
109 to neutralization by many mAbs, when compared to their chimeric VSV counterparts. These data suggest that
110 chimeric VSVs may not be optimal for accurate quantification of neutralizing activity of filovirus antibodies. We
111 also demonstrate the development of a high-throughput system suitable for functional screening and analysis
112 of large panels of filovirus mAbs. Finally, we used the chimeric viruses to demonstrate that BDBV sGP serves
113 as a decoy for a BDBV GP-specific antibody isolated from a BDBV survivor.
114
115
116

MATERIALS AND METHODS

Construction of chimeric EBOV viruses and biological filovirus isolates used in the study. To construct the full-length genome cDNA of EBOV with its GP swapped with that of BDBV, SUDV or MARV, we used the plasmid carrying the genomic RNA of wild-type EBOV (pEBOwt) and its modified version with the transcriptional cassette encoding enhanced green fluorescent protein added between the NP and VP35 genes (pEBO-eGFP) (27), which were provided by Dr. Jonathan Towner and Dr. Stuart Nichol (CDC). First, the pEBOwtΔBamHI-SbfI,AscI-PspOMI plasmid subclone was generated from the pEBOwt construct by consecutive two-step removal of BamHI-SbfI and AscI-PspOMI fragments; after pEBOwt digestion with the each pair of restriction endonucleases, the residual vector part was treated with the Klenow fragment of DNA polymerase I and self-ligated. The resulting subclone was subjected to mutagenesis using the QuikChange site-directed mutagenesis kit (Stratagene, La Jolla, CA) for introduction of NheI and XhoI restriction endonuclease sites flanking the GP open reading frame (ORF). Additionally, the similar pEBOwtΔBamHI-SbfI,AscI-PspOMI subclone was generated with BamHI restriction endonuclease site instead of XhoI downstream of the EBOV GP ectodomain encoding region corresponding to the genomic sequence of EBOV Ebola virus/H.sapiens-tc/COD/1976/Yambuku-Mayinga, nucleotides 6039-7987 (GenBank accession number NC_002549.1). For cloning of GP ORF of MARV, BDBV and SUDV, Vero-E6 cells were infected with Marburg virus/H.sapiens-tc/UGA/2007/Kitaka-200702854, Bundibugyo virus/H.sapiens-tc/UGA/200706291/Butalya-811249, or Sudan virus/H.sapiens-tc/UGA/2000/Gulu-200011676, and subjected to RNA isolation following cell lysis in TRIzol reagent (LifeTechnologies, Carlsbad, CA). Total RNA was reverse-transcribed, and PCR fragments corresponding to GP ORFs of three different filovirus species were generated and cloned into pUC19 vector by SphI and XmaI sites. In order to perform subsequent cloning steps toward generation of full-length clones, the following restriction endonuclease sites were knocked down by introduction of silent mutations: BamHI and XhoI in MARV GP ORF, ApaI and NheI in BDBV GP ORF, and ApaI, SacI and XhoI in SUDV GP ORF. To disable the expression of sGP, the GP gene transcriptional editing site was modified from AAAAAAA to AAGAAGAA (antigenome DNA sense) by site-directed mutagenesis, resulting in a plasmid designated pUC19-BDBV-GPΔsGP. Next, the resulting pUC19 clones were used to PCR amplify BDBV GP

ORF with the following primers: direct,
ACAGTAGCTAGCAACACA*ATGGTTACATCAGGAATTCTACAATTGCCC,* reverse,
ACAGTACTCGAGAAAAA*TTAGAGTAGAAATTTGCAAATACACAGCAGTGC*;
SUDV GP was amplified with the primers: direct, ACAGTAGCTAGCAACACA*ATGGGGGGTCTTAGCCTACT*,
reverse, ACAGTACTCGAGAAAAA*TCAGCAAAGCAGCTTGCAAAC*;
MARV GP was amplified with the primers: direct,
TCTAGCAGGCTAGCAACACA*ATGAGGACTACATGCTTCTT*, reverse,
TCTAGCAGCTCGAGAAAAA*CTATCCAATATATTTAGTAAAGATACGACAA*; and MARV GP ectodomain was
amplified with the primers: direct, TCTAGCAGGCTAGCAACACA*ATGAGGACTACATGCTTCTT,* and reverse,
AGTCACGTGGATCCA*GTCGGATGTCCACCATTTACCACC* (NheI, XhoI or BamHI restriction endonuclease
sites are underlined, the start of GP ORF direct sequence and the end of GP ORF or GP ectodomain
complementary sequences are italicized). The PCR products were used to replace EBOV GP ORF in
pEBOwtΔBamHI-SbfI,AscI-PspOMI subclone with ORF for GP of BDBV, SUDV or MARV by NheI and XhoI
sites, or for the replacement of EBOV GP ectodomain encoding region with that of MARV by NheI and BamHI
sites, respectively. To generate the final full-length constructs, the ApaI-SacI fragments of the generated
subclones were transferred to pEBO-eGFP plasmid for substitution of the existing EBOV GP ORF with an ORF
encoding the GP of BDBV, SUDV, or MARV, or to replace the EBOV GP ectodomain with a MARV GP
ectodomain. For the construction of EBOV full-length clone with its GP replaced by that of LLOV, we first
changed editing site in LLOV GP ORF from 8A to 7A (antigenome DNA sense) by mutagenizing pBsII SK (+)-
LLOV GP plasmid (provided by Dr. Ayato Takada, reference 28) to make it identical to the original LLOV
sequence (6). Also, two existing KpnI restriction endonuclease sites in LLOV GP ORF were knocked down by
introduction of silent mutations. The resulting LLOV GP ORF cDNA was PCR-amplified using the following
primers: direct, TCTAGCAGGCTAGCAACACA*ATGGTGCCCACCTACCCGTA*, and reverse,
TCTAGCAGCTCGAGAAAAA*TCATCGTGTTATTCTGCACA* (NheI or XhoI restriction endonuclease sites are
underlined, the start of LLOV GP ORF direct sequence and the end of LLOV GP ORF complementary
sequence are italicized), and cloned into pEBOwtΔBamHI-SbfI,AscI-PspOMI plasmid. The ApaI-KpnI fragment
from the resulting subclone was transferred to the pEBO-eGFP full-length clone with one of its KpnI sites (in

polymerase L ORF, nucleotides 14292-14297 in EBOV genome) disabled by introduction of a silent mutation for substitution of the existing ORF of EBOV GP with an ORF encoding the GP of LLOV. The chimeric viruses Ebola virus/H.sapiens-rec/COD/1976/Yambuku-Mayinga-eGFP-BDBV_GP (hereafter referred as EBOV/BDBV-GP), its derivative Ebola virus/H.sapiens-rec/COD/1976/Yambuku-Mayinga-eGFP-BDBV_GPdelta_sGP (referred as EBOV/BDBV-GPΔsGP) that is deficient in the production of sGP, Ebola virus/H.sapiens-rec/COD/1976/Yambuku-Mayinga-eGFP-SUDV_GP (referred as EBOV/SUDV-GP), Ebola virus/H.sapiens-rec/COD/1976/Yambuku-Mayinga-eGFP-MARV_GP (referred as EBOV/MARV-GP), Ebola virus/H.sapiens-rec/COD/1976/Yambuku-Mayinga-eGFP-MARV_GPed (referred as EBOV/MARV-GPed), and Ebola virus/H.sapiens-rec/COD/1976/Yambuku-Mayinga-eGFP-LLOV_GP (referred as EBOV/LLOV-GP) were rescued as previously described (29) and propagated by two passages in Vero-E6 cell culture monolayers. Genomic RNA of all recovered viruses was sequenced using Illumina HiSeq 1000 sequencing system as previously described (30) and the 3' and 5' termini were sequenced by RNA circularization as previously described (31). The sequences were deposited in GenBank, accession numbers KU174137-KU174142. Work with the filovirus full-length clones was performed in a laboratory approved by the NIH Recombinant DNA Advisory Committee. Generation of the chimeric viruses was approved by the UTMB Institutional Biosafety Committee. Recovery of the recombinant filoviruses and all work with filoviruses were performed in the BSL-4 facility of the Galveston National Laboratory. The growth kinetics experiments on chimeric EBOV viruses were performed as previously described (29). BDBV and MARV were provided originally by the Special Pathogens Branch of the U.S. Centers for Disease Control and Prevention (CDC) and deposited at the World Reference Center of Emerging Viruses and Arboviruses (WRCEVA) housed at the Galveston National Laboratory, the University of Texas Medical Branch at Galveston. BDBV isolate 200706291 Uganda was isolated originally from the serum of a patient during the first recorded outbreak caused by this virus (5), and passaged three times in Vero-E6 cells. MARV isolate 200702854 Uganda was isolated originally from a subject designated "Patient A" during the outbreak in Uganda in 2007 (32, 33) and underwent four passages in Vero-E6 cells.

Immunostaining of chimeric EBOV plaques. Vero-E6 cell culture monolayers were inoculated with dilutions of chimeric EBOV constructs, covered with 0.9% methylcellulose (Sigma-Aldrich, Saint Louis, MO), and

incubated at 37°C. At day 6 after infection, the overlay was removed, cells were fixed with formalin for 24 hours, taken out of BSL-4, and blocked in 5% skim milk in phosphate buffered saline (PBS) containing 0.1% Tween-20 (Sigma-Aldrich) for one hour. Next, monolayers were incubated for 1 hour at 37°C with the selected mAbs (1 µg/ml) in solution, or with 1:1,000 dilution of rabbit polyclonal serum raised against EBOV isolate Mayinga or MARV isolate Musoke, and then washed three times with blocking solution. Thereafter, the respective goat anti-human or goat anti-rabbit IgG antibodies conjugated with horse radish peroxidase (KPL, Gaithersburg, MD) were added at 1:1,000 dilution in blocking buffer, and monolayers were incubated for one hour at 37°C and washed three times with PBS. Virus plaques were visualized by staining with the 4CN two-component peroxidase substrate system (KPL, Gaithersburg, MD).

Chimeric VSV with filovirus GP proteins. VSV/MARV-GP was constructed and recovered as previously described (34). VSV/BDBV-GP was provided by Dr. Thomas Geisbert (University of Texas Medical Branch at Galveston, Galveston, Texas), and VSV/EBOV-GP (35) was provided by Dr. Heinz Feldmann (Rocky Mountain Laboratories, National Institutes of Health, Hamilton, Montana).

Plaque reduction assay. For plaque-based neutralization assays, 150 PFUs of filoviruses or chimeric VSVs were pre-incubated with varying concentrations of mAbs in 100 µl volume for 1 hour at 37°C in triplicate and placed on monolayers of Vero-E6 cells in 24-well plates. After adsorption of virus for 1 hour at 37°C, cells were overlaid with 1 ml of 0.9% methylcellulose in MEM medium containing 10% of fetal bovine serum (Quality Biologicals, Gaithersburg, MD) and 0.1% of gentamicin sulfate (Mediatech, Manassas, VA) and incubated at 37°C. Chimeric VSV plaques were visualized by staining monolayers with 0.25% crystal violet solution in formalin on day 3, 4 or 5 after infection, and filovirus plaques were immunostained with rabbit anti-EBOV polyclonal serum on day 6 after infection as described above. Plaques were counted, and neutralization curves were plotted as percentages of reduction of plaque numbers as compared to mock-neutralized virus.

High-throughput screening neutralization assay. Four hundred PFUs of recombinant EBOV expressing eGFP or EBOV/BDBV-GP were incubated with varying concentrations of mAbs in black polystyrene 96-well

plates with clear bottoms (Corning, NY) for 1 hour at 37°C in MEM medium containing 10% fetal bovine serum and 0.1% of gentamicin sulfate. Next, 4 x 10^4 Vero-E6 cells in the same medium were added to the virus-antibody mixtures and incubated at 37°C for 4 days. The fluorescence intensity of infected cells at 488 nm wave length was measured in triplicate using the 2104 EnVision multilabel reader (PerkinElmer, Waltham, MA). The signal readout was normalized to virus control aliquots with no mAb added and presented as the percentage of neutralization.

Binding of antibodies to the recombinant GPs of various filovirus species. Soluble forms of GP of BDBV, EBOV, SUDV, MARV or sGP of BDBV, EBOV, SUDV were coated overnight onto 384-well plates (Thermo Scientific Nunc, Waltham, MA) at 1 µg/ml in PBS. Plates were blocked with 25 µl of blocking solution/well for 1 hour. Blocking solution consisted of 10 g powdered milk (Bio-Rad, Hercules, CA), 10 ml of goat serum (Gibco, Waltham, MA), 100 ml of 10x PBS, and 0.5 ml of Tween-20 mixed to a 1 l final volume with distilled water. Purified antibodies were applied to the plates at a concentration 10 µg/ml in blocking solution for 2 hr. The presence of antibodies bound to the GP and sGP proteins was determined using goat anti-human IgG alkaline phosphatase conjugate (Meridian Life Science, Memphis, TN) and p-nitrophenol phosphate substrate tablets (Sigma-Aldrich), with optical density read at 405 nm after 1 hour.

RESULTS

***Filoviruses are resistant to antibody neutralization compared to chimeric VSVs*.** We used human Abs to compare their ability to neutralize filoviruses EBOV or MARV on the one hand or recombinant VSVs expressing the same filovirus GPs on the other hand (Fig. 1A). We first tested a recombinant form of the EBOV-specific antibody KZ52, isolated from a phage display library constructed from antibody genes from a human survivor of natural EBOV infection (36), which is protective in the guinea pig model of EBOV infection (37). The antibody appeared to neutralize authentic EBOV less efficiently than VSV/EBOV-GP. Next,

antibodies BDBV43 and BDBV52, isolated from a human survivor of BDBV infection (38) were tested. Again, authentic BDBV was less efficiently neutralized than VSV/BDBV-GP. Moreover, BDBV52 did not neutralize authentic BDBV at any concentration tested (up to 200 µg/ml), but effectively neutralized VSV/BDBV-GP. Analysis of neutralization by additional BDBV antibodies from the survivor suggested a similar pattern, *i.e.*, less efficient neutralization of authentic as compared to VSV/BDBV-GP (data not shown). Analysis of the antibody MR201 that we isolated previously from a MARV survivor (34) also demonstrated a great difference between the neutralization of authentic MARV and VSV/MARV-GP. For example, 50 µg/ml of MR201 neutralized only 7% of MARV, but as much as 94% of VSV/MARV-GP. Taken together, these data suggest that authentic filoviruses generally are more resistant to neutralization by mAbs compared to chimeric VSVs, which can, as a result of these findings, produce greatly exaggerated data on mAb neutralization.

***Replacement of the EBOV GP with its counterpart from heterologous ebolaviruses results in viable chimeric viruses*.** Infection of cells with the recombinant EBOV expressing eGFP from an added gene results in a bright eGFP fluorescence in infected cells starting at 36-48 hrs post-infection (27), which opens the possibility for use of this virus for development of a high-throughput screening of mAbs. As noted above, the genus *Ebolavirus* includes five virus species whose representatives EBOV, BDBV and SUDV cause a severe disease in humans. We therefore attempted to generate recombinant replication-competent EBOV-derived viruses in which the GP protein was exchanged with that of BDBV or SUDV. We replaced the ORF of EBOV GP in the EBOV full-length clone with that of BDBV or SUDV and used the plasmids in virus recovery experiments, as previously described (27, 29) (Fig. 2A,D). Indeed, the experiments resulted in recovery of viable chimeric viruses expressing eGFP: EBOV/BDBV-GP and EBOV/SUDV-GP (Fig. 3A); sequencing analysis revealed no adventitious mutations in the GP gene or elsewhere in the genome. We then compared the multi-step growth kinetics of the recombinant viruses (Fig. 3B). Contrary to our expectations, EBOV/BDBV-GP replicated slightly faster than EBOV, and EBOV/SUDV-GP replicated much faster than EBOV (Fig. 3B). For example, on day 1 or 2, the respective titers of EBOV/SUDV-GP were greater than those of EBOV by 2.5 or 1.3 $\log_{10}$, although the final viral titers of all viruses were comparable. These data suggest that EBOV can tolerate swapping of GP with its counterparts from heterologous ebolaviruses.

***EBOV can tolerate swapping of the glycoprotein with that of MARV and LLOV*.** The two members of genus *Marburgvirus*, MARV and RAVV, have only partial antigenic relatedness (39), further suggesting the need for development of a single filovirus platform capable of expressing the GPs from individual marburgviruses for accurate characterization of antibodies. Filovirus GP is a type I transmembrane protein (16, 17), which interacts with VP40 (40); its transmembrane domain affects conformation of the protein (41) and is required for incorporation in viral particles (42). Since the MARV GP cytoplasmic tail (amino acids RIFTKVIG) has no similarity to its EBOV GP counterpart (amino acids KFVF), and the transmembrane domains exhibit only a limited similarity (16, 43), the compatibility between MARV GP with EBOV particles was difficult to predict. We therefore initially attempted to replace the EBOV GP ectodomain only (which represents the GP lacking the cytoplasmic tail and the highly conserved transmembrane domain) with that of MARV (Fig. 2B,D). As a result, a fully viable virus designated EBOV/MARV-GPed was recovered (Fig. 3A), which replicated at a rate similar to that of EBOV (Fig. 3B). Since EBOV easily tolerated swapping of the GP ectodomain, we next attempted to replace the whole GP with that of MARV (Fig. 2B). This approach also resulted in recovery of a viable virus (Fig. 3A) that replicated at a level similar to that of EBOV (Fig. 3B), suggesting that the interaction of the GP cytoplasmic tail with VP40 (the matrix protein) may be not highly specific. We also attempted to replace the whole GP with its counterpart from cuevavirus LLOV, whose RNA was identified in a dead bat in Spain (6) but the virus was never isolated. This experiment resulted in recovery of a viable virus designated EBOV/LLOV-GP (Fig. 2A,C), whose replication was slightly reduced as compared to EBOV (Fig. 3B). Again, adventitious mutations were not detected in GP or elsewhere in the genome of EBOV/MARV-GP, EBOV/MARV-GPed and EBOV/LLOV-GP. Thus, EBOV can tolerate swapping GP with its counterparts not only from heterologous ebolaviruses, but also from more distantly related and distinct marburgvirus and cuevavirus.

***The generated chimeric filoviruses produce plaques, which can be stained by mAbs specific to their glycoproteins*.** We next tested the ability of mAbs isolated from filovirus survivors to bind to plaques formed by the constructed viruses. We tested the binding of mAbs BDBV43 or BDBV52 recently isolated from a survivor

Journal of Virology

of BDBV infection (A.I.F. et al., unpublished data) and MR78, MR235 or MR246 from a survivor of MARV infection (34) (Fig. 4A). The comparison was performed in parallel using rabbit hyperimmune serum against EBOV or MARV. We found that rabbit EBOV-specific immune serum was able to stain plaques not only for EBOV, but also for all constructs generated, including EBOV/MARV-GP and EBOV/MARV-GPed. This observation can be explained by the contribution of binding of antibodies in the immune serum that recognize internal EBOV proteins, such as NP and VP40. Interestingly, BDBV43 stained the three ebolavirus GP-based constructs with varying intensity and also EBOV/MARV-GP and EBOV/MARV-GPed, although with a low intensity, while BDBV52 stained EBOV/BDBV-GP and weakly EBOV/MARV-GP and EBOV/MARV-GPed, but not EBOV and EBOV/SUDV-GP. These data suggest the two BDBV mAbs interact with epitopes that are partially conserved across all or some members of the family *Filoviridae*. In contrast, MARV polyclonal antibodies stained plaques of EBOV/MARV-GP or EBOV/MARV-GPed but not the ebolavirus constructs. Again, similarly to polyclonal MARV antibodies, the three MARV mAbs stained only MARV, but not the ebolavirus GP-based constructs. The GP proteins of EBOV and MARV have considerable amino acid similarity (44), with several stretches of four or more identical amino acids located in the receptor-binding region of GP_1 and heptad repeats 1 and 2 in GP_2 (based on comparison of EBOV isolate Mayinga and MARV isolate Uganda, Fig. 4B). In contrast, the mucin-like domains of EBOV and MARV have almost no sequence similarity. Therefore, the two BDBV mAbs react with conserved epitopes, while the two MARV-specific mAbs and the polyclonal MARV Abs are directed against more variable epitopes. These data demonstrate that chimeric filovirus constructs are useful in the characterization of antibodies specific for any filovirus species.

Chimeric filoviruses are neutralized according to the GP ectodomain specificity of mAbs. To determine the binding specificities of the mAbs used in the study, we tested a panel of mAbs for their ability to bind a panel of recombinant filovirus GP or sGP proteins (Fig. 5A). All mAbs tested, with the exception of BDBV43, bound exclusively to full-length GP of the targeted filoviruses, and all of the mAbs except BDBV43 and BDBV52 did not detectably bind to sGP. In contrast, BDBV43 bound to both GP and sGP of all three ebolaviruses: EBOV, BDBV and SUDV, but not to MARV, while BDBV52 bound to both GP and sGP of BDBV only. We next tested the ability of selected mAbs to neutralize EBOV, BDBV, MARV, EBOV/MARV-GP or

EBOV/MARV-GPed (Fig. 5B). As expected, EBOV was neutralized effectively by mAb KZ52 and, to a lesser degree, by BDBV43, but not by BDBV41 or BDBV52. BDBV was neutralized by BDBV41 and BDBV43, but not by BDBV52, despite the fact that this mAb binds to BDBV GP. MARV and the chimeric viruses carrying MARV GP or its ectodomain were neutralized by MR78, but not the other mAbs. Thus, the GP ectodomain specificities of chimeric filoviruses determine the neutralization efficiencies of antibodies, which do not necessary correlate with the protein binding data. These data suggest that chimeric filoviruses are useful for highly specific antibody neutralization tests.

***Use of the chimeric filoviruses for a high-throughput screening (HTS) assay of mAbs*.** Neutralization tests of large panels of mAbs or multiple serum samples against multiple filovirus species by conventional plaque reduction assay, which must be performed in BSL-4 biocontainment, is laborious. We therefore tested the generated chimeric viruses as targets for a HTS neutralization assay in which eGFP fluorescence provided a measure of remaining infectivity and thus a measure of antibody neutralization. In preliminary experiments, we performed test neutralizations of varying doses of EBOV/BDBV-GP ranging from 4 to 4,000 PFUs with varying concentrations of mAb BDBV41. Following a one hour incubation, virus-antibody aliquots were mixed with varying amounts of Vero-E6 cells ranging from 2,500 to 40,000, and then added as a suspension to individual wells of 96-well plates. eGFP fluorescence was read on days 2, 3, 4, 5 and 6. As an example of our preliminary data, infection of 40,000 cells with 150 or 300 PFUs resulted in a two-fold difference in the signal on day 4 (Fig. 6A). In another example, residual infectivity in Vero-E6 cells was measured in a broad range of various concentrations of mAb BDBV41 mixed with EBOV/BDBV-GP in triple aliquots. Quantitation of eGFP signal on a fluorescence plate reader on day 4 post infection demonstrated that the level of eGFP signal was inversely proportional to the amount of mAb added (Fig. 6B). Interestingly, based on visual examination of plates, this antibody inhibited or prevented spread of the viral infection, but did not completely eliminate initial infectious foci even at the greatest concentration tested, 200 µg/ml (Fig. 6C). Based on the optimization experiments, we found that inoculation of 40,000 cells with 400 PFU (MOI of 0.01) of EBOV/BDBV-GP gave the greatest possible dynamic range of the signal at various antibody concentrations (data not shown). Next, we used the optimized assay conditions to determine neutralization potency of BDBV41 in comparison with the

360 classic plaque reduction assay with BDBV, VSV/BDBV-GP or EBOV/BDBV-GP (Fig. 6D). As in the case of
361 KZ52, MR201 and BDBV43 (Fig. 1), VSV/BDBV-GP was more easily neutralized by BDBV41 in classic plaque
362 reduction assays. Use of EBOV/BDBV-GP instead of BDBV for the plaque reduction assay resulted in a similar
363 neutralization curve, and use of EBOV/BDBV-GP in a HTS assay also resulted in a neutralization curve similar
364 to that generated by plaque reduction assays with BDBV or EBOV/BDBV-GP. Thus, chimeric filoviruses
365 expressing eGFP can be used as a substitute for their natural counterparts in plaque reduction assays as well
366 as being used in HTS assays to rapidly identify mAbs neutralizing individual filovirus species.
367
368 ***The sGP protein prevents virus neutralization by BDBV52.*** We next tested the possibility that the
369 generated chimeric viruses are useful for a qualitative characterization of mAbs. We previously demonstrated
370 that the secreted G protein of respiratory syncytial virus, which, similarly to EBOV is a non-segmented negative
371 strand virus, reduces the efficiency of virus neutralization by serving as a decoy for neutralizing antibodies (45).
372 More recently, a similar immune evasion mechanism was demonstrated for EBOV sGP (26). However, these
373 studies involved mouse polyclonal antibodies, and the BDBV sGP study involved a chimeric VSV expressing
374 EBOV GP, and therefore, the importance of this mechanism for pathogenesis of human disease remained
375 unknown. Data presented here show that BDBV52 bound to both BDBV sGP and GP (Fig. 5A). We
376 hypothesized that sGP serves as a decoy for BDBV52 and antibodies with similar epitope specificities, thereby
377 preventing their ability to effectively neutralize BDBV. To test the hypothesis, we modified the GP gene of
378 EBOV/BDBV-GP cDNA to disable the expression of sGP by mutating the transcription-editing site from
379 UUUUUUU to UUCUUCUU (negative-sense RNA strand). As a result, the modified GP gene had the
380 continuous open reading frame encoding GP only. The resulting virus designated EBOV/BDBV-GPΔsGP was
381 recovered and sequencing data confirmed the stability of the mutation and lack of any adventitious mutations
382 in the genome (data not shown). sGP is not required for viral replication in cultured cells . To determine if
383 disabling of expression of sGP makes the virus more sensitive to neutralization by BDBV52, we compared
384 susceptibility of the two viruses to the antibody. We found that while EBOV/BDBV-GP was completely resistant
385 to the antibody, EBOV/BDBV-GPΔsGP was partially neutralized at the highest antibody concentration tested,
386 200 μg/ml (Fig. 7A), suggesting that BDBV52 binds part of sGP shared with GP (Fig. 7B). These data

demonstrate for the first time the ability of an ebolavirus to evade neutralization by a naturally-occurring human mAb isolated from a survivor.

DISCUSSION

The recent devastating outbreak of EBOV in Western Africa (4) demonstrated the pressing need in development of means of treatments and prophylaxes of infections caused by filoviruses. To date, the greatest progress has been achieved, which require detailed characterization of monoclonal or polyclonal Abs. Data presented in this study suggest that surrogate systems such as chimeric VSV expressing filovirus GP may produce misleading results and therefore appear to be suboptimal for reliable characterization of filovirus antibodies. The simultaneous circulation of multiple lineages of filoviruses in the same outbreak (46, 47) along with the emergence of "new" filoviruses (5, 6), and improved methods for isolation of mAbs from survivors (34, 38, 48) along with the utility of their use in therapeutics strongly support the need for improved efficient means of rapid screening and characterization of large panels of mAbs. While a previous study demonstrated the possibility of generation of viable ebolaviruses with some genes replaced with counterparts from a heterologous ebolavirus (49), this study demonstrates that EBOV can easily tolerate exchange of GP not only from ebolaviruses, but also from more distantly related marburgvirus and cuevavirus. Each of the chimeric viruses easily tolerated and expressed eGFP from an added gene. Moreover, we show that chimeric filoviruses are useful for a HTS screening process to identify neutralizing mAbs. In addition, we show that binding to GP does not necessarily predict the ability of a mAb to neutralize a filovirus, the effect most likely related to a different conformation of GP in a free form and in a viral particle. Taken together, these results illustrate the practicality of a quick exchange of GP in EBOV with its counterpart from any circulating filovirus and the use of the resulting chimeric filoviruses for a rapid analysis of large panels of monoclonal or polyclonal Abs.

The present study shows that filoviruses are more resistant to neutralization by mAbs than chimeric VSV with filovirus GP widely used for quantitative analysis of filovirus-specific mAbs. While the exact reason for this

414 phenomenon requires additional studies, we hypothesize that it may be related to a much greater length of
415 filovirus particles, 1,028 nm for EBOV or 876 nm for MARV (50), as compared to 175 nm for VSV (51). The
416 greater length of filovirus particles suggests a greater number of GP trimers per filovirus particle, which require
417 a greater number of bound mAbs to abrogate infectivity, as compared to a chimeric VSV. However, this model
418 cannot explain why for some antibodies, such as KZ52 and BDBV43, the difference between neutralization of a
419 filovirus and the corresponding chimeric VSV is moderate, while for others, such as BDBV52 and MR201, the
420 difference is dramatic (Fig. 1A). Most likely, other factors, such as epitope specificity of mAbs, also affect the
421 observed difference.
422
423 A recently published study demonstrated that sGP interferes with the antibody-mediated neutralization of
424 EBOV GP-lentivirus pseudotype by antisera from sGP or GP immunized mice (26). The importance of this
425 mechanism in the context of human filovirus infections remains unclear. In a separate study we isolated
426 BDBV52, an antibody from a survivor, which binds both the recombinant GP and sGP, but does not neutralize
427 EBOV/BDBV-GP (38). We hypothesized that this mAb can neutralize virus in the absence of sGP. To test the
428 hypothesis, we generated the derivative of EBOV/BDBV-GP, which does not express sGP, EBOV/BDBV-
429 GPΔsGP. Indeed, this virus was partially neutralized by BDBV52. These data represent the first demonstration
430 that ebolavirus survivors have mAbs that bind sGP, which do not neutralize the virus, but can partially
431 neutralize the virus when sGP expression is disabled. Thus, expression of sGP might help the virus to evade
432 effective antibody neutralization. Of note, a recent study demonstrated that disabling of the transcriptional
433 editing site of the GP gene reduces EBOV virulence, but the expression of sGP *per se* did not affect it (52). We
434 are unaware of any comparison of sGP expression by the various ebolaviruses; however, the identical GP
435 transcription editing sites and the high levels of similarity of the polymerase (L) genes of EBOV, BDBV and
436 SUDV (5, 41) suggest that the levels of expression of sGP by these viruses and by EBOV/BDBV-GP and
437 EBOV/SUDV-GP are comparable.
438
439 In summary, these data suggest that (i) chimeric VSV expressing filovirus GP may not provide an accurate
440 prediction of the neutralizing capacity of antibodies, (ii) EBOV can easily tolerate exchange of GP from other

ebolaviruses or the heterologous marburgvirus or cuevavirus, (iii) swapping the GP genes and expression of a fluorescent protein from a recombinant filovirus allows for the rapid screening of large number of antibodies specific for virtually any filovirus, and (iv) sGP serves as a decoy, reducing the effectiveness of virus neutralization during filovirus human infections.

ACKNOWLEDGEMENTS

We thank Dr. Steven G. Widen, Jill K. Thompson and Dr. Thomas G. Wood (the University of Texas Medical Branch at Galveston) for deep sequencing of the viral genomic RNA. We thank Drs. J. Towner and S. Nichol (CDC) for providing the EBOV-eGFP full-length clone, Drs. Y. Kawaoka (University of Wisconsin) and H. Feldmann (NIH) for providing the EBOV NP, VP35, L, VP30, and T7 polymerase plasmids, Dr. H. Feldmann for providing the VSV/EBOV-GP virus, Dr. A. Takada (Hokkaido University, Japan) for providing cDNA of LLOV GP, Dr. T. Geisbert (UTMB) for providing the VSV/BDBV-GP virus, and Drs. Erica Ollmann Saphire and Marnie Fusco (The Scripps Research Institute) for providing the EBOV recombinant glycoprotein. We are grateful Dr. Y. Wolf (NIH) for calculating the degree of difference between the amino acid sequences of EBOV GP and the other filoviruses. This project received support from the Defense Threat Reduction Agency (grant HDTRA1-13-1-0034 to JEC and AB) and U.S. NIH grant U19 AI109711 (to JEC and AB).

460 **REFERENCES**

461

462 1. **Kuhn JH, Bao Y, Bavari S, Becker S, Bradfute S, Brister JR, Bukreyev AA, Chandran K, Davey**
463 **RA, Dolnik O, Dye JM, Enterlein S, Hensley LE, Honko AN, Jahrling PB, Johnson KM, Kobinger**
464 **G, Leroy EM, Lever MS, Mühlberger E, Netesov SV, Olinger GG, Palacios G, Patterson JL,**
465 **Paweska JT, Pitt L, Radoshitzky SR, Saphire EO, Smither SJ, Swanepoel R, Towner JS, van der**
466 **Groen G, Volchkov VE, Wahl-Jensen V, Warren TK, Weidmann M, Nichol ST.** 2013. Virus
467 nomenclature below the species level: a standardized nomenclature for natural variants of viruses
468 assigned to the family Filoviridae. Arch Virol **158:**301-311.
469 2. **CDC** 2015, posting date. Outbreaks Chronology: Ebola Virus Disease.
470 http://www.cdc.gov/vhf/ebola/outbreaks/history/chronology.html
471 3. **CDC** 2014, posting date. Known Cases and Outbreaks of Marburg Hemorrhagic Fever, in
472 Chronological Order.
473 http://www.cdc.gov/vhf/marburg/resources/outbreak-table.html
474 4. **CDC** 2015, posting date. Outbreak of Ebola in Guinea, Liberia, and Sierra Leone.
475 http://www.cdc.gov/vhf/ebola/outbreaks/guinea/
476 5. **Towner JS, Sealy TK, Khristova ML, Albariño CG, Conlan S, Reeder SA, Quan PL, Lipkin WI,**
477 **Downing R, Tappero JW, Okware S, Lutwama J, Bakamutumaho B, Kayiwa J, Comer JA, Rollin**
478 **PE, Ksiazek TG, Nichol ST.** 2008. Newly discovered Ebola virus associated with hemorrhagic fever
479 outbreak in Uganda. PLoS Pathog **4:**e1000212.
480 6. **Negredo A, Palacios G, Vazquez-Moron S, Gonzalez F, Dopazo H, Molero F, Juste J, Quetglas J,**
481 **Savji N, de la Cruz Martinez M, Herrera JE, Pizarro M, Hutchison SK, Echevarria JE, Lipkin WI,**
482 **Tenorio A.** 2011. Discovery of an ebolavirus-like filovirus in europe. PLoS Pathog **7:**e1002304.
483 7. **Dye JM, Herbert AS, Kuehne AI, Barth JF, Muhammad MA, Zak SE, Ortiz RA, Prugar LI, Pratt WD.**
484 2012. Postexposure antibody prophylaxis protects nonhuman primates from filovirus disease. Proc Natl
485 Acad Sci U S A **109:**5034-5039.

8. **Qiu X, Audet J, Wong G, Pillet S, Bello A, Cabral T, Strong JE, Plummer F, Corbett CR, Alimonti JB, Kobinger GP.** 2012. Successful treatment of Ebola virus-infected cynomolgus macaques with monoclonal antibodies. Sci Transl Med **4:**138ra181.

9. **Olinger GG, Jr., Pettitt J, Kim D, Working C, Bohorov O, Bratcher B, Hiatt E, Hume SD, Johnson AK, Morton J, Pauly M, Whaley KJ, Lear CM, Biggins JE, Scully C, Hensley L, Zeitlin L.** 2012. Delayed treatment of Ebola virus infection with plant-derived monoclonal antibodies provides protection in rhesus macaques. Proc Natl Acad Sci U S A **109:**18030-18035.

10. **Qiu X, Wong G, Audet J, Bello A, Fernando L, Alimonti JB, Fausther-Bovendo H, Wei H, Aviles J, Hiatt E, Johnson A, Morton J, Swope K, Bohorov O, Bohorova N, Goodman C, Kim D, Pauly MH, Velasco J, Pettitt J, Olinger GG, Whaley K, Xu B, Strong JE, Zeitlin L, Kobinger GP.** 2014. Reversion of advanced Ebola virus disease in nonhuman primates with ZMapp. Nature **514:**47-53.

11. **Volchkov VE, Feldmann H, Volchkova VA, Klenk HD.** 1998. Processing of the Ebola virus glycoprotein by the proprotein convertase furin. Proc Natl Acad Sci U S A **95:**5762-5767.

12. **Volchkov VE, Volchkova VA, Ströher U, Becker S, Dolnik O, Cieplik M, Garten W, Klenk HD, Feldmann H.** 2000. Proteolytic processing of Marburg virus glycoprotein. Virology **268:**1-6.

13. **Volchkov VE, Becker S, Volchkova VA, Ternovoj VA, Kotov AN, Netesov SV, Klenk HD.** 1995. GP mRNA of Ebola virus is edited by the Ebola virus polymerase and by T7 and vaccinia virus polymerases. Virology **214:**421-430.

14. **Sanchez A, Trappier SG, Mahy BW, Peters CJ, Nichol ST.** 1996. The virion glycoproteins of Ebola viruses are encoded in two reading frames and are expressed through transcriptional editing. Proc Natl Acad Sci U S A **93:**3602-3607.

15. **Mehedi M, Falzarano D, Seebach J, Hu X, Carpenter MS, Schnittler HJ, Feldmann H.** 2011. A New Ebola Virus Nonstructural Glycoprotein Expressed through RNA Editing. J Virol **85:**5406-5414.

16. **Bukreyev A, Volchkov VE, Blinov VM, Netesov SV.** 1993. The GP-protein of Marburg virus contains the region similar to the 'immunosuppressive domain' of oncogenic retrovirus P15E proteins. FEBS Lett **323:**183-187.

17. **Will C, Mühlberger E, Linder D, Slenczka W, Klenk HD, Feldmann H.** 1993. Marburg virus gene 4 encodes the virion membrane protein, a type I transmembrane glycoprotein. J Virol **67:**1203-1210.

18. **Kuhn JH, Bao Y, Bavari S, Becker S, Bradfute S, Brauburger K, Rodney Brister J, Bukreyev AA, Cai Y, Chandran K, Davey RA, Dolnik O, Dye JM, Enterlein S, Gonzalez JP, Formenty P, Freiberg AN, Hensley LE, Hoenen T, Honko AN, Ignatyev GM, Jahrling PB, Johnson KM, Klenk HD, Kobinger G, Lackemeyer MG, Leroy EM, Lever MS, Mühlberger E, Netesov SV, Olinger GG, Palacios G, Patterson JL, Paweska JT, Pitt L, Radoshitzky SR, Ryabchikova EI, Saphire EO, Shestopalov AM, Smither SJ, Sullivan NJ, Swanepoel R, Takada A, Towner JS, van der Groen G, Volchkov VE, Volchkova VA, Wahl-Jensen V, Warren TK, Warfield KL, Weidmann M, Nichol ST.** 2014. Virus nomenclature below the species level: a standardized nomenclature for filovirus strains and variants rescued from cDNA. Arch Virol **159:**1229-1237.

19. **Kajihara M, Marzi A, Nakayama E, Noda T, Kuroda M, Manzoor R, Matsuno K, Feldmann H, Yoshida R, Kawaoka Y, Takada A.** 2012. Inhibition of Marburg virus budding by nonneutralizing antibodies to the envelope glycoprotein. J Virol **86:**13467-13474.

20. **Takada A, Ebihara H, Jones S, Feldmann H, Kawaoka Y.** 2007. Protective efficacy of neutralizing antibodies against Ebola virus infection. Vaccine **25:**993-999.

21. **Audet J, Wong G, Wang H, Lu G, Gao GF, Kobinger G, Qiu X.** 2014. Molecular Characterization of the Monoclonal Antibodies Composing ZMAb: A Protective Cocktail Against Ebola Virus. Scientific reports **4:**6881.

22. **Wool-Lewis RJ, Bates P.** 1998. Characterization of Ebola virus entry by using pseudotyped viruses: identification of receptor-deficient cell lines. J Virol **72:**3155-3160.

23. **Kuhn JH, Radoshitzky SR, Guth AC, Warfield KL, Li W, Vincent MJ, Towner JS, Nichol ST, Bavari S, Choe H, Aman MJ, Farzan M.** 2006. Conserved receptor-binding domains of Lake Victoria marburgvirus and Zaire ebolavirus bind a common receptor. J Biol Chem **281:**15951-15958.

24. **Shedlock DJ, Bailey MA, Popernack PM, Cunningham JM, Burton DR, Sullivan NJ.** 2010. Antibody-mediated neutralization of Ebola virus can occur by two distinct mechanisms. Virology **401:**228-235.

25. **Sullivan NJ, Geisbert TW, Geisbert JB, Shedlock DJ, Xu L, Lamoreaux L, Custers JH, Popernack PM, Yang ZY, Pau MG, Roederer M, Koup RA, Goudsmit J, Jahrling PB, Nabel GJ.** 2006. Immune protection of nonhuman primates against Ebola virus with single low-dose adenovirus vectors encoding modified GPs. PLoS Med **3:**e177.

26. **Mohan GS, Li W, Ye L, Compans RW, Yang C.** 2012. Antigenic subversion: a novel mechanism of host immune evasion by Ebola virus. PLoS Pathog **8:**e1003065.

27. **Towner JS, Paragas J, Dover JE, Gupta M, Goldsmith CS, Huggins JW, Nichol ST.** 2005. Generation of eGFP expressing recombinant Zaire ebolavirus for analysis of early pathogenesis events and high-throughput antiviral drug screening. Virology **332:**20-27.

28. **Maruyama J, Miyamoto H, Kajihara M, Ogawa H, Maeda K, Sakoda Y, Yoshida R, Takada A.** 2014. Characterization of the envelope glycoprotein of a novel filovirus, Lloviu virus. J Virol **88:**99-109.

29. **Lubaki NM, Ilinykh P, Pietzsch C, Tigabu B, Freiberg AN, Koup RA, Bukreyev A.** 2013. The lack of maturation of Ebola virus-infected dendritic cells results from the cooperative effect of at least two viral domains. J Virol **87:**7471-7485.

30. **Ilinykh PA, Lubaki NM, Widen SG, Renn LA, Theisen TC, Rabin RL, Wood TG, Bukreyev A.** 2015. Different Temporal Effects of Ebola Virus VP35 and VP24 Proteins on Global Gene Expression in Human Dendritic Cells. J Virol **89:**7567-7583.

31. **Kuzmin IV, Wu X, Tordo N, Rupprecht CE.** 2008. Complete genomes of Aravan, Khujand, Irkut and West Caucasian bat viruses, with special attention to the polymerase gene and non-coding regions. Virus Res **136:**81-90.

32. **CDC.** 2009. Imported case of Marburg Hemorrhagic Fever - Colorado, 2008. Morbidity and Mortality Weekly Report **58:**1377-1381.

33. **Towner JS, Amman BR, Sealy TK, Carroll SA, Comer JA, Kemp A, Swanepoel R, Paddock CD, Balinandi S, Khristova ML, Formenty PB, Albariño CG, Miller DM, Reed ZD, Kayiwa JT, Mills JN, Cannon DL, Greer PW, Byaruhanga E, Farnon EC, Atimnedi P, Okware S, Katongole-Mbidde E, Downing R, Tappero JW, Zaki SR, Ksiazek TG, Nichol ST, Rollin PE.** 2009. Isolation of genetically diverse Marburg viruses from Egyptian fruit bats. PLoS Pathog **5:**e1000536.

566 34. **Flyak AI, Ilinykh PA, Murin CD, Garron T, Shen X, Fusco ML, Hashiguchi T, Bornholdt ZA,**
567 **Slaughter JC, Sapparapu G, Klages C, Ksiazek TG, Ward AB, Saphire EO, Bukreyev A, Crowe**
568 **JE, Jr.** 2015. Mechanism of human antibody-mediated neutralization of Marburg virus. Cell **160:**893-
569 903.
570 35. **Garbutt M, Liebscher R, Wahl-Jensen V, Jones S, Möller P, Wagner R, Volchkov V, Klenk HD,**
571 **Feldmann H, Ströher U.** 2004. Properties of replication-competent vesicular stomatitis virus vectors
572 expressing glycoproteins of filoviruses and arenaviruses. J Virol **78:**5458-5465.
573 36. **Maruyama T, Rodriguez LL, Jahrling PB, Sanchez A, Khan AS, Nichol ST, Peters CJ, Parren PW,**
574 **Burton DR.** 1999. Ebola virus can be effectively neutralized by antibody produced in natural human
575 infection. J Virol **73:**6024-6030.
576 37. **Parren PW, Geisbert TW, Maruyama T, Jahrling PB, Burton DR.** 2002. Pre- and postexposure
577 prophylaxis of Ebola virus infection in an animal model by passive transfer of a neutralizing human
578 antibody. J Virol **76:**6408-6412.
579 38. **Flyak AI, Shen X, Murin CD, Turner HL, Fusco ML, Lampley R, Kose N, Ilinykh PA, Kuzmina N,**
580 **Branchizio A, King H, Brown L, Bryan C, Davidson E, Doranz BJ, Slaughter JC, Sapparapu G,**
581 **Klages C, Ksiazek TG, Saphire EO, Ward AB, Bukreyev A, Crowe JE, Jr.** 2016. Cross-reactive and
582 potent neutralizing antibody responses in human survivors of natural Ebolavirus infection. Cell **D-15-**
583 **01816R1 In press**.
584 39. **Hevey M, Negley D, Geisbert J, Jahrling P, Schmaljohn A.** 1997. Antigenicity and vaccine potential
585 of Marburg virus glycoprotein expressed by baculovirus recombinants. Virology **239:**206-216.
586 40. **Licata JM, Johnson RF, Han Z, Harty RN.** 2004. Contribution of Ebola virus glycoprotein,
587 nucleoprotein, and VP24 to budding of VP40 virus-like particles. J Virol **78:**7344-7351.
588 41. **Mittler E, Kolesnikova L, Hartlieb B, Davey R, Becker S.** 2011. The cytoplasmic domain of Marburg
589 virus GP modulates early steps of viral infection. J Virol **85:**8188-8196.
590 42. **Mittler E, Kolesnikova L, Strecker T, Garten W, Becker S.** 2007. Role of the transmembrane domain
591 of Marburg virus surface protein GP in assembly of the viral envelope. J Virol **81:**3942-3948.
592 43. **Kuhn JH.** 2008. Filoviruses, 1 ed. Springer, Wien New York.

593 44. **Sanchez A, Kiley MP, Holloway BP, Auperin DD.** 1993. Sequence analysis of the Ebola virus
594 genome: organization, genetic elements, and comparison with the genome of Marburg virus. Virus Res
595 **29:**215-240.
596 45. **Bukreyev A, Yang L, Fricke J, Cheng L, Ward JM, Murphy BR, Collins PL.** 2008. The secreted form
597 of respiratory syncytial virus G glycoprotein helps the virus evade antibody-mediated restriction of
598 replication by acting as an antigen decoy and through effects on Fc receptor-bearing leukocytes. J Virol
599 **82:**12191-12204.
600 46. **Grard G, Biek R, Tamfum JJ, Fair J, Wolfe N, Formenty P, Paweska J, Leroy E.** 2011. Emergence
601 of divergent Zaire ebola virus strains in Democratic Republic of the Congo in 2007 and 2008. J Infect
602 Dis **204 Suppl 3:**S776-784.
603 47. **Bausch DG, Nichol ST, Muyembe-Tamfum JJ, Borchert M, Rollin PE, Sleurs H, Campbell P,**
604 **Tshioko FK, Roth C, Colebunders R, Pirard P, Mardel S, Olinda LA, Zeller H, Tshomba A, Kulidri**
605 **A, Libande ML, Mulangu S, Formenty P, Grein T, Leirs H, Braack L, Ksiazek T, Zaki S, Bowen**
606 **MD, Smit SB, Leman PA, Burt FJ, Kemp A, Swanepoel R.** 2006. Marburg hemorrhagic fever
607 associated with multiple genetic lineages of virus. N Engl J Med **355:**909-919.
608 48. **Smith SA, Crowe JE.** 2015. Use of Human Hybridoma Technology To Isolate Human Monoclonal
609 Antibodie. Microbiology Spectrum **3:**AID-0027-2014.
610 49. **Groseth A, Marzi A, Hoenen T, Herwig A, Gardner D, Becker S, Ebihara H, Feldmann H.** 2012. The
611 Ebola virus glycoprotein contributes to but is not sufficient for virulence in vivo. PLoS Pathog
612 **8:**e1002847.
613 50. **Bharat TA, Noda T, Riches JD, Kraehling V, Kolesnikova L, Becker S, Kawaoka Y, Briggs JA.**
614 2012. Structural dissection of Ebola virus and its assembly determinants using cryo-electron
615 tomography. Proc Natl Acad Sci U S A **109:**4275-4280.
616 51. **McCombs RM, Melnick MB, Brunschwig JP.** 1966. Biophysical studies of vesicular stomatitis virus.
617 Journal of bacteriology **91:**803-812.
618 52. **Volchkova VA, Dolnik O, Martinez MJ, Reynard O, Volchkov VE.** 2015. RNA Editing of the GP
619 Gene of Ebola Virus is an Important Pathogenicity Factor. J Infect Dis **212 Suppl 2:**S226-233.

520 **FIGURE LEGENDS**

521

522 **Figure 1. Filoviruses are resistant to neutralization by mAbs.** Percentage of neutralization of filoviruses
523 EBOV, BDBV or MARV or the corresponding pseudotyped VSVs by human mAbs isolated from survivors.
524 Asterisks indicate concentrations of mAbs which gave different ($p < 0.05$) percentages of neutralization for
525 filoviruses versus pseudotyped VSVs.

526

527 **Figure 2. Swapping of GP or their ectodomains with their counterparts from heterologous filoviruses**
528 **result in viable chimeric filoviruses. A-C.** Cloning strategy for generation of EBOV/BDBV-GP, EBOV/SUDV-
529 GP, or EBOV/MARV-GP (**A**), EBOV/MARV-GPed (**B**), and EBOV/LLOV-GP (**C**) full-length clones. **D.**
530 Schematic representation of the recombinant eGFP-expressing filovirus constructs.

531

532 **Figure 3. Swapping of filovirus GP has only a minimal effect on the efficiency of viral replication.**
533 **A.** Fluorescent plaques of recombinant wild-type and chimeric filoviruses on day 3 after inoculation of Vero-E6
534 cell culture monolayers. The micrographs were taken at 10x magnification. **B.** Growth kinetics of the EBOV
535 chimeras in Vero-E6 cells inoculated at an MOI of 0.1 PFU/cell. The red curve corresponding to EBOV/BDBV-
536 GP is completely hidden under the blue curve representing EBOV/MARV-GP since these two viruses have
537 similar growth kinetics. Asterisks or pound symbol show differences ($p < 0.05$) in viral titers of the chimeric
538 viruses compared to EBOV on days 1 – 6.

539

540 **Figure 4. Plaques of chimeric filoviruses can be immunostained by mAbs specific to ectodomains of**
541 **their GP proteins. A.** Vero-E6 cell culture monolayers were inoculated with dilutions of the indicated viruses,
542 covered with 0.9% methylcellulose, and incubated for six days. Viral plaques were immunostained as
543 described in Materials and Methods. **B.** Top: the degree of difference between the amino acid sequences of
544 BDBV, SUDV or MARV GP versus EBOV GP calculated as 1.00-H where H is position homogeneity (53).
545 Bottom: parts of GP1 and GP2 are designated in colors as follows: SS, signal sequence, RBR, receptor-
546 binding region, GC, glycan cap, MD, mucin-like domain, IFL, internal fusion loop, HR1, heptad repeat 1, HR2,

heptad repeat 2, MPER, membrane-proximal external region, TM, transmembrane domain, CT, cytoplasmic tail (adapted from reference (54) . Note that the lengths of the proteins, as indicated in the plots, are greater than that of BDBV, SUDV, EBOV and MARV GP due to the gaps introduced in the alignments.

Figure 5. Chimeric filoviruses are neutralized according to GP ectodomain specificity of antibodies. A. Binding of filovirus-specific human mAbs to recombinant GP or sGP of the indicated filovirus species. **B.** Percentages of neutralization of wild type or chimeric filoviruses by various concentrations of human mAbs.

Figure 6. Use of chimeric filoviruses for high throughput screening (HTS) of mAbs. A. Comparison of the levels of fluorescence on day 4 after inoculation of cells with 150 or 300 PFU of EBOV/BDBV-GP. **B.** Levels of eGFP fluorescence in triplicate Vero-E6 cell suspensions inoculated with 400 PFU of EBOV/BDBV-GP pre-treated with various concentrations of BDBV41. **C**. UV fluorescent microscopy of Vero-E6 cells inoculated with 400 PFU of EBOV/BDBV-GP pre-treated with various concentrations of BDBV41; mAb concentrations and the levels of fluorescence for representative wells I – IV are indicated on Panel B. **D**. Comparison of the neutralizing activities of BDBV41 in plaque reduction assay with a biological isolate of BDBV, recombinant EBOV/BDBV-GP filovirus or pseudotyped VSV (VSV/BDBV-GP), and in HTS with EBOV/BDBV-GP chimera.

Figure 7. The sGP protein reduces virus neutralization by mAb BDBV52. A. Percent neutralization of EBOV/BDBV-GP or EBOV/BDBV-GPΔsGP by BDBV52 or BDBV41. Disabling of sGP expression makes the virus partially susceptible to BDBV52. In contrast, both viruses are equally susceptible to BDBV41, suggesting that the increased susceptibility of EBOV/BDBV-GPΔsGP to BDBV52 is not a result of the altered properties of viral particles. **B.** Binding of BDBV52 to both GP and sGP. Parts of GP are designated in colors as in Fig. 4B. sGP shares with GP the N-terminal part, including SS, RBD, and most of GC, and also has the unique part (UP) at the C-terminus (13, 14). The most likely location of BDBV52 epitope identified in Flyak et al., unpublished, is indicated for both sGP and $GP_{1,2}$.

Fig. 1

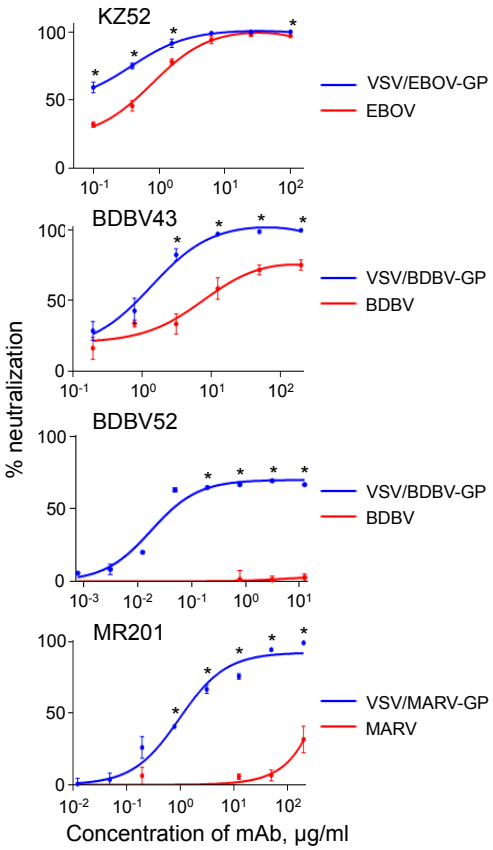

Fig. 2

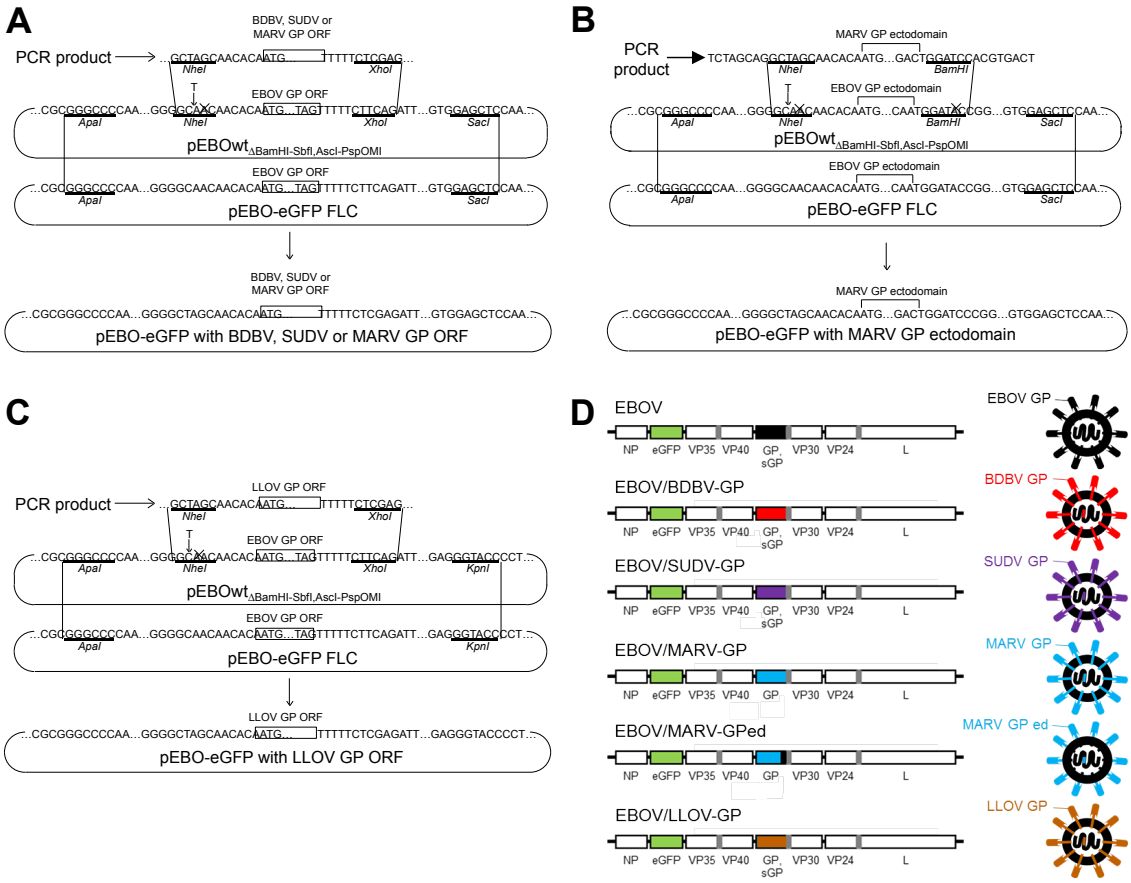

Fig. 3

A

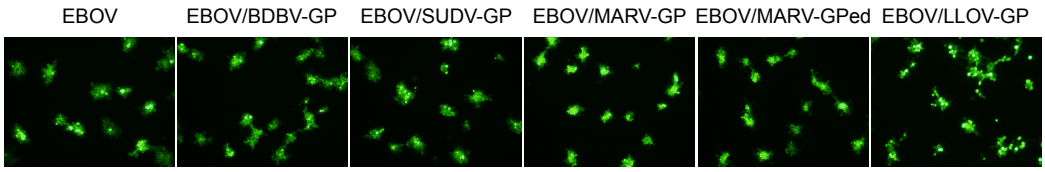

B

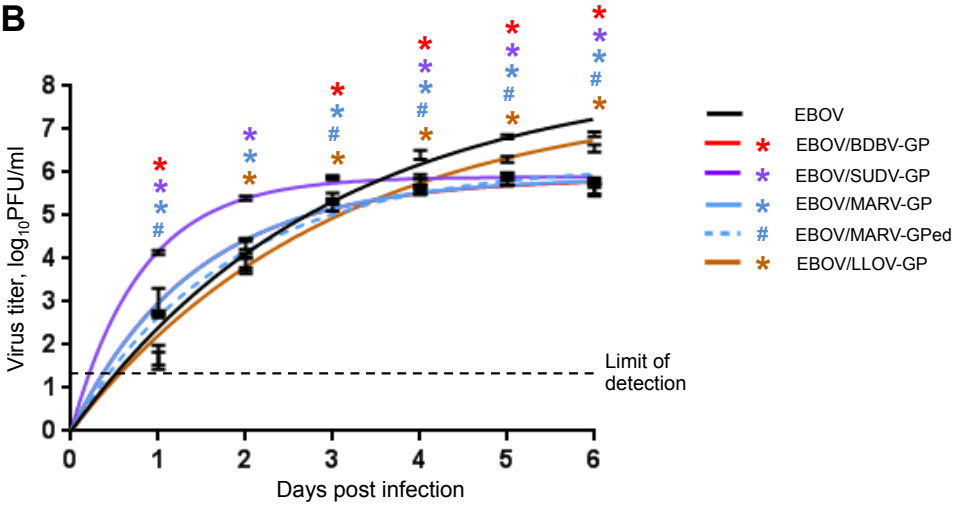

Fig. 4

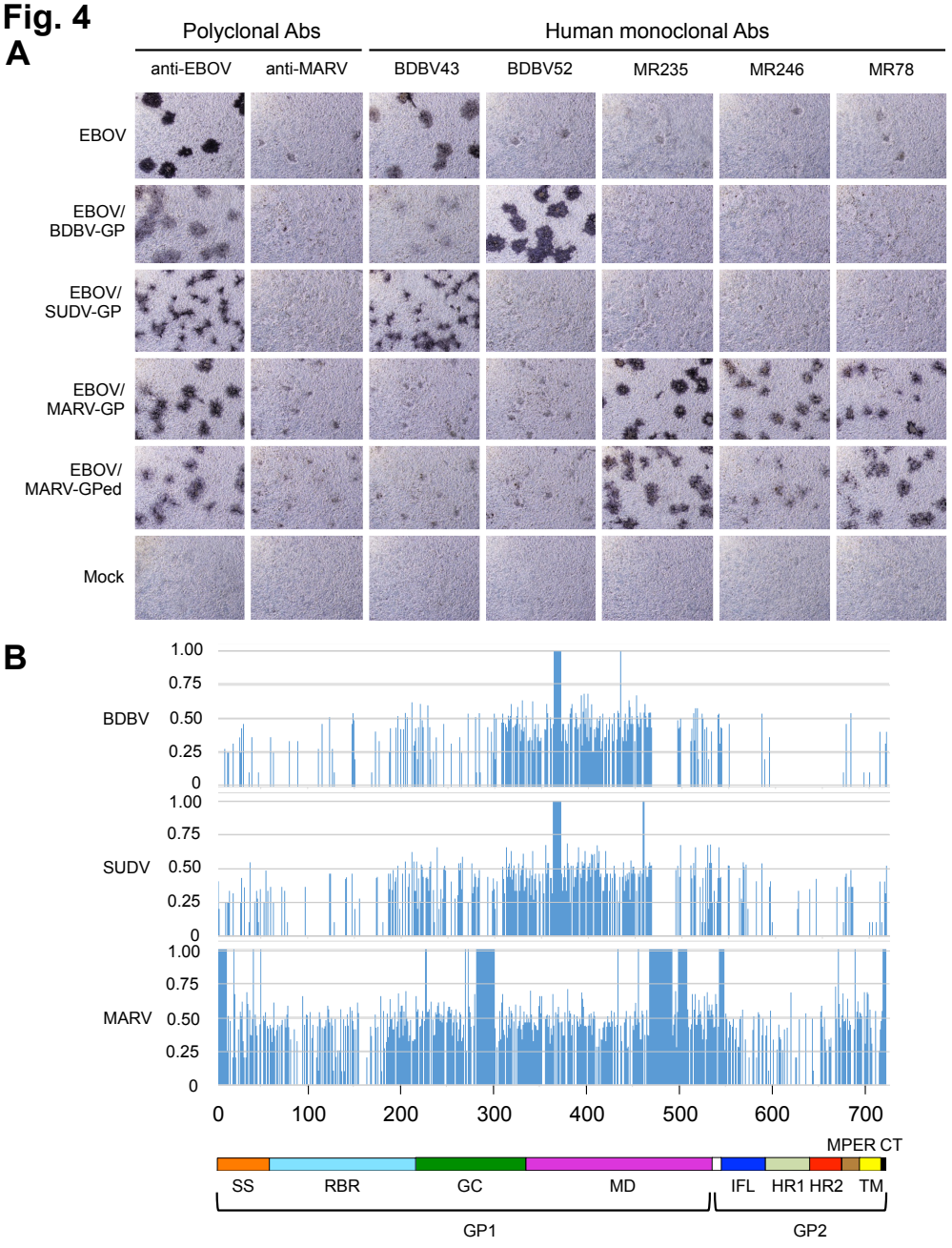

Fig 5

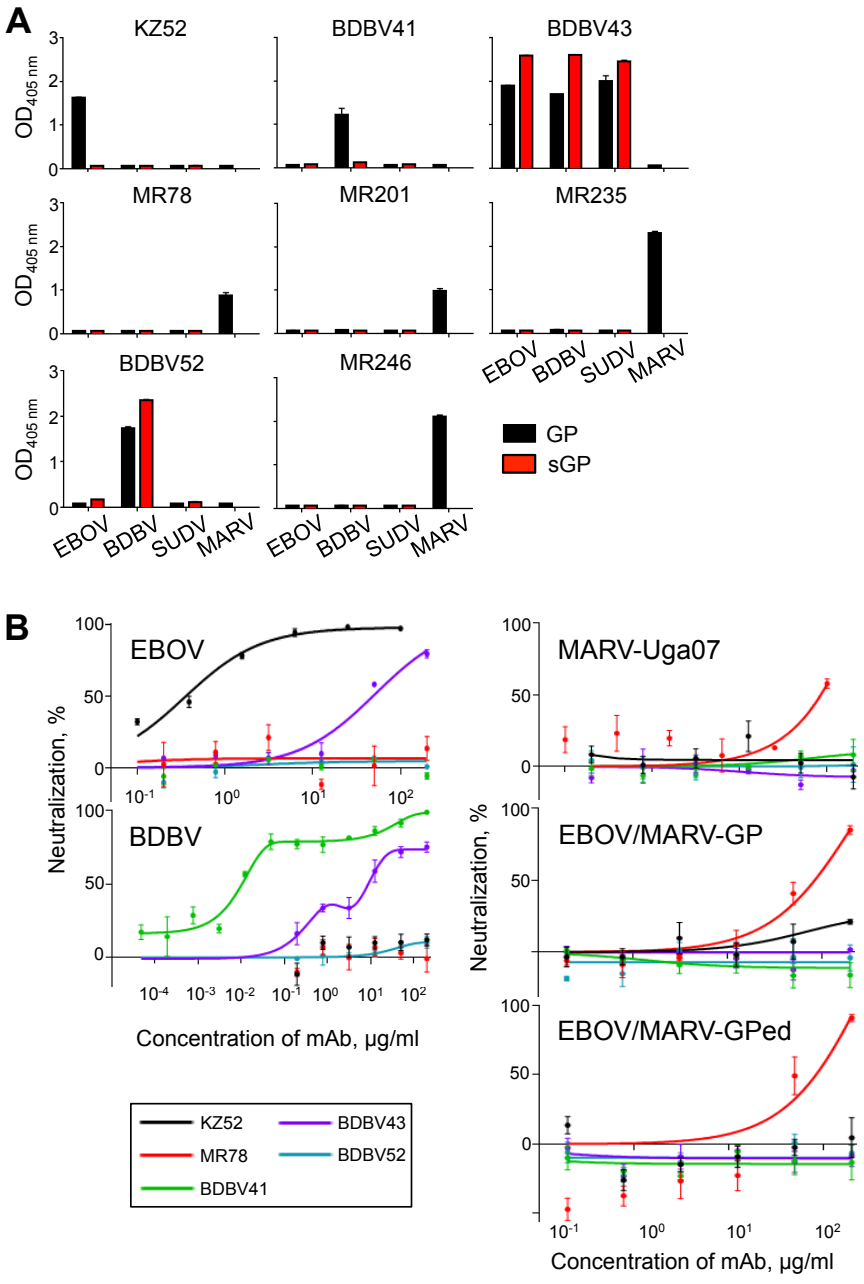

Fig. 6

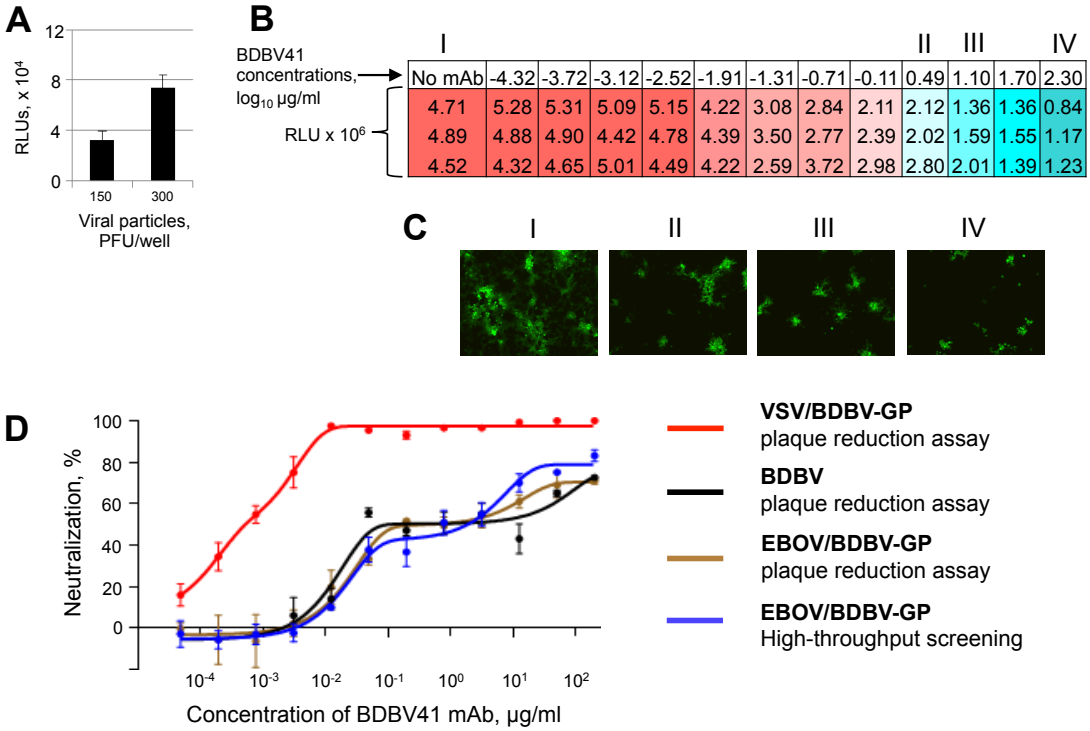

Fig. 7

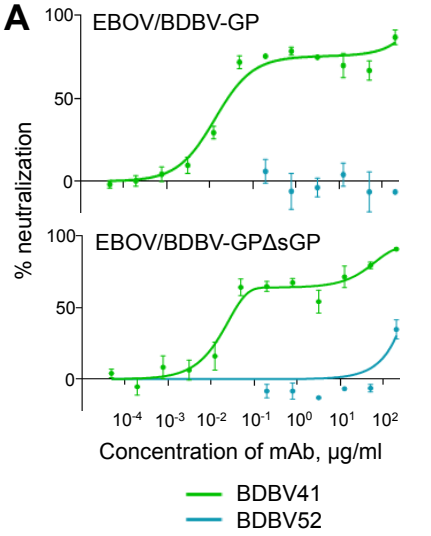

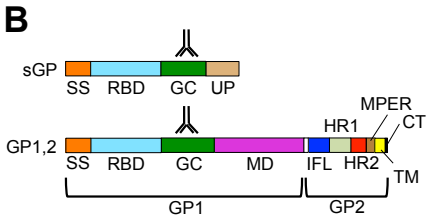

Article

Cell

Cross-Reactive and Potent Neutralizing Antibody Responses in Human Survivors of Natural Ebolavirus Infection

Graphical Abstract

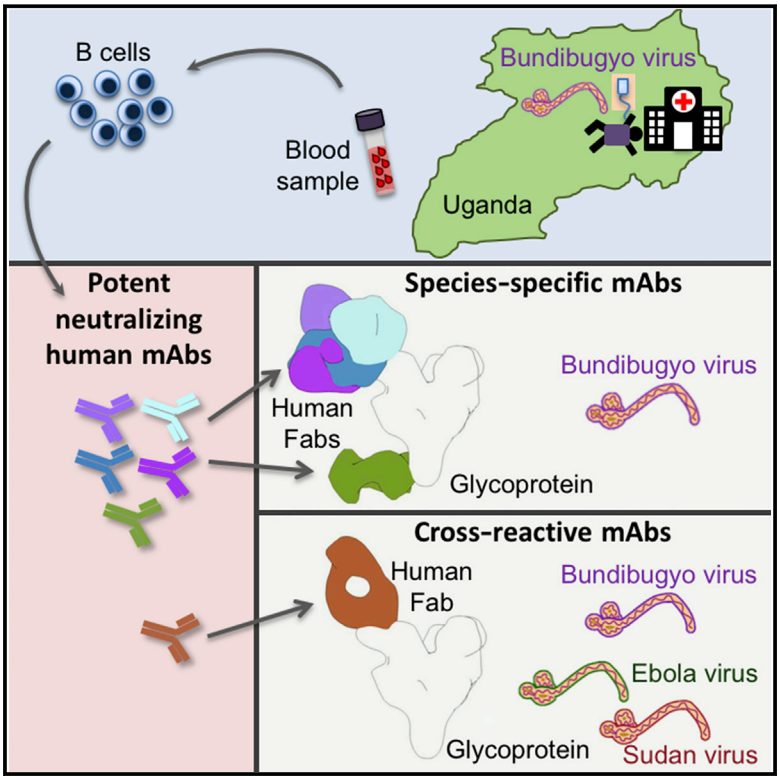

Highlights

- Natural Ebolavirus infection induced B cells encoding cross-reactive antibodies
- Some cross-reactive human antibodies neutralized multiple Ebolavirus species
- A large proportion of BDBV-neutralizing antibodies bound to the glycan cap
- Glycan cap-specific antibodies exhibited very potent neutralizing activity

Authors

Andrew I. Flyak, Xiaoli Shen, Charles D. Murin, ..., Andrew B. Ward, Alexander Bukreyev, James E. Crowe, Jr.

Correspondence

alexander.bukreyev@utmb.edu (A.B.), james.crowe@vanderbilt.edu (J.E.C.)

In Brief

Natural Ebola virus infection causes the induction of B cells that encode potent neutralizing human antibodies, which possess, in some cases, a surprising level of cross-reactivity for multiple species of filoviruses. The neutralizing antibody repertoire recognizes diverse features on the surface glycoprotein, but most of the potent antibodies recognize the glycan cap region.

Flyak et al., 2016, Cell *164*, 392–405
January 28, 2016
http://dx.doi.org/10.1016/j.cell.2015.12.022

CellPress

Cell

Article

Cross-Reactive and Potent Neutralizing Antibody Responses in Human Survivors of Natural Ebolavirus Infection

Andrew I. Flyak,[1] Xiaoli Shen,[5] Charles D. Murin,[8,9] Hannah L. Turner,[8] Joshua A. David,[8] Marnie L. Fusco,[9] Rebecca Lampley,[3] Nurgun Kose,[3] Philipp A. Ilinykh,[5] Natalia Kuzmina,[5] Andre Branchizio,[3] Hannah King,[3] Leland Brown,[3] Christopher Bryan,[11] Edgar Davidson,[11] Benjamin J. Doranz,[11] James C. Slaughter,[3,4] Gopal Sapparapu,[3] Curtis Klages,[7] Thomas G. Ksiazek,[5,6,7] Erica Ollmann Saphire,[9,10] Andrew B. Ward,[8] Alexander Bukreyev,[5,6,7,*] and James E. Crowe, Jr.[1,2,3,*]

[1]Department of Pathology, Microbiology and Immunology, Vanderbilt University, Nashville, TN 37232, USA
[2]Department of Pediatrics, Vanderbilt University, Nashville, TN 37232, USA
[3]Vanderbilt Vaccine Center, Vanderbilt University, Nashville, TN 37232, USA
[4]Department of Biostatistics, Vanderbilt University, Nashville, TN 37232, USA
[5]Department of Pathology, University of Texas Medical Branch, Galveston, TX 77555, USA
[6]Department of Microbiology and Immunology, University of Texas Medical Branch, Galveston, TX 77555, USA
[7]Galveston National Laboratory, Galveston, TX 77550, USA
[8]Department of Integrative Structural and Computational Biology, The Scripps Research Institute, La Jolla, CA 92037, USA
[9]Department of Immunology and Microbial Science, The Scripps Research Institute, La Jolla, CA 92037, USA
[10]The Skaggs Institute for Chemical Biology, The Scripps Research Institute, La Jolla, CA 92037, USA
[11]Integral Molecular Inc., Philadelphia, PA 19104, USA
*Correspondence: alexander.bukreyev@utmb.edu (A.B.), james.crowe@vanderbilt.edu (J.E.C.)
http://dx.doi.org/10.1016/j.cell.2015.12.022

SUMMARY

Recent studies have suggested that antibody-mediated protection against the *Ebolaviruses* may be achievable, but little is known about whether or not antibodies can confer cross-reactive protection against viruses belonging to diverse *Ebolavirus* species, such as Ebola virus (EBOV), Sudan virus (SUDV), and Bundibugyo virus (BDBV). We isolated a large panel of human monoclonal antibodies (mAbs) against BDBV glycoprotein (GP) using peripheral blood B cells from survivors of the 2007 BDBV outbreak in Uganda. We determined that a large proportion of mAbs with potent neutralizing activity against BDBV bind to the glycan cap and recognize diverse epitopes within this major antigenic site. We identified several glycan cap-specific mAbs that neutralized multiple ebolaviruses, including SUDV, and a cross-reactive mAb that completely protected guinea pigs from the lethal challenge with heterologous EBOV. Our results provide a roadmap to develop a single antibody-based treatment effective against multiple *Ebolavirus* infections.

INTRODUCTION

The genus *Ebolavirus*, family *Filoviridae*, contains three viral species that are known to cause large deadly disease outbreaks in Africa: *Zaire ebolavirus* represented by Ebola virus (EBOV), *Sudan ebolavirus* represented by Sudan virus (SUDV), and *Bundibugyo ebolavirus* represented by Bundibugyo virus (BDBV). The most recent EBOV outbreak has caused more than 28,000 cases and more than 11,000 deaths (according to the October 14, 2015, World Health Organization [WHO] Ebola Situation Report). While there is no FDA-approved treatment for filovirus infections, several experimental therapeutics against EBOV are being investigated, including small interfering RNAs (Geisbert et al., 2010; Thi et al., 2015), antisense oligonucleotides (Warren et al., 2010, 2015), a nucleoside analog (Warren et al., 2014), therapeutic vaccines (Feldmann et al., 2007; Geisbert et al., 2008), and monoclonal antibody (mAb) cocktails (Olinger et al., 2012; Qiu et al., 2012, 2014). Of these, preliminary treatment studies suggest that the effect of the ZMapp mAb cocktail exceeded the efficacy and treatment window of other experimental therapeutics described so far (Qiu et al., 2014).

The ZMapp cocktail is composed of three EBOV glycoprotein (GP)-specific mAbs (designated c13C6, c2G4, and c4G7) that were isolated initially from mice (Qiu et al., 2011; Wilson et al., 2000), chimerized with human antibody-constant regions, and then produced in *Nicotiana benthamiana* (Qiu et al., 2014). Single-particle electron microscopy (EM) reconstructions of these mAbs in complex with EBOV surface protein have revealed key sites of vulnerability on the EBOV GP (Murin et al., 2014). One such site lies within the GP base at the GP1/GP2 interface; two of three mAbs from the ZMapp cocktail (c2G4 and c4G7) bind to overlapping epitopes located in this region. The third mAb from the ZMapp cocktail, c13C6, binds a second antigenic site, which is located in the glycan cap region. GP base region-specific mAbs c2G4 and c4G7 displayed high neutralization activity in vitro (IC_{50} < 0.1 μg/ml), whereas the glycan cap-specific mAb c13C6 weakly neutralized EBOV only in the presence of complement (IC_{50} > 1.0 μg/ml) (Qiu et al., 2014). The lower

A

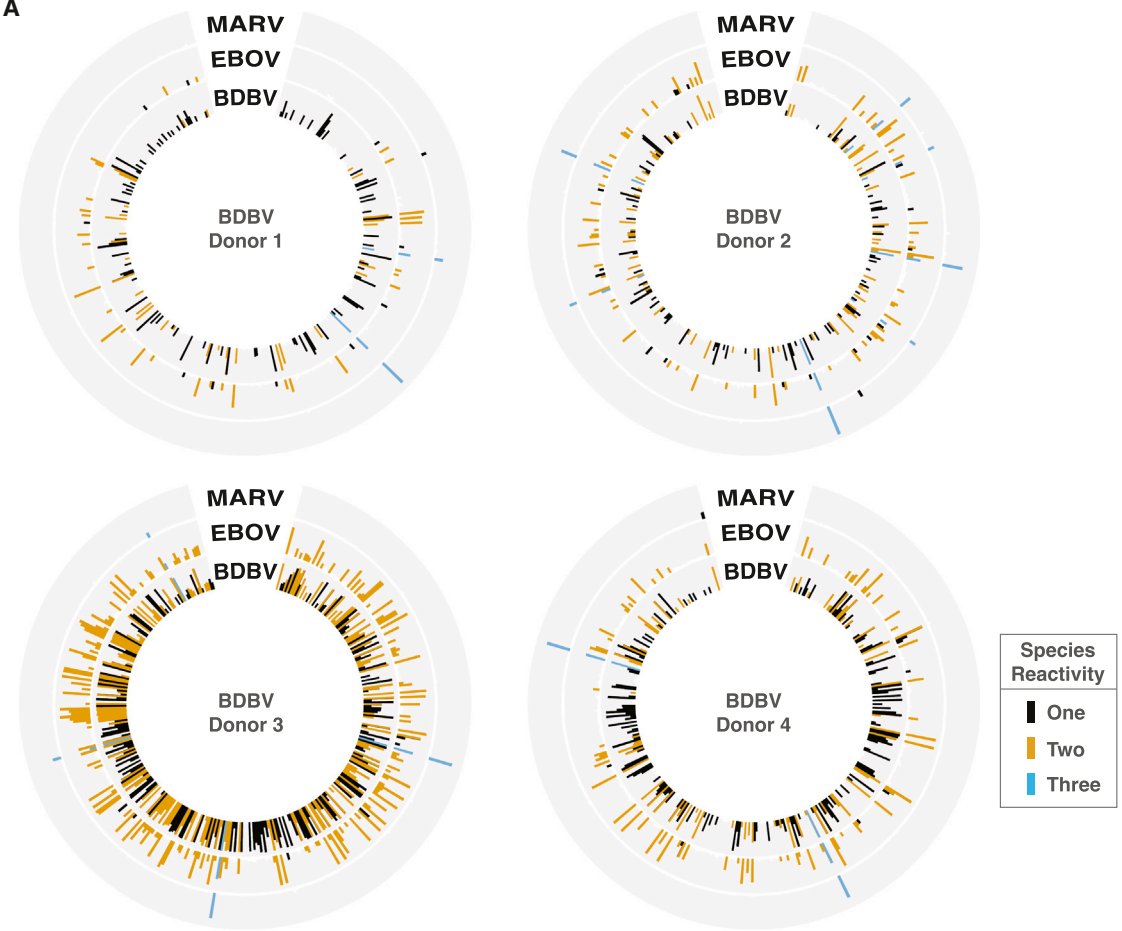

B

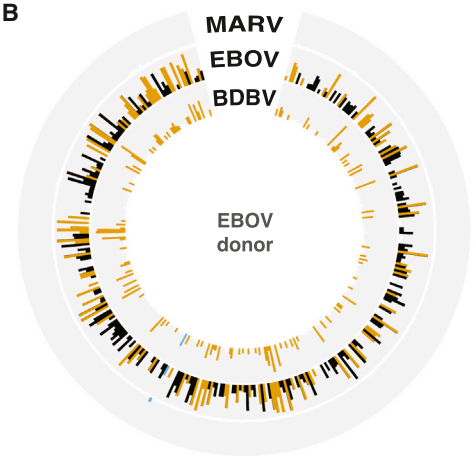

C

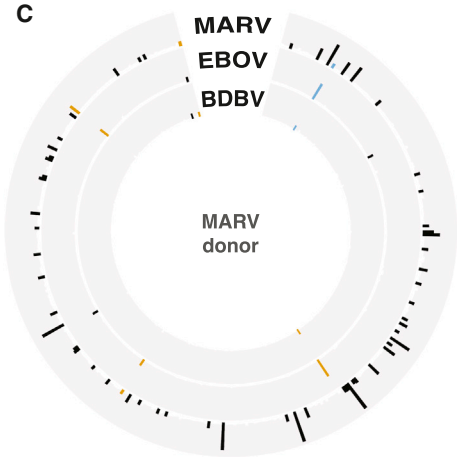

D

Subject	Total number of GP-specific lines	Reactivity of GP-specific B cell lines with diverse GPs (%)				
		BDBV-specific	BDBV/EBOV cross-reactive	EBOV-specific	BDBV/EBOV/MARV cross-reactive	MARV-specific
BDBV						
Donor 1	127	65.0	24.0	8.0	2.0	1.0
Donor 2	158	46.2	39.2	9.5	4.4	0.6
Donor 3	318	46.9	50.0	1.9	1.3	0
Donor 4	208	63.0	32.2	3.4	1.0	0.5
EBOV	281	0	36.3	63.3	0.4	0
MARV	64	1.6	1.6	4.8	1.6	90.3

(legend on next page)

in vitro neutralization activity of glycan cap-specific antibodies may be due to the removal of the glycan cap by host proteases (Chandran et al., 2005; Côté et al., 2011; Misasi et al., 2012) inside the endosome before GP engagement with the Niemann-Pick C1 receptor (Carette et al., 2011; Côté et al., 2011).

The ability of mAbs to bind to conserved neutralizing epitopes present on the surface of highly variable viral proteins has been documented extensively for HIV (Burton et al., 2012), influenza viruses (Pappas et al., 2014), dengue virus (Rouvinski et al., 2015), paramyxoviruses (Corti et al., 2013), and alphaviruses (Fox et al., 2015). Despite similar requirements for virus entry into the cell (Misasi et al., 2012), GPs from BDBV, EBOV, and SUDV strains differ by over 30% at the amino acid level (Towner et al., 2008). This overall genetic divergence among species of genus *Ebolavirus* has hampered the development of ebolavirus cross-neutralizing Abs. The key components of multiple antibody cocktails developed over the last decade neutralize only viruses of species *Zaire ebolavirus*. A weakly neutralizing mAb c13C6 was shown to cross-react with SUDV GPs (Wilson et al., 2000), but it is unknown whether this mAb can neutralize SUDV. Recently, several studies have shown that cross-reactive antibodies in serum can be elicited during natural infection in humans or vaccination of animals. The serum of individuals who survived BDBV, EBOV, or SUDV infections contained ebolavirus cross-reactive IgG, but not IgM (Macneil et al., 2011). Other studies demonstrated that mice immunized with a vaccine bearing the GP of EBOV generated cross-reactive polyclonal mAbs to other ebolaviruses, such as BDBV and SUDV (Meyer et al., 2015; Ou et al., 2012). Four broadly reactive non-neutralizing mAbs were isolated in mice after vaccinating animals with recombinant vesicular stomatitis virus (rVSV) expressing EBOV GP and then boosting initial immune response with the heterologous virus containing SUDV GP (Hernandez et al., 2015). The epitopes recognized by such cross-reactive mAbs are unknown.

In this study, we isolated a large panel of BDBV-specific and ebolavirus cross-reactive mAbs from B cells of survivors of BDBV infection. The results show that a large proportion of mAbs with potent neutralizing activity against BDBV bind to the glycan cap and recognize diverse epitopes within this major antigenic site. We identified several glycan cap-specific mAbs that neutralized multiple *Ebolavirus* species and a cross-reactive mAb that completely protected guinea pigs from the lethal challenge with heterologous EBOV when used as monotherapy. Several of these naturally occurring antibodies exhibit the most potent protective capacity reported, and they possessed unprecedented cross-reactivity for multiple *Ebolavirus* species, including SUDV, for which neutralizing human mAbs have not been reported.

RESULTS

Isolation of Human mAbs

To generate human cell lines secreting human mAbs to BDBV, we transformed peripheral blood B cells from seven survivors of the 2007 Uganda BDBV outbreak with Epstein-Barr virus, as described in the Experimental Procedures. To determine the breadth of antibody response in survivors of ebolavirus infection, we screened supernatants from EBV-transformed B cell lines for binding to GPs from diverse representatives of filovirus species: BDBV, EBOV, or Marburg virus (MARV) (Figures 1A and S1). We also used the same GP panel to screen supernatants from transformed B cell lines derived from a survivor of the 2014 EBOV outbreak (Figure 1B) or from a donor who survived MARV infection (Figure 1C). We color coded GP-reactive supernatants based on the cross-reactivity pattern as follows: species-specific cell lines are highlighted in black; and cross-reactive lines to two or three species are shown in yellow or blue, respectively (Figures 1A–1C and S1).

While approximately half of GP-specific B cell lines obtained from BDBV survivors produced antibodies specific to BDBV GP, 24%–50% of GP-reactive B cell culture supernatants also cross-reacted with EBOV GP (Figures 1A and 1D). Similarly, 36% of GP-specific B cell lines obtained from the EBOV survivor cross-reacted with the heterologous BDBV GP (Figures 1B and 1D). Despite the apparent presence of B cells encoding cross-reactive antibodies in survivors of BDBV or EBOV infections to GPs from heterologous *Ebolavirus* species, we detected a very limited cross-reactivity with GPs from MARV, which belongs to a different genus in the family *Filoviridae* (Figures 1A and 1D). In line with this finding, 90% of GP-reactive B cell lines obtained from the MARV survivor reacted with autologous GP, and only 2% of antigen-specific B cell lines produced *Ebolavirus* cross-reactive Abs (Figures 1C and 1D). The limited cross-reactivity of mAbs to GPs from *Ebolavirus* and *Marburgvirus* species likely is due in part to low sequence conservation between GPs from two genera (only 27% amino acid identity between BDBV and MARV GP) as well as differences in epitope availability caused by different positions of the mucin-like domains on the GP surface of *Ebolavirus* and *Marburgvirus* (Flyak et al., 2015; Fusco et al., 2015; Hashiguchi et al., 2015).

Binding and Neutralizing Activity of Human mAbs

We fused transformed cells from B cell lines producing BDBV GP-reactive Abs with myeloma cells and generated 90 cloned hybridomas secreting BDBV GP-reactive human mAbs. To determine the breadth of mAb binding, we screened the mAbs

Figure 1. Cross-Reactive B Cell Responses in Filovirus Immune Donors

(A–C) Supernatants from EBV-transformed PBMC samples isolated from survivors were screened in ELISA-binding assays using BDBV, EBOV, or MARV GPs. Results for four BDBV survivors (A), one EBOV survivor (B), and one MARV survivor (C) are shown. Height of the bars indicates $OD_{405\ nm}$ values in ELISA binding to full-length extracellular domain of GP of the indicated virus species. Reactive supernates are color coded based on the cross-reactivity pattern as follows: species-specific cell lines are highlighted in black; and cross-reactive lines to two or three species are shown in yellow or blue, respectively. Previous work has shown that the amino acid sequence of GP differs between BDBV and EBOV by over 34% and between BDBV and MARV by over 72%.

(D) Percentages of lines secreting antibodies specific to BDBV, EBOV, or MARV GPs or cross-reactive antibodies to BDBV and EBOV (designated BDBV/EBOV) or BDBV, EBOV, and MARV (designated BDBV/EBOV/MARV) are shown. Increasing intensity of the pink cell fill color corresponds to increasing reactivity for the indicated virus.

See also Figure S1.

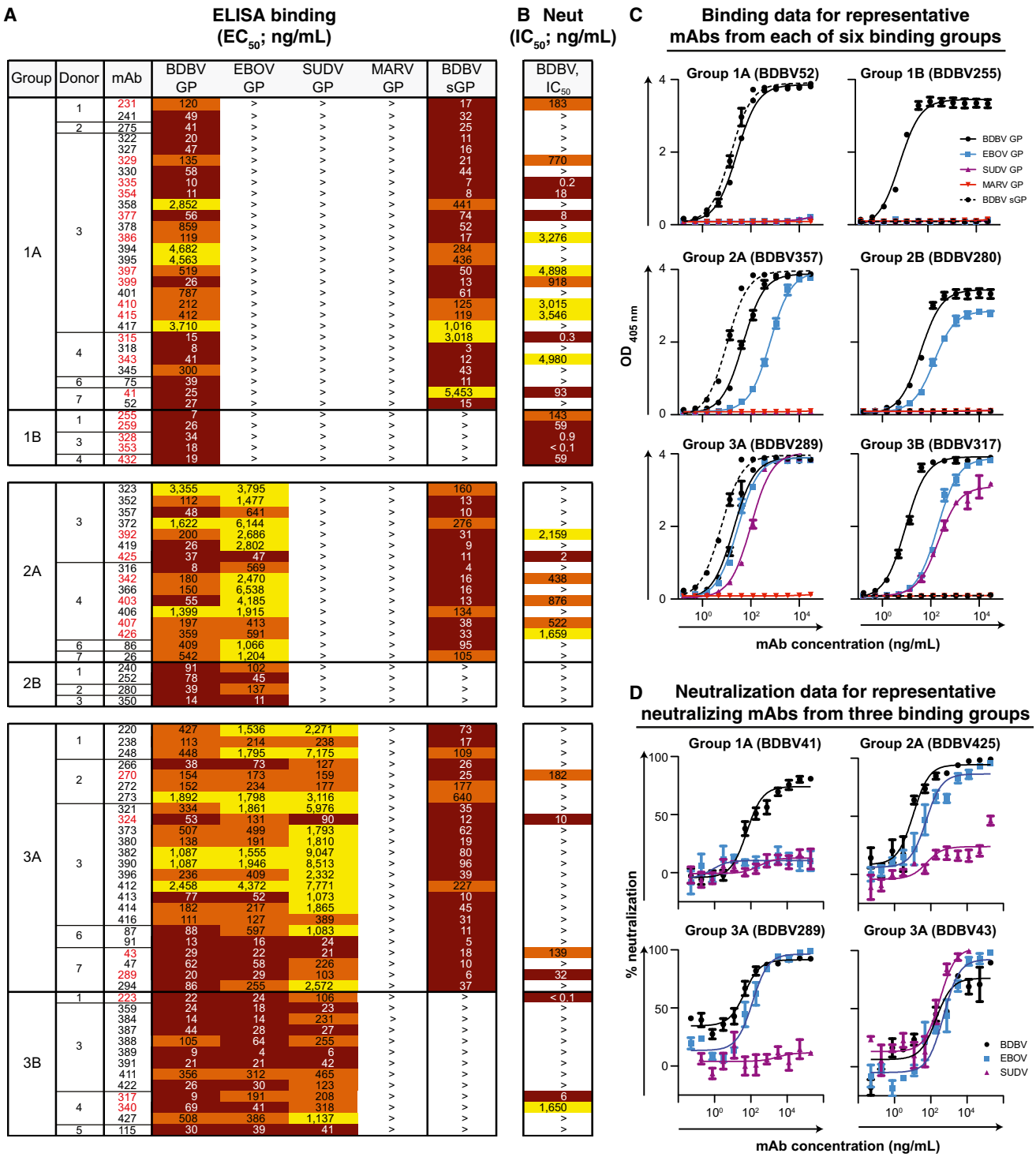

Group	Donor	mAb	BDBV GP	EBOV GP	SUDV GP	MARV GP	BDBV sGP	BDBV, IC_{50}
1A	1	231	120	>	>	>	17	183
		241	49	>	>	>	32	>
	2	275	41	>	>	>	25	>
	3	322	20	>	>	>	11	>
		327	47	>	>	>	16	>
		329	135	>	>	>	21	770
		330	58	>	>	>	44	>
		335	10	>	>	>	7	0.2
		354	11	>	>	>	8	18
		358	2,852	>	>	>	441	>
		377	56	>	>	>	74	8
		378	859	>	>	>	52	>
		386	119	>	>	>	17	3,276
		394	4,682	>	>	>	284	>
		395	4,563	>	>	>	436	>
		397	519	>	>	>	50	4,898
		399	26	>	>	>	13	918
		401	787	>	>	>	61	>
		410	212	>	>	>	125	3,015
		415	412	>	>	>	119	3,546
		417	3,710	>	>	>	1,016	>
	4	315	15	>	>	>	3,018	0.3
		318	8	>	>	>	3	>
		343	41	>	>	>	12	4,980
		345	300	>	>	>	43	>
	6	75	39	>	>	>	11	>
	7	41	25	>	>	>	5,453	93
		52	27	>	>	>	15	>
1B	1	255	7	>	>	>	>	143
		259	26	>	>	>	>	59
	3	328	34	>	>	>	>	0.9
		353	18	>	>	>	>	< 0.1
	4	432	19	>	>	>	>	59
2A	3	323	3,355	3,795	>	>	160	>
		352	112	1,477	>	>	13	>
		357	48	641	>	>	10	>
		372	1,622	6,144	>	>	276	>
		392	200	2,686	>	>	31	2,159
		419	26	2,802	>	>	9	>
		425	37	47	>	>	11	2
	4	316	8	569	>	>	4	>
		342	180	2,470	>	>	16	438
		366	150	6,538	>	>	16	>
		403	55	4,185	>	>	13	876
		406	1,399	1,915	>	>	134	>
		407	197	413	>	>	38	522
		426	359	591	>	>	33	1,659
	6	86	409	1,066	>	>	95	>
	7	26	542	1,204	>	>	105	>
2B	1	240	91	102	>	>	>	>
		252	78	45	>	>	>	>
	2	280	39	137	>	>	>	>
	3	350	14	11	>	>	>	>
3A	1	220	427	1,536	2,271	>	73	>
		238	113	214	238	>	17	>
		248	448	1,795	7,175	>	109	>
	2	266	38	73	127	>	26	>
		270	154	173	159	>	25	182
		272	152	234	177	>	177	>
		273	1,892	1,798	3,116	>	640	>
	3	321	334	1,861	5,976	>	35	>
		324	53	131	90	>	12	10
		373	507	499	1,793	>	62	>
		380	138	191	1,810	>	19	>
		382	1,087	1,555	9,047	>	80	>
		390	1,087	1,946	8,513	>	96	>
		396	236	409	2,332	>	39	>
		412	2,458	4,372	7,771	>	227	>
		413	77	52	1,073	>	10	>
		414	182	217	1,865	>	45	>
		416	111	127	389	>	31	>
	6	87	88	597	1,083	>	11	>
		91	13	16	24	>	5	>
	7	43	29	22	21	>	18	139
		47	62	58	226	>	10	>
		289	20	29	103	>	6	32
		294	86	255	2,572	>	37	>
3B	1	223	22	24	106	>	>	< 0.1
	3	359	24	18	23	>	>	>
		384	14	14	231	>	>	>
		387	44	28	27	>	>	>
		388	105	64	255	>	>	>
		389	9	4	6	>	>	>
		391	21	21	42	>	>	>
		411	356	312	465	>	>	>
		422	26	30	123	>	>	>
	4	317	9	191	208	>	>	6
		340	69	41	318	>	>	1,650
		427	508	386	1,137	>	>	>
	5	115	30	39	41	>	>	>

Figure 2. Cross-Neutralizing Antibodies from Survivors of Natural BDBV Infection

(A) Heatmap showing the binding of BDBV mAbs to a panel of filovirus GPs. The EC_{50} value for each GP-mAb combination is shown, with dark red, orange, yellow, or white shading indicating high, intermediate, low, or no detectable binding, respectively. EC_{50} values greater than 10,000 ng/ml are indicated (>). NAb names are highlighted in red.

(B) Heatmap showing the neutralization potency of BDBV GP-specific mAbs against BDBV. The IC_{50} value for each virus-mAb combination is shown. IC_{50} values greater than 10,000 ng/ml are indicated (>). Neutralization assays were performed in triplicate.

(legend continued on next page)

in ELISA-binding assays using recombinant GPs from multiple filoviruses: BDBV, EBOV, SUDV, or MARV GPs. While 33 Abs recognized only the autologous BDBV GP (designated groups 1A and 1B), 20 Abs recognized both BDBV and EBOV GPs (groups 2A and 2B), and 37 Abs recognized all three GPs from BDBV, EBOV, and SUDV (groups 3A and 3B) (Figures 2A and 2C; Data S1). The relative proportions of antibodies that recognize GPs from 1, 2, or 3 *Ebolavirus* species did not correlate fully with the B cell line frequencies in the initial screen, which can be explained by our prioritization on recovery of a high number of cross-reactive mAbs. We were not able to isolate Abs that bind to the heterologous MARV GP (Figures 2A and 2C; Data S1).

We further characterized the binding of species-specific or cross-reactive mAbs to recombinant GPs by performing a binding assay with the recombinant form of GP that is secreted from the cell to the extracellular space during natural infection (sGP, secreted GP) (Sanchez et al., 1996; Volchkov et al., 1995). While the *Ebolavirus* GP is a trimer, sGP forms dimers in which each protomer shares only the amino-terminal 295 amino acids with GP. The majority of mAbs recognized epitopes shared between BDBV GP and BDBV sGP (designated groups 1A, 2A, or 3A) (Figures 2A and 2C). We also identified antibodies that bound to BDBV GP, but failed to bind BDBV sGP in ELISA (designated groups 1B, 2B, or 3B) (Figures 2A and 2C). Antibodies from groups 1B, 2B, or 3B also bound the recombinant GP form that lacks highly glycosylated mucin-like domains (BDBV GPΔmuc), suggesting that mAbs from these three groups target epitopes outside of mucin-like domains (Figure S2).

To evaluate the inhibitory activity of isolated mAbs, we tested mAbs in a BDBV neutralization assay. Of the 90 BDBV GP-reactive mAbs, 31 had half-maximal inhibitory concentration (IC_{50}) values <10 μg/ml, and we defined these as neutralizing antibodies (nAbs) (Figures 2B, where nAb names are highlighted in red, and S3). Several nAbs displayed an extremely high neutralizing potency, with IC_{50} values below 1 ng/ml (Figure 2B). Also, 18 of 31 nAbs bound only to BDBV GP in ELISA, six nAbs recognized BDBV and EBOV GPs, and the remaining seven nAbs bound to GPs from representatives of three *Ebolavirus* species, BDBV, EBOV, and SUDV. These results suggested that cross-reactive mAbs in our panel might possess neutralizing activity to multiple ebolaviruses. To test this hypothesis, we screened BDBV425 (a group 2A nAb) in an EBOV neutralization assay as the nAb with the lowest half-maximal effective concentration (EC_{50}) value to the heterologous EBOV GP, and we determined that BDBV425 neutralized the heterologous EBOV. Encouraged by this result, we tested nAbs from groups 3A and 3B in EBOV or SUDV neutralization assays to determine whether cross-reactive nAbs can neutralize three *Ebolavirus* species. We found two cross-reactive nAbs from group 3A (BDBV43 and BDBV324) that neutralized all three ebolaviruses BDBV, EBOV, and SUDV (Figure 2D, BDBV43). The remaining five nAbs from groups 3A and 3B neutralized BDBV and EBOV, but failed to neutralize SUDV (Figure 2D, BDBV289). Analysis of the Ab heavy-chain variable domain sequences for 26 nAbs revealed that all BDBV-specific and cross-reactive nAbs were encoded by unique Ab genes (Table S1).

Major Antigenic Sites Recognized by Human mAbs

To determine whether Abs from distinct binding groups targeted different antigenic regions on the BDBV GP surface, we performed a quantitative competition-binding assay using a real-time biosensor. We tested four BDBV nAbs from binding group 1A, five nAbs from binding group 1B, four nAbs from group 3A, and three nAbs from group 3B in a tandem blocking assay, in which BDBV GP was attached to the biosensor. We also tested five non-neutralizing antibodies from group 1A to determine whether non-neutralizing antibodies target a unique epitope on GP surface. Non-neutralizing and neutralizing mAbs from group 1A and nAbs from group 3A blocked binding of each other to the GP antigen and segregated into a single competition-binding group (Figure 3). These results suggest that mAbs from groups 1A and 3A target a single antigenic region that contains epitopes shared between GP and sGP (Figure 2A). The nAbs from group 3B that did not recognize sGP in ELISA (Figure 2A) segregated into a separate competition-binding group. Group 1B antibodies were interesting in that two nAbs in this group competed for binding with group 3B nAbs, while three nAbs from the group competed for binding with antibodies from group 3A (Figure 3). These findings suggested that there are at least two major antigenic regions recognized by human BDBV nAbs, based on competition-binding studies. The first major antigenic region contains epitopes that both sGP and GP share (recognized by mAbs from groups 1A and 3A) as well as epitopes that are present only on the GP surface (recognized by three mAbs from group 1B). The second major antigenic region contains only epitopes that are present on the GP surface, but not sGP (recognized by two mAbs from group 1B and three mAbs from group 3B).

Diverse Patterns of Molecular Recognition Defined by Negative-Stain EM

To determine the location of the two major antigenic regions targeted by human BDBV nAbs, we performed negative-stain single-particle EM studies using antibodies from groups 1A and 1B. The EM class averages and reconstructions showed clearly that the two major antigenic regions, defined in competition-binding experiments, corresponded to two distinct sites on the GP surface: the glycan cap and the GP base.

Comparison of the structures of glycan cap-directed mAbs from group 1A with those in group 1B revealed that the antibodies have partially overlapping epitopes, but approach the glycan cap at distinct angles (Figures 4A, 4B, and S4). We fitted a previously determined atomic resolution structure of SUDV GPΔmuc (Bale et al., 2012), which reveals more residues of the

(C) Binding of representative mAbs from six distinct binding groups to the filovirus GPs is shown.
(D) Neutralization activity of representative neutralizing mAbs from three binding groups against BDBV, EBOV, or SUDV. Error bars represent the SE of the experiment, performed in triplicate.
See also Table S1, Data S1, and Figures S2 and S3.

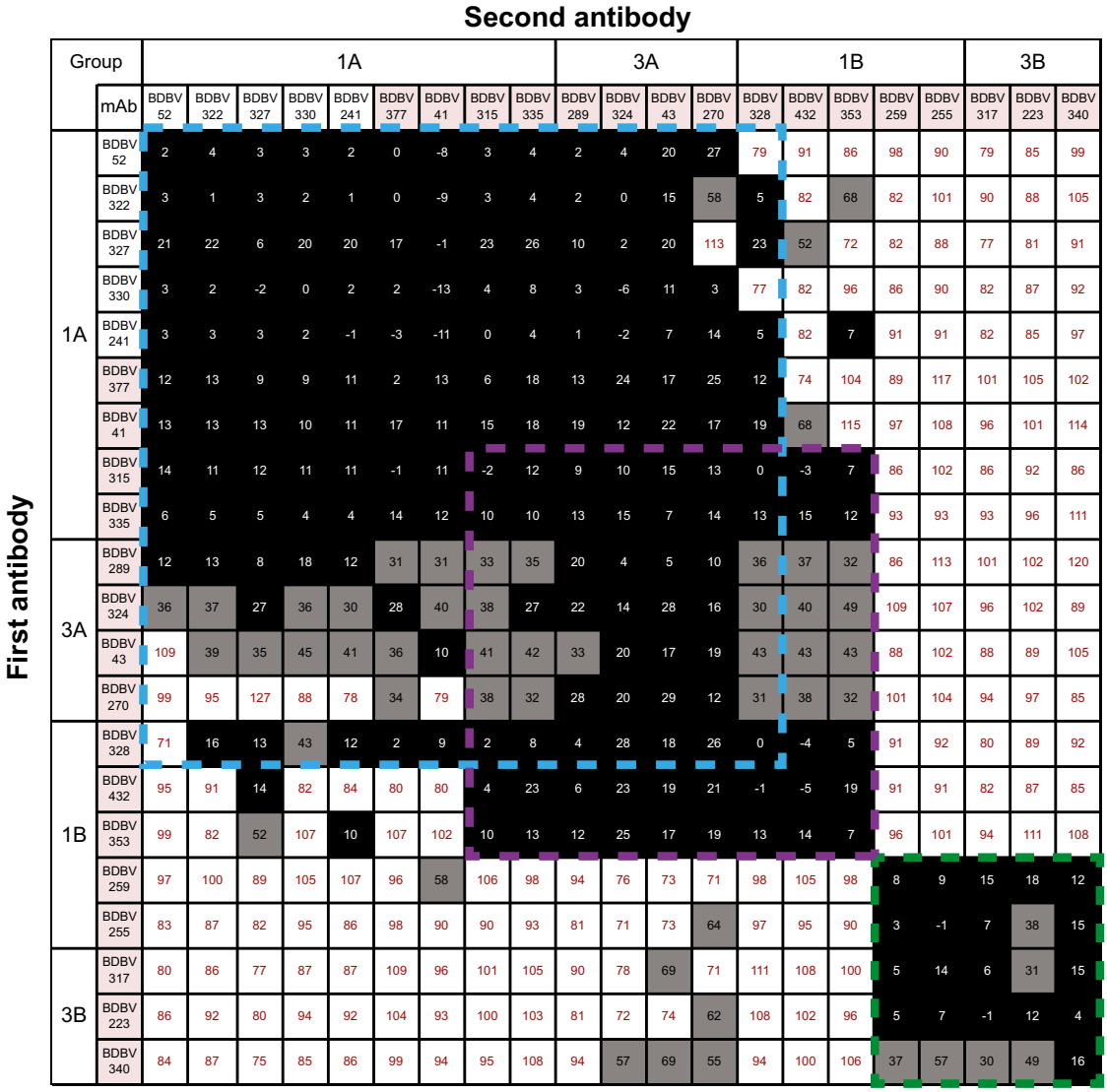

Figure 3. BDBV-Neutralizing Antibodies Target at Least Two Distinct Antigenic Regions of the GP Surface

Data from competition-binding assays using non-neutralizing mAbs from binding group 1A (white background) and neutralizing mAbs from binding groups 1A, 1B, 3A, or 3B (pink background). Numbers indicate the percentage binding of second mAb in the presence of the first mAb compared to binding of un-competed second mAb. MAbs were judged to compete for the same site if maximum binding of the second mAb was reduced to <30% of its un-competed binding (black boxes with white numbers). The mAbs were considered non-competing if maximum binding of the second mAb was >70% of its un-competed binding (white boxes with red numbers). Gray boxes with black numbers indicate an intermediate phenotype (competition resulted in between 30% and 70% of un-competed binding). Blue, purple, and green dashed lines indicate what appear to be major competition groups; the blue and purple groups overlap substantially, but not completely.

glycan cap region than the equivalent EBOV structure, into the envelope of GP from the EM reconstructions, and we determined the regions targeted by each mAb (Figures 4D and 4E). BDBV335, which binds GP and sGP equally well, mainly targets a region between residues 274 and 282. This region appears well defined in the BDBV335 EM map, indicated by the large lobe on the outside of the glycan cap that closely resembles that region in the GP crystal structure. When viewed along the 3-fold axis of GP, BDBV41 binds to the right of BDBV335, further up on the glycan cap, close to a loop that extends from residue 266 to 277. Consistent with this position, we passaged a chimeric VSV in which the G protein was replaced with BDBV GP as a sole surface protein (VSV/BDBV-GP) in the presence of mAb BDBV41 to generate a neutralization escape mutant virus that was completely resistant to the antibody and that possessed two amino acid substitutions, G271R and T272S (Figure S5). The mutation at the 272 position likely explains why BDBV41 is a group 1 antibody, i.e., only recognizes BDBV (with T272), but not EBOV or SUDV (which have the alternate residue K272). BDBV41 also may make contacts with a loop that extends

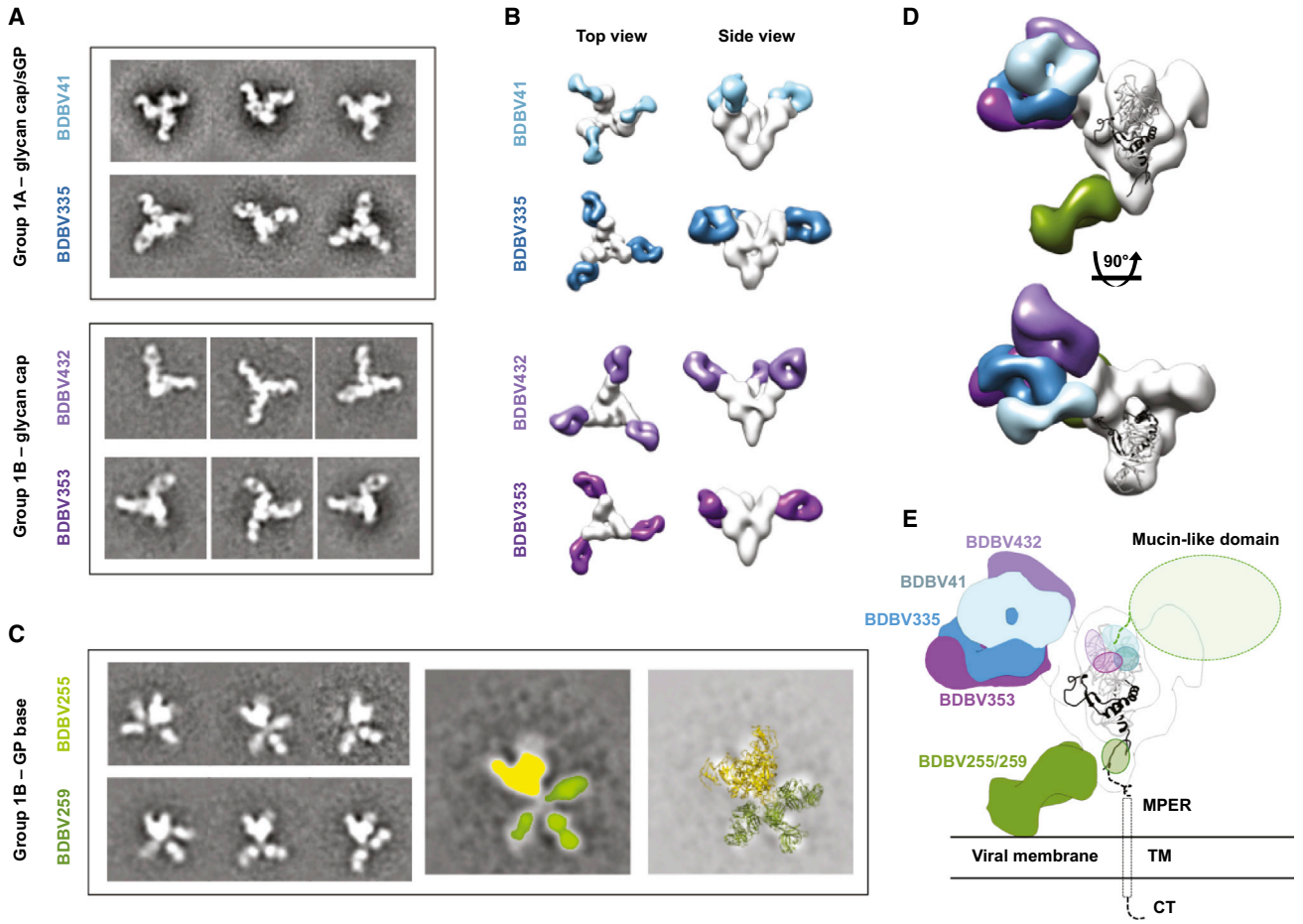

Figure 4. BDBV-Neutralizing Antibodies Bind to the Glycan Cap or Base Region of GP

(A) Shown are negative-stain EM reference-free 2D class averages of group 1A antibodies that bind both the glycan cap of GP and sGP, and group 1B antibodies that bind the glycan cap of GP, but not sGP. BDBV GP or GPΔmuc was used to generate complexes.

(B) 3D reconstructions of glycan cap binders from groups 1A and 1B reveal that these antibodies bind the glycan cap at overlapping but distinct epitopes. Top (left) and side (right) views of the complexes are shown.

(C) Reference-free 2D class averages of group 1B antibodies (left) reveal that these antibodies bind an epitope below the base of GP that is flexible. In the middle image, GP is colored yellow and each Fab is colored green. The righthand panel illustrates a superimposition of crystal structures of SUDV GPΔmuc (PDB: 3VE0) and Fabs (PDB: 3CSY) to demonstrate how Fabs may bind to GP.

(D) The composite model delineates the epitopes of the glycan cap mAbs in group 1A or 1B. Side (above) and top (below) views are shown.

(E) Docking a crystal structure of SUDV GPΔmuc (PDB: 3VE0) (Bale et al., 2012), which contains a more complete model of the glycan cap region targeted by group 1A/B mAbs, reveals how group 1A/B mAbs target a broad region in the GP1 centered on the glycan cap, near the beginning of the mucin-like domains. Group 1B mAbs that target the base likely bind to a loop near the membrane proximal external region (MPER) that is flexible and has not yet been resolved at high resolution. TM, transmembrane region; CT, cytoplasmic tail.

See also Figure S4.

toward the mucin-like domains, from residue 309 to 312 or further in regions that were unresolved in the GP crystal structure. BDBV432 binds to the left of BDBV335, at the top of a helix loop at residues 259–266, and likely makes extensive contacts with a loop from residues around 302–312. Despite a lack of binding to sGP, BDBV432, as well as BDBV353, binds in the glycan cap region, suggesting that these mAbs make contacts with residues that are exclusive to GP.

The other antibodies in group 1B bind to an epitope at the base of GP. These antibodies, including BDBV255 and BDBV259, bind further down on GP than has been observed previously with murine mAbs, possibly contacting residues within GP2 that are part of the membrane proximal external region (MPER) (Figures 4C–4E). These antibodies were refractory to a reconstruction by EM due to predominant side views of the particles and also apparent flexibility. The class averages, however, clearly show that these antibodies bind an epitope that extends down below the base of GP. Three Fabs can be seen in some of the class averages, indicating that despite the apparent small size of this region, three antibodies can be accommodated on one GP trimer. Although the Fabs adopt various positions in each class average, there is not a continuous range of flexibility

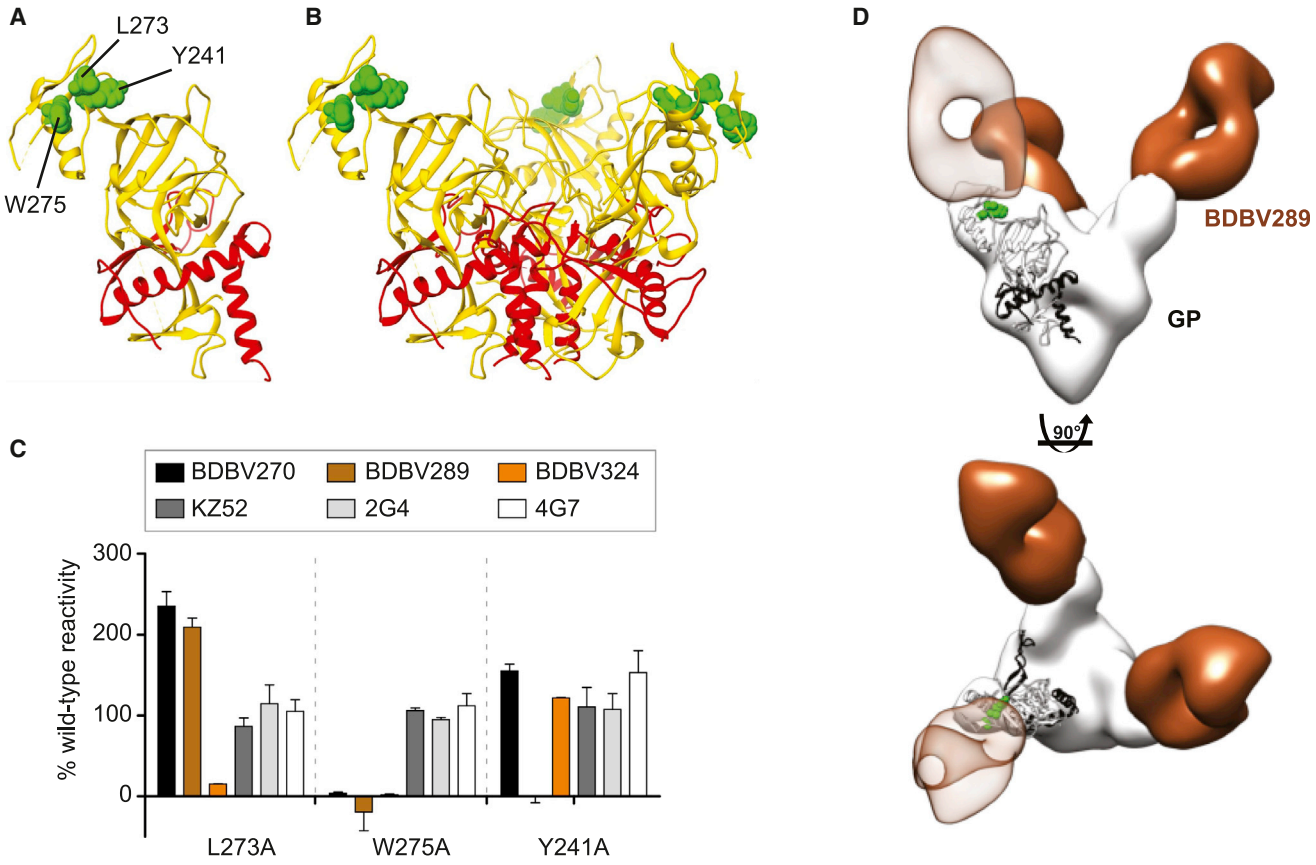

Figure 5. Epitope Mapping of Group 3A mAbs Using Saturation Mutagenesis and Negative-Stain EM

(A and B) Epitope residues for three nAbs from group 3A (BDBV270, BDBV289, and BDBV324) were identified as those for which mutation to alanine specifically reduced binding of these antibodies. GP residue W275 was common to all three nAbs, while L273 was specific for BDBV324 and Y241 was specific for BDBV289. The mutated residues are shown in space-filling forms on a ribbon diagram of the EBOV GP structure, based on PDB: 3CSY.

(C) Binding values for nAbs and previously isolated mAbs KZ52, 2G4, and 4G7 to library clones with mutations at residues L273, W275, and Y241. The Ab reactivities against each mutant EBOV GP clone were calculated relative to reactivity with wild-type EBOV GP.

(D) BDBV289 (brown) binds at the top of the viral GP near the glycan cap region. Complexes are of BDBV antibody Fab fragments bound to BDBV GPΔTM with side view (top panel) or top view (bottom panel). A representative Fab crystal structure is fit in the Fab density for each reconstruction (from PDB: 3CSY). A monomer of the GP trimer crystal structure (PDB: 3CSY) is also fit in the GP density, with white corresponding to GP1 and black to GP2. Two critical residues for binding by BDBV289 (W275 and Y241, determined using saturation mutagenesis) are highlighted in green.

See also Figure S5.

since the Fabs themselves are well resolved. These antibodies may require the full MPER and transmembrane (TM) regions, as well as a membrane, in order to bind stably. These features are all lacking in the current recombinant protein used here, a soluble form of the extracellular domain of GP. While the GP2 region is well conserved across the filoviruses, these BDBV-specific mAbs likely bind non-conserved regions in GP2 proximal to the TM region.

Epitope Mapping of Group 3A mAbs Using Saturation Mutagenesis and Negative-Stain EM

As the group 3A (cross-reactive) nAbs competed for binding with group 1A (BDBV-specific) nAbs (Figure 3), we hypothesized that some structural features of the glycan cap are conserved among GPs from multiple *Ebolavirus* species. We sought to identify critical amino acids that defined epitopes for three group 3 nAbs (BDBV270, BDBV289, and BDBV324) using a comprehensive EBOV GP alanine-scanning mutation library (Davidson et al., 2015). Epitope mapping identified critical residues for binding by each nAb as follows: W275 for BDBV270, W275 and Y241 for BDBV289, and W275 and L273 for BDBV324. Residues for which mutation reduced binding of three nAbs from group 3A were visualized on the surface of the high-resolution structure of EBOV GP (PDB: 3CSY). This finding suggests that each of these antibodies recognizes overlapping epitopes in the GP glycan cap (Figures 5A and 5B). The previously described murine nAbs 2G4 and 4G7 and the human nAb KZ52 were shown previously to bind the base region of the GP (Lee et al., 2008; Murin et al., 2014), and mutations of the W275 or L273 residue did not reduce the binding of these nAbs (Figure 5C). We passaged VSV/BDBV-GP in the presence of BDBV223 or BDBV289 in an attempt to generate escape mutant viruses, but could not detect

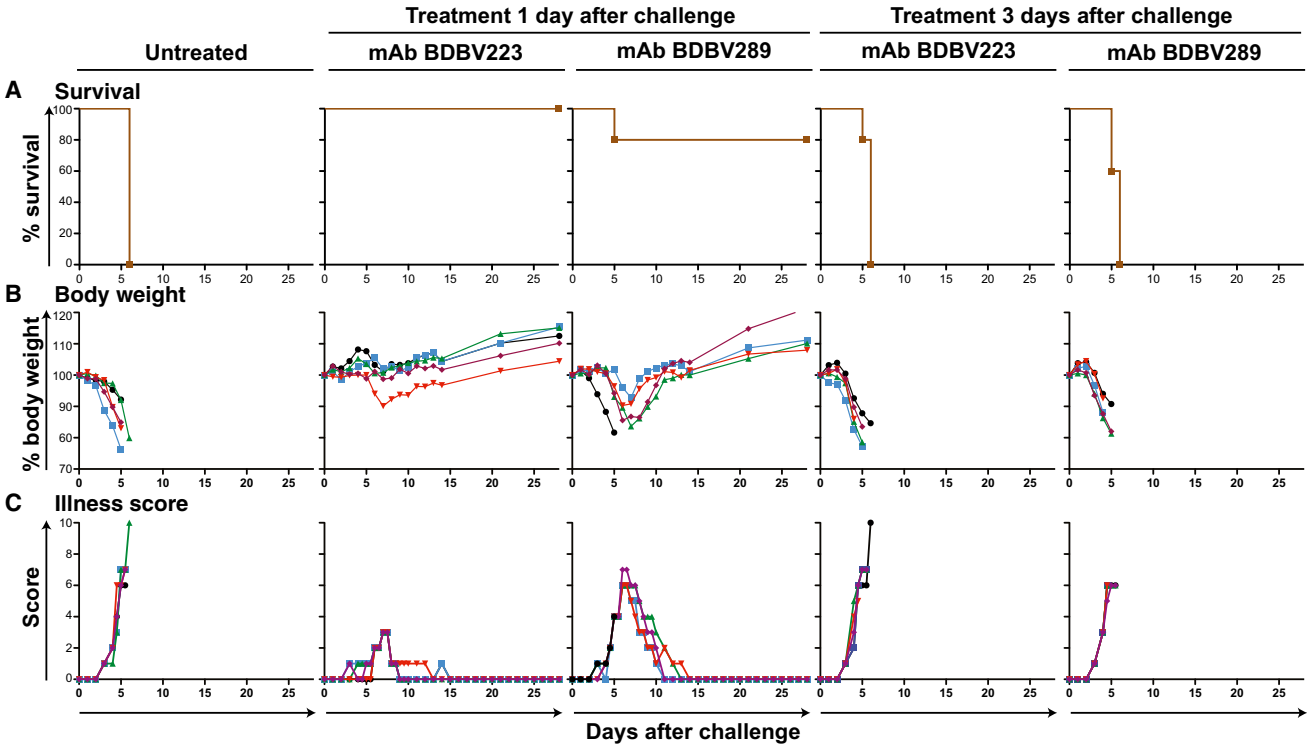

Figure 6. Survival and Clinical Signs of EBOV-Inoculated Mice Treated with BDBV mAbs

Groups of five mice in each group were injected with individual mAbs by the i.p. route 1 day after EBOV challenge, using 100 μg mAb per treatment. Animals treated with dengue virus-specific human mAb 2D22 served as controls.

(A) Kaplan-Meier survival curves are shown.

(B) Body weight is shown.

(C) Illness score is shown.

neutralization-resistant viruses. An isolate passaged in the presence of BDBV223 with a R574H polymorphism in heptad repeat 1 (HR1) region was identified, and for BDBV289 an isolate with an I584M polymorphism in the HR1 region alone or in combination with an E149K substitution in the receptor-binding domain was identified. However, none of these mutations was associated with the ability of those viruses to resist neutralization by the corresponding mAb.

We further characterized BDBV289 by single-particle EM studies of antibody in complex with GP. BDBV289 binds the glycan cap region of GP, centered on the residues W275 and Y241 (Figures 5D and S4). The angle of approach resembles that of the mAb 1H3 from the antibody cocktail ZMab, although 1H3 is specific to EBOV and is weakly neutralizing (Murin et al., 2014; Qiu et al., 2011). Further, BDBV289 also binds sGP, which shares the first 295 amino acids of GP1 with GP, including the glycan cap region (Sanchez et al., 1996; Volchkov et al., 1995). Therefore, despite previous hypotheses that propose that sGP is an immune decoy and that cleavage of the glycan cap prevents neutralizing antibodies from binding this region (Mohan et al., 2012; Murin et al., 2014), we have now identified several antibodies that challenge these ideas. Interestingly, BDBV289 targets an overlapping epitope with antibodies that we identified to be specific to BDBV and that do not bind sGP (Figure 4). Therefore, the glycan cap region is a major antigenic site that contains epitopes with subtle features that influence sGP and GP binding, neutralization, and species cross-reactivity of targeting mAbs.

Therapeutic Efficacy of Human mAbs in Small Animal Models of EBOV Infection

To determine the therapeutic activity of cross-neutralizing Abs, we tested several antibodies in mice. We focused on cross-reactive antibodies, and we studied the heterologous effect of BDBV survivor mAbs against EBOV challenge. We selected two nAbs from groups 3A (BDBV289) and 3B (BDBV223) that bound non-overlapping antigenic regions in the competition-binding experiments (Figure 3). The 7-week-old BALB/c mice received 100 μg antibody by the intraperitoneal (i.p.) route 1 or 3 days after inoculation with 1,000 plaque-forming units (PFUs) of mouse-adapted EBOV, strain Mayinga (Bray et al., 1998). BDBV223 and BDBV289 reduced disease and protected mice from death when delivered 1 day after challenge with EBOV (Figure 6). We did not observe a therapeutic effect in the mice receiving the antibodies 3 days after the challenge.

Finally, we set out to test in vivo efficacy of the cross-reactive nAbs BDBV289 and BDBV223 using a guinea pig model of EBOV infection. The 5- to 6-week-old guinea pigs, strain Hartley, were injected with 5 mg antibody by the i.p. route once (day 1) or twice

(days 1 and 3) after inoculation with 1,000 PFU of guinea pig-adapted EBOV, strain Mayinga. BDBV223 provided marginal protection, as only one of five animals survived the lethal challenge (Figure 7). Surprisingly, a glycan cap-specific nAb, BDBV289, fully protected guinea pigs when delivered twice after the virus challenge. The protective efficiency of BDBV289 with a single treatment against a heterologous EBOV (Figure 7, three of five animals survived) was higher than the protective efficiency of the equivalent glycan-cap-specific mAb c13C6, a component of the ZMapp cocktail (one of six animals survived) (Qiu et al., 2014). To determine whether a combination of two mAbs that target two neutralizing epitopes on the EBOV GP surface confer better protection than treatment with a single mAb alone, we tested the combination of BDBV223 and BDBV289 in guinea pigs. The combination of two antibodies provided complete protection against a heterologous EBOV with only a single treatment (Figure 7). We isolated viral RNA from blood of representative animals that were treated with mAbs BDBV223 or BDBV289 but died, and then sequenced the genes encoding the GP (Table S2). Several polymorphisms were detected, but none appeared to be directly related to the epitope specificity of the mAb used for treatment.

DISCUSSION

This study reveals that natural BDBV infection in humans triggers the development of ebolavirus cross-reactive antibodies that target epitopes on the GP surface that are conserved in diverse species of genus *Ebolavirus*. During these studies, we isolated 90 human mAbs from humans following BDBV infection and found 57 cross-reactive mAbs that recognized heterologous EBOV GPs. Remarkably, some of the isolated cross-reactive mAbs not only bound but also neutralized multiple *Ebolavirus* species. The majority of cross-reactive mAbs neutralized BDBV and EBOV, but we also isolated two antibodies that displayed potent neutralizing activity against representatives of three *Ebolavirus* species, BDBV, EBOV, and SUDV. We tested two cross-neutralizing mAbs in mice and guinea pigs and showed that they protected animals from lethal challenge with a heterologous species of EBOV. These data suggest that cross-neutralizing mAbs can be used to develop a universal treatment against multiple ebolaviruses, and they imply that highly immunogenic vaccines with proper presentation of GP from one species could induce some measure of cross-protection against viruses of the other species. The ability of these mAbs to bind and neutralize a broad range of *Ebolavirus* species also suggests that such antibodies might offer protection against emerging filoviruses in the future.

Our study highlights the neutralization and protective potencies of human glycan cap-specific antibodies. It has been suggested previously that glycan cap-binding mAbs may not neutralize well because cathepsins remove this region during viral entry (Murin et al., 2014). However, several of the BDBV glycan cap-specific mAbs isolated here exhibit very potent neutralizing activity, and they recognize diverse epitopes within this major antigenic site. Furthermore, a single glycan cap-specific nAb, BDBV289, provided complete protection in EBOV-challenged guinea pigs. The mechanism used by glycan cap-binding mAbs to neutralize the virus in vitro is unclear. The glycan cap-specific antibodies described here bind to sites distant from the putative cathepsin cleavage site (located at residue 190), so they are unlikely to interfere with GP cleavage. While the amino acid sequence of the GP1 region is generally less well conserved than that of GP2 in viruses of diverse filovirus species, the five neutralizing glycan cap mAbs studied with EM imaging here target conserved residues, indicating that these regions may be important to the viral life cycle. Therefore, these mAbs may block some yet undefined function of the glycan cap.

Several antibody-based treatments provided a complete species-specific protection from EBOV in a non-human primate model of infection (Qiu et al., 2014). However, antibody-based therapeutics against other members of the *Ebolavirus* genus, such and BDBV and SUDV, are not yet available. While one strategy would be to develop separate antibody treatments for each filovirus infection, an alternative strategy would be to have a universal treatment effective against diverse *Ebolavirus* species. The development of universal antibody treatments for ebolaviruses seems inevitable, given recent progress in the identification of broad and potent neutralizing antibodies against viruses that exhibit more antigenic diversity than the filoviruses such as HIV (Burton et al., 2012), influenza viruses (Pappas et al., 2014), dengue virus (Rouvinski et al., 2015), alphaviruses (Fox et al., 2015), and paramyxoviruses (Corti et al., 2013). Our results provide a roadmap to develop a single antibody-based treatment effective against multiple *Ebolavirus* infections. We propose that the principal components of such treatment should include cross-neutralizing mAbs that target conserved elements of the non-overlapping major neutralizing antigenic sites on the GP surface.

EXPERIMENTAL PROCEDURES

Donors

De-identified peripheral blood mononuclear cells (PBMCs) from seven survivors of the 2007 BDBV outbreak in Uganda (Towner et al., 2008) were obtained from a repository at Makerere University (Kampala, Uganda) managed in collaboration with the U.S. Military HIV Research Program MHRP, which is part of the Walter Reed Army Institute of Research. PBMCs were obtained after informed consent from a U.S. survivor of EBOV infection who was infected while delivering health care in Liberia during the 2014 Ebola virus outbreak with Makona virus. Cells from the EBOV survivor were obtained about 11 weeks after infection and about 7 weeks after discharge from hospital, following several negative PCR tests for presence of virus. PBMCs were obtained from a U.S. survivor of MARV infection who developed the disease in early 2008 following exposure to fruit bats in the Python Cave in Queen Elizabeth National Park, Uganda. This donor's clinical course was documented previously (Centers for Disease Control and Prevention, 2009), and we have reported previously on isolation of human antibodies from this donor (Flyak et al., 2015). Peripheral blood from the donor was obtained in 2012, 4 years after the illness, following informed consent. The studies were approved by the Vanderbilt University Institutional Review Board.

Viruses

BDBV strain 200706291 Uganda was isolated originally from the serum of a patient during the first recorded outbreak caused by this virus (Towner et al., 2008) and passaged three times in Vero E6 cells. The virus was provided originally by the Special Pathogens Branch of the U.S. Centers for Disease Control and Prevention (CDC) and deposited at the World Reference Center of Emerging Viruses and Arboviruses (WRCEVA), housed at the University of Texas Medical Branch (UTMB). The chimeric EBOV/BDBV-GP,

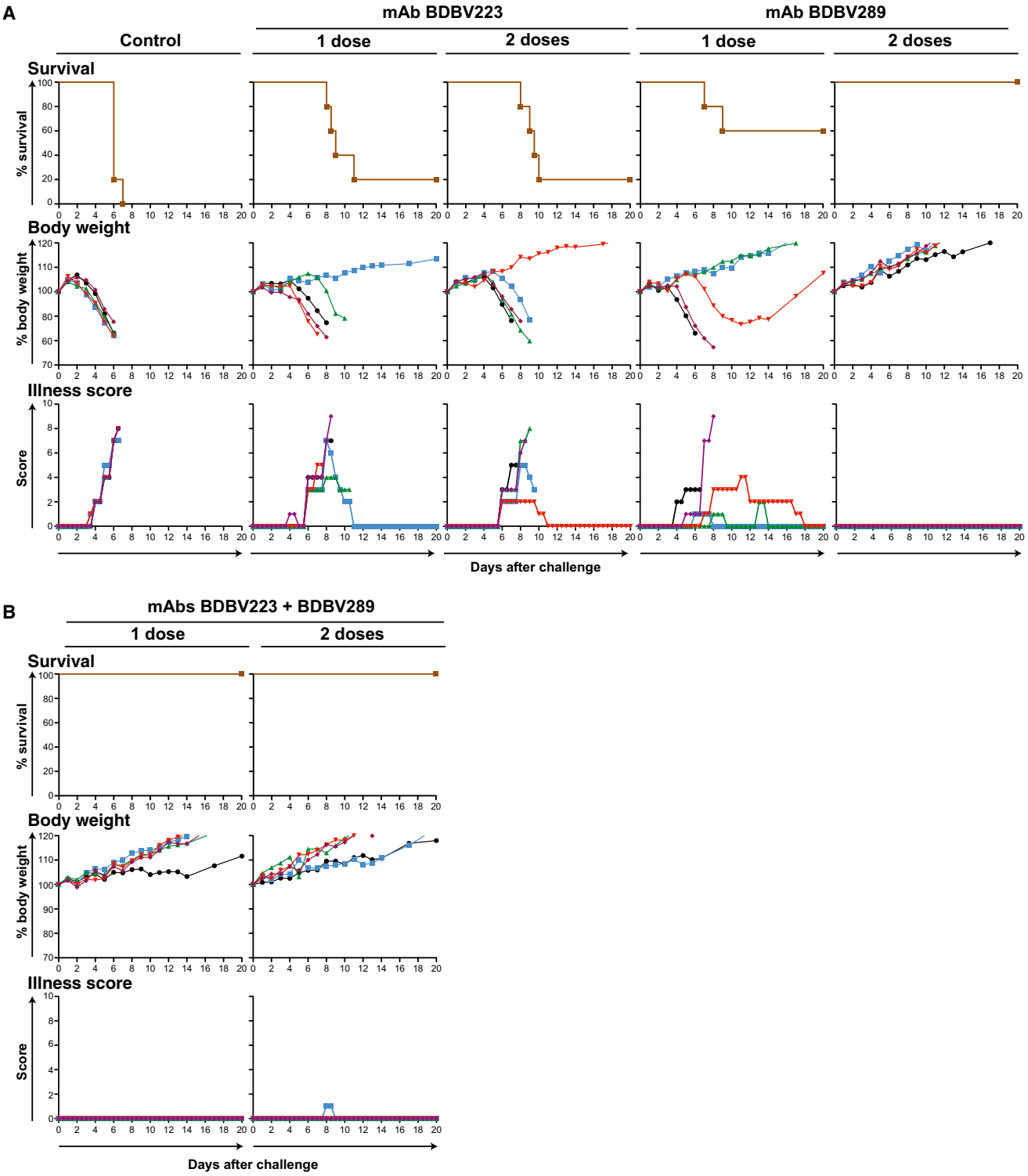

Figure 7. Survival and Clinical Signs of EBOV-Inoculated Guinea Pigs Treated with BDBV mAbs

(A and B) Groups of five guinea pigs per group were injected with individual mAbs by the i.p. route 1 day or 1 and 3 days after EBOV challenge, using 5 mg of individual mAb (A) or 5 mg of the combination of two mAbs per treatment (B), as indicated. Animals treated with dengue virus-specific human mAb 2D22 served as controls. The survival curves are based on morning and evening observations. Mortality in the morning is shown in whole day numbers, in the evening in half-day values. The body weight and illness scores are shown with one value per day. See also Table S2.

EBOV/MARV-GP, and EBOV/SUDV-GP constructs expressing EGFP were obtained by replacing the gene encoding EBOV GP with that of BDBV, MARV, or SUDV, respectively (P.A. Ilinykh, unpublished data) and passaged two times in Vero E6 cells. Additional details are reported in the Supplemental Experimental Procedures.

Generation of Human Hybridomas Secreting mAbs

Human hybridomas were generated as described previously (Flyak et al., 2015). In brief, previously cryopreserved samples were transformed with Epstein-Barr virus, CpG, and additional supplements. After 7 days, cells from each well of the 384-well culture plates were expanded into four 96-well culture plates using cell culture medium containing irradiated heterologous human PBMCs (recovered from blood unit leukofiltration filters, Nashville Red Cross) and incubated for an additional 4 days. Plates were screened for BDBV GP antigen-specific antibody-secreting cell lines using ELISAs. Cells from wells with supernates reacting with antigen in an ELISA were fused with HMMA2.5 myeloma cells using an established electrofusion technique (Yu et al., 2008).

Human mAb and Fab Production and Purification

After fusion, hybridoma cell lines were cloned by single-cell fluorescence-activated cell sorting and expanded in post-fusion medium as previously described (Flyak et al., 2015). HiTrap Protein G or HiTrap MabSelectSure columns were used to purify antibodies from filtered supernates. Fab fragments were generated by papain digestion, as described previously (Flyak et al., 2015).

Expression and Purification of Filovirus GPs

BDBV GP ectodomain (BDBV GP, residues 1–637) or the sGP dimer (BDBV sGP, residues 1–316) was used to screen supernatants of transformed B cells. Recombinant GPs were engineered with a C-terminal double strep tag and cloned into a modified pMTpuro vector for expression in *Drosophila* S2 cells. Briefly, plasmids were transfected into S2 cells using Effectene reagent (QIAGEN) followed by stable cell selection with 6 μg/ml puromycin. S2 cells first were cultured in Schneider's medium supplemented with 10% (v/v) fetal calf serum (FCS, Lonza), and later they were adapted to Insect Xpress medium for large-scale expression in 2-l shaker flasks. Stable cells were induced with 0.5 mM $CuSO_4$ and harvested after 4 to 5 days at 27°C. Tangential flow filtration then was used to buffer exchange the supernatants into 100 mM Tris-HCl, 150 mM NaCl, 1 mM EDTA, and 15 μg/ml avidin (pH 8.0), and target proteins were purified using Streptactin Superflow affinity (QIAGEN). GP ectodomains were purified further with S200 size exclusion chromatography (SEC); sGP was purified with S75 SEC. Recombinant ectodomains for EBOV, SUDV, or MARV were designed and expressed similarly.

Screening and EC_{50} ELISA-Binding Analysis

Soluble forms of the full-length extracellular domain of BDBV, EBOV, SUDV, or MARV GPs or the sGP form of BDBV GP were coated overnight onto 384-well plates at 1 μg/ml. For screening ELISA, 10 μl supernate from a well of a tissue-culture plate was transferred to each well of a 384-well ELISA plate. For EC_{50}-binding analysis by ELISA, purified antibodies were applied to the plates at a concentration range of 30 μg/ml to 170 ng/ml, using 3-fold serial dilutions. The presence of antibodies bound to the GP was determined using goat anti-human IgG alkaline phosphatase conjugate and p-nitrophenol phosphate substrate tablets, with optical density read at 405 nm after 120 min. A non-linear regression analysis was performed on the resulting curves using Prism version 5 (GraphPad) to calculate EC_{50} values. The Circos software package was used for data visualization (Krzywinski et al., 2009).

EBOV and MARV Neutralization Experiments

Isolated mAbs were screened initially in a high-throughput neutralization assay using EBOV/BDBV-GP with or without 5% guinea pig complement (MP Biomedicals) (P.A. Ilinykh, unpublished data). The mAbs that exhibited neutralizing activity also were screened for neutralization of EGFP-expressing EBOV (Towner et al., 2005). Several mAbs were tested for neutralization of EBOV/SUDV-GP and EBOV/MARV-GP by the same approach. Additional information is given in the Supplemental Experimental Procedures.

Biolayer Interferometry Competition-Binding Assay

Competition binding studies using biolayer interferometry and biotinylated BDBV GP (EZ-link Micro NHS-PEG_4-Biotinylation Kit, Thermo Scientific 21955) (5 μg/ml) were performed on an Octet RED biosensor (ForteBio), as described previously (Flyak et al., 2015). In brief, the antigen was immobilized onto streptavidin-coated biosensor tips. After a brief washing step, biosensor tips were immersed first into the wells containing first antibody at a concentration of 100 μg/ml and then into the wells containing a second mAb at a concentration of 100 μg/ml. The percentage binding of the second mAb in the presence of the first mAb was determined by comparing the maximal signal of the second mAb applied after the first mAb complex to the maximal signal of the second mAb alone.

Sequence Analysis of Antibody Variable Region Genes

Antibody variable gene sequence analysis was performed as previously described (Flyak et al., 2015). Heavy-chain antibody variable region sequences were analyzed using the IMGT/V-Quest program (Brochet et al., 2008; Giudicelli et al., 2011).

EM and Sample Preparation

Fabs were added in 10 M excess to BDBV GPdMuc and subsequently purified and stained as previously described (Murin et al., 2014).

Image Processing of Protein Complexes

Particles were automatically picked using DoG Picker (Voss et al., 2009) and particle stacks were generated using Appion (Lander et al., 2009). Subsequently, reference-free two-dimensional (2D) class averages were generated using iterative multi-reference alignment (MRA)/multivariate statistical analysis (MSA) (van Heel et al., 1996). Non-GP complexes and those with a clear lack of full saturation by Fab were removed to generate a final stack for reconstructions. In some cases, orientation bias or flexibility of Fabs prevented convergence of an acceptable model, although examination of class averages allowed a general assignment of the epitope. Final stack class averages were used to generate initial models using EMAN2 common lines (Tang et al., 2007). A model matching its reference projections was further refined using the entire raw particle stack with EMAN2, as described previously (Murin et al., 2014). For the BDBV41 reconstruction, the EMAN2 reconstruction lacked important features that were present in the class averages, indicating that perhaps some particles lacked full Fab saturation. To circumvent this problem, we utilized the Relion package, which allows three-dimensional (3D) classification to remove particles that may only contain two Fabs, significantly improving the quality of the final EM map (Scheres, 2012). Modeling fitting and EM figures were generated using UCSF Chimera (Pettersen et al., 2004).

Epitope Mapping Using an EBOV GP Alanine-Scan Mutation Library

Comprehensive high-throughput alanine scanning (shotgun mutagenesis) was carried out on an expression construct for EBOV GP (Yambuku-Mayinga variant GP; UniProt: Q05320) (Davidson et al., 2015). Additional details are reported in the Supplemental Experimental Procedures.

In Vivo Testing

The animal protocols for testing of mAbs in mice and guinea pigs were approved by the Institutional Animal Care and Use Committee of the UTMB. The 7-week-old BALB/c mice (Charles River Laboratories) were placed in the ABSL-4 facility of the Galveston National Laboratory. Groups of mice at five animals per group were injected with 1,000 PFU of the mouse-adapted EBOV by the i.p. route. Then 24 or 72 hr later, animals were injected with individual mAbs by the i.p. route using 100 μg per treatment. Animals treated with the antibody specific to dengue virus 2D22 served as controls. Animals were weighed and monitored daily over the 2-week period after challenge. Once animals were symptomatic, they were examined no less than twice per day. The disease was scored using the following parameters: dyspnea (possible scores 0–5), recumbency (0–9), unresponsiveness (0–5), and bleeding/hemorrhage (0–5). To test the protective efficacy of mAbs in guinea pigs, five- to six-week-old animals (strain Hartley) were placed in the ABSL-4 facility of the Galveston National Laboratory. Groups of five animals per group were injected

with 1,000 PFU of guinea pig-adapted EBOV by the i.p. route. Then 24 or 24 and 72 hr later, animals were injected with individual mAbs (5 mg per treatment) or a cocktail of two mAbs (2.5 mg of each mAb per treatment). Animals were weighed and monitored daily for 28 days. After animals became symptomatic, they were examined no less than twice per day. The disease was scored using the following parameters: appearance (possible scores 0–3), body condition (0–3), natural behavior (0–3), and provoked behavior (0–3).

ACCESSION NUMBERS

The accession numbers for the EM reconstructions reported in this paper are Electron Microscopy Data Bank: EMD-6527 through EMD-6532.

SUPPLEMENTAL INFORMATION

Supplemental Information includes Supplemental Experimental Procedures, five figures, two tables, and a data file and can be found with this article online at http://dx.doi.org/10.1016/j.cell.2015.12.022.

AUTHOR CONTRIBUTIONS

A.I.F., A.B., and J.E.C. conceived the study. A.I.F., X.S., C.D.M., M.L.F., H.L.T., J.A.D., R.L., N. Kose, N. Kuzmina, P.A.I., H.K., L.B., G.S., C.K., C.B., and T.G.K. performed experiments. A.I.F., X.S., P.A.I., N. Kose, N. Kuzmina, A.B., E.D., B.J.D., J.C.S., E.O.S., A.B.W., A.B., and J.E.C. analyzed data. A.I.F., P.A.I., A.B., and J.E.C. wrote the paper.

ACKNOWLEDGMENTS

This project received support from the Defense Threat Reduction Agency (grant HDTRA1-13-1-0034 to J.E.C. and A.B.), U.S. NIH grant U19 AI109711 (to J.E.C. and A.B.), U19 AI109762 (to E.O.S. and A.B.W.), NIH contract HHSN272201400058C (to B.J.D.), and R01 AI067927 (to E.O.S.). E.O.S. is an Investigator in the Pathogenesis of Infectious Disease of the Burroughs Wellcome Fund. The project was supported by NCRR Grant UL1 RR024975-01 and is now at the National Center for Advancing Translational Sciences, Grant 2 UL1 TR000445-06. The content is solely the responsibility of the authors and does not necessarily represent the official views of the NIH. We thank the donors and Cheryl Stewart and Jill Janssen in the Vanderbilt Clinical Trials Center for help in sample acquisition in the United States. We thank Monica Millard and Hannah Kibuuka of the Makerere University Walter Reed Project (MUWRP) in Kampala, Uganda, who provided repository samples from the Long-term Bundibugyo Ebola virus survivors study done in collaboration with U.S. Army Medical Research Institute of Infectious Diseases. We thank Frances Smith-House at Vanderbilt and Kathleen Pommert at Scripps for excellent technical support. L.B. was a summer undergraduate research fellow at the Vanderbilt Vaccine Center, and J.A.D. was a summer undergraduate research fellow at The Scripps Research Institute. We thank Andrew McNeal and Rachel Fong for assistance with epitope mapping. We also thank Dr. Alexander Freiberg (UTMB) for providing the guinea-pig-adapted EBOV strain. Flow cytometry experiments were performed in the VMC Flow Cytometry Shared Resource, supported by NIH grants P30 CA68485 and DK058404. The EM work was conducted at The Scripps Research Institute electron microscopy facility. C.D.M. is supported by a National Science Foundation Graduate Research Fellowship.

Received: August 8, 2015
Revised: October 17, 2015
Accepted: December 3, 2015
Published: January 21, 2016

REFERENCES

Bale, S., Dias, J.M., Fusco, M.L., Hashiguchi, T., Wong, A.C., Liu, T., Keuhne, A.I., Li, S., Woods, V.L., Jr., Chandran, K., et al. (2012). Structural basis for differential neutralization of ebolaviruses. Viruses *4*, 447–470.

Bray, M., Davis, K., Geisbert, T., Schmaljohn, C., and Huggins, J. (1998). A mouse model for evaluation of prophylaxis and therapy of Ebola hemorrhagic fever. J. Infect. Dis. *178*, 651–661.

Brochet, X., Lefranc, M.P., and Giudicelli, V. (2008). IMGT/V-QUEST: the highly customized and integrated system for IG and TR standardized V-J and V-D-J sequence analysis. Nucleic Acids Res. *36*, W503–508.

Burton, D.R., Poignard, P., Stanfield, R.L., and Wilson, I.A. (2012). Broadly neutralizing antibodies present new prospects to counter highly antigenically diverse viruses. Science *337*, 183–186.

Carette, J.E., Raaben, M., Wong, A.C., Herbert, A.S., Obernosterer, G., Mulherkar, N., Kuehne, A.I., Kranzusch, P.J., Griffin, A.M., Ruthel, G., et al. (2011). Ebola virus entry requires the cholesterol transporter Niemann-Pick C1. Nature *477*, 340–343.

Centers for Disease Control and Prevention (CDC) (2009). Imported case of Marburg hemorrhagic fever - Colorado, 2008. MMWR Morb. Mortal. Wkly. Rep. *58*, 1377–1381.

Chandran, K., Sullivan, N.J., Felbor, U., Whelan, S.P., and Cunningham, J.M. (2005). Endosomal proteolysis of the Ebola virus glycoprotein is necessary for infection. Science *308*, 1643–1645.

Corti, D., Bianchi, S., Vanzetta, F., Minola, A., Perez, L., Agatic, G., Guarino, B., Silacci, C., Marcandalli, J., Marsland, B.J., et al. (2013). Cross-neutralization of four paramyxoviruses by a human monoclonal antibody. Nature *501*, 439–443.

Côté, M., Misasi, J., Ren, T., Bruchez, A., Lee, K., Filone, C.M., Hensley, L., Li, Q., Ory, D., Chandran, K., and Cunningham, J. (2011). Small molecule inhibitors reveal Niemann-Pick C1 is essential for Ebola virus infection. Nature *477*, 344–348.

Davidson, E., Bryan, C., Fong, R.H., Barnes, T., Pfaff, J.M., Mabila, M., Rucker, J.B., and Doranz, B.J. (2015). Mechanism of binding to Ebola virus glycoprotein by the ZMapp, ZMAb, and MB-003 cocktail antibodies. J. Virol *89*, 10982–10992.

Feldmann, H., Jones, S.M., Daddario-DiCaprio, K.M., Geisbert, J.B., Ströher, U., Grolla, A., Bray, M., Fritz, E.A., Fernando, L., Feldmann, F., et al. (2007). Effective post-exposure treatment of Ebola infection. PLoS Pathog. *3*, e2.

Flyak, A.I., Ilinykh, P.A., Murin, C.D., Garron, T., Shen, X., Fusco, M.L., Hashiguchi, T., Bornholdt, Z.A., Slaughter, J.C., Sapparapu, G., et al. (2015). Mechanism of human antibody-mediated neutralization of Marburg virus. Cell *160*, 893–903.

Fox, J.M., Long, F., Edeling, M.A., Lin, H., van Duijl-Richter, M.K., Fong, R.H., Kahle, K.M., Smit, J.M., Jin, J., Simmons, G., et al. (2015). Broadly Neutralizing Alphavirus Antibodies Bind an Epitope on E2 and Inhibit Entry and Egress. Cell *163*, 1095–1107.

Fusco, M.L., Hashiguchi, T., Cassan, R., Biggins, J.E., Murin, C.D., Warfield, K.L., Li, S., Holtsberg, F.W., Shulenin, S., Vu, H., et al. (2015). Protective mAbs and Cross-Reactive mAbs Raised by Immunization with Engineered Marburg Virus GPs. PLoS Pathog. *11*, e1005016.

Geisbert, T.W., Daddario-DiCaprio, K.M., Williams, K.J., Geisbert, J.B., Leung, A., Feldmann, F., Hensley, L.E., Feldmann, H., and Jones, S.M. (2008). Recombinant vesicular stomatitis virus vector mediates postexposure protection against Sudan Ebola hemorrhagic fever in nonhuman primates. J. Virol. *82*, 5664–5668.

Geisbert, T.W., Bausch, D.G., and Feldmann, H. (2010). Prospects for immunisation against Marburg and Ebola viruses. Rev. Med. Virol. *20*, 344–357.

Giudicelli, V., Brochet, X., and Lefranc, M.P. (2011). IMGT/V-QUEST: IMGT standardized analysis of the immunoglobulin (IG) and T cell receptor (TR) nucleotide sequences. Cold Spring Harb. Protoc. *2011*, 695–715.

Hashiguchi, T., Fusco, M.L., Bornholdt, Z.A., Lee, J.E., Flyak, A.I., Matsuoka, R., Kohda, D., Yanagi, Y., Hammel, M., Crowe, J.E., Jr., and Saphire, E.O. (2015). Structural basis for Marburg virus neutralization by a cross-reactive human antibody. Cell *160*, 904–912.

Hernandez, H., Marceau, C., Halliday, H., Callison, J., Borisevich, V., Escaffre, O., Creech, J., Feldmann, H., and Rockx, B. (2015). Development and Characterization of Broadly Cross-reactive Monoclonal Antibodies Against All Known Ebolavirus Species. J. Infect. Dis. *212* (*Suppl 2*), S410–S413.

Krzywinski, M., Schein, J., Birol, I., Connors, J., Gascoyne, R., Horsman, D., Jones, S.J., and Marra, M.A. (2009). Circos: an information aesthetic for comparative genomics. Genome Res. *19*, 1639–1645.

Lander, G.C., Stagg, S.M., Voss, N.R., Cheng, A., Fellmann, D., Pulokas, J., Yoshioka, C., Irving, C., Mulder, A., Lau, P.W., et al. (2009). Appion: an integrated, database-driven pipeline to facilitate EM image processing. J. Struct. Biol. *166*, 95–102.

Lee, J.E., Fusco, M.L., Hessell, A.J., Oswald, W.B., Burton, D.R., and Saphire, E.O. (2008). Structure of the Ebola virus glycoprotein bound to an antibody from a human survivor. Nature *454*, 177–182.

Macneil, A., Reed, Z., and Rollin, P.E. (2011). Serologic cross-reactivity of human IgM and IgG antibodies to five species of Ebola virus. PLoS Negl. Trop. Dis. *5*, e1175.

Meyer, M., Garron, T., Lubaki, N.M., Mire, C.E., Fenton, K.A., Klages, C., Olinger, G.G., Geisbert, T.W., Collins, P.L., and Bukreyev, A. (2015). Aerosolized Ebola vaccine protects primates and elicits lung-resident T cell responses. J. Clin. Invest. *125*, 3241–3255.

Misasi, J., Chandran, K., Yang, J.Y., Considine, B., Filone, C.M., Côté, M., Sullivan, N., Fabozzi, G., Hensley, L., and Cunningham, J. (2012). Filoviruses require endosomal cysteine proteases for entry but exhibit distinct protease preferences. J. Virol. *86*, 3284–3292.

Mohan, G.S., Li, W., Ye, L., Compans, R.W., and Yang, C. (2012). Antigenic subversion: a novel mechanism of host immune evasion by Ebola virus. PLoS Pathog. *8*, e1003065.

Murin, C.D., Fusco, M.L., Bornholdt, Z.A., Qiu, X., Olinger, G.G., Zeitlin, L., Kobinger, G.P., Ward, A.B., and Saphire, E.O. (2014). Structures of protective antibodies reveal sites of vulnerability on Ebola virus. Proc. Natl. Acad. Sci. USA *111*, 17182–17187.

Olinger, G.G., Jr., Pettitt, J., Kim, D., Working, C., Bohorov, O., Bratcher, B., Hiatt, E., Hume, S.D., Johnson, A.K., Morton, J., et al. (2012). Delayed treatment of Ebola virus infection with plant-derived monoclonal antibodies provides protection in rhesus macaques. Proc. Natl. Acad. Sci. USA *109*, 18030–18035.

Ou, W., Delisle, J., Jacques, J., Shih, J., Price, G., Kuhn, J.H., Wang, V., Verthelyi, D., Kaplan, G., and Wilson, C.A. (2012). Induction of ebolavirus cross-species immunity using retrovirus-like particles bearing the Ebola virus glycoprotein lacking the mucin-like domain. Virol. J. *9*, 32.

Pappas, L., Foglierini, M., Piccoli, L., Kallewaard, N.L., Turrini, F., Silacci, C., Fernandez-Rodriguez, B., Agatic, G., Giacchetto-Sasselli, I., Pellicciotta, G., et al. (2014). Rapid development of broadly influenza neutralizing antibodies through redundant mutations. Nature *516*, 418–422.

Pettersen, E.F., Goddard, T.D., Huang, C.C., Couch, G.S., Greenblatt, D.M., Meng, E.C., and Ferrin, T.E. (2004). UCSF Chimera–a visualization system for exploratory research and analysis. J. Comput. Chem. *25*, 1605–1612.

Qiu, X., Alimonti, J.B., Melito, P.L., Fernando, L., Ströher, U., and Jones, S.M. (2011). Characterization of Zaire ebolavirus glycoprotein-specific monoclonal antibodies. Clin. Immunol. *141*, 218–227.

Qiu, X., Audet, J., Wong, G., Pillet, S., Bello, A., Cabral, T., Strong, J.E., Plummer, F., Corbett, C.R., Alimonti, J.B., and Kobinger, G.P. (2012). Successful treatment of ebola virus-infected cynomolgus macaques with monoclonal antibodies. Sci. Transl. Med. *4*, 138ra81.

Qiu, X., Wong, G., Audet, J., Bello, A., Fernando, L., Alimonti, J.B., Fausther-Bovendo, H., Wei, H., Aviles, J., Hiatt, E., et al. (2014). Reversion of advanced Ebola virus disease in nonhuman primates with ZMapp. Nature *514*, 47–53.

Rouvinski, A., Guardado-Calvo, P., Barba-Spaeth, G., Duquerroy, S., Vaney, M.C., Kikuti, C.M., Navarro Sanchez, M.E., Dejnirattisai, W., Wongwiwat, W., Haouz, A., et al. (2015). Recognition determinants of broadly neutralizing human antibodies against dengue viruses. Nature *520*, 109–113.

Sanchez, A., Trappier, S.G., Mahy, B.W., Peters, C.J., and Nichol, S.T. (1996). The virion glycoproteins of Ebola viruses are encoded in two reading frames and are expressed through transcriptional editing. Proc. Natl. Acad. Sci. USA *93*, 3602–3607.

Scheres, S.H. (2012). RELION: implementation of a Bayesian approach to cryo-EM structure determination. J. Struct. Biol. *180*, 519–530.

Tang, G., Peng, L., Baldwin, P.R., Mann, D.S., Jiang, W., Rees, I., and Ludtke, S.J. (2007). EMAN2: an extensible image processing suite for electron microscopy. J. Struct. Biol. *157*, 38–46.

Thi, E.P., Mire, C.E., Lee, A.C., Geisbert, J.B., Zhou, J.Z., Agans, K.N., Snead, N.M., Deer, D.J., Barnard, T.R., Fenton, K.A., et al. (2015). Lipid nanoparticle siRNA treatment of Ebola-virus-Makona-infected nonhuman primates. Nature *521*, 362–365.

Towner, J.S., Paragas, J., Dover, J.E., Gupta, M., Goldsmith, C.S., Huggins, J.W., and Nichol, S.T. (2005). Generation of eGFP expressing recombinant Zaire ebolavirus for analysis of early pathogenesis events and high-throughput antiviral drug screening. Virology *332*, 20–27.

Towner, J.S., Sealy, T.K., Khristova, M.L., Albariño, C.G., Conlan, S., Reeder, S.A., Quan, P.L., Lipkin, W.I., Downing, R., Tappero, J.W., et al. (2008). Newly discovered ebola virus associated with hemorrhagic fever outbreak in Uganda. PLoS Pathog. *4*, e1000212.

van Heel, M., Harauz, G., Orlova, E.V., Schmidt, R., and Schatz, M. (1996). A new generation of the IMAGIC image processing system. J. Struct. Biol. *116*, 17–24.

Volchkov, V.E., Becker, S., Volchkova, V.A., Ternovoj, V.A., Kotov, A.N., Netesov, S.V., and Klenk, H.D. (1995). GP mRNA of Ebola virus is edited by the Ebola virus polymerase and by T7 and vaccinia virus polymerases. Virology *214*, 421–430.

Voss, N.R., Yoshioka, C.K., Radermacher, M., Potter, C.S., and Carragher, B. (2009). DoG Picker and TiltPicker: software tools to facilitate particle selection in single particle electron microscopy. J. Struct. Biol. *166*, 205–213.

Warren, T.K., Warfield, K.L., Wells, J., Swenson, D.L., Donner, K.S., Van Tongeren, S.A., Garza, N.L., Dong, L., Mourich, D.V., Crumley, S., et al. (2010). Advanced antisense therapies for postexposure protection against lethal filovirus infections. Nat. Med. *16*, 991–994.

Warren, T.K., Wells, J., Panchal, R.G., Stuthman, K.S., Garza, N.L., Van Tongeren, S.A., Dong, L., Retterer, C.J., Eaton, B.P., Pegoraro, G., et al. (2014). Protection against filovirus diseases by a novel broad-spectrum nucleoside analogue BCX4430. Nature *508*, 402–405.

Warren, T.K., Whitehouse, C.A., Wells, J., Welch, L., Heald, A.E., Charleston, J.S., Sazani, P., Reid, S.P., Iversen, P.L., and Bavari, S. (2015). A single phosphorodiamidate morpholino oligomer targeting VP24 protects rhesus monkeys against lethal Ebola virus infection. MBio *6*, e02344-14.

Wilson, J.A., Hevey, M., Bakken, R., Guest, S., Bray, M., Schmaljohn, A.L., and Hart, M.K. (2000). Epitopes involved in antibody-mediated protection from Ebola virus. Science *287*, 1664–1666.

Yu, X., McGraw, P.A., House, F.S., and Crowe, J.E., Jr. (2008). An optimized electrofusion-based protocol for generating virus-specific human monoclonal antibodies. J. Immunol. Methods *336*, 142–151.

AMERICAN SOCIETY FOR MICROBIOLOGY | mBio®

RESEARCH ARTICLE

Host-Primed Ebola Virus GP Exposes a Hydrophobic NPC1 Receptor-Binding Pocket, Revealing a Target for Broadly Neutralizing Antibodies

Zachary A. Bornholdt,[a] Esther Ndungo,[b] Marnie L. Fusco,[a] Shridhar Bale,[a] Andrew I. Flyak,[c] James E. Crowe, Jr.,[c,d,e] Kartik Chandran,[b] Erica Ollmann Saphire[a,f]

Department of Immunology and Microbial Science, The Scripps Research Institute, La Jolla, California, USA[a]; Department of Microbiology and Immunology, Albert Einstein College of Medicine, Bronx, New York, USA[b]; Department of Pathology, Microbiology and Immunology,[c] Department of Pediatrics,[d] and Vanderbilt Vaccine Center,[e] Vanderbilt University, Nashville, Tennessee, USA; The Skaggs Institute for Chemical Biology, The Scripps Research Institute, La Jolla, California, USA[f]

Z.A.B. and E.N. contributed equally to this article.

This is manuscript number 29196 from The Scripps Research Institute.

ABSTRACT **The filovirus surface glycoprotein (GP) mediates viral entry into host cells. Following viral internalization into endosomes, GP is cleaved by host cysteine proteases to expose a receptor-binding site (RBS) that is otherwise hidden from immune surveillance. Here, we present the crystal structure of proteolytically cleaved Ebola virus GP to a resolution of 3.3 Å. We use this structure in conjunction with functional analysis of a large panel of pseudotyped viruses bearing mutant GP proteins to map the Ebola virus GP endosomal RBS at molecular resolution. Our studies indicate that binding of GP to its endosomal receptor Niemann-Pick C1 occurs in two distinct stages: the initial electrostatic interactions are followed by specific interactions with a hydrophobic trough that is exposed on the endosomally cleaved GP_1 subunit. Finally, we demonstrate that monoclonal antibodies targeting the filovirus RBS neutralize all known filovirus GPs, making this conserved pocket a promising target for the development of panfilovirus therapeutics.**

IMPORTANCE **Ebola virus uses its glycoprotein (GP) to enter new host cells. During entry, GP must be cleaved by human enzymes in order for receptor binding to occur. Here, we provide the crystal structure of the cleaved form of Ebola virus GP. We demonstrate that cleavage exposes a site at the top of GP and that this site binds the critical domain C of the receptor, termed Niemann-Pick C1 (NPC1). We perform mutagenesis to find parts of the site essential for binding NPC1 and map distinct roles for an upper, charged crest and lower, hydrophobic trough in cleaved GP. We find that this 3-dimensional site is conserved across the filovirus family and that antibody directed against this site is able to bind cleaved GP from every filovirus tested and neutralize viruses bearing those GPs.**

Received 31 December 2015 **Accepted** 8 January 2016 **Published** 23 February 2016

Citation Bornholdt ZA, Ndungo E, Fusco ML, Bale S, Flyak AI, Crowe JE, Jr, Chandran K, Saphire EO. 2016. Host-primed Ebola virus GP exposes a hydrophobic NPC1 receptor-binding pocket, revealing a target for broadly neutralizing antibodies. mBio 7(1):e02154-15. doi:10.1128/mBio.02154-15.

Editor Peter Palese, Icahn School of Medicine at Mount Sinai

Address correspondence to Kartik Chandran, kartik.chandran@einstein.yu.edu, and Erica Ollmann Saphire, erica@scripps.edu.

This article is a direct contribution from a Fellow of the American Academy of Microbiology. External solicited reviewers: Thomas Geisbert, University of Texas Medical Branch; Benhur Lee, Icahn School of Medicine at Mount Sinai.

Ebola virus (EBOV) and Marburg virus (MARV) are both members of the *Filoviridae* family of enveloped negative-strand RNA viruses and are the causative agents of a highly lethal disease for which no approved vaccines or treatments are currently available (1, 2). Due to their virulence and biothreat potential, filoviruses are classified as category A pathogens. The ongoing EBOV epidemic in West Africa is the longest and most widespread filovirus outbreak on record (3).

Like all filoviruses, EBOV displays a single virus-encoded protein, the viral glycoprotein (GP), on the surface of the virion. EBOV GP is a 676-residue class I membrane fusion glycoprotein. However, EBOV GP differs from canonical class I fusion proteins, such as those of human immunodeficiency virus and influenza A virus, in that the architecture of its fusion loop more closely resembles those of class II and III glycoproteins (4, 5). EBOV GP is synthesized as a precursor polypeptide, GP_0, which assembles into trimers in the endoplasmic reticulum. Each GP_0 subunit is then posttranslationally cleaved by the Golgi endoprotease furin to yield disulfide-linked GP_1 (≈55 kDa) and GP_2 (≈20 kDa) subunits. The final GP assembly, which is an ≈450 kDa trimer of $GP_{1,2}$ heterodimers, is then displayed on the surface of mature EBOV virions (4, 5). GP_1 contains the receptor-binding site and regulates the triggering of the membrane fusion machinery in the GP_2 subunit (6).

The GP_1 structure can be divided into three subdomains: the mucin domain, glycan cap, and GP_1 core. The outer mucin domain (GP_1 residues 313 to 464), is predicted to be loosely structured and heavily glycosylated, incorporating five N-linked gly-

cans and 12 to 17 predicted O-linked glycans (5). Interior to the mucin-like domain is the glycan cap (GP_1 residues 227 to 313), which sits atop the GP_1 core. The glycan cap is more ordered than the mucin-like domain and contains four N-linked glycosylation sites. Neither the mucin nor the glycan cap domain is essential for viral entry. Indeed, removal of these domains enhances infection by viruses pseudotyped with EBOV GP (7–9). Therefore, it is currently hypothesized that a primary function of the mucin domain and glycan cap is to shield the GP_1 core from immune surveillance (4, 5, 10, 11).

EBOV virions are internalized into cells via a macropinocytosis-like mechanism and undergo trafficking to late endosomes (12–15). There, host endosomal cysteine proteases, including cathepsins L (CatL) and B (CatB), cleave GP_1 to remove the mucin and glycan cap domains. Cleavage generates a fusion-competent GP trimer (GP_{CL}) comprising the 19-kDa GP_1 core domain and GP_2 (8, 9, 16). Cleavage of $GP_{1,2}$ to GP_{CL} is a prerequisite for viral recognition of the host endosomal receptor Niemann-Pick C1 (NPC1) (10, 17–20), strongly suggesting that the receptor-binding site in the GP_1 core structure is unmasked by the cleavage of GP_1 in late endosomes. Thus, GP_{CL} represents the structure of EBOV GP in a conformation that is competent for receptor binding.

In order to observe possible structural changes in GP_{CL} and to illustrate definitively which surfaces and residues are unveiled upon endosomal proteolysis, we determined the crystal structure of the EBOV GP_{CL} trimer at a resolution of 3.3 Å, in complex with the neutralizing human antibody Fab KZ52 (21). We found that the main feature exposed upon priming of EBOV GP is a wave-like morphology at the top of GP_{CL}, with a polar/basic crest rising above a large, recessed, hydrophobic trough, previously occupied by the glycan cap prior to priming by host cathepsins. Extensive structure-directed mutagenesis of EBOV GP_{CL} revealed that the basic character of the polar crest is crucial to the EBOV-receptor interaction, likely because it confers an initial electrostatic attraction between GP_{CL} and the second luminal domain of NPC1, domain C. We also find that the trough makes specific hydrophobic contacts that are essential to high-affinity GP_{CL}-NPC1 domain C binding. Finally, we demonstrate that host-programmed unmasking of the NPC1-binding site in EBOV GP creates a broadly conserved target for neutralization by monoclonal antibodies (MAbs) recently isolated from a human survivor of MARV infection (22). Our results thus suggest a novel approach for developing engineered MAbs with broad-spectrum activity against filoviruses.

RESULTS

The crystal structure of EBOV GP_{CL} reveals the NPC1 receptor-binding site that is unmasked upon endosomal cleavage. Purified EBOV $GP_{1,2}$ ectodomains (expressed without mucin-like domains; hereinafter referred to as GP) were treated with thermolysin, which mimics host endosomal protease processing of EBOV GP (8), in order to generate EBOV GP_{CL} trimers for crystallization. EBOV GP_{CL} crystallizes in the space group H3 (R3:H) with four GP monomers and four KZ52 Fabs in the asymmetric unit (ASU). The ASU contains one full GP trimer and one remaining GP monomer, which itself forms a biologically relevant trimer with two symmetry-related protomers about a crystallographic 3-fold axis. The overall changes to the tertiary structure upon cleavage of GP are minimal, reflected in a root mean square deviation (RMSD) of 0.419 Å compared to the structure of uncleaved EBOV GP (Fig. 1A) (4). This finding corroborates a previous model of EBOV GP_{CL} which suggested only limited changes in the GP_{CL} structure upon thermolysin digestion (23). The structure of EBOV GP_{CL} is more compact than that of EBOV GP and exhibits more stable crystal packing, less disorder, and improved resolution of X-ray diffraction over that of the previously determined uncleaved GP (4).

New regions of EBOV GP can now be visualized in the EBOV GP_{CL} structure. These include C-terminal residues of GP_2, the disulfide link between C53 of GP_1 and C609 of GP_2, and an intra-GP_2 disulfide bond between C601 and C610. As EBOV GP_2 descends from the base of the GP trimer structure, it forms a tightly ordered loop structure that is stabilized by the intra-GP_2 disulfide bond between C601 and C610. This disulfide link turns the peptide chain back toward the body of GP where it is anchored to GP_1 by the C53-C609 inter-$GP_{1,2}$ disulfide bond prior to turning downward toward the transmembrane domain and viral membrane (Fig. 1B).

The most striking structural feature of GP_{CL} is the full exposure of a charged hydrophilic crest and a large hydrophobic trough structure in immediate proximity to the GP_2 fusion loop. The trough becomes exposed upon proteolytic excision of the glycan cap from EBOV GP and is 13 Å wide, 23 Å long, and 10 Å deep (Fig. 1C). Residues I113 and L111 form an exposed hydrophobic face inside the trough, while residues V79, T83, W86, F88, L122, V141, and I170 line the bottom of the trough.

Mutation of GP residues exposed after removal of the glycan cap affects viral infectivity and binding to the filovirus receptor NPC1. Previous work utilizing scanning mutagenesis of EBOV GP identified multiple residues important for viral infectivity (24–26). These studies were carried out prior to the availability of a crystal structure of EBOV GP (4) or GP_{CL} (this work) and prior to identification of the endosomal receptor, NPC1 (17, 18). Here, we map these residues onto the crystal structure of EBOV GP_{CL} and determine whether mutations in EBOV GP that reduce infectivity specifically correlate with defects in GP_{CL}-NPC1 binding. Previous work identified three lysines at positions 114, 115, and 140 (16, 25) and hydrophobic residues F88, L111, and L122 (25–27) for which mutation to alanine diminishes infectivity (16, 25). These deficits in infectivity correlate with reductions in NPC1 binding, as determined by co-immunoprecipitation (28).

The crystal structure of EBOV GP_{CL} illustrates that K114, K115, and K140 lie along the crest and F88, L111, and L122 line the trough of EBOV GP_{CL}. These hydrophobic residues are buried in uncleaved EBOV GP (4) but become solvent exposed in the trough of EBOV GP_{CL}. We systematically mutated residues that the GP_{CL} crystal structure shows to be surface-exposed after cleavage, in order to determine their importance for NPC1 binding and viral infectivity and to define the GP_1 receptor-binding site (RBS).

We pseudotyped vesicular stomatitis virus (VSV) particles with 73 mutant GP proteins and tested them for viral incorporation of GP relative to the incorporation of the wild-type (WT) protein, and for binding to the conformational antibody KZ52 (4, 21), which only recognizes properly folded GP (see Fig. S4 in the supplemental material). The 68 VSV-GP mutants that met these quality benchmarks were then evaluated for their capacity to recognize a purified, soluble form of human NPC1 domain C in an

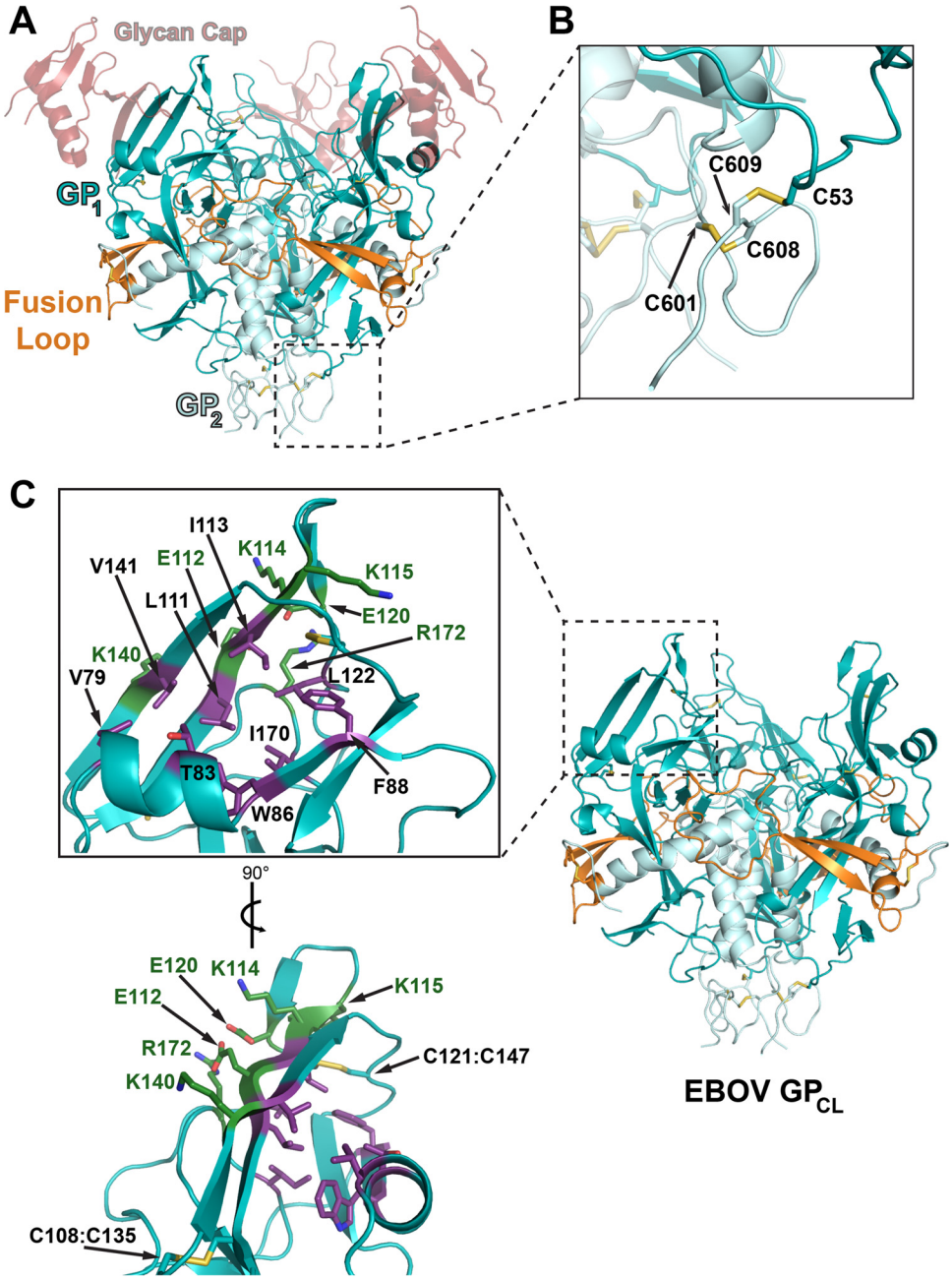

FIGURE 1 Crystal structure of ebolavirus GP_{CL}. (A) The trimeric EBOV GP_{CL} structure is shown, with GP_1 colored teal, GP_2 colored light blue, the fusion loop colored orange, and disulfide bonds displayed as sticks and colored gold. The former position of the glycan cap, now absent in the GP_{CL} structure, is illustrated in semitransparent red and is derived from an alignment with the uncleaved EBOV GP structure (PDB code 3CSY). (B) Additional residues at the C terminus of GP_2 are now visible in this higher-resolution structure. These residues include C601-C608, contained within GP_2, as well as the C53-C609 disulfide bond that cross-links GP_1 and GP_2 together. (C) The structure of EBOV GP_{CL} is displayed to the right, with the same coloring as described for panel A. An enlarged illustration of the putative EBOV GP_1 RBS is shown to the left, in two orientations. Residues forming the hydrophilic crest and hydrophobic trough are labeled and colored green and purple, respectively. The disulfide bonds present around the crest and trough, C108-C135 and C121-C145, are colored gold.

enzyme-linked immunosorbent assay (ELISA), as described previously (27, 29). We report that WT EBOV GP_{CL} binds to NPC1 domain C with a 50% effective concentration (EC_{50}) of ≈0.5 nM, consistent with a high-avidity binding interaction between these proteins. In comparison, we find that mutants that demonstrate reduced infectivity are also defective for binding to NPC1 domain C (see Fig. S1 and S2 in the supplemental material). Furthermore, a few single point mutations that cause drastic reductions (>10-fold) in the GP_{CL}-NPC1 domain C-binding EC_{50} are located in or around the hydrophobic trough and hydrophilic crest. These mutants allow us to map those residues of EBOV GP_1 that are critical to NPC1 domain C onto the EBOV GP_{CL} structure and to better

define the RBS (see Fig. S1 and S2). Interestingly, mutation to alanine of two trough residues, F88 and L111, reduces viral infectivity dramatically (by >3 $\log_{10}$ units) but has more modest effects on GP_{CL}-NPC1 binding (see Fig. S2A). The disparity between strong reduction in infectivity but modest effect on NPC1 binding suggests that these residues may be important for steps in viral entry post-NPC1 binding and prior to membrane fusion, such as conformational changes or release of GP2.

The hydrophobic trough exposed on GP1 upon endosomal cleavage is the primary binding site of NPC1 domain C. We performed further mutagenesis of the hydrophobic trough to better define its precise role. Since most of the point mutations to alanine within the hydrophobic trough had only modest effects, we postulated that replacing them with bulkier methionine residues would more completely occlude the trough and prevent GP-NPC1 binding. We selected two trough residues, T83 and I113, which did not inhibit NPC1 binding when mutated to alanine, for additional mutagenesis to methionine (Fig. 2A and B). To prevent misfolding or disruption of the GP structure, we engineered compensatory mutations with interacting residues of the glycan cap to fit the larger methionine residues and prevent steric clashing. We engineered the following mutants: I113M (trough)/F225A (cap), T83M (trough)/F225V+Y232F (cap), and T83M+I113M (trough)/F225A+Y232F (cap) (Fig. 2C to E). For simplicity, since the compensatory mutations are removed along with the glycan cap upon proteolysis, we will only refer to these mutants by the mutations remaining on EBOV GP_{CL}: T83M, I113M, and T83M+I113M. All engineered VSV-GP mutants maintain high levels of incorporation compared to the incorporation of WT GP (see Fig. S2 in the supplemental material). As posited, the single T83M and I113M mutations, as well as the T83M+I113M double mutation, lead to defects in NPC1 domain C binding and pseudovirus infectivity by GP_{CL} bearing them (Fig. 2A to C). We further find that a single point mutation, L122A, located in the bottom of the trough, abrogates both NPC1 domain C binding and pseudotyped virus infectivity (Fig. 2E). The position of L122 suggests that it has a structural role; the L122A mutation may destabilize the local trough structure, preventing NPC1 binding and subsequent infectivity. Together, these findings provide evidence that supports a direct correlation between NPC1 binding and infectivity and effectively maps the GP_{CL} trough as a critical component of the NPC1-binding site.

An overall basic charge on the GP_1 crest is required for GP binding to NPC1 domain C and viral infectivity. Experiments performed prior to the identification of the filovirus endosomal receptor NPC1 demonstrated that K114A, K115A, and K140A mutations (now mapped to the GP_{CL} crest) significantly reduce viral infectivity (16, 25). Here, we investigated whether the observed reductions in viral infectivity from these mutations correlate with defects in binding to NPC1 domain C. We show that while the individual mutations K114A and K115A have only modest effects (see Fig. S1 and S2 in the supplemental material), the double mutation (K114A+K115A) dramatically inhibits GP_{CL}-NPC1 domain C binding and viral entry (Fig. 3A and B). In contrast, the K140A mutant showed no significant defect in viral infectivity or NPC1 domain C binding (see Fig. S2). To test the hypothesis that these crest residues participate in electrostatic interactions with NPC1 during virus-receptor engagement, we engineered and analyzed VSV-GPs in which these lysines were replaced with either basic or acidic residues. The K114R+K115R double mutant, which maintains the basic charge, remains fully functional. In contrast, the K114E+K115E double mutant, which reverses charge, displays an even greater deficit in receptor-binding function and entry activity than the neutral K114A+K115A mutant (Fig. 3A and B). To determine whether it is the overall charge of the site or specific basic residues within the site that are important, we mutated two glutamic acid residues in proximity to positions 114 and 115 to alanine. The resulting quadruple mutant (K114A+K115A+E112A+E120A), which is predicted to have WT-like electrostatics, exhibits receptor-binding activity and infectivity at nearly WT levels (Fig. 3A and B). The importance of a set of basic residues but lack of a specific requirement for any one of them individually suggest a need to maintain an overall basic charge on the GP_{CL} crest (Fig. 3C).

Neutralizing antibodies raised from a Marburg virus survivor demonstrate potential panfilovirus neutralization activity. The high degree of sequence and structural conservation in the NPC1-binding site of filovirus glycoproteins makes it an attractive target for the development of broadly neutralizing MAbs with therapeutic potential (see Fig. S3 in the supplemental material). Unfortunately, no such MAbs against ebolaviruses have been isolated. Instead, most known neutralizing anti-ebolavirus MAbs target a conformational epitope at the base of the $GP_{1,2}$ trimer (4, 5, 30, 31). Recently, however, several MAbs isolated from a human survivor of MARV infection were found to recognize the hydrophobic GP_{CL} trough and inhibit GP-NPC1 domain C binding (11, 22). Of significance, one anti-MARV MAb from that study, MR72, cross-reacts with purified GP and GP_{CL} of EBOV, while three other MAbs, MR78, MR111, and MR191, cross-react only with EBOV GP_{CL} (22). MR72, MR78, MR111, and MR191 bind to similar locations on MARV GP but approach from significantly different angles (22). The third complementarity-determining region of the heavy chain variable region (CDRH3) of MR78 binds into the expected MARV GP_1 RBS (see Fig. S3) (11).

As the RBS is conserved in sequence and structure across known filoviruses, we evaluated the capacity of MR72 and two additional GP_{CL}-reactive antibodies, MR78 and MR191 (22), to recognize and neutralize VSV bearing GP_{CL} from four ebolaviruses (Sudan virus [SUDV], Bundibugyo virus [BDBV], Taï Forest virus [TAFV], and Reston virus [RESTV]) and the cuevavirus Lloviu virus (LLOV) (2, 32). Remarkably, we find that MR72 effectively neutralizes VSVs pseudotyped with GP_{CL} derived from all known filoviruses (Fig. 4A). In contrast, MR191 neutralizes VSV bearing other filovirus GPs only weakly, and MR78 fails to neutralize VSVs bearing GP_{CL} derived from any species other than MARV. We speculate that the steeper angle of approach of MR191 to MARV GP_{CL} compared to that of MR78 may enhance the breadth of neutralization by improving access to the shared RBS (Fig. 4A and S3). Of significance, we found that MR72 failed to bind VSVs bearing uncleaved EBOV GP on the surface (see Fig. S3 in the supplemental material). This finding is in contrast to a previous observation of MR72 binding to uncleaved soluble EBOV GP ectodomain (see Fig. S3) (22). It is likely that there are differences in the presentation of EBOV GP on the surface of actual virions that prevent MR72 from binding and effectively neutralizing either wild-type EBOV or VSV bearing uncleaved EBOV GP.

The contrasting neutralization breadth properties of MR72 and MR78, despite their similar binding angles and shared epitope, led us to explore our panel of GP_{CL} mutations to identify

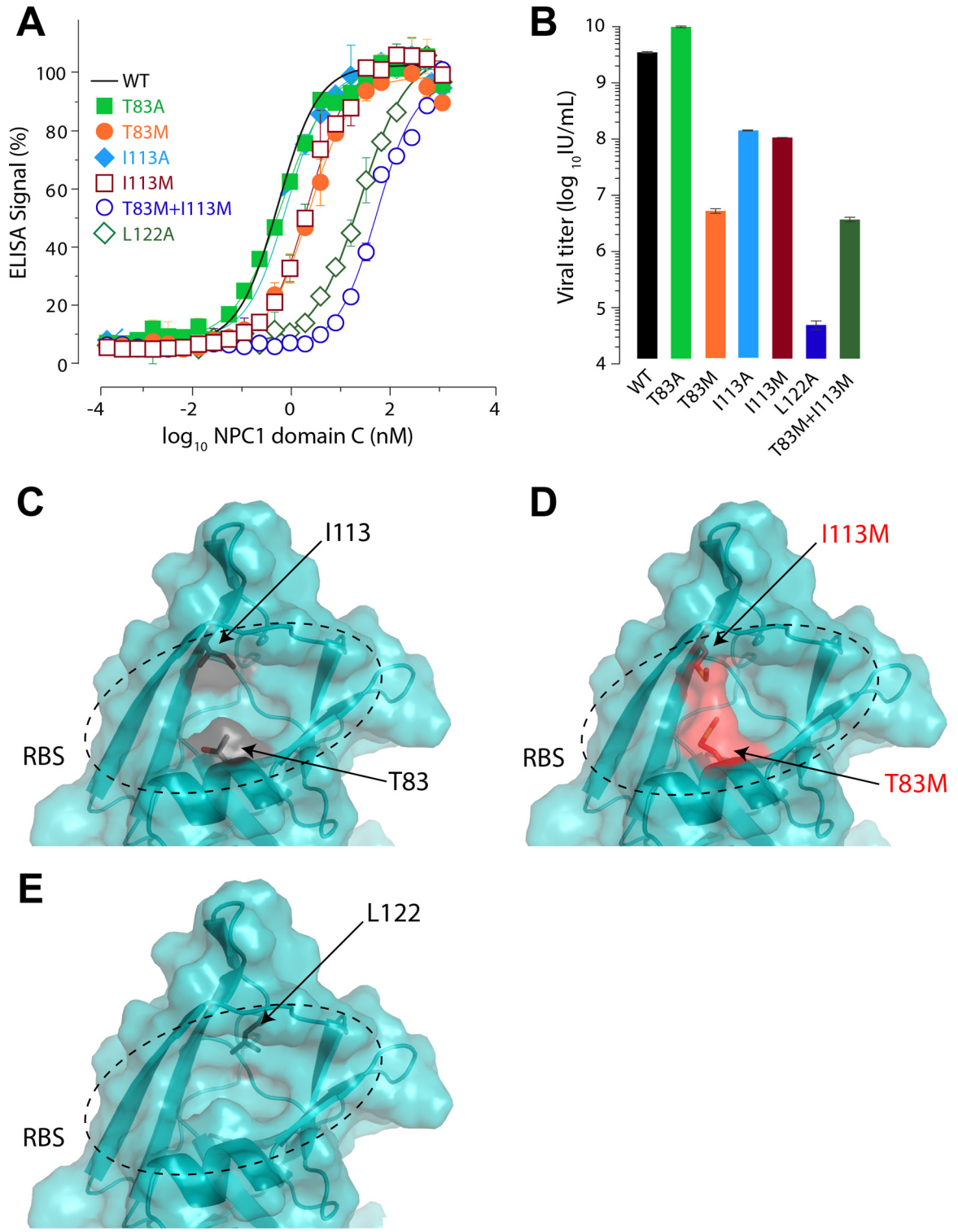

FIGURE 2 Mutagenic occlusion of the EBOV GP_1 receptor-binding site. (A) Alanine or methionine mutations were made to key residues in the RBS. The affinities of wild-type and mutant GP_{CL} for NPC1 domain C were analyzed via ELISA. Note that the L122A and T83M+I113M mutations significantly reduce binding to NPC1 domain C. Means ± SD ($n = 4$) from a representative experiment are shown. (B) Graph displaying titers of VSV pseudoviruses harboring GP_1 RBS mutations. Means ± SD ($n = 2–4$) from a representative experiment are shown. (C) A semitransparent surface has been placed over the cartoon model of the WT RBS on EBOV GP_1 to display the RBS pocket (within the dashed oval outline). Residues T83 and I113 are illustrated as sticks (black). (D) Model of EBOV RBS bearing the mutations T83M and I113M (red). The longer side chains of the introduced methionine residues fill the RBS pocket and likely prevent NPC1 domain C binding by occluding the NPC1 binding site. (E) The buried location of L122 (black) is displayed in the EBOV GP_1 RBS. See also Fig. S1, S2, and S4 in the supplemental material.

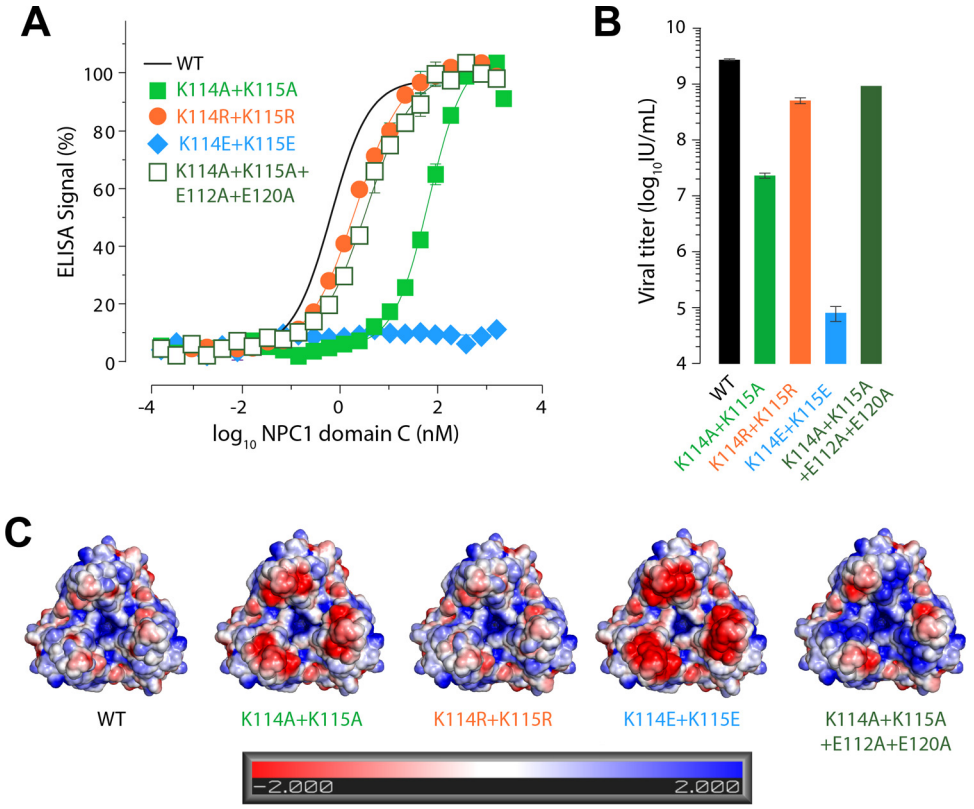

FIGURE 3 The basic electrostatic potential of the GP_1 crest is vital to receptor binding. (A) ELISA analysis of binding of wild-type or mutant GP_{CL} to NPC1 domain C. Replacement of positively charged K114 and K115 with neutral alanines or negatively charged glutamic acids reduces and abrogates NPC1 binding, respectively. Concomitant mutation of neighboring E112 and E120 to neutral alanine residues restores affinity for NPC1 domain C. Means ± SD ($n = 4$) from a representative experiment are shown. (B) Growth titers of VSV pseudotyped with electrostatic mutants of EBOV GP correlate with the NPC1 domain C affinities shown by the results in panel A: reduction in growth correlates with loss of positive charge. Means ± SD ($n = 2–4$) from a representative experiment are shown. (C) The electrostatic surface potential is calculated for each of the mutant EBOV GPs using APBS in PyMol (The PyMOL Molecular Graphics System, version 1.5.0.4. [Schrödinger, LLC], and APBS plugin for PyMol, M. G. Lerner and H. A. Carlson, University of Michigan, Ann Arbor, MI, 2006; 48). The view is looking down onto the EBOV GP trimer. Mutants with an overall negative charge on the surface of GP_1 demonstrate defects in both affinity for NPC1 domain C and viral growth. See also Fig. S1, S2, and S4 in the supplemental material.

specific residues in the GP RBS that can affect MR78's neutralization of EBOV GP_{CL} (see Fig. S2 in the supplemental material). We find that a single point mutation, V79A, allows MR78 to neutralize EBOV GP_{CL}: although MR78 cannot neutralize VSV bearing wild-type EBOV GP_{CL}, it can neutralize V79A-bearing VSV-EBOV GP_{CL} (Fig. 4B). Position 79 in EBOV GP is equivalent to position 63 in MARV. Structural alignment of EBOV GP_{CL} with MARV in the MARV GP-MR78 crystal structure (11) suggests that the wild-type V79 may sterically clash with the light chain of MR78. Replacement of valine with the smaller alanine residue (V79A) may improve neutralization by relieving the steric clash (Fig. 4B).

Furthermore, previous studies have shown that, unlike MR72, MR78 fails to block NPC1 domain C binding to EBOV GP_{CL} (11). Therefore, we performed NPC1 domain C competitive-binding assays to determine whether MR78 neutralizes EBOV GP_{CL}-V79A by inhibiting GP-NPC1 binding. Curiously, even though MR78 is now able to neutralize VSV bearing EBOV GP_{CL}-V79A, it remains unable to prevent binding of NPC1 domain C to EBOV GP_{CL} or EBOV GP_{CL}-V79A (Fig. 4B). MR72, however, does block NPC1 binding to EBOV GP_{CL}. Therefore, our data suggest that MAbs MR72 and MR78 may neutralize by distinct mechanisms. MR72 effectively blocks GP_{CL}-NPC1 binding for all filoviruses, whereas MR78 does not block EBOV GP_{CL}-NPC1 binding. We speculate that MR78 neutralizes EBOV entry by inhibiting viral membrane fusion downstream from virus receptor recognition.

In order to gauge the neutralization potentials of MR72 and MR78 relative to those of other MAbs with demonstrated protective efficacy *in vivo*, we performed a comparative analysis with the combined MAbs of the EBOV-specific ZMapp cocktail: 2G4, 4G7, and 13C6 (31, 33), as well as with KZ52, a known neutralizing MAb from a human survivor (21). Our analysis demonstrates that MR72 can neutralize pseudoviruses at 10-fold lower concentrations of antibody than are required for KZ52 and the ZMapp cocktail (Fig. 4C). Thus, MAbs such as MR72, which target the highly conserved GP_1 RBS, represent a novel avenue for both broad and potent neutralization of filoviruses, if they can be delivered to the endosomal compartments where GP_{CL} is generated during entry.

DISCUSSION

In this study, we present the 3.3-Å crystal structure of thermolysin-cleaved EBOV GP (GP_{CL}), which is primed for interaction with the filovirus receptor, NPC1. Thermolysin has previously been demonstrated to mimic host CatB and CatL proteolytic processing of

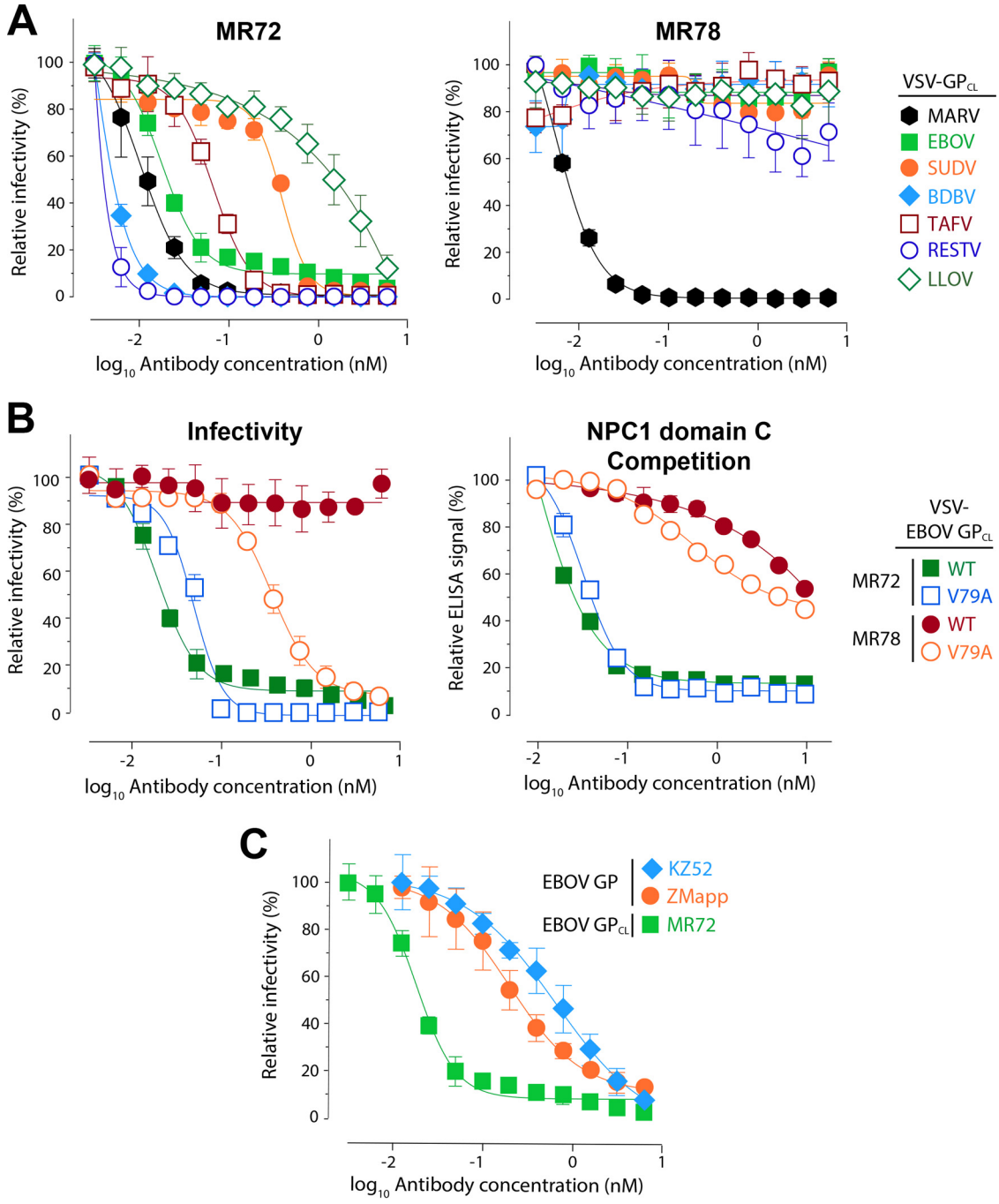

FIGURE 4 Monoclonal antibodies targeting the conserved GP_1 RBS demonstrate panfilovirus neutralization activity. (A) VSV pseudotyped with GPs from different species of filovirus (as indicated in the key to the right) were preprimed with thermolysin to expose the GP_1 RBS and then analyzed for reduction in relative infectivity following treatment with MR72 or MR78. (B) The graph to the left shows a comparative analysis of the neutralization of VSV-EBOV GP_{CL} and VSV-EBOV GP_{CL}-V79A by MR72 and MR78. The graph to the right displays the results of competitive binding assays detecting NPC1 domain C binding in the presence of increasing concentrations of MR72 or MR78 for EBOV GP_{CL} and EBOV GP_{CL}-V79A. The key for both graphs is on the far right. (C) Graph showing the results of comparative infectivity assays of nonprimed VSV pseudotyped with EBOV GP treated with MAbs from the ZMapp cocktail (2G4, 4G7, and 13C6) (33) or the neutralizing EBOV antibody KZ52 (21). MR72 neutralizes primed EBOV GP_{CL} pseudovirions at >10-fold lower concentrations than are required for ZMapp or KZ52 to neutralize EBOV GP pseudovirions. See also Fig. S3 in the supplemental material. Means ± SD ($n = 2-4$) from a representative experiment are shown in each panel.

EBOV GP, which occurs in the endosome and is required for receptor binding and membrane fusion (8–10, 16). This high-resolution structure of EBOV GP_{CL} has now defined the intermolecular disulfide bridge between C53 in GP_1 and C609 in GP_2, a region previously unresolved for EBOV GP. The disulfide bridge likely contributes to the inherent stability of ebolavirus GP despite proteolytic processing. This stability is reflected in a high degree of structural conservation between uncleaved EBOV GP (4) and

GP_{CL}; the aligned structures have an RMSD of 0.419 Å. The crystal structure of EBOV GP_{CL} presented here also illustrates how proteolytic priming removes the glycan cap of EBOV GP_1 to expose the binding site for the filovirus receptor NPC1. The GP_{CL} crystal structure suggests that the glycan cap may act as a final layer of defense, shielding the critical and conserved NPC1 domain C binding site from host immune surveillance prior to cellular entry. We show that this RBS has a crest-and-trough morphology and exists at the apex of the GP_{CL} trimer.

The crest is lined with hydrophilic basic residues, while the trough is recessed and entirely hydrophobic. Mutagenic analysis of EBOV GP_{CL} demonstrates that the crest is involved in nonspecific electrostatic interactions with NPC1, requiring an overall basic charge to facilitate binding of NPC1 domain C. Mutations in EBOV GP (such as K114E+K115E) that reverse the electrostatic charge on the GP_{CL} crest consistently abrogate receptor binding and reduce infectivity. In contrast, the GP_{CL} trough is involved in more specific hydrophobic interactions with NPC1 domain C. Structure-based mutants with mutations designed to obstruct the structure of the trough (such as T83M+I113M) diminish the affinity of GP for NPC1 domain C and severely restrict the infectivity of VSV pseudotypes bearing these mutations. Based on the crystal structure and results of mutagenesis reported here, we propose that the NPC1 receptor binds GP in a two-stage process. First, GP_{CL} recruits the NPC1 domain C receptor through nonspecific electrostatic interactions between NPC1 and the basic crest region on GP_{CL}. Without this interaction, there is no detectable GP-receptor binding. Next, specific hydrophobic interactions are initiated between the GP_1 RBS trough and NPC1 domain C. The specificity of these interactions likely explains the differential effects of individual mutations in the trough (Fig. 3 and 4), whereas the effects of mutations in the crest were determined by charge, not specific amino acid position.

We also further analyzed two mutants with a mutation in the hydrophobic trough, F88A or L111A, which have been described previously as unable to support infection (25, 26). These two mutants are outliers in our analysis. Their infectivities are reduced by more than three $\log_{10}$ infectious units relative to that of WT EBOV GP, despite only modest defects in binding of NPC1 domain C. We postulate that these mutants are defective at a step downstream from NPC1 binding. They will provide useful tools to further decipher precisely how GP_{CL}-NPC1 binding facilitates fusion triggering and membrane fusion.

Recent work has identified multiple neutralizing MAbs from a patient who survived MARV infection. The MAbs from those studies were found to bind to the apex of MARV GP_1 (11, 22)—the site we have confirmed here to be the filovirus GP_1 receptor-binding site. Since ebolavirus, marburgvirus, and cuevavirus GP proteins all use the NPC1 protein as a receptor, it is not unexpected that the structure of the GP_1 RBS would be highly conserved across all filoviruses (10, 17–19, 32). Thus, we hypothesized that the MAbs identified by Flyak et al. (22), shown to target the RBS trough on MARV GP_1 (11), should be broadly neutralizing. However, unlike the GP proteins of marburgviruses, those of the ebolaviruses and cuevavirus maintain a glycan cap structure that effectively shields the GP_1 RBS from immune surveillance. Therefore, by proteolytically priming filovirus GPs on the surface of VSV particles (such as VSV-EBOV GP_{CL}), we were able to analyze the neutralization potential of MAbs targeting the otherwise-occluded filovirus RBS. Analysis of GP_{CL}-bearing VSVs would tell us if it was worthwhile to target such antibodies to the endosome as future therapeutics.

Of the panel of neutralizing MAbs from an MARV survivor described by Flyak et al. (22), only one, MR72, demonstrates significant cross-reactivity to uncleaved EBOV GP. Three other MAbs, MR78, MR111, and MR191, only react with EBOV GP_{CL}. We focused our analysis on the EBOV GP-reactive MR72 and the EBOV GP_{CL}-reactive MR78 and MR191, which approach GP from different angles. Here, we show that MR72 effectively neutralizes VSV pseudovirions bearing GP_{CL} from EBOV, SUDV, BDBV, TAFV, RESTV, or LLOV. MR191 neutralizes the EBOV, BDBV, TAFV, and LLOV VSV-GP_{CL} virions weakly (and RESTV and SUDV GP_{CL} not at all), with infectivity never reduced below 50% (see Fig. S3 in the supplemental material). In contrast, MR78 can only neutralize MARV GP_{CL}. It cannot neutralize EBOV GP_{CL}-bearing VSVs, even though it is able to bind them.

The crystal structures of MARV GP_{CL} and EBOV GP_{CL} bound to MR78 suggest that MR78 binds the same site in both viruses. However, the resolution of the EBOV GP_{CL}-MR78 complex was too low to identify subtle differences imposed by sequence deviations from MARV GP that might explain why MR78 fails to neutralize EBOV GP_{CL} (11). Hence, we used a panel of VSV-EBOV GP RBS mutants to understand which sequence variations could prevent MR78-mediated neutralization of EBOV GP_{CL}. Surprisingly, the introduction of a single point mutation (V79A) within the EBOV RBS allows MR78 to neutralize VSV-EBOV GP_{CL}-V79A. Of significance, BDBV, TAFV, and RESTV GPs also encode valine at this position, while SUDV and LLOV GPs encode isoleucine and leucine, respectively. The larger Val, Ile, and Leu aliphatic residues encoded by the ebolaviruses and cuevavirus may prevent MR78 from neutralizing their GP_{CL}-bearing particles (Fig. 4A; see also Fig. S3 in the supplemental material). We note that, unlike MR78, MR191 exhibits no improvement in neutralization of VSV-EBOV GP_{CL}-V79A (see Fig. S3 in the supplemental material). How MR72 but not MR78 is able to overcome divergent amino acids at position 79 to broadly neutralize filovirus GP_{CL} is the subject of continued structural and biochemical study.

Remarkably, enhanced neutralization of EBOV GP_{CL}-V79A by MR78 was not accompanied by a commensurate increase in its capacity to block NPC1 binding of this GP (Fig. 4). This apparent uncoupling of neutralization and receptor blockage raises the possibility that MR78 may act as an allosteric inhibitor, preventing membrane fusion by binding to GP_1 subunits in the trimer that are not occupied by NPC1 domain C in the endosome. There, it may inhibit events that occur after receptor binding in order to trigger GP-mediated membrane fusion. Mutations like L111A, which eliminate infectivity without affecting receptor binding, may target these same post-receptor-binding steps.

Recent events, including the unprecedented EBOV epidemic in West Africa (3, 34), coinciding with human cases of MARV emerging in central Africa (35) and the emergence of BDBV (36) and re-emergence of SUDV (37) in this decade, highlight the urgent need for broad-spectrum antifilovirus therapeutics (38). Here, we demonstrate that the highly conserved binding site for the essential intracellular receptor NPC1 provides an attractive and underexplored target for broadly protective antibodies or small-molecule therapeutics. However, one crucial challenge to the development of such antibodies as therapeutics is an evolved feature of the filovirus entry mechanism—the unavailability of its NPC1-binding site to extracellular antibodies. The success of this

antiviral strategy therefore requires novel protein engineering approaches to deliver GP_{CL}-specific MAbs to late endosomes and/or lysosomes, where the NPC1-binding site is unmasked by host proteases.

MATERIALS AND METHODS

Expression and purification of GP_{CL}-KZ52 complex for crystallization. Ebola virus GP (lacking the mucin domain [residues 312 to 462]) was produced by stable expression in *Drosophila melanogaster* S2 cells. Briefly, Effectene (Qiagen) was used to transfect S2 cells with a modified pMT-puro vector plasmid containing the GP gene of interest, followed by stable selection of transfected cells with 6 μg/ml puromycin. Cells were cultured at 27°C in complete Schneider's medium for selection and then adapted to Insect Xpress medium (Lonza) for large-scale expression in 2-liter Erlenmeyer flasks. Secreted GP ectodomain expression was induced with 0.5 mM $CuSO_4$, and supernatant harvested after 4 days. Ebola virus GP was engineered with a double Strep-tag at the C terminus to facilitate purification using Strep-Tactin resin (2-1201-010) (Qiagen) and then further purified by Superdex 200 size exclusion chromatography (SEC) in 10 mM Tris-buffered saline (Tris-HCl, pH 7.5, 150 mM NaCl [TBS]). EBOV GP_{CL} was produced by incubation of 1 mg GP with 0.02 mg thermolysin overnight at room temperature in TBS containing 1 mM $CaCl_2$ and purified by using Superdex 200 SEC. Trimeric EBOV GP_{CL} was then complexed with a KZ52 Fab fragment prior to crystallization as previously described (4).

Crystallization, data collection, and structure determinations. The purified EBOV GP_{CL}-KZ52 Fab complex was concentrated to 3.5 mg/ml in TBS. The crystal drops consisted of a 1:1 ratio of protein/well solution. The well solution consisted of 25% polyethylene glycol monomethyl ether 550 (PEG MME 550), 10% 2-propanol, 5% ethylene glycol, 100 mM sodium acetate, pH 4.7, and 100 mM calcium chloride. Crystals grew over the course of a month and were flash frozen directly out of the crystal drop into liquid nitrogen for data collection. Data were collected remotely at the Argonne National Laboratory, Advanced Photon Source (APS), from the GM/CA beamline 23-ID-D. The structure was determined using molecular replacement with PHASER (39), within the CCP4 suite (40), using a modified EBOV GP-KZ52 complex model (PDB code 3CSY) with all the residues corresponding to the glycan cap removed (4). Refinement of the EBOV GP_{CL} crystal structure was done through iterative cycles of model building using COOT, followed by refinement with Refmac5 and PHENIX (41–43). Translation/libration/screw (TLS) motion was applied during refinement with the TLS Motion Determination (TLSMD) server used to determine the TLS structure partitions (44, 45). Five percent of the data was set aside prior to refinement for the R_{free} calculations for each data set (46). The statistics and stereochemistry of the crystal structure were checked using the MolProbity server until ranking at least at the >95th percentile (see Fig. S2A in the supplemental material) (47). All of the structural figures were rendered using PyMOL (PyMOL Molecular Graphics System, version 1.5.0.4; Schrödinger, LLC).

Cells and viruses. African grivet monkey kidney (Vero) cells were maintained at 37°C and 5% CO_2 in high-glucose Dulbecco's modified Eagle medium (DMEM; Invitrogen Corp., Carlsbad, CA) supplemented with 10% fetal calf serum. Replication-incompetent vesicular stomatitis virus (VSV) (serotype Indiana) pseudotyped viruses were generated as previously described (49). The wild type (VSV-WT GP) encodes enhanced green fluorescence protein (eGFP) in place of the VSV-G gene to allow scoring of infection and bears the EBOV GPΔmuc gene (Mayinga isolate, GenBank accession number AF086833) but lacks the mucin-like domain (residues 309 to 489 [Δmuc]) (6). Point mutants and multiple mutants were generated by subcloning GP fragments containing the mutation(s) to replace EBOV GPΔmuc. Cleaved VSV-GP_{CL} particles were generated by incubating VSV-GP pseudotypes with thermolysin (250 μg/ml) for 1 h at 37°C. The reaction was stopped by adding phosphoramidon (1 mM) and incubating on ice for 5 min.

Normalization of GP for ELISA. Normalization of GP_{CL} amounts to be used in the binding experiments was done by ELISA, as illustrated in Fig. S4 in the supplemental material. Briefly, high-binding 96-well ELISA plates (Corning) were coated with serial dilutions of GP_{CL} in phosphate-buffered saline (PBS), and allowed to bind at 37°C for 1 h. The plates were blocked with PBS containing 3% bovine serum albumin (PBSA), followed by incubation with the anti-GP monoclonal antibody KZ52 (2 μg/ml in PBS) (21) and a horseradish-conjugated anti-human secondary antibody (Santa Cruz Biotechnology), which was detected by ultra-TMB (3,3′,5,5′-tetramethylbenzidine) substrate (Thermo Scientific). Absorbance readings were subjected to a nonlinear regression analysis (GraphPad Prism software) to generate binding curves and calculate an EC_{50} value. Additionally, the virions were normalized for GP incorporation by comparing the amount of GP to the amount of the VSV matrix protein (M). Equal amounts of purified virions were resolved on SDS-PAGE and blotted for the VSV matrix protein using a mouse anti-VSV M antibody (23H12). Quantification was done using a LI-COR IR dye-conjugated anti-mouse Alexa Fluor 680 secondary antibody (Invitrogen) on the Odyssey Imaging Station and Image Studio 2.1 software (LI-COR Biosciences), and the results were normalized to the WT control. Virus particles that had less than 25% incorporation of mutant GP compared to the incorporation of WT GP or that were highly sensitive to proteolysis were excluded from our analysis.

GP-NPC1 domain C capture ELISA. Binding of GP to NPC1 domain C was performed as previously described (10, 32). Briefly, high-binding 96-well ELISA plates (Corning) were coated with the anti-GP monoclonal antibody KZ52 (2 μg/ml in PBS) (21). Following a blocking step, either uncleaved or *in vitro*-cleaved GP_{CL} pseudotypes were captured on the plate. Unbound GP was washed off, and serial dilutions of Flag-tagged purified soluble human NPC1 domain C (0 to 40 μg/ml) were added. Bound NPC1 domain C was detected by a horseradish-conjugated anti-Flag antibody (Sigma-Aldrich), using ultra-TMB substrate (Thermo Scientific). EC_{50}s were calculated from binding curves generated by nonlinear regression analysis using GraphPad Prism software. Binding ELISAs were done in duplicate in at least two independent experiments. All incubation steps were done at 37°C for 1 h or at 4°C overnight.

Pseudovirus neutralization assays. Serial dilutions of MAbs and of a no-antibody control were mixed with either cleaved or uncleaved VSV-GP particles and allowed to bind for 1 h at room temperature. Monolayers of Vero cells were inoculated with the antibody-virus mixture in duplicate and incubated at 37°C in 5% CO_2. Infection was scored 12 to 16 h postinfection by enumeration of eGFP-positive cells under a fluorescence microscope. The ZMapp cocktail MAbs 2G4, 4G7, and 13C6, as well as MAb KZ52, prepared as previously described (33), were generously provided by Mapp Biopharmaceutical. MAbs MR78 and MR72 were prepared as previously described (22).

Protein structure accession number. Coordinates and structure factors have been deposited into the Protein Data Bank under accession number 5HJ3.

SUPPLEMENTAL MATERIAL

Supplemental material for this article may be found at http://mbio.asm.org/lookup/suppl/doi:10.1128/mBio.02154-15/-/DCSupplemental.

Figure S1, PDF file, 2.7 MB.
Figure S2, PDF file, 0.3 MB.
Figure S3, PDF file, 1.2 MB.
Figure S4, PDF file, 0.2 MB.

ACKNOWLEDGMENTS

We thank the beamline scientists at GM/CA 23-ID for support during data collection.

E.O.S. was supported by NIAID R01 AI101436 and R01 AI081982 and an Investigators in the Pathogenesis of Infectious Disease award from the Burroughs Wellcome Fund. K.C. acknowledges support from NIAID R01 AI088027 and R01 AI101436, and J.E.C. was supported by NIAID U19

AI109711 and by the Defense Threat Reduction Agency (HDTRA1-13-1-0034).

FUNDING INFORMATION

HHS | NIH | National Institute of Allergy and Infectious Diseases (NIAID) provided funding to Erica Ollmann Saphire under grant numbers R01 AI101436 and R01 AI081982. HHS | NIH | National Institute of Allergy and Infectious Diseases (NIAID) provided funding to Kartik Chandran under grant numbers R01 AI088027 and R01 AI101436. HHS | NIH | National Institute of Allergy and Infectious Diseases (NIAID) provided funding to James E. Crowe under grant number U19 AI109711. DOD | Defense Threat Reduction Agency (DTRA) provided funding to James E. Crowe under grant number HDTRA1-13-1-0034.

REFERENCES

1. **De la Vega MA, Stein D, Kobinger GP.** 2015. Ebolavirus evolution: past and present. PLoS Pathog **11:**e1005221. http://dx.doi.org/10.1371/journal.ppat.1005221.
2. **Negredo A, Palacios G, Vázquez-Morón S, González F, Dopazo H, Molero F, Juste J, Quetglas J, Savji N, de la Cruz Martínez M, Herrera JE, Pizarro M, Hutchison SK, Echevarría JE, Lipkin WI, Tenorio A.** 2011. Discovery of an ebolavirus-like filovirus in Europe. PLoS Pathog **7:**e1002304. http://dx.doi.org/10.1371/journal.ppat.1002304.
3. **Baize S, Pannetier D, Oestereich L, Rieger T, Koivogui L, Magassouba N, Soropogui B, Sow MS, Keïta S, De Clerck H, Tiffany A, Dominguez G, Loua M, Traoré A, Kolié M, Malano ER, Heleze E, Bocquin A, Mély S, Raoul H, Caro V, Cadar D, Gabriel M, Pahlmann M, Tappe D, Schmidt-Chanasit J, Impouma B, Diallo AK, Formenty P, Van Herp M, Gunther S.** 2014. Emergence of Zaire Ebola virus disease in Guinea. N Engl J Med **371:**1418–1425. http://dx.doi.org/10.1056/NEJMoa1404505.
4. **Lee JE, Fusco ML, Hessell AJ, Oswald WB, Burton DR, Saphire EO.** 2008. Structure of the Ebola virus glycoprotein bound to an antibody from a human survivor. Nature **454:**177–182. http://dx.doi.org/10.1038/nature07082.
5. **Lee JE, Saphire EO.** 2009. Neutralizing ebolavirus: structural insights into the envelope glycoprotein and antibodies targeted against it. Curr Opin Struct Biol **19:**408–417. http://dx.doi.org/10.1016/j.sbi.2009.05.004.
6. **Jeffers SA, Sanders DA, Sanchez A.** 2002. Covalent modifications of the Ebola virus glycoprotein. J Virol **76:**12463–12472. http://dx.doi.org/10.1128/JVI.76.24.12463-12472.2002.
7. **Kaletsky RL, Simmons G, Bates P.** 2007. Proteolysis of the Ebola virus glycoproteins enhances virus binding and infectivity. J Virol **81:**13378–13384. http://dx.doi.org/10.1128/JVI.01170-07.
8. **Schornberg K, Matsuyama S, Kabsch K, Delos S, Bouton A, White J.** 2006. Role of endosomal cathepsins in entry mediated by the Ebola virus glycoprotein. J Virol **80:**4174–4178. http://dx.doi.org/10.1128/JVI.80.8.4174-4178.2006.
9. **Chandran K, Sullivan NJ, Felbor U, Whelan SP, Cunningham JM.** 2005. Endosomal proteolysis of the Ebola virus glycoprotein is necessary for infection. Science **308:**1643–1645. http://dx.doi.org/10.1126/science.1110656.
10. **Miller EH, Obernosterer G, Raaben M, Herbert AS, Deffieu MS, Krishnan A, Ndungo E, Sandesara RG, Carette JE, Kuehne AI, Ruthel G, Pfeffer SR, Dye JM, Whelan SP, Brummelkamp TR, Chandran K.** 2012. Ebola virus entry requires the host-programmed recognition of an intracellular receptor. EMBO J **31:**1947–1960. http://dx.doi.org/10.1038/emboj.2012.53.
11. **Hashiguchi T, Fusco ML, Bornholdt ZA, Lee JE, Flyak AI, Matsuoka R, Kohda D, Yanagi Y, Hammel M, Crowe JE, Jr., Saphire EO.** 2015. Structural basis for Marburg virus neutralization by a cross-reactive human antibody. Cell **160:**904–912. http://dx.doi.org/10.1016/j.cell.2015.01.041.
12. **Mulherkar N, Raaben M, de la Torre JC, Whelan SP, Chandran K.** 2011. The Ebola virus glycoprotein mediates entry via a non-classical dynamin-dependent macropinocytic pathway. Virology **419:**72–83. http://dx.doi.org/10.1016/j.virol.2011.08.009.
13. **Saeed MF, Kolokoltsov AA, Albrecht T, Davey RA.** 2010. Cellular entry of Ebola virus involves uptake by a macropinocytosis-like mechanism and subsequent trafficking through early and late endosomes. PLoS Pathog **6:**e1001110. http://dx.doi.org/10.1371/journal.ppat.1001110.
14. **Mingo RM, Simmons JA, Shoemaker CJ, Nelson EA, Schornberg KL, D'Souza RS, Casanova JE, White JM.** 2015. Ebola virus and severe acute respiratory syndrome coronavirus display late cell entry kinetics: evidence that transport to NPC1+ endolysosomes is a rate-defining step. J Virol **89:**2931–2943. http://dx.doi.org/10.1128/JVI.03398-14.
15. **Nanbo A, Imai M, Watanabe S, Noda T, Takahashi K, Neumann G, Halfmann P, Kawaoka Y.** 2010. Ebolavirus is internalized into host cells via macropinocytosis in a viral glycoprotein-dependent manner. PLoS Pathog **6:**e1001121. http://dx.doi.org/10.1371/journal.ppat.1001121.
16. **Dube D, Brecher MB, Delos SE, Rose SC, Park EW, Schornberg KL, Kuhn JH, White JM.** 2009. The primed ebolavirus glycoprotein (19-kilodalton GP1,2): sequence and residues critical for host cell binding. J Virol **83:**2883–2891. http://dx.doi.org/10.1128/JVI.01956-08.
17. **Carette JE, Raaben M, Wong AC, Herbert AS, Obernosterer G, Mulherkar N, Kuehne AI, Kranzusch PJ, Griffin AM, Ruthel G, Dal Cin P, Dye JM, Whelan SP, Chandran K, Brummelkamp TR.** 2011. Ebola virus entry requires the cholesterol transporter Niemann-Pick C1. Nature **477:**340–343. http://dx.doi.org/10.1038/nature10348.
18. **Côté M, Misasi J, Ren T, Bruchez A, Lee K, Filone CM, Hensley L, Li Q, Ory D, Chandran K, Cunningham J.** 2011. Small molecule inhibitors reveal Niemann-Pick C1 is essential for Ebola virus infection. Nature **477:**344–348. http://dx.doi.org/10.1038/nature10380.
19. **Krishnan A, Miller EH, Herbert AS, Ng M, Ndungo E, Whelan SP, Dye JM, Chandran K.** 2012. Niemann-Pick C1 (NPC1)/NPC1-like1 chimeras define sequences critical for NPC1's function as a flovirus entry receptor. Viruses **4:**2471–2484. http://dx.doi.org/10.3390/v4112471.
20. **Herbert AS, Davidson C, Kuehne AI, Bakken R, Braigen SZ, Gunn KE, Whelan SP, Brummelkamp TR, Twenhafel NA, Chandran K, Walkley SU, Dye JM.** 2015. Niemann-Pick C1 is essential for ebolavirus replication and pathogenesis in vivo. mBio **6:**e00565-15. http://dx.doi.org/10.1128/mBio.00565-15.
21. **Maruyama T, Rodriguez LL, Jahrling PB, Sanchez A, Khan AS, Nichol ST, Peters CJ, Parren PW, Burton DR.** 1999. Ebola virus can be effectively neutralized by antibody produced in natural human infection. J Virol **73:**6024–6030.
22. **Flyak AI, Ilinykh PA, Murin CD, Garron T, Shen X, Fusco ML, Hashiguchi T, Bornholdt ZA, Slaughter JC, Sapparapu G, Klages C, Ksiazek TG, Ward AB, Saphire EO, Bukreyev A, Crowe JE, Jr.** 2015. Mechanism of human antibody-mediated neutralization of Marburg virus. Cell **160:**893–903. http://dx.doi.org/10.1016/j.cell.2015.01.031.
23. **Bale S, Liu T, Li S, Wang Y, Abelson D, Fusco M, Woods VL, Jr., Saphire EO.** 2011. Ebola virus glycoprotein needs an additional trigger, beyond proteolytic priming for membrane fusion. PLoS Negl Trop. Dis **5:**e1395. http://dx.doi.org/10.1371/journal.pntd.0001395.
24. **Brindley MA, Hughes L, Ruiz A, McCray PB, Jr., Sanchez A, Sanders DA, Maury W.** 2007. Ebola virus glycoprotein 1: identification of residues important for binding and postbinding events. J Virol **81:**7702–7709. http://dx.doi.org/10.1128/JVI.02433-06.
25. **Manicassamy B, Wang J, Jiang H, Rong L.** 2005. Comprehensive analysis of Ebola virus GP1 in viral entry. J Virol **79:**4793–4805. http://dx.doi.org/10.1128/JVI.79.8.4793-4805.2005.
26. **Mpanju OM, Towner JS, Dover JE, Nichol ST, Wilson CA.** 2006. Identification of two amino acid residues on Ebola virus glycoprotein 1 critical for cell entry. Virus Res **121:**205–214. http://dx.doi.org/10.1016/j.virusres.2006.06.002.
27. **Martinez O, Ndungo E, Tantral L, Miller EH, Leung LW, Chandran K, Basler CF.** 2013. A mutation in the Ebola virus envelope glycoprotein restricts viral entry in a host species- and cell-type-specific manner. J Virol **87:**3324–3334. http://dx.doi.org/10.1128/JVI.01598-12.
28. **Miller EH, Harrison JS, Radoshitzky SR, Higgins CD, Chi X, Dong L, Kuhn JH, Bavari S, Lai JR, Chandran K.** 2011. Inhibition of Ebola virus entry by a C-peptide targeted to endosomes. J Biol Chem **286:**15854–15861. http://dx.doi.org/10.1074/jbc.M110.207084.
29. **Miller EH, Chandran K.** 2012. Filovirus entry into cells—new insights. Curr Opin Virol **2:**206–214. http://dx.doi.org/10.1016/j.coviro.2012.02.015.
30. **Dias JM, Kuehne AI, Abelson DM, Bale S, Wong AC, Halfmann P, Muhammad MA, Fusco ML, Zak SE, Kang E, Kawaoka Y, Chandran K, Dye JM, Saphire EO.** 2011. A shared structural solution for neutralizing ebolaviruses. Nat Struct Mol Biol **18:**1424–1427. http://dx.doi.org/10.1038/nsmb.2150.
31. **Murin CD, Fusco ML, Bornholdt ZA, Qiu X, Olinger GG, Zeitlin L, Kobinger GP, Ward AB, Saphire EO.** 2014. Structures of protective

antibodies reveal sites of vulnerability on Ebola virus. Proc Natl Acad Sci U S A **111:**17182–17187. http://dx.doi.org/10.1073/pnas.1414164111.

32. **Ng M, Ndungo E, Jangra RK, Cai Y, Postnikova E, Radoshitzky SR, Dye JM, Ramírez de Arellano E, Negredo A, Palacios G, Kuhn JH, Chandran K.** 2014. Cell entry by a novel European filovirus requires host endosomal cysteine proteases and Niemann-Pick C1. Virology **468–470:**637–646. http://dx.doi.org/10.1016/j.virol.2014.08.019.
33. **Qiu X, Wong G, Audet J, Bello A, Fernando L, Alimonti JB, Fausther-Bovendo H, Wei H, Aviles J, Hiatt E, Johnson A, Morton J, Swope K, Bohorov O, Bohorova N, Goodman C, Kim D, Pauly MH, Velasco J, Pettitt J, Olinger GG, Whaley K, Xu B, Strong JE, Zeitlin L, Kobinger GP.** 2014. Reversion of advanced Ebola virus disease in nonhuman primates with ZMapp. Nature **514:**47–53. http://dx.doi.org/10.1038/nature13777.
34. **Carroll MW, Matthews DA, Hiscox JA, Elmore MJ, Pollakis G, Rambaut A, Hewson R, García-Dorival I, Bore JA, Koundouno R, Abdellati S, Afrough B, Aiyepada J, Akhilomen P, Asogun D, Atkinson B, Badusche M, Bah A, Bate S, Baumann J, Becker D, Becker-Ziaja B, Bocquin A, Borremans B, Bosworth A, Boettcher JP, Cannas A, Carletti F, Castilletti C, Clark S, Colavita F, Diederich S, Donatus A, Duraffour S, Ehichioya D, Ellerbrok H, Fernandez-Garcia MD, Fizet A, Fleischmann E, Gryseels S, Hermelink A, Hinzmann J, Hopf-Guevara U, Ighodalo Y, Jameson L, Kelterbaum A, Kis Z, Kloth S, Kohl C, Korva M.** 2015. Temporal and spatial analysis of the 2014–2015 Ebola virus outbreak in West Africa. Nature **524:**97–101. http://dx.doi.org/10.1038/nature14594.
35. **Maganga GD, Kapetshi J, Berthet N, Kebela Ilunga B, Kabange F, Mbala Kingebeni P, Mondonge V, Muyembe JJ, Bertherat E, Briand S, Cabore J, Epelboin A, Formenty P, Kobinger G, González-Angulo L, Labouba I, Manuguerra JC, Okwo-Bele JM, Dye C, Leroy EM.** 2014. Ebola virus disease in the Democratic Republic of the Congo. N Engl J Med **371:**2083–2091. http://dx.doi.org/10.1056/NEJMoa1411099.
36. **Towner JS, Sealy TK, Khristova ML, Albariño CG, Conlan S, Reeder SA, Quan PL, Lipkin WI, Downing R, Tappero JW, Okware S, Lutwama J, Bakamutumaho B, Kayiwa J, Comer JA, Rollin PE, Ksiazek TG, Nichol ST.** 2008. Newly discovered Ebola virus associated with hemorrhagic fever outbreak in Uganda. PLoS Pathog **4:**e1000212. http://dx.doi.org/10.1371/journal.ppat.1000212.
37. **Shoemaker T, MacNeil A, Balinandi S, Campbell S, Wamala JF, McMullan LK, Downing R, Lutwama J, Mbidde E, Ströher U, Rollin PE, Nichol ST.** 2012. Reemerging Sudan Ebola virus disease in Uganda, 2011. Emerg Infect Dis **18:**1480–1483. http://dx.doi.org/10.3201/eid1809.111536.
38. **Mylne A, Brady OJ, Huang Z, Pigott DM, Golding N, Kraemer MU, Hay SI.** 2014. A comprehensive database of the geographic spread of past human Ebola outbreaks. Sci Data **1:**140042. http://dx.doi.org/10.1038/sdata.2014.42.
39. **McCoy AJ, Grosse-Kunstleve RW, Adams PD, Winn MD, Storoni LC, Read RJ.** 2007. Phaser crystallographic software. J Appl Crystallogr **40:**658–674. http://dx.doi.org/10.1107/S0021889807021206.
40. **Collaborative Computational Project Number 4.** 1994. The CCP4 suite: programs for protein crystallography. Acta Crystallogr D Biol Crystallogr **50:**760–763. http://dx.doi.org/10.1107/S0907444994003112.
41. **Emsley P, Cowtan K.** 2004. Coot: model-building tools for molecular graphics. Acta Crystallogr D Biol Crystallogr **60:**2126–2132. http://dx.doi.org/10.1107/S0907444904019158.
42. **Evans P.** 2006. Scaling and assessment of data quality. Acta Crystallogr D Biol Crystallogr **62:**72–82. http://dx.doi.org/10.1107/S0907444905036693.
43. **Adams PD, Afonine PV, Bunkóczi G, Chen VB, Davis IW, Echols N, Headd JJ, Hung LW, Kapral GJ, Grosse-Kunstleve RW, McCoy AJ, Moriarty NW, Oeffner R, Read RJ, Richardson DC, Richardson JS, Terwilliger TC, Zwart PH.** 2010. PHENIX: a comprehensive python-based system for macromolecular structure solution. Acta Crystallogr D Biol Crystallogr **66:**213–221. http://dx.doi.org/10.1107/S0907444909052925.
44. **Painter J, Merritt EA.** 2006. Optimal description of a protein structure in terms of multiple groups undergoing TLS motion. Acta Crystallogr D Biol Crystallogr **62:**439–450. http://dx.doi.org/10.1107/S0907444906005270.
45. **Painter J, Merritt EA.** 2006. TLSMD web server for the generation of multi-group TLS models. J Appl Crystallogr **39:**109–111. http://dx.doi.org/10.1107/S0021889805038987.
46. **Brünger AT.** 1992. Free R-value—a novel statistical quantity for assessing the accuracy of crystal-structures. Nature **355:**472–475. http://dx.doi.org/10.1038/355472a0.
47. **Chen VB, Arendall WB, Headd JJ, Keedy DA, Immormino RM, Kapral GJ, Murray LW, Richardson JS, Richardson DC.** 2010. MolProbity: all-atom structure validation for macromolecular crystallography. Acta Crystallogr D Biol Crystallogr **66:**12–21. http://dx.doi.org/10.1107/S0907444909042073.
48. **Baker NA, Sept D, Joseph S, Holst MJ, McCammon JA.** 2001. Electrostatics of nanosystems: application to microtubules and the ribosome. Proc Natl Acad Sci U S A **98:**10037–10041. http://dx.doi.org/10.1073/pnas.181342398.
49. **Takada A, Robison C, Goto H, Sanchez A, Murti KG, Whitt MA, Kawaoka Y.** 1997. A system for functional analysis of Ebola virus glycoprotein. Proc Natl Acad Sci U S A **94(26):**14764–14769.